Biofilm Development and Destruction

EPRI

EPRI CS-1554
Project 902-1
Final Report
September 1980

Keywords:
Biofouling
Microbial Fouling
Condenser
Chlorine
Cooling Systems
Water Treatment

Prepared by
Rice University
Houston, Texas

ELECTRIC POWER RESEARCH INSTITUTE

Master

Biofilm Development and Destruction

CS-1554
Research Project 902-1

Final Report, September 1980

Prepared by

RICE UNIVERSITY
6100 South Main
P. O. Box 1892
Houston, Texas 77001

Principal Investigator
W. G. Characklis

Prepared for

Electric Power Research Institute
3412 Hillview Avenue
Palo Alto, California 94304

EPRI Project Manager
R. M. Jorden

Water Quality Control and Heat Rejection Program
Coal Combustion Systems Division

ORDERING INFORMATION

Requests for copies of this report should be directed to Research Reports Center (RRC), Box 50490, Palo Alto, CA 94303, (415) 965-4081. There is no charge for reports requested by EPRI member utilities and affiliates, contributing nonmembers, U.S. utility associations, U.S. government agencies (federal, state, and local), media, and foreign organizations with which EPRI has an information exchange agreement. On request, RRC will send a catalog of EPRI reports.

NOTICE

This report was prepared by the organization(s) named below as an account of work sponsored by the Electric Power Research Institute, Inc. (EPRI). Neither EPRI, members of EPRI, the organization(s) named below, nor any person acting on their behalf: (a) makes any warranty or representation, express or implied, with respect to the accuracy, completeness, or usefulness of the information contained in this report, or that the use of any information, apparatus, method, or process disclosed in this report may not infringe privately owned rights; or (b) assumes any liabilities with respect to the use of, or for damages resulting from the use of, any information, apparatus, method, or process disclosed in this report.

Prepared by
Rice University
Houston, Texas

ABSTRACT

This investigation was restricted to the study of fouling biofilm formation, its effects on energy losses and, finally, its destruction.

The project objectives included the following:

1. Develop a better understanding of fouling biofilm accumulation and factors affecting its rate.
2. Determine the effectiveness of fouling biofilm destruction by chemical oxidants.
3. Develop a practical, reliable, sensitive device for monitoring biofouling.

Special apparatus and simulated cooling water were used in the laboratory. Two reactor configurations were used:

1. a tubular reactor
2. an annular reactor consisting of a stationary outer cylinder and a rotating inner cylinder

Experiments and apparatus were designed to isolate the effects of biofouling from other processes such as corrosion or particulate fouling which could complicate data interpretation.

Biofilm development rate is affected by fluid velocity, wall temperature, and nutrient concentration. Increase in fluid frictional resistance, resulting from biofilm formation, is a good indication of biofouling after the biofilm reaches a critical thickness corresponding to the viscous sublayer thickness. Changes in heat transfer are the net result of (1) decrease in conductive heat transfer due to biofilm accumulation and, (2) increase in convective heat transfer due to increase in fluid frictional resistance.

Destruction of biofilms by chemical oxidants is a diffusion-limited process. Consequently, oxidants are more effective when applied at high concentration for short periods. High flow rates enhance biofilm destruction by oxidants.

Several promising techniques for monitoring biofouling film development and destruction were developed and tested.

EPRI PERSPECTIVE

PROJECT DESCRIPTION

Slime formation (microbial fouling) on condenser tubes leads to higher heat rates and reduced plant output. Chlorination has been one traditional control method, but current and proposed regulations may make it more difficult to maintain adequate cleanliness.

The overall objective of the biofouling control work at EPRI is to provide the technological basis for effective, economical, and environmentally acceptable methods of biofouling control in power plants. Specific projects develop data bases, design guidelines, chlorine reduction techniques, and alternatives to chlorination. The results will be published in a Biofouling Guidelines Manual.

This final report on RP902-1 describes a study of the growth and destruction of microbial slime films and determines the implications for condenser design and operation. The contractor also reviews several instruments for the detection and measurement of films for use in research projects and for in-plant operation and control.

PROJECT OBJECTIVES

The objectives of this project are to:

- Develop an understanding of and a model for the mechanisms of biofilm development and destruction
- Determine the effectiveness of biofilm destruction by chemical oxidants
- Develop a device for monitoring microbial fouling

PROJECT RESULTS

Film properties and growth:

- Slime films are 95-98% water and have the thermal conductivity of water. They are filamentous and pliable and have a maximum thickness of 100-500μ. Therefore:

  --Thermal resistance can be estimated from the film thickness.

  --Pressure drop is much higher than would be caused by a rigid film of equal thickness.

- Film growth: This occurs in three stages--induction, growth, and plateau stage; rates are controlled by water temperature, velocity, and organic carbon level.

- Control methods: These should focus on detection during the induction period. Continuous, low-level chlorination is most effective for prevention; high-level, short-duration dosage is most effective for destruction of an established film.

- Film measurement methods: Measurement and instrumentation studies showed that tube site pressure drop and loss of heat transfer efficiency can both be used for detecting fouling at film thicknesses above 50 μm, with measurement of pressure drop being the preferred method.

The report is intended both as a guide for researchers in the biofouling field and as an aid to utility engineers and equipment designers in achieving effective biofouling control.

Results of this study will lead to the development of improved microbial fouling control methods and a measurement-control concept. The development and demonstration of the methods will be integrated into Phase II work of RP1132, Biofouling Control Practice--Assessment and Evaluation.

R. M. Jorden, Project Manager
R. W. Kosage, Project Manager
Coal Combustion Systems Division

ACKNOWLEDGMENTS

The laboratory research reported herein was accomplished by a motivated group of young scientists and engineers. Their interest, enthusiasm and energy are largely responsible for any progress resulting from this work. They are as follows:

James D. Bryers, Graduate Research Assistant

Duane Marks, Research Technician

Michael Nimmons, Graduate Research Assistant

Frank L. Roe, Ph.D., Post-Doctoral Research Associate

Eileen Swinford, Research Technician

Michael Trulear, Graduate Research Assistant

Nicholas Zelver, Graduate Research Assistant

The project director also gratefully acknowledges the following:

Funding support from the Electric Power Research Institute (RP 902-1) and the National Science Foundation (ENG74-11957 and ENG77-26934).

Technical advice and assistance in graduate student direction from Dr. Basil F. Picologlou, Department of Mechanical Engineering, Rice University.

Technical advice and contributions from Dr. Larry V. McIntire and John Kirkpatrick, Department of Chemical Engineering, Rice University.

Administrative support and manuscript preparation by Linda Graetz, Maurine Lee and Audrey Yarletts under trying circumstances.

The Swiss Federal Institute for Water Resources and Water Pollution Control, Dubendorf, Switzerland.

Houston Lighting and Power Co. for permitting us to conduct tests at two of their stations.

Blank Page

CONTENTS

ILLUSTRATIONS

TABLES

SUMMARY

The term fouling refers to the formation of inorganic and/or organic deposits on surfaces. These films can impede the flow of heat across the surface, increase the fluid frictional resistance past the surface and increase the rate of corrosion at the surface. In most cases, the fouling media is water.

The U.S. power industry uses water at the rate of 6700 m^3/sec and approximately sixty percent is freshwater (1). The water is used to condense steam that has driven turbines to generate electricity. The water flows through surface condensers which are large bundles of tubes from 20-28 mm (0.8-1.1 in) and over 15 m (50 ft) long. A power plant with 240 MW capacity will have a surface condenser with approximately 3000 m^2 (32,300 ft^2) tube area.

BACKGROUND

Four types of fouling, and their combinations, may occur in these heat exchangers (1):

1. crystalline fouling - precipitation of inverse solubility sales (e.g., $CaCO_3$, $CaSO_4$) on the heated tube surface.
2. corrosion fouling - corrosion of tube metal which results in insulating layers of oxides on the tubes.
3. particulate fouling - attachment of particulate material on the tube surfaces.
4. biological fouling - formation of biological deposits on the tube surfaces.

Biological fouling, or biofouling, is perhaps the least understood of the fouling processes. Some of the confusion regarding biofouling

undoubtedly arises because of the interaction of several of the fouling processes at a given plant location. Mechanistically, fouling biofilm accumulation may be described as the net result of the following processes or variables:

1. Transport and accumulation of material from the cooling water to the tube surface. Materials can be soluble (microbial nutrients and inorganic salts) or particulate (viable microorganisms, their detritus, or inorganic particles. Also suspended particles of sufficient mass may control films by "scouring" action.

2. Microbial growth within the film. Attached microbial growth and extracellular polymers produced by the biofilm add film bulk and they can promote adherence of particles and significantly influence fouling rate.

3. Fluid shear stress at the surface of the film. Such forces can limit the overall extent of the fouling accumulation.

4. Metal condenser material and roughness. These material properties can influence micro-mixing near the surface and corrosion processes. In addition, some metals may release toxic components into the biofilm inhibiting growth and/or attachment.

5. Fouling control procedures. Chlorine, the most commonly used chemical, oxidizes film polymers causing disruption and partial removal in the shear stress field. Inactiviation of a portion of the microbial population also occurs. Altered film "roughness" and decreased viability will influence "regrowth" rates of the biofilm. Mechanical cleaning physically removes a portion of attached films.

There can be no doubt that fouling biofilms that form on surface condensers reduce heat transfer and lower plant efficiency. The most common method of controlling biofilm accumulation is periodic chlorination. Chlorine dosage and application schedule are typically governed by observation of plant steam back pressure or operator experience.

PRESENT CONCERNS

Recently, concern over toxicity from hypochlorous acid, or its reaction products, has resulted in federal regulations which limit the allowable concentrations of free available chlorine in cooling water discharges to 0.2 mg/l average (0.5 mg/l maximum). Discharge is re-

stricted to less than two hours daily per unit. The impact of the limitations is unknown but will vary significantly with location. At present, there is no sound basis for assessing the impact of these regulations.

This research project stems from the apparent need for a better basic understanding of fouling biofilm development and fouling biofilm destruction so that the impact of these new regulations on power plant operations can be evaluated. This project had the following goals:

1. Develop a better understanding of fouling biofilm development, with particular emphasis on the effects of fluid flow rate, bulk water temperature, wall surface temperature and limiting nutrient concentration.

2. Determine the effectiveness of fouling biofilm destruction by chemical oxidants, primarily chlorine.

3. Develop a practical, reliable, sufficiently sensitive device for monitoring biofouling and for effectively operating and controlling biofouling destruction processes at operating power plants.

PROCEDURES AND METHODS

To facilitate measurement, control and experimental reproducibility essential for understanding biofouling processes, special apparatus and simulated cooling water were adapted for use in the laboratory. Two reactor configurations were used:

1. a tubular reactor

2. an annular reactor consisting of a stationary outer cylinder and a rotating inner cylinder

The tubular reactor geometry and its turbulent flow regime are identical to those existing in power plant condensers. The annular reactor was tested as a biofouling monitor because it is very sensitive and also easy to operate and maintain. The annular reactor could be more conveniently used in a sidestream from the cooling water supply at a power plant to continuously monitor biofouling and control the addition of biocide.

The simulated cooling water had to be recirculated past the fouling surfaces to attain representative velocities and yet keep the cost

of water preparation reasonable. In order to study microbial growth in reasonable times, seed organisms and nutrients had to be added to the water. Glucose was used as the sole energy source for microbial growth in all experiments. It has several advantages and, in addition, has been used in many other reported biofilm studies which can be used for data comparison. Trypticase Soy Broth, a synthetic media, was used as a carbon source in most of the experiments. TSB contains a diverse number of organic compounds and therefore contributes to the stability of a mixed microbial population during an experiment. Some experiments were performed with glucose as the sole energy and carbon source.

Biofouling in the experimental reactors was measured by observing changes in the following parameters:

1. biofilm thickness
2. attached biomass
3. fluid frictional resistance
4. heat transfer resistance

The first two methods are direct measures of biofilm production, while the latter two are effects of biofilm development.

LIMITATIONS OF THE REPORTED RESULTS

Most of the reported results were obtained from laboratory experimentation. Several fundamental limitations must be considered when attempting to apply the results to biofouling in operating power plant condensers:

1. Glass or plastic surfaces were used to eliminate corrosion so that observed effects could be attributed solely to the presence of fouling biofilms. Power plant condensers are composed of a variety of metals or metal alloys which may significantly influence the fouling process observed in the field.

2. A soluble substrate (glucose) was used as the sole energy source for microbial growth in this research. Cooling waters for power plants most likely contain more complex carbon and energy sources at low concentrations. Furthermore, they probably vary enormously with plant location and other environmental factors.

3. The microbial inoculum for all laboratory experiments was composed of a variety of microbial species. Use of a single substrate, however, essentially precludes the maintenance of a stable mixed population. Therefore, as an experiment progressed, the microbial population was probably dominated by a very few species which could compete better for the available nutrients under the imposed experimental conditions. Microbial population diversity entering power plant condensers will vary with location, water quality, and many other environmental factors.

4. The feed water to the laboratory experimental reactors used in this research contained less than 1 mg/l suspended solids. Although biofouling may enhance the adsorption of inert suspended solids to condenser surfaces in operating power plants, suspended solids were not an influence on fouling in the reported laboratory experiments.

5. Concentration of other water quality parameters, besides the limiting nutrient, were not considered in this research. Biofouling in operating power plants is probably affected by other soluble and colloidal components of the cooling water such as calcium, magnesium, silica, and iron compounds.

SUMMARY OF COMPLETED WORK

Within the stated limitations, this research has contributed to the understanding of fouling biofilm development and destruction processes. Specifically,

1. The sensitivity of fouling biofilm development to fluid flow rate, bulk water temperature, wall surface temperature, and limiting nutrient concentration has been tested.

2. The thermal conductivity of biofilm has been estimated from experimental data.

3. The effect of biofilm development on fluid frictional resistance and heat transfer resistance has been determined.

4. Several non-destructive techniques for measurement of biofouling have been developed and tested. The feasibility of using these methods in full-size power plant condensers has been considered.

5. The rate and stoichiometry of the chlorine-biofilm reaction have been determined. Other chemical oxidants were tested in a limited number of experiments.

6. The effects of repeated chlorine addition on "regrowth" of biofilm has been observed.

7. The effects of flow reversal, bulk water temperature increase, and wall surface temperature increase on biofilms have been observed within a narrow range of experimental conditions.

CONCLUSIONS

The conclusions listed below have resulted from laboratory experimental work reported here. It cannot be overemphasized that the conclusions are valid for conditions and range of test variable encompassed by this study. The precise relevance of each of these conclusions to biofouling control in power plants must, unfortunately, await future laboratory/field studies in parallel.

Biofilm Properties

Biofilm density increases with increasing glucose loading rate (0-200 mg/m^2-min)* and fluid shear stress at the wall (2.9-7.24 ft/sec).** Biofilm density ranged from 10-40 mg/cm^3.

Biofilms are viscoelastic and exhibit a high viscous modulus.

In situ biofilms are primarily composed of water (95-98%).

Biofilm thermal conductivity is not significantly different from the thermal conductivity of water at the same temperature.

Biofilms are frequently characterized by filamentous structures. Filaments as long as 0.25 cm were observed in the flow reactors. The filamentous habit was especially evident at low glucose loadings.

---

*A glucose loading rate of 200 mg/m^2-min is equivalent to that observed in a 7/8" OD 18 BWG gage tube, 30 ft long, when average fluid velocity is 6 ft/sec and the intake water contains 0.14 mg/l soluble organic carbon.

**In a 7/8" OD 18 BWG gage tube.

Biofilm Development

Biofilm development on a clean surface, as measured by an increase in biofilm thickness or biofilm mass, occurs in three sequential phases:

1. the lag or induction phase characterized by little measurable change in frictional resistance or heat transfer resistance. The induction phase observed in the field lasted from 10-14 days and, consequently, special methods were used to accelerate this phase in the laboratory.

2. the growth phase characterized by an exponential increase in biofilm.

3. the plateau phase characterized by a relatively constant biofilm thickness and mass.

The rate of biofilm development, as determined in the growth phase, varies in the following way:

1. increases linearly with glucose loading rate at low glucose loading rates (approx. 0-20 mg/m^2-min)* and is independent of glucose loading rate at higher loading rates (up to 200 mg/m^2-min).*

2. increases with bulk water temperature up to approximately 35°C and then decreases.

3. decreases with increasing wall temperature greater than 35°C.

4. decreases with increasing shear stress at the wall (equivalent to 4.7-7.3 ft/sec).**

The extent of biofilm development, as characterized by biofilm thickness or biofilm mass in the plateau phase, varies in the following way:

---

*A glucose loading rate of 200 mg/m^2-min is equivalent to that observed in a 7/8" OD 18 BWG gage tube, 30 ft long, when average fluid velocity is 6 ft/sec and the intake water contains 0.14 mg/l soluble organic carbon.

**In a 7/8" OD 18 BWG gage tube.

1. increases with increasing glucose loading rate (0-200 mg/m^2-min).*

2. decreases with increasing shear stress at the wall (equivalent to 2.9-7.3 ft/sec).**

3. decreases with increasing wall temperature greater than 35°C.

Maximum biofilm thicknesses were generally in the range of 100-500 μm.

Fluid Frictional Resistance

Increase in fluid frictional resistance corresponds to an increase in biofilm thickness or biofilm mass.

Increase in biofilm thickness corresponds to the calculated increase in equivalent sand roughness.

Increase in frictional resistance is characterized by an induction period at small biofilm thicknesses followed by a rapid increase when the biofilm thickness reaches a critical value. The critical biofilm thickness compares favorably with the viscous sublayer thickness (e.g., 50 μm at a flow velocity of 6 ft/sec).*

Constriction of the tube due to biofilm production accounts for only a small fraction of the frictional resistance (approximately 10%).

The effect of Reynolds number on friction facter (e.g., Moody diagram) for a tube with an attached biofilm is similar to a tube with a rigid rough surface in the range of Reynolds number tested (5,000-48,000).

---

*A glucose loading rate of 200 mg/m^2-min is equivalent to that observed in a 7/8" OD 18 BWG gage tube, 30 ft long, when average fluid velocity is 6 ft/sec and the intake water contains 0.14 mg/l soluble organic carbon.

**In a 7/8" OD 18 BWG tube.

The viscoelastic properties and the filamentous nature of the biofilm contribute to the increase in frictional resistance.

Heat Transfer Resistance

The biofilm thermal conductivity is not significantly different from the thermal conductivity of water at the same temperature.

The changes in heat transfer observed during biofilm development are the net result of the following:

1. increase in convective heat transfer due to increase in "roughness,"

2. decrease in conductive heat transfer due to the increased thickness of the stagnant water layer adjacent to the tube wall. The calculated thickness of the stagnant water layer compares favorably with the measured biofilm thickness.

Biofilm Destruction by Chemical Methods

Chemical oxidants (chlorine, chloramines, hydrogen peroxide, and ozone) disrupt the biofilm structure resulting in only partial removal of the biofilm. Relative effectiveness of chemical oxidants is dependent on pH and, perhaps, other variables.

Rate of oxidant consumption is proportional to oxidant concentration (i.e., first order). As a consequence, for power plants which periodically add oxidant, pulse-injection of oxidant at relatively high concentrations will be more effective than low-level continuous chlorination for biofilm destruction. For example, three 5-minute pulses representing an average oxidant concentration of 1 mg/l would be more effective than continuous addition for 30 minutes at 0.5 mg/l. Continuous low-level oxidant addition, however, may be effective for prevention of biofouling film formation.

The extent of biofilm destruction is dependent on the amount of biofilm present prior to the addition of oxidant.

Biofilm development subsequent to oxidant treatment is more rapid than biofilm development observed on a new, clean surface.

Microscopic observations (430x) indicate that the tube surface was never completely restored to the new, clean condition with chlorine addition.

The stoichiometric chlorine demand of biofilm is 0.31 mg Cl_2/mg biofilm.

Biofilm Destruction by Physical Methods

Rapid increase in bulk water temperature provided more effective treatment than flow reversal or increase in surface temperature within the ranges tested.

Measurement of Biofouling

Frictional resistance in a tube is the most promising method for monitoring biofilm development in full-size condensers of those approaches investigated. The method, however, will only detect biofilms whose thickness is greater than the viscous sublayer (approximately 50 μm for a clean, smooth 7/8" OD 18 BWG gage tube at 6 ft/sec).

Frictional resistance in a rotating annular reactor is the most promising method for monitoring biofilm development in a sidestream parallel to a full-size condenser.

The frictional resistance methods can be used with readily available transducers capable of providing alarms and/or actuating pumps for feeding chemical control compounds.

Change in heat transfer resistance can be effectively used for monitoring biofilm development. However, an increase in heat transfer resistance may not be detected until the biofilm develops to a thickness equal to the viscous sublayer thickness (approximately 50 μm for a clean, smooth 7/8" OD 18 BWG gage tube at 6 ft/sec).

For laboratory research, the following methods have been tested and found useful for determining quantity of biofilm:

1. Biofilm thickness determination by volumetric displacement can detect biofilms down to a thickness of 10 μm with a precision of ± 9 μm.

2. Biofilm thickness determination using the mechanical stage of an optical microscope can detect biofilms down to a thickness of 10 μm with a precision of ± 10 μm.

3. Biofilm mass could be detected below 0.11 mg/cm^2. Biofilm density is calculated from biofilm mass and thickness measurements.

Relevance of Laboratory Conditions to Power Plant Condensers

The laboratory system appeared to provide a satisfactory simulation of fouling in a power plant cooling water when compared to the limited field data available.

RECOMMENDATIONS

The research work reported herein has contributed significantly to the understanding of the biofouling process. In so doing, many new questions have evolved. This section summarizes recommendations for future investigation on the topic of biofouling and its importance to the power industry.

In general, further laboratory research is necessary to evaluate the influence of other potentially important environmental variables on biofouling film development and destruction. The laboratory offers an inexpensive yet effective method for screening the effects of variables under controlled conditions.

Instrumentation and apparatus developed for monitoring biofilm development and its effects on fluid frictional resistance and heat transfer resistance must be improved where possible. Higher sensitivity and precision are necessary without sacrificing the durability of the device in the field.

Parallel field testing of the instrumentation and apparatus must be conducted to determine their value as laboratory research tools and field measurement and/or control devices.

Field Testing

Most importantly, field investigations are necessary to determine the relevance of instrumentation, apparatus, and data from laboratory re-

search and their value as monitoring and control tools.

Field investigations must be conducted in parallel with a power plant condenser which has been adequately instrumented to allow comparison with the instruments and apparatus in the sidestreams.

Factors Affecting Biofouling Film Development and Destruction

The initial period of attachment (i.e., the induction phase) is affected by the flow rate, the number concentration of particles and their size distribution. The roughness and composition of the surface will also influence the attachment process. More investigative effort must be directed at these initial events in a system capable of turbulent flow rates where all of the above variables can be controlled.

Particulate material has been implicated as the cause of increased biofouling and has also been suggested as a means of biofouling control. The effect of inert particulate concentration and particle characteristics (e.g., specific gravity, size, composition) on biofouling must be determined.

It is postulated that chemical species such as calcium, magnesium and silica are believed to influence the extracellular polymer matrix which is responsible for holding the biofilm together. Magnesium has been reported to play an important role in filament formation in attached growths. The effects of these constituents on biofilm properties and biofilm development rates must be determined, especially since chelants (e.g., EDTA, NTA) have been observed to be effective in partially removing biofilm from surfaces.

In recirculating cooling systems, pH and total dissolved solids (TDS) are set by considerations of corrosion and scaling control. In addition, cycles of concentration, which affect TDS, are also selected independently of biofouling considerations. Both pH and TDS may affect biofouling rates and biofouling control effectiveness. Laboratory studies should determine the extent to which biofouling film development and destruction are affected by pH and TDS.

Much effort has been directed to identifying specific organisms responsible for biofouling without any conclusive evidence that the organism population distribution is important. Controlled experiments with defined mixed populations should be conducted to determine whether the influence of the population distribution is significant as compared to the environmental variables.

Biofouling Control

The effects of flow rate, temperature and pH on oxidant effectiveness should be considered in greater depth.

Extensive testing of biofouling film destruction/control options and their combinations is necessary under controlled conditions. This testing should be accomplished in the laboratory and a portion should be conducted with closely simulated field conditions.

Effort should be directed towards methods for applying the oxidant directly onto the biofouling film, directly in the viscous sublayer rather than in the bulk fluid, or recycling the oxidant. Such procedures would make the most effective use of the oxidant and minimize the oxidant residual concentration in the cooling water discharge. Other avenues might involve enhancing extracellular polymer hydrolysis.

From trickling filter experience, it is postulated that absence of dissolved oxygen in the lower layers of the biofilm can be responsible for the sloughing of biofilm under certain circumstances. The effect of dissolved oxygen on biofouling should be determined and its use as a biofouling control procedure evaluated.

Instrumentation and Apparatus

Decreasing the gap width of the annular reactor will increase its sensitivity, i.e., it will be able to detect the presence of thinner films from a torque reading. Changes in the tube size and/or length of the tubular reactor will also alter sensitivity.

The benefits of providing a heat flux to the annular fouling reactor

should be determined in a laboratory study. The added heat flux may provide an even closer simulation of power plant condensers.

Techniques utilizing sound or light wave absorbance or reflectance should be considered and tested as biofilm thickness monitoring devices.

Techniques are needed for detecting biofouling during the induction phase. Promising methods included organic carbon or chemical oxygen demand analysis on tubes from a sidestream apparatus. Direct microscopic observation may also be useful in a sidestream system.

Section 1

INTRODUCTION

The term fouling refers to the formation of inorganic and/or organic deposits on surfaces. In cooling systems, these deposits form on condenser tube walls increasing fluid frictional resistance, accelerating corrosion and impairing heat transfer. Four types of fouling, alone or in combinations may occur:

1. crystalline fouling caused by precipitation of $CaCO_3$, $CaSO_4$ or silicates
2. corrosion fouling resulting from formation of insulating layers of metal oxides on the tubes
3. fouling due to adherence of particulate matter on tube surfaces
4. biological fouling resulting from attachment and growth of microbial organisms

This investigation was restricted to the study of biological fouling.

The most common method for controlling the fouling biofilm development and maintaining condenser performance is periodic chlorination. Chlorine, added to the cooling water, serves either to kill the microorganism or to hydrolyze the extracellular polymers which hold the biofilm together. The chlorine dosage and application schedule is typically determined by (1) observation of condenser performance as indicated by plant steam back-pressure, or (2) operator experience.

Recently, concern over residual toxicity from hypochlorous acid or its reaction products has resulted in federal regulations which limit the allowable concentrations of free available chlorine in cooling water discharges. At the present time, there is no sound basis for assessing the impact of the regulations. This investigation stems from the apparent need for a better basic understanding

of fouling biofilm development and fouling biofilm destruction so that the impact of these new regulations on power plant operations can be evaluated.

Laboratory experiments and a limited number of field tests were conducted with two reactor configurations:

1. a tubular reactor
2. an annular reactor consisting of a stationary outer cylinder and a rotating inner cylinder.

The tubular reactor geometry and its turbulent flow regime are identical to those existing in power plant condensers. The annular reactor was tested as a biofouling monitor because it is very sensitive to fouling and is easy to operate and maintain. The annular reactor has the potential of being used in a sidestream from the cooling water supply at a power plant to continuously monitor biofouling for control of the addition of oxidant. Biofouling in the experimental reactors was measured by observing changes in the following parameters:

1. biofilm thickness
2. attached biomass
3. fluid frictional resistance
4. heat transfer resistance

The project goals included the following:

1. Develop a better understanding of fouling biofilm development, with particular emphasis on the effects of fluid flow rate, bulk water temperature, wall surface temperature and limiting nutrient concentration.
2. Determine the effectiveness of fouling biofilm destruction by chemical oxidants, primarily chlorine.
3. Develop a practical, reliable, sufficiently sensitive device for monitoring biofouling and for effectively operating and controlling biofouling destruction processes at operating power plants.

Section 2

EXPERIMENTAL METHODS

The experimental methods used in this laboratory study were chosen to simulate the fundamental processes of biofilm development and destruction occurring in a small portion of a power plant condenser. The laboratory environment was necessary to attain good control on the variables of interest, i.e., flow rate, temperature and water quality.

Recycle reactor systems were used in all cases in the laboratory to minimize the cost of nutrient and organic carbon additions which would have been extravagant in a high-rate, once-through flow system. Nutrients, glucose and, in some cases, a synthetic growth media were added to provide the necessary mineral, energy and carbon requirements for microbial growth. The feed water to the various experimental reactors was tap water which had been treated to remove residual suspended solids and chlorine.

Experiments were initiated by inoculating with a mixed population of microorganisms and operating the reactors in a batch mode (as opposed to continuous flow) until some surface colonization occurred. This technique minimizes the induction period (see Figure 4-1) which can last for weeks under some of the conditions tested.

There are always risks in applying results from a laboratory simulation to a problem in the field. Some such limitations for this study are presented in the DISCUSSION section.

EXPERIMENTAL APPARATUS

Two reactor geometries were used in this research to study biofilm development and destruction:

1. The circular tube was used because it is the prevalent geometry in power plant condensers.

2. The sensitivity of the rotating annular reactor was tested because it could provide a more practical, reliable means for monitoring biofouling in the field since it requires little maintenance or support equipment.

Biofilm development was measured in two ways:

1. attached biomass
2. biofilm thickness

Indirectly biofouling was observed by measuring:

1. fluid frictional resistance
2. heat transfer resistance

Five apparati employing the tubular geometry and one employing the annular configuration were assembled so that several experimental programs could be conducted simultaneously. Specifically,

1. Tubular Fouling Reactor 1 (TFR1) (see Figures 2-1 and 2-2) was used for determining the effect of fluid shear rate at the wall, bulk water temperature, and limiting substrate concentration on biofilm development as determined by attached biomass, biofilm thickness and fluid frictional resistance. TFR1 was also used in the studies of the chlorine-biofilm reaction. Tubular Fouling Reactor 3 (TFR3) was an improved version of TFR1.

2. Tubular Fouling Reactor 2 (TFR2) (see Figure 2-3) was used for determining the effect of surface temperature on biofilm development. In addition, the effects of physical stress on biofilm were observed in this system. Attached biomass, biofilm thickness, and fluid frictional resistance were monitored.

3. Tubular Fouling Reactor 4 (TFR4) (see Figure 2-5) was used for determining biofilm thermal conductivity. Biofilm thickness, fluid frictional resistance, and heat transfer resistance were measured by TFR4 experiments.

4. Field Fouling Reactor (FFR) (see Figure 2-7) was used for observing biofouling in the field in terms of attached biomass and fluid frictional resistance.

5. Annular Fouling Reactor (AFR) (see Figure 2-8) was used for determining the effect of fluid shear rate at the wall, bulk temperature, and limiting substrate concentration on biofilm development as determined by biofilm thickness and fluid frictional resistance. AFR was also used for studying the chlorine-biofilm reaction.

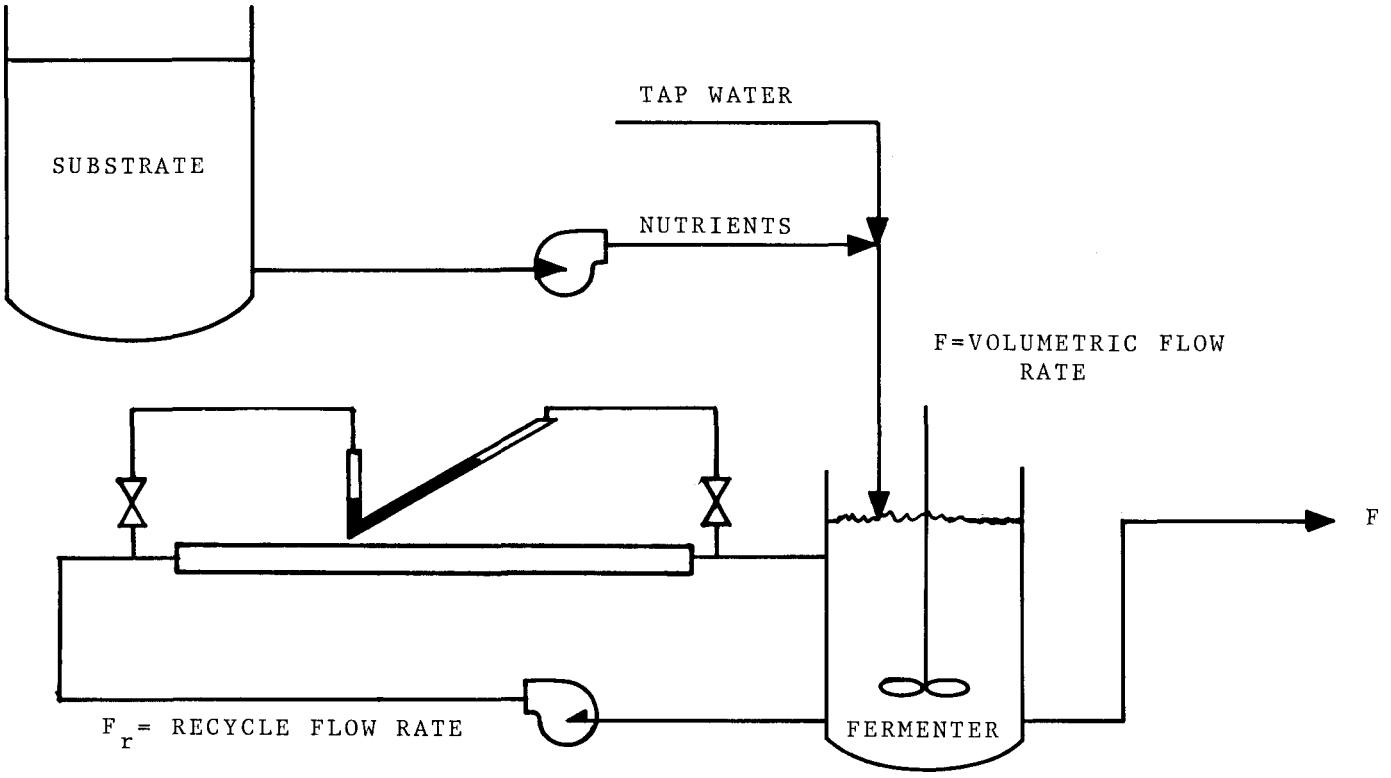

Figure 2-1. Schematic Diagram of Tubular Fouling Reactor System

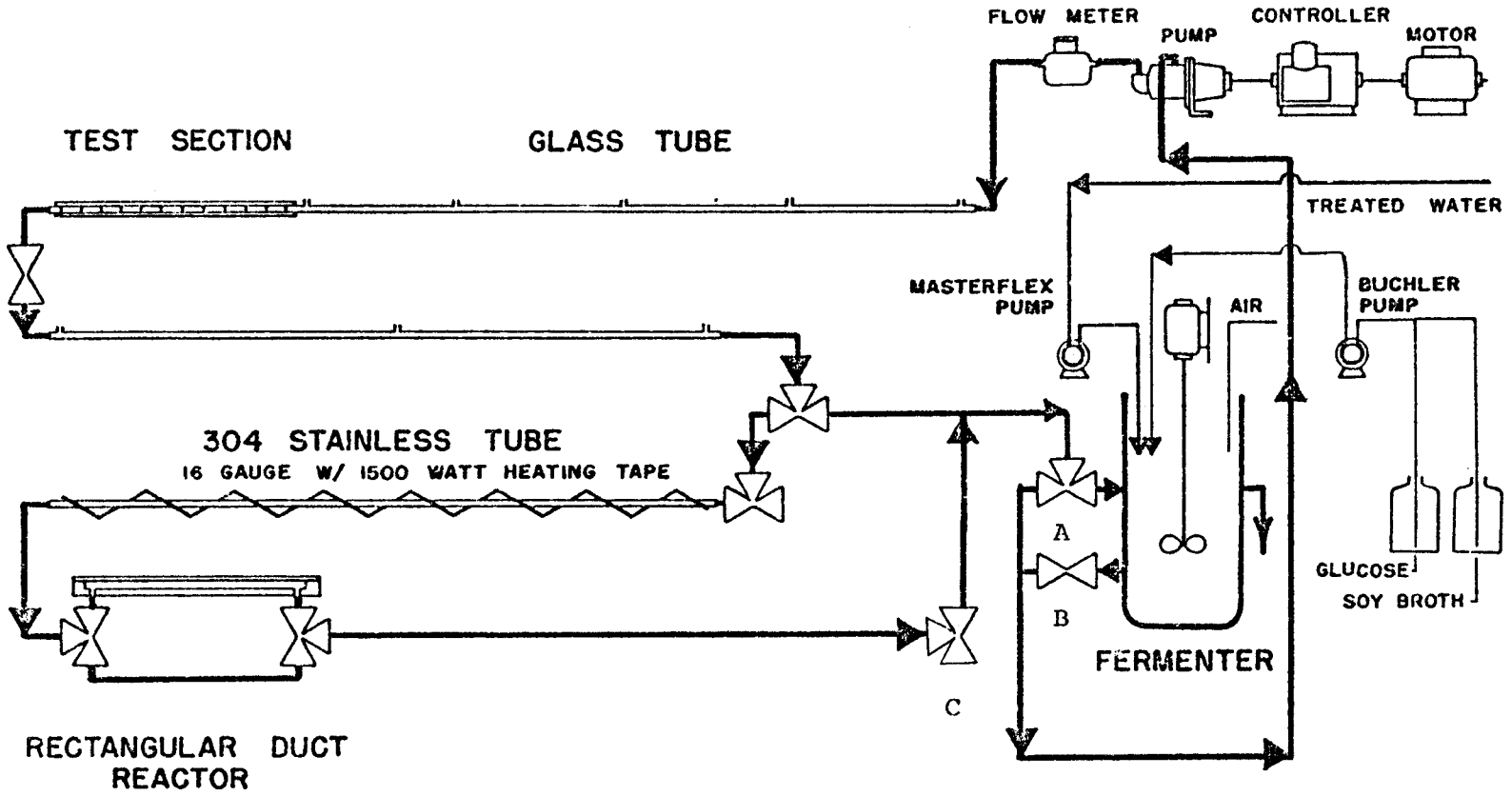

Figure 2-2. Tubular Fouling Reactor 1

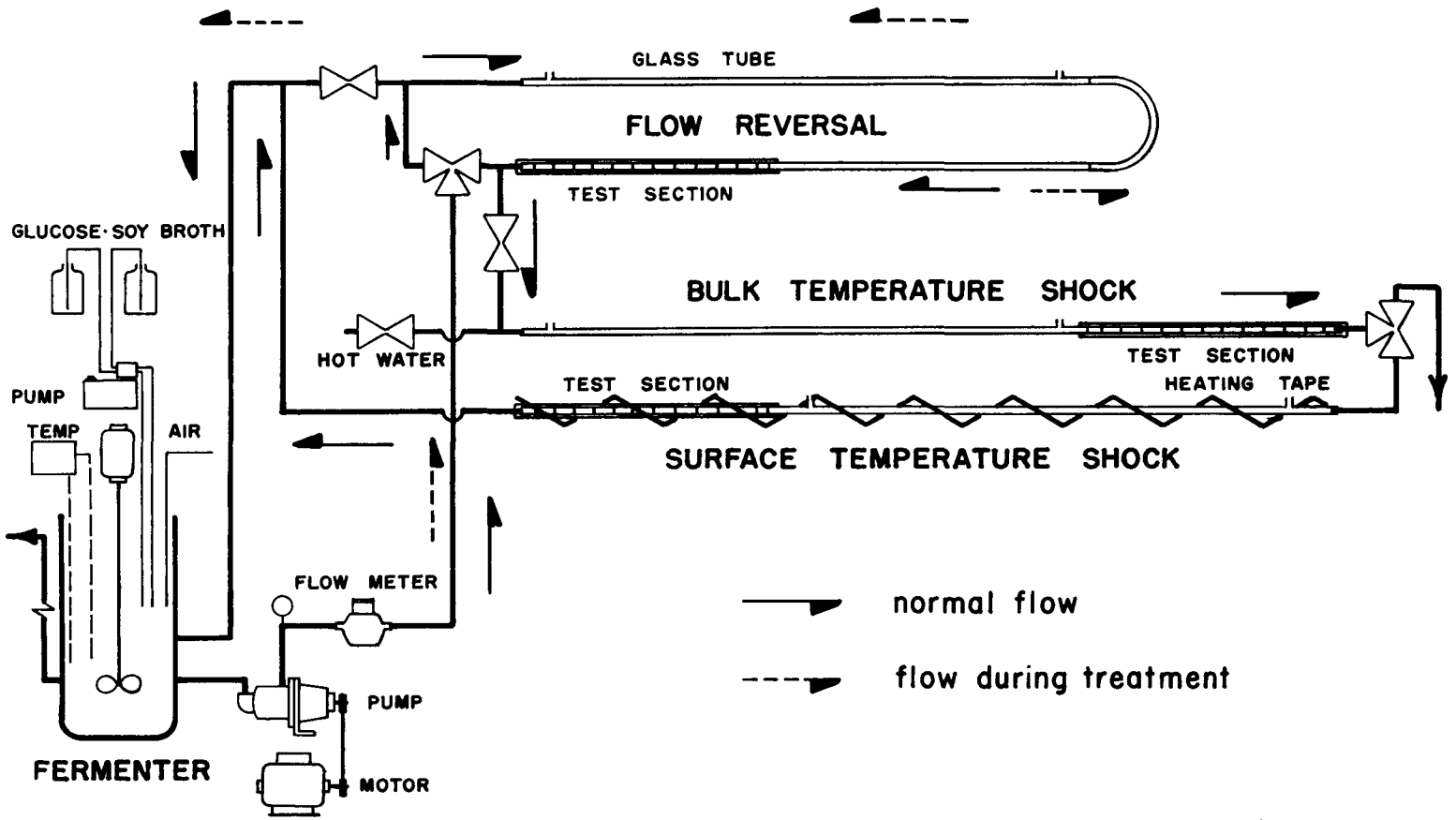

Figure 2-3. Tubular Fouling Reactor 2

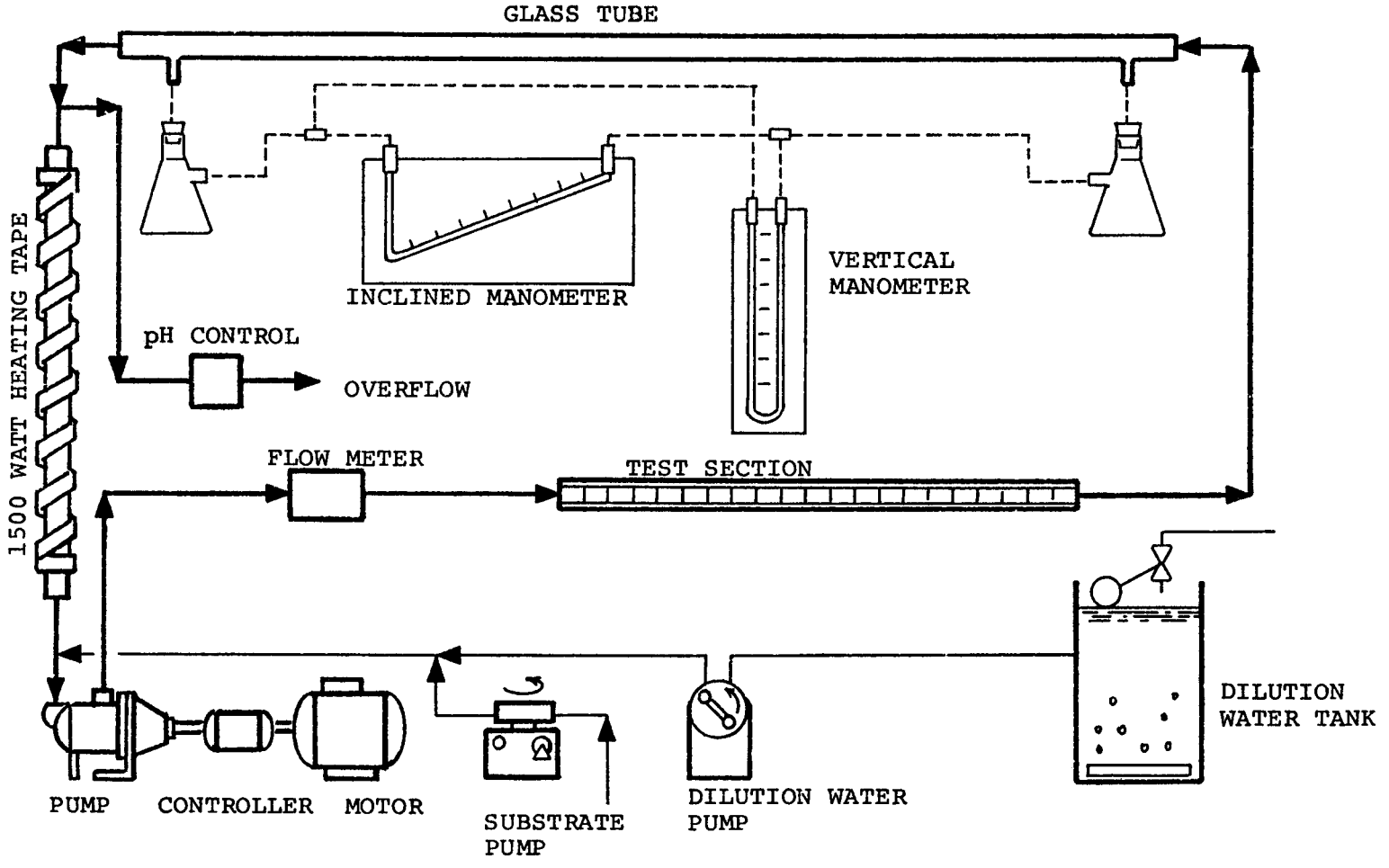

Figure 2-4. Tubular Fouling Reactor 3

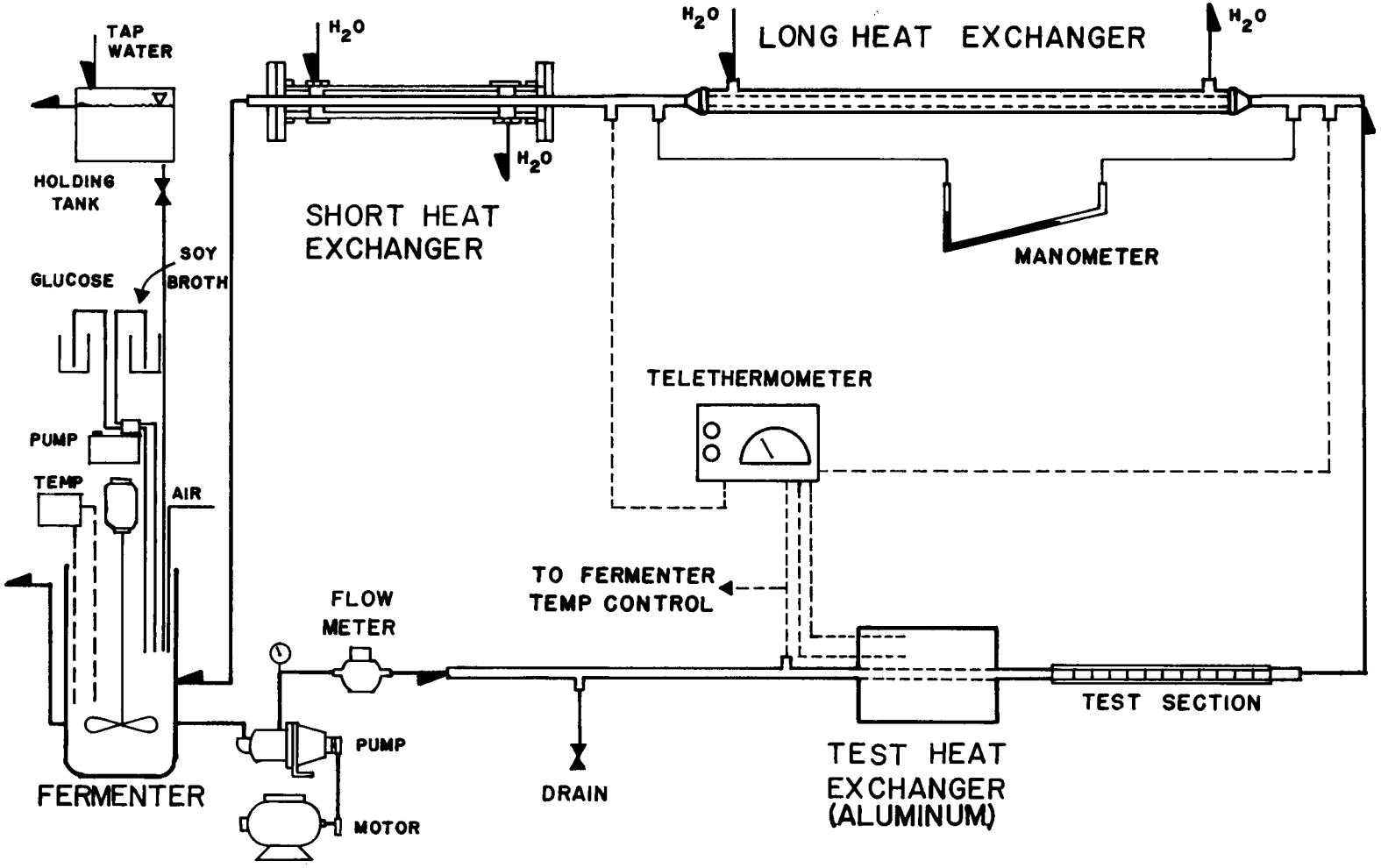

Figure 2-5. Tubular Fouling Reactor 4

r_i = 1.37 cm

r_{ii} = 6.48 cm

r_1 = .654 cm (0.695 cm)*

r_2 = 6.985 cm

*rebored system

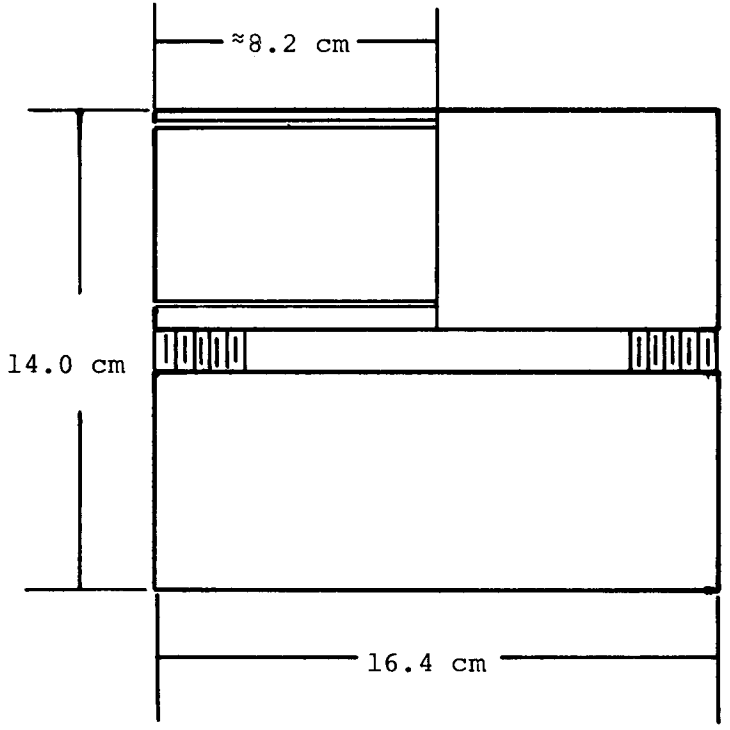

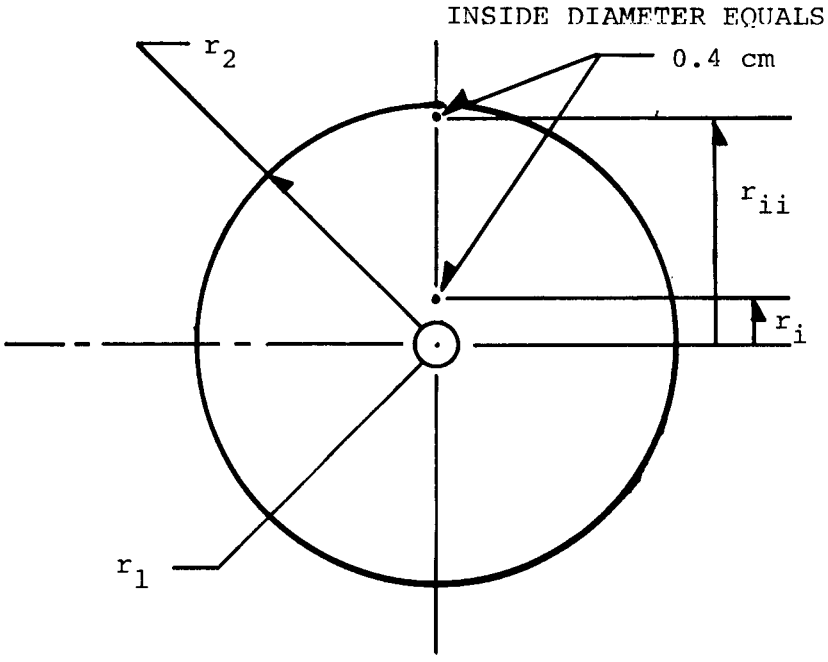

Figure 2-6. Aluminum Test Heat Exchanger (THE)

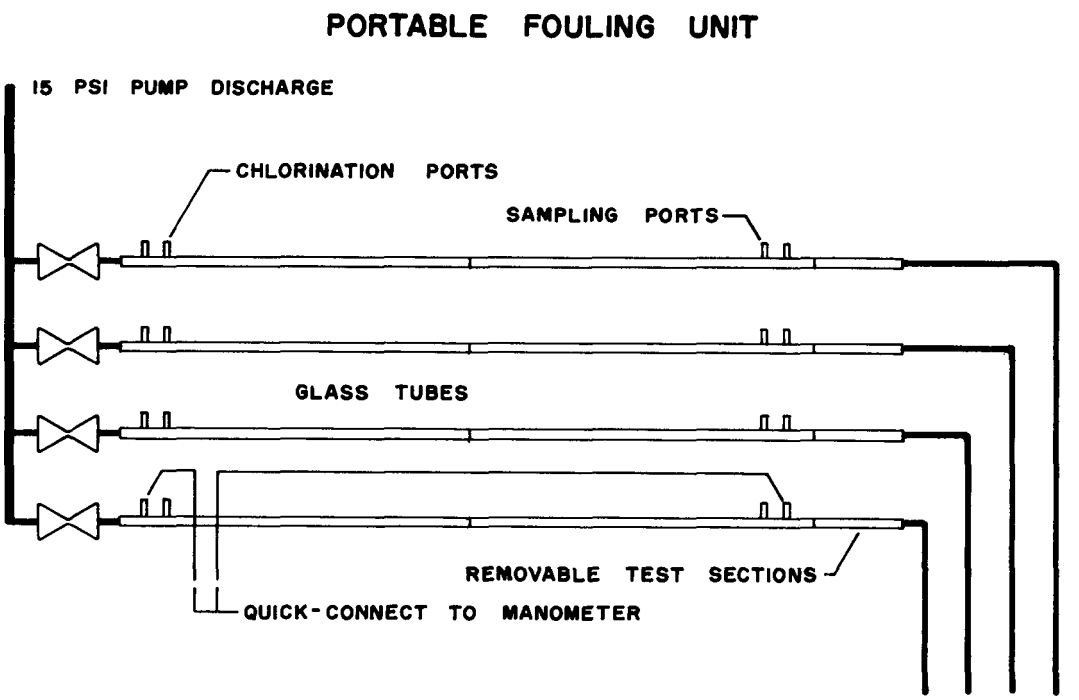

Figure 2-7. Detailed Diagram of FTU

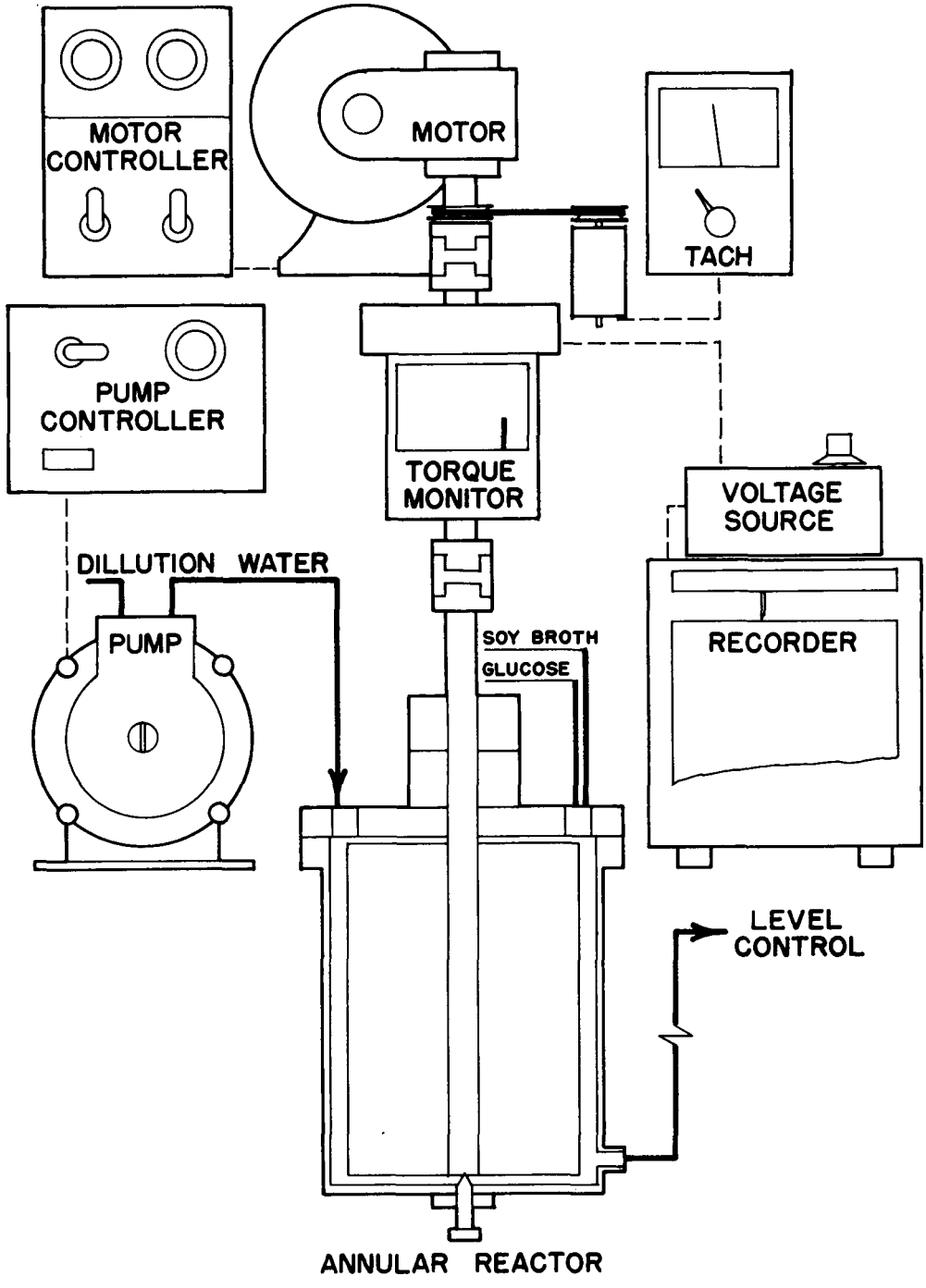

Figure 2-8. Annular Fouling Reactor System

The flow diagrams for all of these reactors, except for the FFR, are presented in Figure 3-7. All employ a recycle flow rate except for the FFR which was operated on a once-through basis. The recycle flow in the AFR (not evident in Figure 3-7) is by virtue of the pumping action of the impeller and four draft tubes situated in the inner, rotating cylinder (see Figure 2-9).

The Tubular Fouling Reactors

The tubular fouling reactors are chemostats (continuous stirred tank reactors) with internal recycle as indicated in Figure 2-1. Advantages of this configuration for laboratory experimentation include the following:

1. At high recycle rates employed ($F_r >> F$), the reactor contents are completely mixed and no concentration gradients exist. This simplifies mathematical descriptions and sampling. It also provides a relatively uniform biofilm in the recycle section while allowing simple control of pH and temperature. From a practical standpoint, this system minimized the consumption of water and microbial nutrient medium.

2. A short mean residence time can be maintained which minimizes biomass activity in the bulk fluid and restricts microbial activity to the reactor surfaces.

3. Fluid shear stress at the wall in the recycle loop is independent of mean residence time in the reactor system.

Tubular Fouling Reactor 1. A detailed diagram of the TFR1 system is presented in Figure 2-2. Recycle flow rate was maintained constant during an experiment by an electronic feedback system controlling a positive displacement screw pump. Bulk temperature was controlled with ± 0.3°C, pH was maintained at 7.0 ± 0.1 by H_2SO_4 and NaOH addition. Diffused air in the fermenter maintained aerobic conditions. System volume, including the fermenter, was 6719 cm^3 and surface area available for growth was 10,751 cm^2. Substrate and treated dilution water were pumped through peristaltic pumps (Model No. 6100, Buchler Co., Fort Lee, N.J., and Model No. WZLR0031, Cole-Parmer Instrument Co., Chicago, Ill., respectively). The reactor was insulated to minimize temperature gradients across the tubular cross sections.

The fermenter (Model No., MMF-07, New Brunswick Scientific Co., New Brunswick, N.J.) operating volume during the TFR1 experiments was 2950 cm^3 with a liquid depth of 19.0 cm. The fermenter was equipped with a temperature controller (Model No. 74, Yellow Springs Instrument Co., Yellow Springs, Ohio) and agitation control. The impeller was composed of three paddles 5 cm across and located 6.35, 10.15 and 13.10 cm below liquid level. Air was supplied to an orifice located beneath the stirring paddles at approximately 1500 cm^3/min. A summary of relevant characteristics and important dimensions for TFR1 is presented in Table 2-1.

Tubular Fouling Reactor 2. TFR2 was used for laboratory experiments testing the effect of wall surface temperature on biofilm development and the effect of physical stress on biofilm destruction. TFR2 was similar to TFR1 except that there was no provision for pH or flow control. The pH of the reactor feed was constant (pH = 8.3). At high influent substrate concentration, pH dropped significantly in the effluent (as low as pH = 7.9). The influence of pH, if any, on biofilm development and biofilm properties is not known at present. The absence of flow rate control in TFR2 resulted in decreasing flow rates as biofilm development progressed. Changes in friction factor could still be determined however, since pressure drop and flow rate were monitored.

Each of the three 244 cm tubular reactor sections in the recycle loop were equipped for providing a different type of physical stress to the biofilms:

1. flow reversal using a valving arrangement
2. bulk temperature shock employing hot tap water
3. surface temperature shock provided by heating tape

Each loop had its own test section, similar to the one in the TFR1, for monitoring biofilm accumulation. A detailed diagram of TFR2 is presented in Figure 2-3. Surface area was 7600 cm^2 and system volume was 4500 cm^3 with liquid depth of 16.5 cm in the fermenter which was identical to that in the TFR1. The three paddles were located 7.60,

Table 2-1

REVELANT CHARACTERISTICS AND IMPORTANT DIMENSIONS FOR TFR1 SYSTEM

System		
operating volume	6719	cm^3
wetted surface area	10750	cm^2
Fermenter		
material of construction	glass	
operating volume	2950	cm^3
Tubular Reactor		
material of construction	glass	
length	2194	cm
inside diameter	1.7	cm
outside diameter	1.91	cm
distance between pressure ports	232	cm
Test Section		
material of construction	acrylic plastic	
length	76	cm
inside diameter	1.9	cm
outside diameter	2.3	cm
Sample Tubes		
material of construction	glass	
number in test section	14	
length	5	cm
inside diameter	1.27	cm
outside diameter	1.91	cm
Volumetric flow rate(nutrient plus dilution water)	440	cm^3/min
Volumetric flow rate of air to fermenter	1500	cm^3/min
System mean residence time	15	min
pH	7.0 ± 0.1	
Temperature	$\pm 0.3^{\circ}C$	

10.15 and 12.70 cm below the liquid level. Air was supplied at approximately 1500 cm^3/min at a point just below the impeller. The fermenter was not insulated. A summary of relevant characteristics and important dimensions for TFR2 is presented in Table 2-2.

Tubular Fouling Reactor 3. TFR3 differed from TFR1 and TFR2 in that the fermenter was eliminated from the experimental system. Biofilm development experiments were conducted with TFR3 in an attempt to eliminate inconsistencies attributed to non-uniform growth conditions in the fermenters of TFR1 and TFR2. A major operational difference in TFR3 was that fluid shear stress was maintained constant by maintaining a constant pressure drop. In TFR1 and TFR2, volumetric flow rate was maintained constant. Pressure drop as high as 800 N/m^2 was monitored with an inclined manometer (Model B-627, Merian Instrument Co., Cleveland, Ohio). A vertical mercury manometer (Model 1230-50, Dwyer Instruments, Inc., Michigan City, Ind.) measured pressure drop from 8000-70,000 N/m^2. A detailed diagram of TFR3 is presented in Figure 2-4.

Temperature and pH were controlled in a manner similar to TFR1. In experiments TFR3-2 to TFR3-8, pH control was poor because of the pH probe location and pH as low as 5.3 was recorded in the reactor. Repositioning of the probe improved control but not to the level achieved in the TFR1 system. System volume was 2100 cm^3 and surface area available for growth was 3467 cm^2. A summary of relevant characteristics and important dimensions for TFR3 is presented in Table 2-3.

Tubular Fouling Reactor 4. TFR was used for determining biofilm thermal conductivity and heat transfer resistance. It was very similar to TFR1 and TFR2. A detailed diagram of the TFR4 system is presented in Figure 2-5. A rotary screw pump (Teel Model No. IP 898, Dayton Electric Mfg. Co., Chicago, Ill.) recirculated the fermenter contents through the recycle loop. Flow rate was determined by a volume displacement meter (Model No. 82AP, Carlon Meter Co.). Temperature was controlled within $\pm$ 0.3°C but there was no pH control. Diffused air in the fermenter maintained aerobic conditions. System volume was 5670 cm^3 and surface area available for growth was 6950 cm^2. Sub-

Table 2-2

RELEVANT CHARACTERISTICS AND IMPORTANT DIMENSIONS FOR TFR2 SYSTEM

System		
operating volume	4500	cm^3
wetted surface area	7600	cm^2
Fermenter		
material of construction	glass	
operating volume	2562	cm^3
liquid depth	16.5	cm
Tubular Reactor		
material of construction	glass	
length	1755	cm
inside diameter	1.27	cm
outside diameter	1.90	cm
distance between pressure ports	232	cm
Test Sections (3 in system)		
material of construction	acrylic plastic	
length	76	cm
inside diameter	1.9	cm
outside diameter	2.3	cm
Sample Tubes		
material of construction	glass	
number in test section	14	
length	5	cm
inside diameter	1.27	cm
Volumetric flow rate(nutrient plus dilution water)	300	cm^3/min
Volumetric flow rate of air to fermenter (23°C)	1500	cm^3/min
System mean residence time	15	min
pH	variable (7.9-8.3)	
Temperature control	±0.3°C	

Table 2-3

CHARACTERISTICS AND IMPORTANT DIMENSIONS FOR TFR3 SYSTEM

System		
operating volume	2100	cm^3
wetted surface area	3467	cm^2
Fermenter		
none		
Tubular Reactor		
material of construction	glass	
length	869	cm
inside diameter	1.27	cm
outside diameter	1.91	cm
distance between pressure ports	120	cm
Test Sections		
material of construction	stainless steel	
length	100	cm
inside diameter	1.25	cm
outside diameter	2.30	cm
Sample Tubes		
material of construction	glass	
number in test section	20	
length	5	cm
inside diameter	1.27	cm
outside diameter	1.91	cm
Volumetric flow rate (nutrient plus dilution water)	140	cm^3/min*
	or 280	cm^3/min**
System mean residence time	15	min
	or 7.5	min
pH	7.0 ± 0.5	
Temperature control	±0.3°C	

* Experiments TFR3-1 to TFR3-4
** Experiments TFR3-5 to TFR3-16

strate was pumped through a peristaltic pump (Model No. 6100, Buchler Co., Fort Lee, N.J.). Untreated dilution water flowed to the fermenter by gravity from a holding tank.

The fermenter (Model No. MMf-07, New Brunswick Scientific Co., New Brunswick, N.J.) operating volume was 1955 cm^3 with a liquid depth of 17.2 cm. The fermenter was equipped with a temperature controller (Model No. 74, Yellow Springs Instruments Co., Yellow Springs, Ohio) and agitation control. The impeller was composed of three paddles 5 cm across and located 10.2, 7.6, and 5.4 cm below the liquid level. Air was supplied to an orifice beneath the stirring paddles at approximately 2000 cm^3/min at 23°C.

Biofilm thermal conductivity was calculated from heat transfer measurements in the test heat exchanger (THE) described in Figure 2-6. The heat source was an electric heater (Model No. 060150C1, 120 volts, 450 watts, Watlow Co., St. Louis, Mo.) bonded to the outside surface of the aluminum THE. Temperature at two radial distances within THE was measured by a thermistor and monitored by a telethermometer (Model 45-TUC, Yellow Springs Instrument Co., Yellow Springs, Ohio). THE was insulated by 5.1 cm of pipe insulation.

The test section (see Figure 2-5) containing eight stainless sample tubes, is heated in a furnace (Model No. 55035, Lindberg Hevi-Duty, Watertown, Wisconsin) to provide a sample tube wall surface temperature equal to the THE surface temperature.

The long heat exchanger (see Figure 2-5) is also used for measurement of fluid frictional resistance. The tube is identical to the sample tubes and was maintained at a similar surface temperature during a given experiment. Pressure drop is measured at pressure ports immediately before and after the heat exchange shell with an inclined mercury manometer (Model No. 109, Dwyer Instruments, Inc., Michigan City, Ind.). Heating or cooling water was passed on the shell side depending on the desired temperature. The shell was composed of 1.25 in. nominal size pipe (3.51 cm) and was insulated.

A short shell and tube heat exchanger (see Figure 2-5) was used for supplemental cooling in some experiments.

A summary of relevant characteristics and important dimensions for TFR4 is presented in Table 2-4.

Field Fouling Reactor. The field fouling reactor (FFR) was used to conduct field investigations with actual power plant intake waters. Tests were conducted at two Houston Lighting and Power generating stations: Deepwater Power Station on the Houston Ship Channel and P. H. Robinson Power Station. The FFR was operated on a once-through flow in order to simulate the conditions in the power plant condenser. The simulation, to be accurate, presumed the surface material (metal in the condenser vs. glass in the FFR) and the temperature difference between the wall and the bulk fluid in the FFR (approximately 10°C in the condenser vs 0°C in the FFR) to have no effect on biofouling. These assumptions suggest caution in applying these results to actual condensers. The field fouling reactor consisted of four parallel, glass, tubular reactors (1.27 cm ID and 244 cm long). Flow was supplied from a sidestream on the discharge side of a supply pump to an operating condenser. The water entered a manifold and flowed through individual valves which controlled flow rate to each tubular reactor. Reactor effluent was wasted. A diagram of the FFR is presented in Figure 2-7.

Two ports were located at the inlet and outlet of each reactor for use as pressure taps, chemical injection, and sampling. A 15.2 cm removable section was located at the outlet end of each tubular reactor and provided data on film accumulation and film properties.

Chlorine was added in pulse doses of 38.4 mg by injecting a measured volume of stock solution with a syringe through a septum in the port at the inlet. In some experiments, the reactors were cleaned (as evidenced by inspection of the glass tubes) by passing larger quantities of chlorine through the tubes. After this procedure, induction periods were considerably shorter than those observed with the "virgin" tubes.

Annular Fouling Reactor

The annular fouling reactor (AFR) was tested as a potential biofouling monitor because of its sensitivity, particularly to changes in fric-

Table 2-4

RELEVANT CHARACTERISTICS AND IMPORTANT DIMENSIONS FOR THE TFR4 SYSTEM

System		
operating volume	5670	cm^3
wetted surface area	6950	cm^2
Fermenter		
material of construction	glass	
operating volume	1955	cm^3
liquid depth	17.5	cm
Test Heat Exchanger		
material of construction	6061-T6 aluminum	
length	16.4	cm
inside diameter	1.31	cm
	1.39	cm*
outside diameter	14	cm
Other Heat Exchangers		
material of construction	304 stainless steel	
length		
heat exchanger with pressure drop measurement	329	cm
heat exchanger for cooling	99	cm
distance between pressure ports	310	cm
inside diameter	1.66	cm
outside diameter	1.91	cm
Test Section		
material of construction	304 stainless steel	
length	39.4	cm
inside diameter	1.98	cm
outside diameter	2.22	cm
Sample Tubes		
material of construction	304 stainless steel	
number in test section	8	
length	5.1	cm
inside diameter	1.66	cm
outside diameter	1.91	cm
Volumetric flow rate(nutrient plus dilution water)	474	cm^3/min
Volumetric flow rate of air to the fermenter (23^oC)	2000	cm^3/min
System mean residence time	12	min
pH	variable (range 7.8-8.9)	
Temperature control	$\pm$ 0.3^oC	

tional resistance. Furthermore, changes can be monitored continuously and non-destructively. Thus the AFR offers the potential for use in a sidestream parallel with a power plant condenser to continuously monitor biofouling and possibly control biocide addition. It remains to be determined how comparable the biofouling rates in the AFR are to those in an actual condenser.

The AFR was constructed of acrylic plastic and consisted of two concentric cylinders, a stationary outer cylinder and a rotating inner cylinder. A torque transducer (Model No. M1, General Thermodynamics, Inc., Wilmington, Mass.), mounted on the shaft between the cylinder and the motor drive, monitored drag force. Rotational velocity was controlled electronically (Model No. ASH 401, Bodine Electric Co., Chicago, Ill.) and was displayed continuously. A removable slide, which formed an integral fit with the inside wall of the outer cylinder, was used to determine biofilm thickness and film density. The reactor was completely mixed by virtue of the pumping action of four draft tubes and an impeller mounted at the bottom of the inner cylinder (2). Nutrients and treated dilution water were measured by peristaltic pumps (Model No. 2-7100, Buchler Instrument Co., Chicago, Ill., and Model No. WZ1R057, Cole-Parmer Instruments Co., Chicago, Ill., respectively). Dilution water passed through a mixing chamber (volume 4500 cm^3) for temperature adjustment before entering the AFR. Temperature control was $\pm$ 0.3°C.

The shear force at the inner wall could be varied independently of mean residence time which was maintained at 10 minutes. The reactor volume was 570 cm^3 and surface area available for growth was 1800 cm^2 not including the draft tubes (another 226 cm^2). The AFR was insulated to minimize temperature gradients. Figure 2-8 illustrates the AFR experimental system and Figure 2-9 and 2-10 present details of the reactor. Table 2-5 presents relevant characteristics and important dimensions of the AFR.

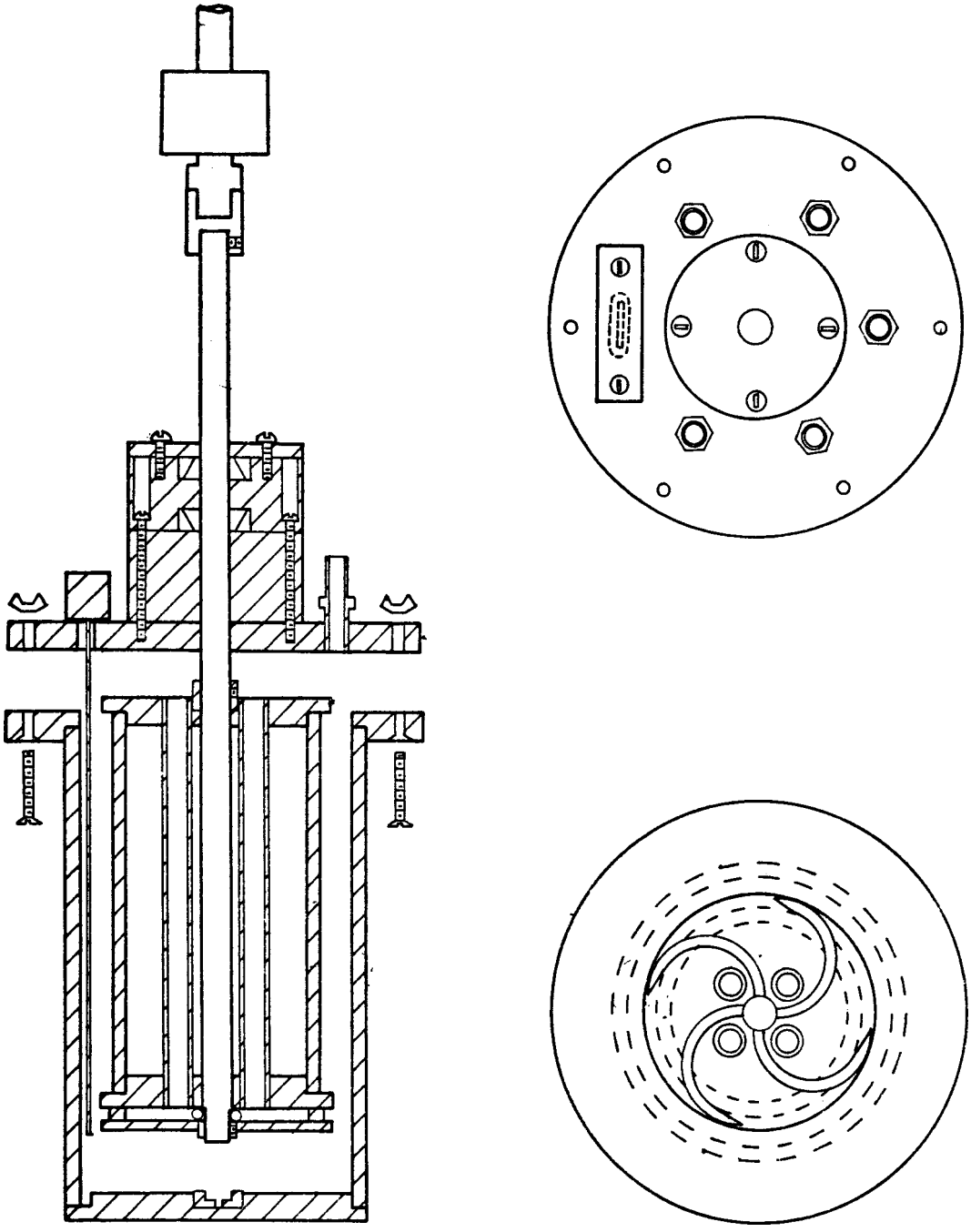

Figure 2-9. Annular Fouling Reactor

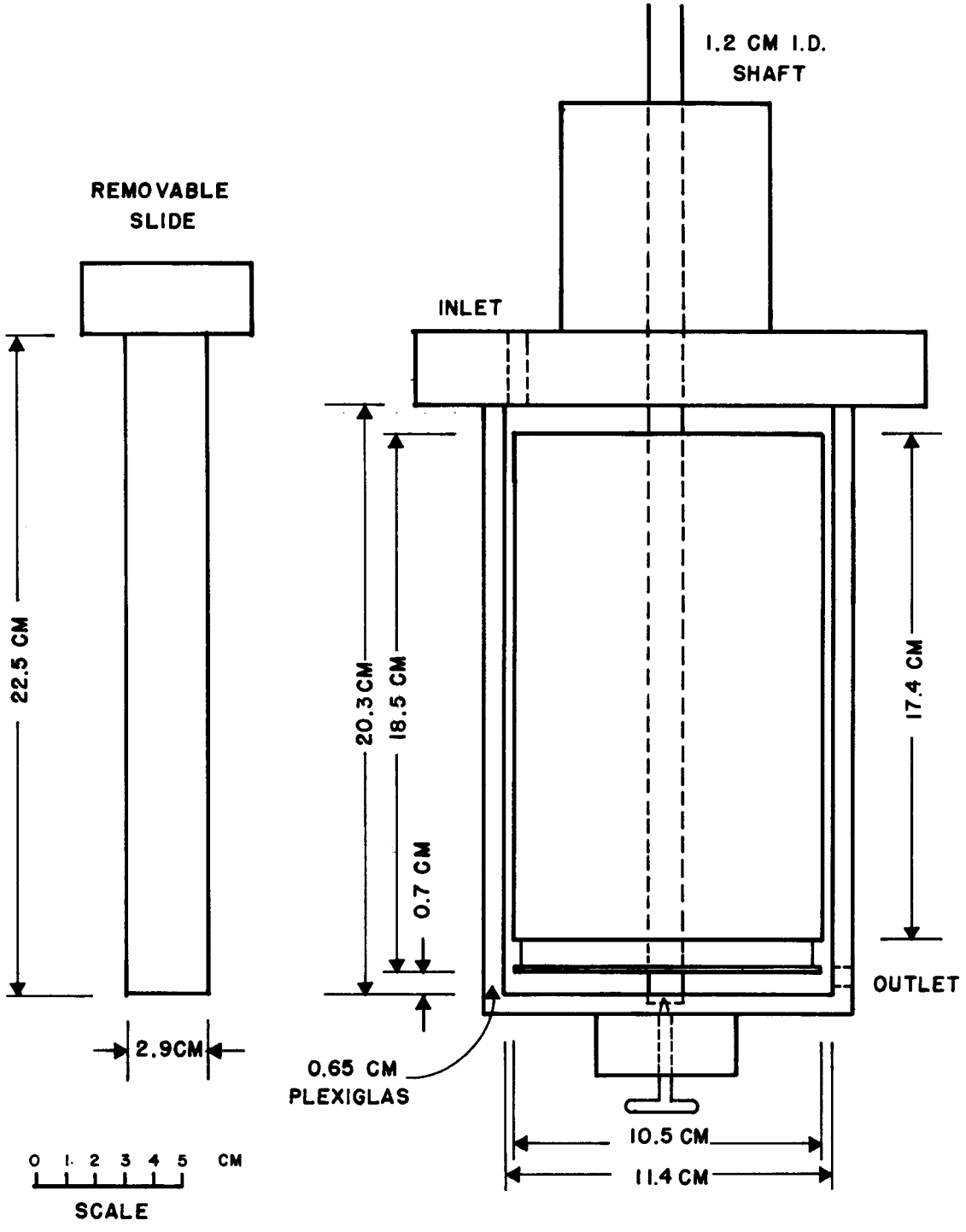

Figure 2-10. Scale drawing of AFR with all dimensions.

Table 2-5

RELEVANT CHARACTERISTICS AND IMPORTANT DIMENSIONS
FOR THE ANNULAR FOULING REACTOR SYSTEM

System		
material of construction	acrylic plastic	
operating volume	570	cm^3
wetted surface area (including draft tubes)	2027	cm^2
wetted surface area of draft tubes	266	cm^2
outside diameter of inner cylinder	10.5	cm
width of annular gap	0.45	cm
wetted height of inner cylinder	17.4	cm
wetted height of outer cylinder	20.2	cm
Removable Slide		
height	22.5	cm
width	2.9	cm
Volumetric flow rate (nutrient plus dilution water)	57	cm^3/min
System mean residence time	10	min
pH	variable	(7.9-8.3)
Temperature control		$\pm 0.3^oC$

EXPERIMENTAL PROCEDURES

The reactor feed was the result of combining the three constituents: dilution water, nutrient, and microbial inoculum.

Dilution Water

Rice University tap water was the source of dilution water for all laboratory experiments. The tap water was treated prior to entering the TFR1 and AFR experimental systems in the following way:

1. Flow through an in-line filter (Model No. 1M1, AMF Cuno Co.) to remove particulates.
2. Flow through a downflow carbon adsorption column for removal of residual chlorine.
3. Storage in an aerated metal storage drum (203 liters) coated with epoxy paint.

A chemical analysis of the tap water is presented in Table 2-6. Experiments in TFR2, TFR3 and TFR4 used untreated tap water.

Table 2-6

CHEMICAL ANALYSIS OF RICE UNIVERSITY TAP WATER

Constituent	Concentration (mg/l)
Dissolved Residue at 350°C	311
Total Dissolved Solids	452
Silica	14 (as SiO_2)
Calcium	13 (as Ca)
Magnesium	4 (as Mg)
Sodium (diff) Na + K	111 (as Na)
Carbonate	0 (as CO_3)
Bicarbonate	278 (HCO_3)
Sulfate	7 (as SO_4)
Chloride	38 (as Cl)
Total Iron	0.15 (as Fe)
Total Hardness	48 (as $CaCO_3$)
Total Alkalinity	228 (as $CaCO_3$)
Free Carbon Dioxide	0.3 (as CO_2)
	Units as Indicated
Conductance (as 25°C)	553 micromhos/cm
Color	2 color units
Turbidity	1 JTU
pH	8.12

Microbial Inoculum

A standard inoculum was prepared in order to minimize the effects of population distribution differences in the laboratory experiments. Twenty liters of mixed liquor from a domestic wastewater treatment plant (Bellaire, Texas) was settled and the concentrated sludge mixed with glycerol to approximately 25 vol% glycerol. Ten milliliter aliquots of the resulting suspension were transferred to glass ampules which were "quick frozen" in liquid nitrogen and then stored at -20°C. Growth rate tests on the standard inocula were conducted periodically by inoculating 250 ml Trypticase Soy Broth (12 g/l) with an ampule (10 cm^3) and observing growth indirectly by light transmittance measurements. Results are presented in Table 2-7 and indi-

cate no significant changes over a period of one year. A new inoculum was prepared and utilized for experiments in TFR3 as well as AFR experiments utilizing glucose but not Trypticase Soy Broth. The growth rate of the new inoculum was approximately 25% of the rate observed previously. Differences have been attributed to a change in procedure, although population differences undoubtedly affect the viability to some extent.

The first standard inoculum has been characterized to the extent that some 20 organisms have been isolated and identified as to their colonial morphology and Gram stain. Preserved microscope slides of biofilm samples from various experiments have been prepared and are available for further observation.

One ampule (10 cm^3) was added to the reactors to begin each batch induction period (see below).

Table 2-7

GROWTH RATES OF STANDARD INOCULA IN 250 ml TSB (12 g/l)

Inoculum I	Growth Rate (hrs^{-1})	Mean Generation Time
November 24, 1976	1.38 ± 0.09 (6)*	43 min
December 7, 1976	1.56 ± 0.16 (2)	40 min
January 21, 1977	1.43 ± 0.03 (2)	43 min
November 10, 1977	1.22 ± 0.08 (2)	50 min
Inoculum II		
December 30, 1977	0.31 ± 0.03	200 min

* Number in parentheses refers to number of replicate tests.

Nutrient Composition

The majority of laboratory experiments conducted during this study used a synthetic media consisting of a 1:1 wt/wt glucose and Trypticase Soy Broth (TSB). TSB is an enzymatic hydrolysate (Becton Dickenson & Co., Cockeysville, Md.). A typical quantitative analysis for such hydrolysates is indicated in Table 2-8 . The resulting influent mixture of glucose and TSB was 43.5 wt% carbon, 4 wt% nitrogen and 4.5 wt% phosphorous. Glucose stock solutions were prepared with deionized water and were not autoclaved. TSB stock solutions were prepared with tap water and were autoclaved. The stock solutions were combined with dilution water in the reactor to obtain the desired reactor influent concentration.

A smaller number of experiments (certain TFR3 and AFR experiments) used a defined medium consisting of glucose and mineral salts in the concentrations indicated in Table 2-9.

Table 2-8

TYPICAL QUANTITATIVE ANALYSIS OF ENZYMATIC HYDROLYSATES (4)

Constituent	wt%
Total nitrogen	13.76
Ammonia nitrogen	0.01
Phosphorous	0.72
Organic sulfur	0.57
Inorganic sulfur	0.04
Calcium	0.12
Magnesium	0.08
Iron	0.008
Sodium	2.77
Potassium	0.50
Ash content	8.45
Organic carbon	45.0 (approximately)

Glucose was used as the sole energy source for microbial growth in all reported experiments. Glucose analysis is accurate, precise, and simple, even for very low concentrations. In addition, glucose

has been used in many other reported biofilm studies which can be used for data comparison. Trypticase Soy Broth (TSB), a synthetic media, was used as a carbon source in most of the experiments. TSB contains a diverse number of organic compounds and therefore contributes to the stability of a mixed microbial population during an experiment. Some experiments (primarily TFR3 experiments) were performed with glucose as the sole energy and carbon source.

Biomass yield determinations verify that glucose was the sole energy source in the synthetic media mixture. Two TFR3 experiments were conducted under identical conditions except that one used the synthetic media and another the defined media with influent glucose concentrations being equal in both cases. The yield values calculated through the experiment were 0.25 ± 0.08 and 0.22 ± 0.06 for the synthetic and defined media, respectively. The yield calculation is discussed in the RESULTS section.

Table 2-9

COMPOSITION OF DEFINED MEDIA

Constituents	Reactor Influent Concentration
Glucose	0 - 250 mg/l
$(NH_4)_2SO_4$	0.4 x Glucose Conc.
K_2HPO_4	0.2 x Glucose Conc.
$FeCl_3 \cdot 6H_2O$	0.25 mg/l
$MnSO_4 \cdot H_2O$	0.05 mg/l
$CaCl_2$	3.8 mg/l
$CuSO_4 \cdot 5H_2O$	0.03 mg/l
$NaMoO_4 \cdot 2H_2O$	0.06 mg/l
$ZnCl_2$	0.103 mg/l
$CoCl_2 \cdot 6H_2O$	0.10 mg/l
K_2HPO_4	4.44 mg/l
$MgSO_4 \cdot 7H_2O$	4.0 mg/l

EXPERIMENTAL PROTOCOL

Cleaning Procedures

Standard cleaning procedures were established to ensure relatively uniform surface conditions for initial attachment and growth. The details of the cleaning procedures can be found in Appendix A. Brush and acid washing of the entire system between each experiment was assumed to result in bacteria-free surfaces at the initiation of each test.

Batch Induction Period

The time necessary for primary attachment of microorganisms, i.e., the induction period, can be as long as two weeks. The length of the induction period is, in part, dependent on the characteristics of the attachment surface (e.g., composition, roughness). Consequently, a study of the induction period was beyond the scope of this project. As a result, an initial period of batch operation was chosen to minimize the time for initial attachment. The details of this procedure are presented in Appendix B.

Oxidizing Biocide Tests

These tests were only conducted in TFR1 (although the fermenter was by-passed) and AFR. After the film growth period, the reactor was flushed with activated carbon-treated tap water for approximately thirty minutes and then biofilm thickness was determined. Experimental conditions (e.g., volumetric flow rate) were adjusted and pressure drop or torque recorded. A predetermined amount of sodium hypochlorite or hydrogen peroxide was injected into the reactor and oxidant decay was monitored. After treatment, biofilm thickness was determined again.

The exposure history of the biofilm to the oxidant compares favorably to chlorination in a cooling tower which is "blocked in," i.e., there is no flow out. The major purpose of the experimental procedure however, was not simulation but an attempt to obtain fundamental rate data for the reaction between the oxidant and the biofilm.

Ozonation tests were conducted only in TFR1. After flushing with activated carbon-treated water, the recycle loop was isolated from the fermenter. Ozone (Model No. T-408, Welsbach Corp., Phildelphia, Pa.) was introduced into the fermenter until a predetermined concentration was attained. The ozone supply was then switched off, the fermenter rejoined to the recycle loop, and ozone decay was monitored. Biofilm thickness and pressure drop were recorded before and after ozonation.

Chloramine tests were conducted in TFR1 by injecting 10 ml $(NH_4)_2SO_4$ (150 mg/l) into the recycle loop followed by 0.7 ml NaOCl (53.5 g/l). The resulting solution contained a 20.1 wt/wt ratio of ammonium ion to chlorine required for a mixed chloramine solution (5).

Control experiments were conducted to determine oxidant decay without biofilm present. The reactors were cleaned with acid (5N HCl), base (5N NaOH), and sodium hypochlorite (10 g/l) before being flushed with carbon-treated tap water. Oxidants were then introduced and oxidant decay monitored.

Stoichiometric Chlorine Demand of Biofilm

Biofilm developed in TFR1 system was scraped from a sample tube into 150 ml demineralized water and blended for 6 seconds. The blended suspension was placed in the sample container of an amperometric titrator, diluted to 200 ml, and buffered at pH 7.0. Hypochlorite titrant (535 mg/l) was slowly added until no further decrease in diffusion current was observed and excess chlorine was back-titrated with phenylarsene oxide. The difference between initial chlorine concentration and phenylarsene oxide consumed is the hypochlorite demand of the biofilm.

Biofilm thickness was determined on the sample tube before its transfer to the demineralized water. Biofilm thickness was also determined on another sample tube withdrawn at the same time. A dry weight was also determined from the second sample tube.

Analytical Procedures

Analytical procedures which required further development for this study were those involving biofilm volume, biofilm thickness and biofilm mass. All other analytical procedures were relatively routine and are presented in Appendix C.

Biofilm Volume. Small sample tubes (1.27 cm ID, 5 cm long) were inserted as an integral part of the tubular reactors. The sample tubes were inserted end-to-end in an acrylic plastic test section 1.9 cm ID and 76 cm long (Figure 2-11). The test section was connected to the TFR1 recycle loop with pipe unions to provide easy access to the sample tubes. At designated intervals, a sample tube was removed from the TFR and a clean sample tube inserted in its place, and the volumetric displacement of the biofilm was determined using the apparatus pictured in Figure 2-12. The fouled sample tube is drained for 2.5 minutes before being inserted in the displacement cell. There is a significant effect of drain time on the biofilm volume determination (see Appendix D). The displacement cell was filled with an aqueous surfactant solution (0.3% vol/vol turgitol). Initial liquid level (i.e., without the sample tube immersed) was measured by lowering the conductive probe, by means of micromanipulator, until contact was made with the water surface, indicated by deflection of the ammeter or observed visually. The ammeter was in series with the cell and a 1.5v power source. A 5 x 1.27 cm (ID) fouled sample tube was then immersed in the displacement cell, and the new liquid level (and hence, displacement) due to fouled sample tube determined. The sample tube was then cleaned, dried and again immersed in the cell. Alternatively, the clean, dry tube can be weighed since density of the glass tube does not change (see Appendix E). The difference between the displacements of the fouled and clean sample tubes was the film volume. Wet film thickness was determined by dividing film volume by the surface area of the sample tube.

This method was calibrated by measuring displacement of copper wire segments of known mass and, therefore, known volume. Precision, based on repeated volume displacement measurements with a clean tube,

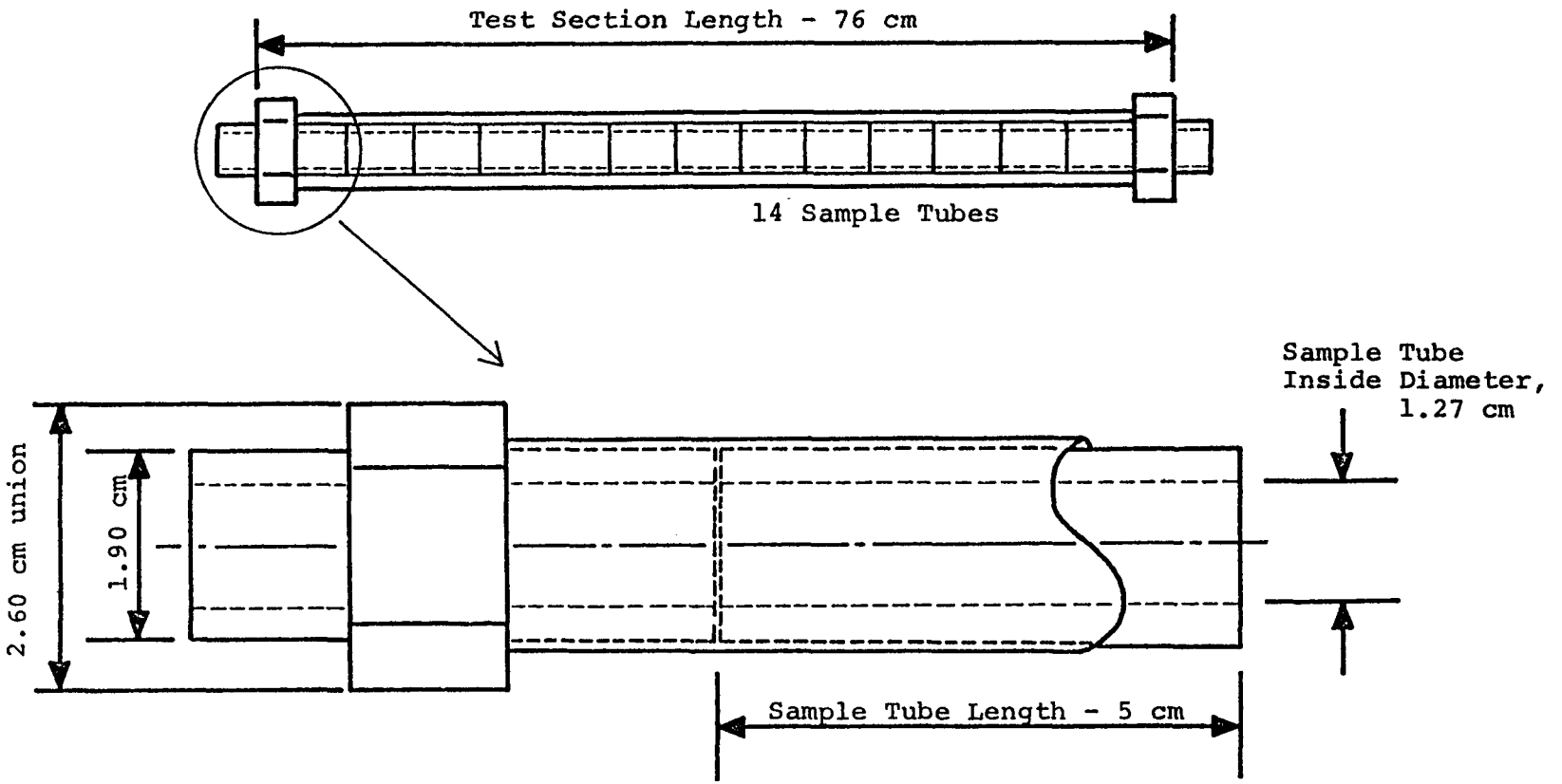

Figure 2-11. Test section and enclosed sample tubes for biofilm thickness and mass measurements.

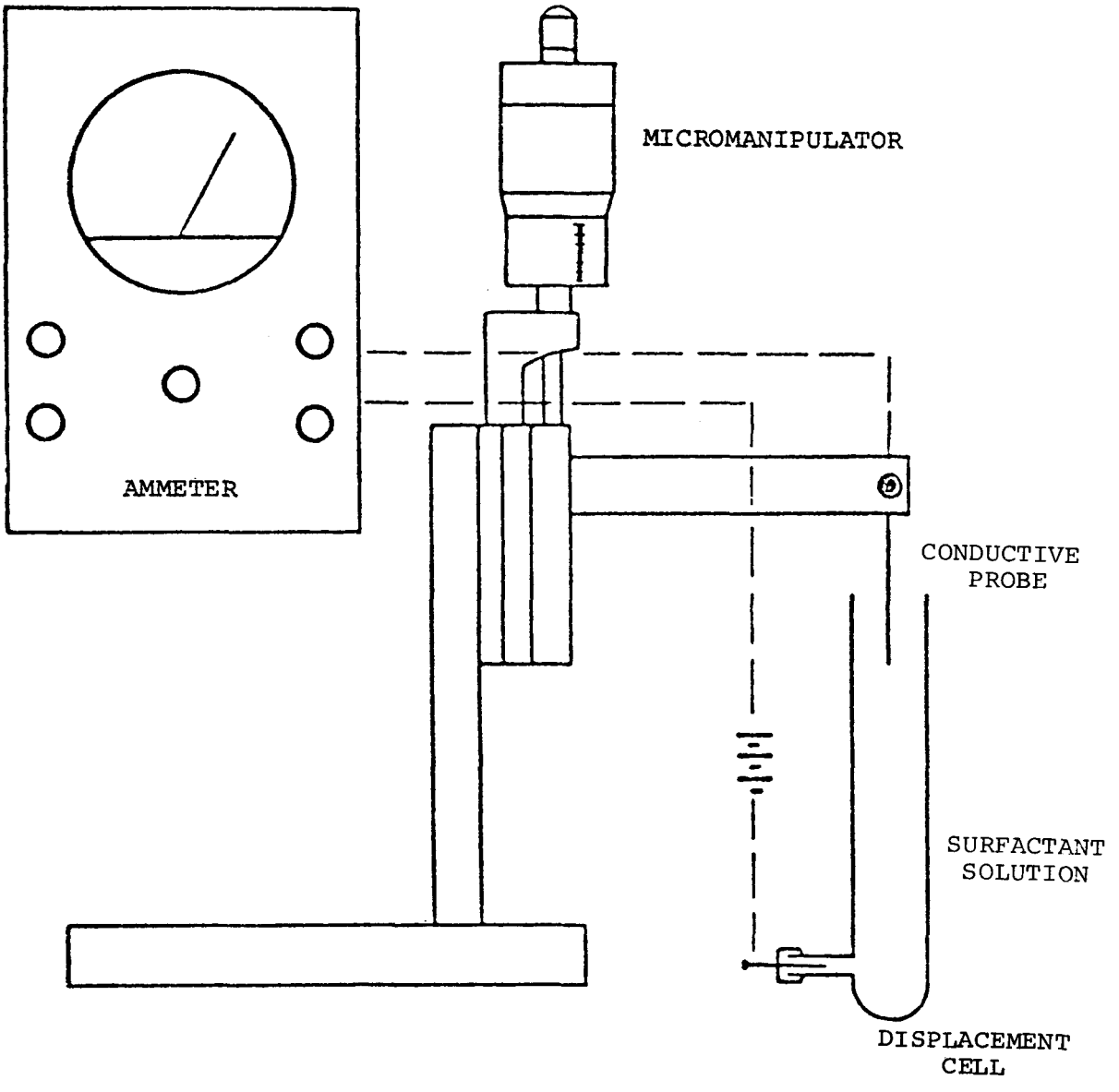

Figure 2-12. Experimental apparatus for measuring film volume.

was ± 9μm. Standard deviation based on duplicate measurements was initially 22μm and included variation in film thickness from one sample tube to another. Standard deviation decreased to 9μm after approximately six months operation (see Appendix F). Average inside surface area of test sections was 20.0 cm^2 with a range of 1.2%.

Biofilm Thickness. This technique was adapted from other work (3) and requires film growth on a transparent surface. In the case of the AFR, microbial film develops on a thin acrylic plastic slide which forms an integral part of the AFR reactor wall. The slide is withdrawn from the reactor and placed on a microscope stage. The 10X objective is lowered until the film surface is in focus and the fine adjustment dial setting is recorded. The objective is then lowered further until the inert plastic growth surface is in focus (Figure 2-13). The difference in fine adjustment settings is compared with a calibration curve (see Appendix G) and the thickness obtained. Sample standard deviation of measurement was 11.9 initially but was reduced to 9μm (see Appendix H). The variation included any irregularities in the film surface.

Biofilm Mass. Sample tube sections are an integral part of TFR1, TFR2,3 and FFR systems. At regular intervals, a sample tube is removed, dried (60°C) for three hours, and weighed. The tube is then cleaned, dried and weighed again. The difference in the two measurements is the dry film mass. The length and diameter of the tubes is known so an areal mass density can be determined. If film thickness or film volume has been measured, volumetric film density can be determined.

After the last film thickness measurement in an AFR experiment the removable slide is dried (60°C) and weighed. The slide is then cleaned, dried and weighed again. The difference in the two measurements is the dry film mass. Areal and volumetric film density can then be calculated.

The volumetric film density has units of dry mass per unit wet volume. The areal film density has units of dry mass per unit area of growth surface.

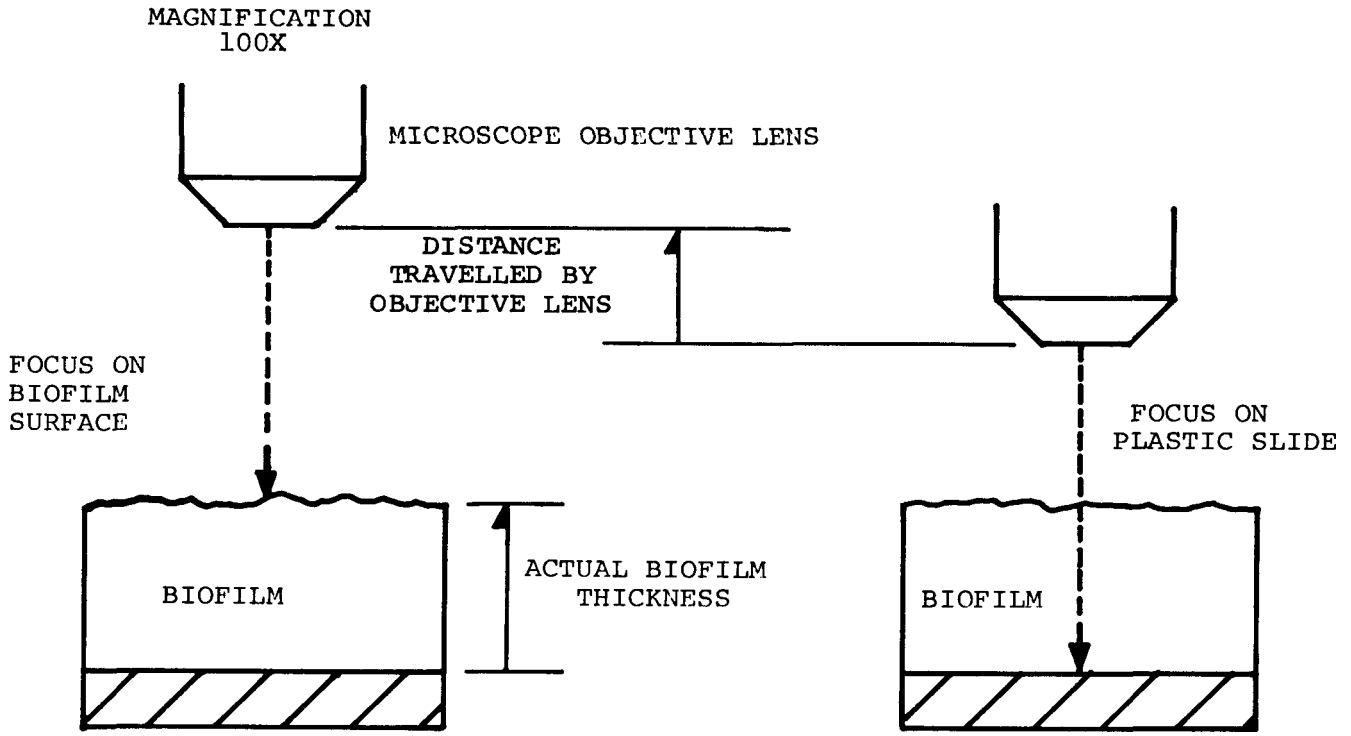

Figure 2-13. Biofilm thickness measurement by optical microscope technique.

Section 3

RESULTS

Data summaries for TFR1,* TFR2, TFR3, TFR4 and AFR are contained in Appendixes I - L. This section will describe the results in general and illustrate some important trends. The relevance of the data to biofilm development and biofouling, especially in operating power plants, and a discussion of all results appear in Section 4.

BIOFILM PROPERTIES

Observation and/or measurement of several biofilm properties were conducted primarily in the tubular fouling reactors. These properties include the following:

1. chemical composition
2. dry mass density
3. water content
4. rheological properties
5. bacterial number density
6. biofilm morphology
7. thermal conductivity

Chemical Composition

The chemical composition of biofilm developed in TFR1 is compared to field data (from an actual power plant condenser) and other relevant experimental results in Table 3-1. The data suggest the following:

1. The composition of the biofilm obtained from the condenser is low in carbon. This may be the result of a high inorganic or ash content.

*Notation and symbols are defined in the Notation Section

2. The carbon to nitrogen ratio (C/N) in the condenser biofilm ranges from 2-27 and suggests a nitrogen limitation since C/N<10 is characteristic of carbon-limited growth. The other data in Table 3-1 are from carbon-limited systems.

Table 3-1

CHEMICAL COMPOSITION OF BIOFILMS

	% of dry weight					
	C	N	P	Fixed Solids	C/N	C/P
Biofilm-this study	19.0	9.2	1.8	20	2.1	10.5
Biofilm-power plant condenser (6)	6.4-13.8	0.51-3.0	--	--	2-27	--
Biofilm-laboratory AFR (2)	42.8	10.0	--	--	4.3	--
E. coli (7)	50.0	14.0	3.	--	3.6	16.7
TFR feed composition (synthetic medium consisting of glucose and Trypticase Soy Broth in a 1:1 wt/wt)	43.5	4.0	4.5	10*	10.9	9.7

*Approximate value calculated from analysis of Trypticase Soy Broth and dilution water analysis.

Inorganic composition of biofilms varies considerably and undoubtedly affects their physical and biological properties. Inorganic particulates embedded in the biofilm will affect the composition and density. Calcium, magnesium and iron may affect the extent of cross-linking of polymers within the biofilm. Table 3-2 presents literature data pertaining to the inorganic composition of fouling biofilms (8,9). Although biofilm in this research was approximately 80% volatile solids (as % dry weight), the effluent suspended solids ranged from 88 - 100% volatile solids. This suggests that the sloughed solids are newly-formed cells or active mass from the biofilm.

Table 3-2

WATER CONTENT AND INORGANIC COMPOSITION OF FOULING BIOFILM AND TRICKLING FILTER BIOFILMS

	Range Reported in References (8) and (9) wt%	This Study wt%
Water	85.6 - 95.4	96
Volatile Solids	1.9 - 3.2	3.2
Fixed Solids	1.4 - 11.7	0.8
	as % of fixed solids	
Si	85.6 - 95.4	
Fe	1.9 - 3.2	
Al	3.9 - 7.5	
Ca	1.0 - 5.6	
Mg	2.5 - 3.2	
Mn	4.9 - 59.5	

A visible inorganic film formed on the tubular reactor surface after an extended period of experimentation. The inorganic film in TFR3 was primarily iron but contained significant quantities of calcium, copper and zinc (see Appendix M). Corrosion in the pump was the probable source of iron although the water supply was a possible contributing factor. The flow meter was bronze and could account for the copper and zinc. The source of calcium is not known.

Biofilm Dry Mass Density

Biofilm dry mass density (ρ_{Th}) reflects the attached dry mass per unit of wet biofilm volume. Consequently, ρ_{Th} is directly related to the biofilm thickness or volume measurement. Results in the tubular fouling reactors indicate that ρ_{Th} is dependent on fluid shear

stress at the wall (τ_w) and glucose loading rate on the biofilm.

During the TFR1 and TFR2 experiments, volumetric flow was held constant and pressure drop and shear stress at the wall increased as the biofilm developed. Figure 3-1 illustrates the effect of the initial shear stress (i.e., shear stress in the clean tube) for a given experiment on ρ_{Th}. Glucose loading rate on the biofilm in these experiments varied from 1.1-23 mg/m^2 min and bulk temperature varied from 28-40^{o}C. Increasing wall shear stress resulted in high ρ_{Th}.

In the TFR3, pressure drop and therefore, shear stress at the wall, were maintained constant during a given experiment. The effect of shear stress on ρ_{Th} in nine TFR3 experiments is presented in Figure 3-2. Glucose loading rate on the biofilm in these experiments varied from 1.57-22.8 mg/m^2-min. Temperature varied from 30-35^{o}C. Again, ρ_{Th} was directly proportional to the wall shear stress maintained during the experiment.

Glucose loading rate also affected ρ_{Th}. The results from a series of TFR3 experiments conducted with a wall shear stress of 7.9 N/m^2 are presented in Figure 3-3. An increased loading rate resulted in higher ρ_{Th}.

Figures 3-1 to 3-3 indicate that biofilm density is a function of glucose loading rate and fluid shear stress at the wall.

Water Content

Biofilm water content is dependent, to some extent, on the measurement technique. Biofilm from TFR3-9 was 96 wt% water which is consistent with values obtained by other researchers (Table 3-2).

Rheological Properties

Rheological measurements conducted with a Weissenburg Rheogoniometer on an *in situ* biofilm (TFR1-10) indicate that the biofilm is viscoelastic.

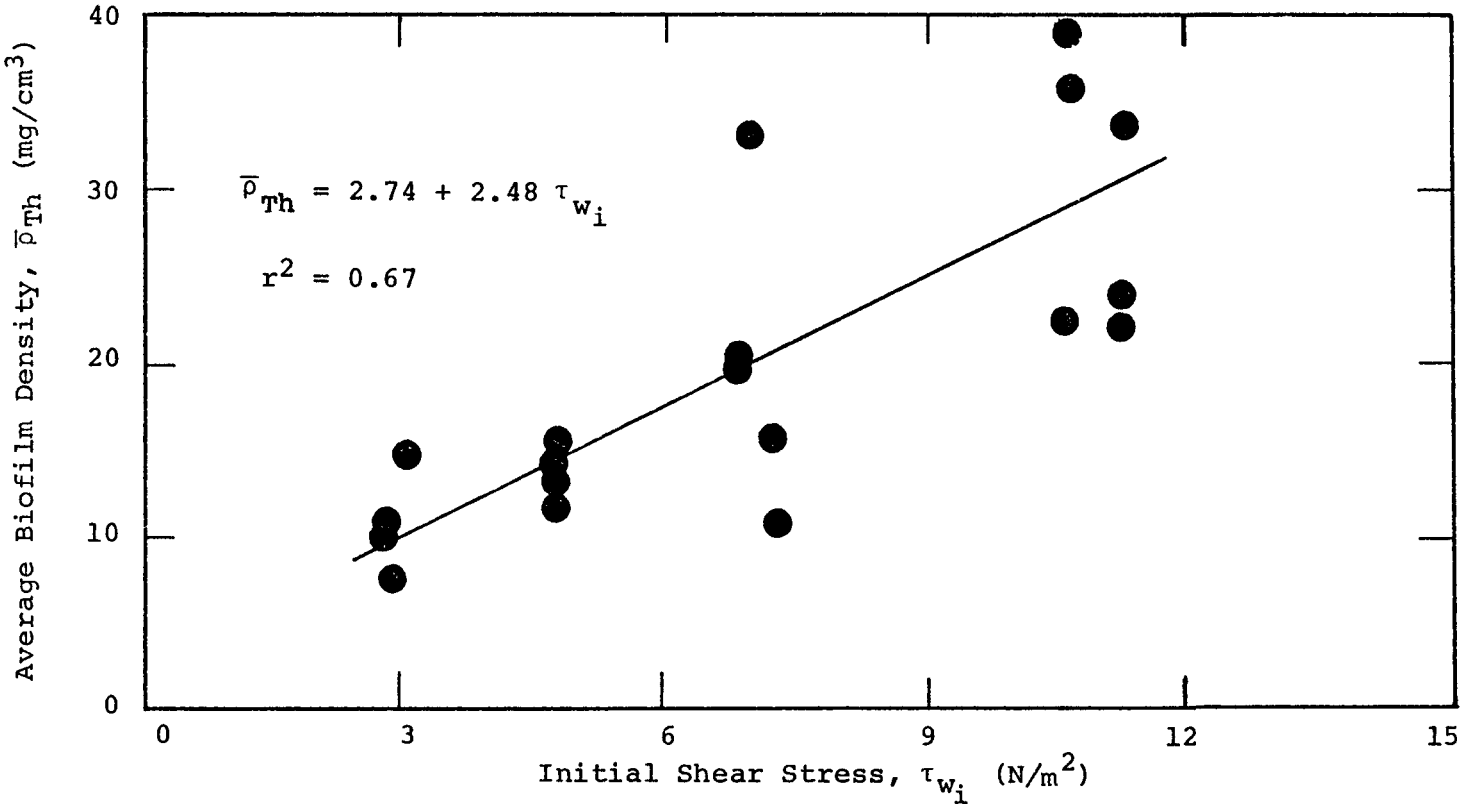

Figure 3-1. Change in biofilm density with initial fluid shear stress for constant flow experiments (TFR1 and TFR2). Glucose loading rate is 23 mg/m^2-min or less.

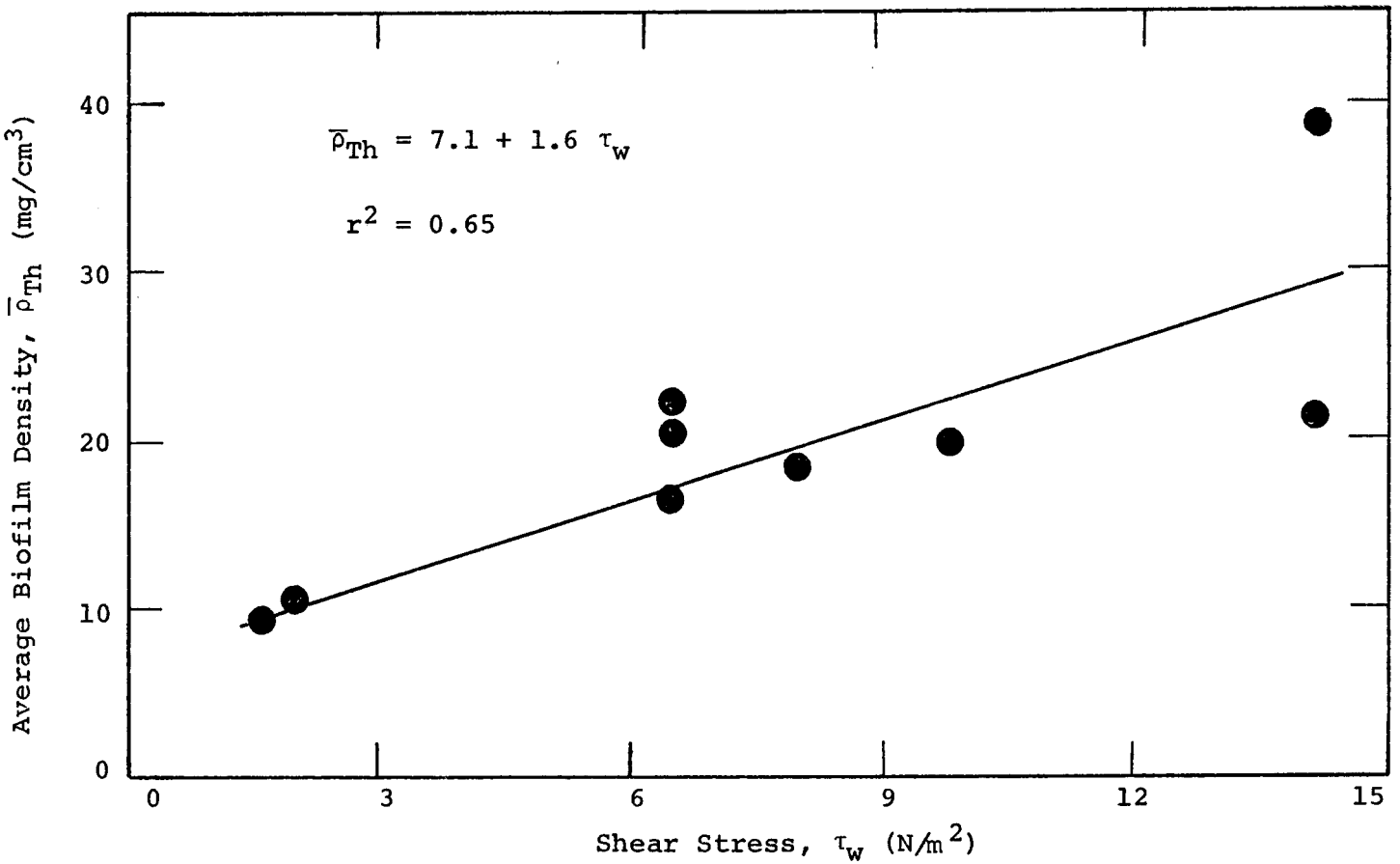

Figure 3-2. Change in biofilm density with fluid shear stress for constant pressure drop experiments (TFR3). Glucose loading rate is 23 mg/m^2-min or less.

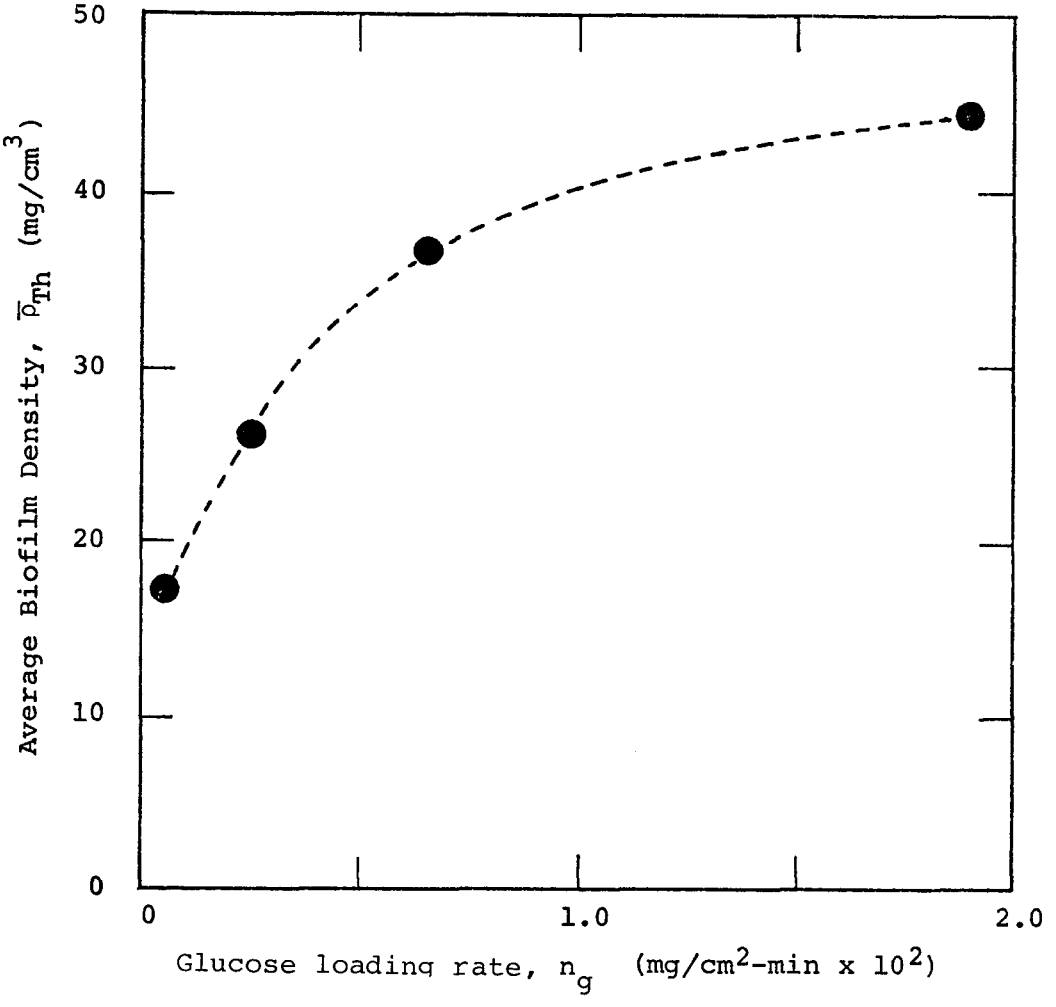

Figure 3-3. Change in biofilm density with glucose loading rate for constant pressure drop experiments (TFR3) at a fluid shear stress of 7.9 N/m^2.

The quantitative resuls of the rheological tests on biofilm are compared with those on coagulated fibrinogen (a cross-linked protein gel) in Table 3-3. Elastic and viscous moduli for the biofilm at various excitation frequencies are presented in Appendix N.

Table 3-3

A COMPARISON OF THE VISCOELASTIC PROPERTIES OF BIOFILM AND COAGULATED FIBRINOGEN. MEASUREMENTS WERE CONDUCTED ON A WEISSENBURG RHEOGONIOMETER AT AN EXCITATION FREQUENCY OF 6 Hz.

Material	Elastic (Storage) Modulus, G' (N/m^2)	Viscous (Loss) Modulus, G" (N/m^2)
Biofilm in TFR1-10 T_b = 40°C τ_w = 3.3 N/m^2 n_s = 6.2 mg/m^2-min	59.5	118
Coagulated Fibrinogen (ID) (230 mg/100 ml plasma) (10)	85	7

Biofilm Cell Number Density

Estimation of the number of viable cells per unit biofilm volume consistently resulted in 10^6-10^8 cells per cm^3 of biofilm despite varying experimental conditions. Number density in the bulk fluid was typically 10^4-10^6 cells per cm^3 (see Appendix C for methods).

Biofilm Morphology

The first visible (by the naked eye) sign of biofilm development was usually small "colonies" of cells distributed randomly on the attachment surface. The "colonies" exhibited an elongated shape in the direction of flow. As the experiment progressed, the "colonies" grew together to form a relatively uniform biofilm.

Most of the biofilms observed in the laboratory were characterized by an abundance of filaments. It is not clear whether this was due to natural selection of filamentous organisms or whether the dominant organisms grew in a filamentous form to gain an ecological advantage. In the AFR, this was especially true at low glucose loading rates. Filament length increased with time during a given experiment, sometimes reaching a length of 0.25 cm.

Thermal Conductivity

The thermal conductivity of the biofilms has been determined indirectly as described in the sub-section EFFECT OF BIOFILM DEVELOPMENT ON HEAT TRANSFER. Results indicate that the thermal conductivity is equal to that in water within experimental error.

Table 3-4

THERMAL CONDUCTIVITY OF BIOFILM

Experiment #	Biofilm Thermal Conductivity (watt/m-^{o}C)	Bulk Temperature (^{o}C)
TFR4-6	0.68 ± 0.27 (4)	28.3 ± 0.3
TFR4-8	0.71 ± 0.39 (5)	26.7 ± 0.3
TFR4-9	0.57 ± 0.10 (5)	28.3 ± 0.3
Grand Mean:	0.65 ± 0.27 (4)	
Water	0.61	26.7
Water	0.62	28.3

DEVELOPMENT OF BIOFILMS

One of the major objectives of this study was to develop a better understanding of fouling biofilm development with particular emphasis on the effects of fluid shear stress at the attachment surface, bulk water temperature, wall surface temperature, and limiting nutrient concentration. Mathematical analysis of the experimental reactor systems, based on macroscopic material balances, provided the basis for the kinetic analysis. A microscopic model for biofilm development and its effect on heat transfer in a circular tube has been described elsewhere (11).

Experimental Measurements

The following measurements were necessary during an experiment to complete a material balance across the reactors:

1. influent and effluent glucose
2. biofilm thickness and/or biofilm mass
3. effluent suspended solids

Influent and effluent glucose concentrations determined the overall reaction rate in the reactor (Figure 3-4). Glucose was utilized for biomass production and resulted in an increase in attached (Figure 3-5) and suspended biomass (Figure 3-6).

Model for Biofilm Development in Laboratory Reactor Systems

Schematic diagrams of the laboratory reactor systems are presented in Figure 3-7. The general material balance equations for limiting reactor nutrient and suspended biomass are the same for all reactor systems. For glucose, which was the limiting nutrient in the reactors, the following equation results:

$$V \cdot \frac{dS}{dt} = F \cdot (S_i - S) - R_v \qquad (3\text{-}1)$$

where F = volumetric flow rate (L^3/t)

R_v = glucose removal rate (m/t)

S = reactor glucose concentration (m/L^3)

S_i = inlet glucose concentration (m/L^3)

t = time (t)

V = reactor volume (L^3)

The glucose removal can be attributed to the attached and suspended biomass in the system. Therefore, Eq. 3-1 becomes

$$V \cdot \frac{dS}{dt} = F \cdot (S_i - S) - (R''A + R' \cdot X \cdot V) \qquad (3\text{-}2)$$

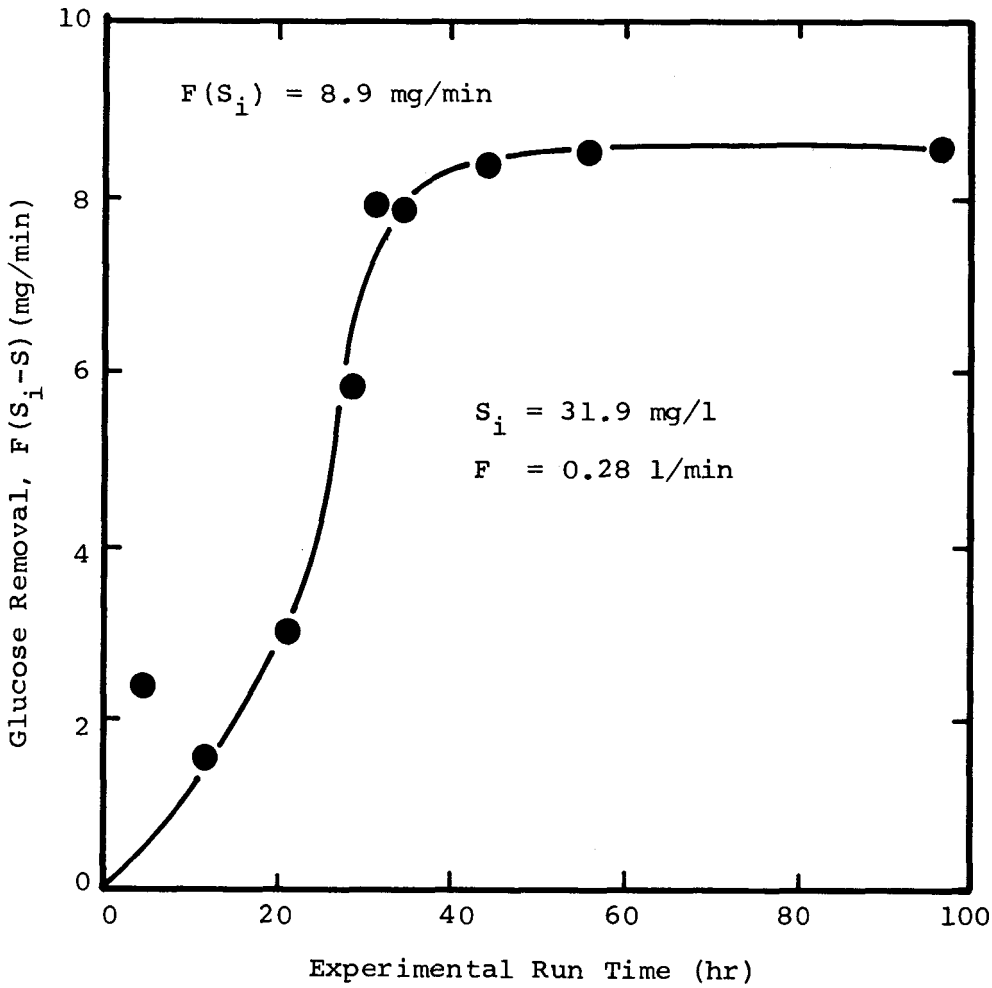

Figure 3-4. Glucose removal during experiment TFR3-5.

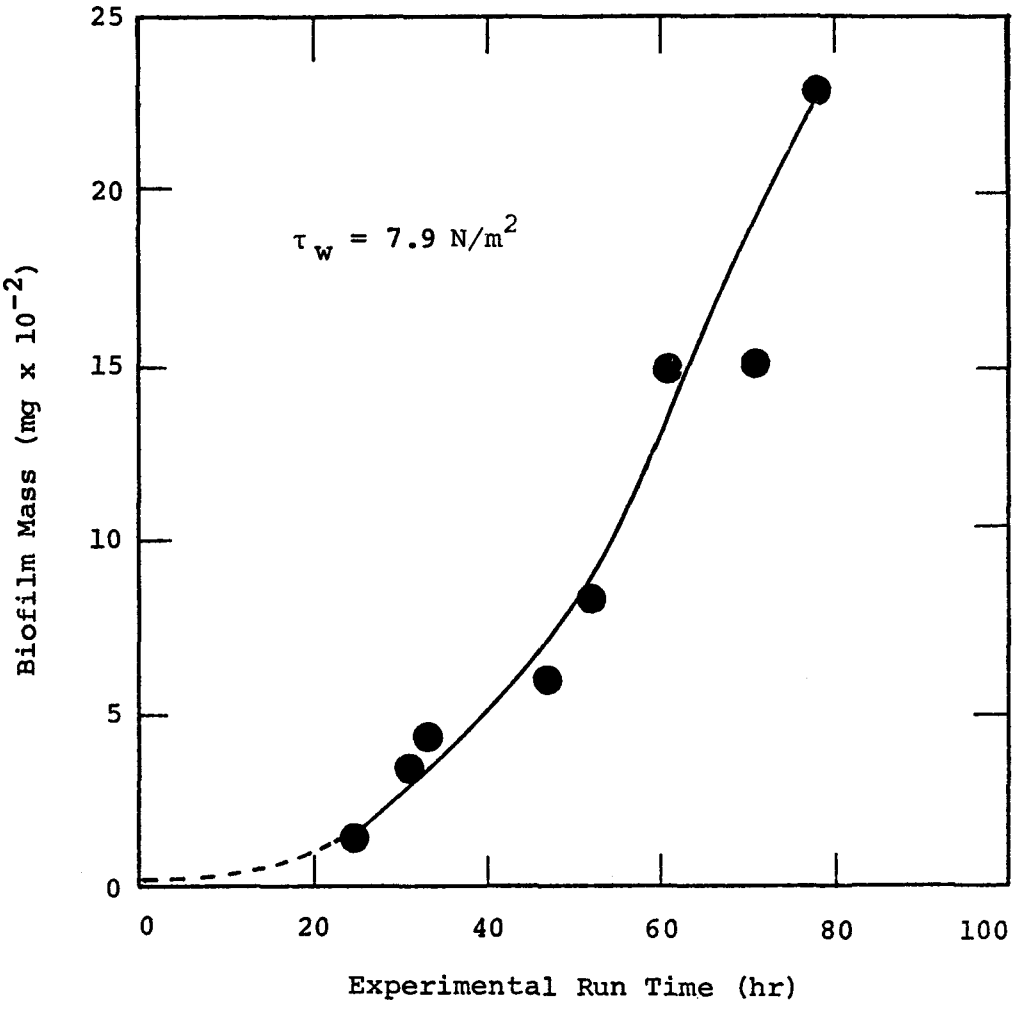

Figure 3-5. Change in biofilm mass with time for a constant pressure drop experiment (TFR3-7).

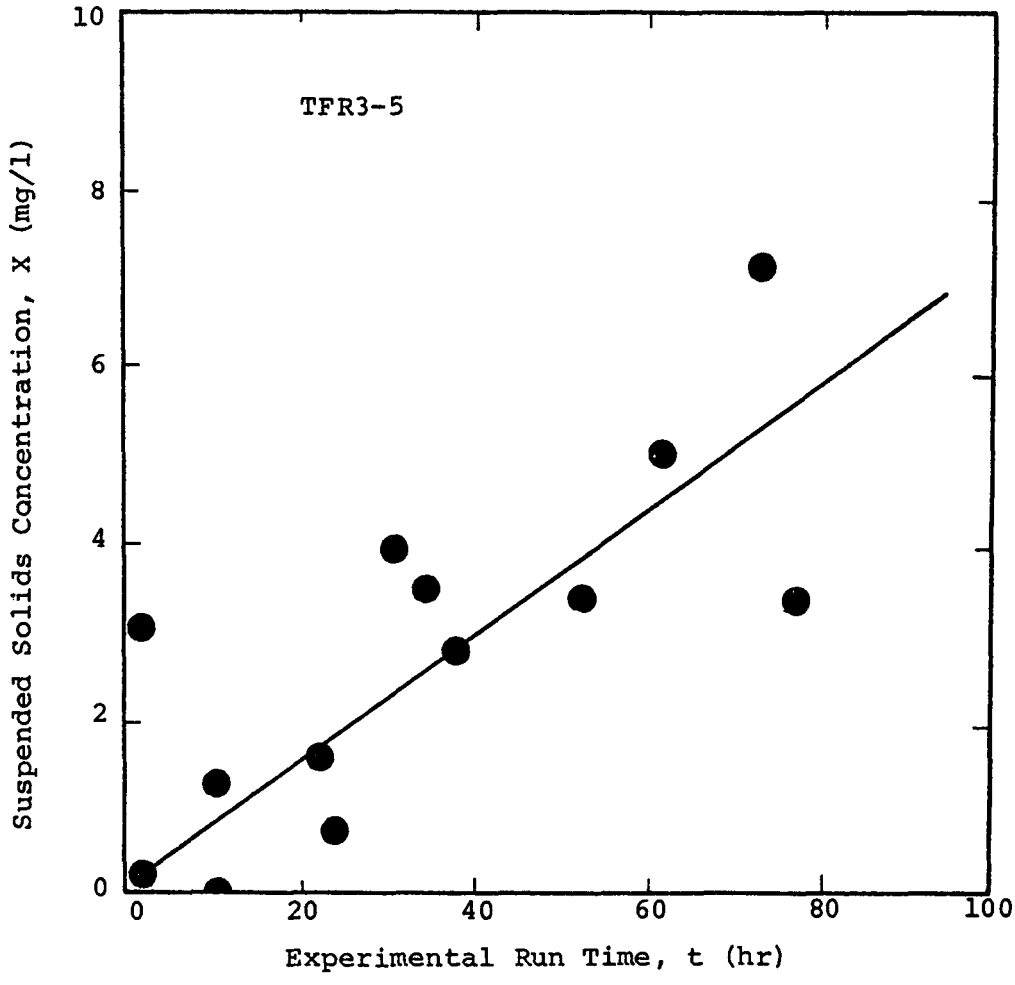

Figure 3-6. Suspended solids concentration as a function of time.

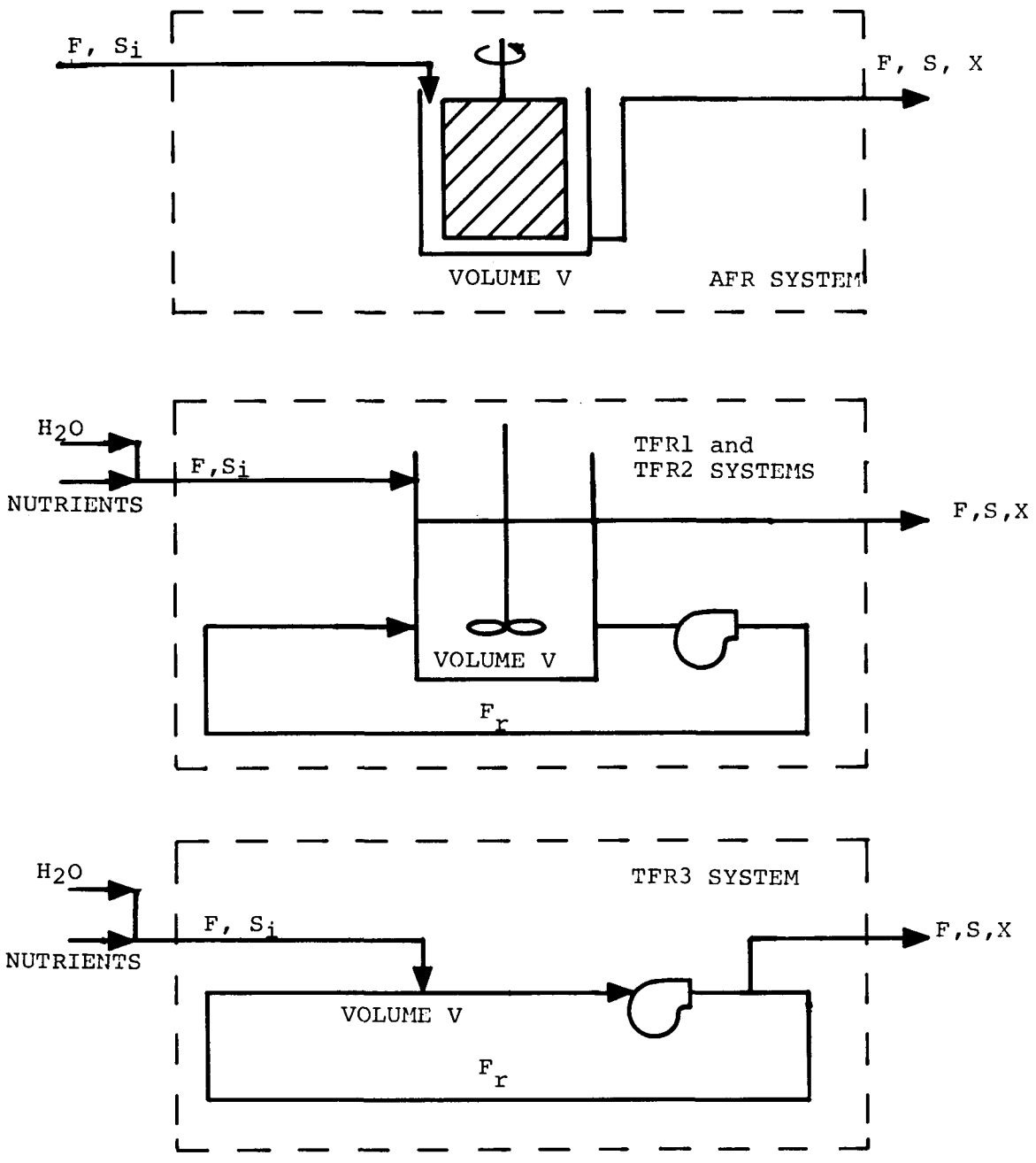

Figure 3-7. Schematic representation of the experimental reactor system used in this study with the boundaries for the system material balances indicated by the dotted lines.

where A = wetted surface area (L^2)

R' = glucose removal rate per unit suspended biomass ($m/m \cdot t$)

R" = glucose removal rate per unit wetted surface area ($m/L^2 \cdot t$)

X = suspended biomass concentration (m/L^3)

In all experimental reactors used in this research, mean hydraulic residence time (θ) was 15 min or less. Consequently, glucose removal due to suspended biomass was assumed negligible. Therefore,

$$V \cdot \frac{dS}{dt} = F \cdot (S_i - S) - R'' \cdot A \tag{3-3}$$

In the experimental reactors (see Figure 3-8), $V \cdot \frac{dS}{dt} << F(S_i - S)$ so

$$F(S_i - S) = R''A \tag{3-4}$$

The general form for the stoichiometric equation describing the microbial reaction is as follows:

$$\underset{\left(\begin{matrix}\text{energy}\\ \text{source}\end{matrix}\right)}{\text{glucose}} + \underset{\left(\begin{matrix}\text{carbon, nitrogen and}\\ \text{phosphorous source}\end{matrix}\right)}{\text{Trypticase Soy Broth}} \longrightarrow \underset{\left(\begin{matrix}\text{synthesis}\\ \text{products}\end{matrix}\right)}{\text{biomass}} + \underset{\left(\begin{matrix}\text{respiration}\\ \text{products}\end{matrix}\right)}{CO_2 + H_2O} \tag{3-5}$$

A significant portion of the glucose removed provides chemical energy for synthesis of biomass which consists of attached and suspended material. A net yield (Y) can be defined based on Eq. 3-3 as follows:

$$Y = \frac{\text{biomass production rate}}{\text{glucose removal rate}} = \frac{r}{R'' \cdot A} \tag{3-6}$$

where r = rate of production of biomass (m/t).

Because mean hydraulic retention time (θ) was small, biomass production in suspension was presumed negligible. Therefore, the suspended biomass was a result of sloughing from the biofilm. In the reactor at any instant,

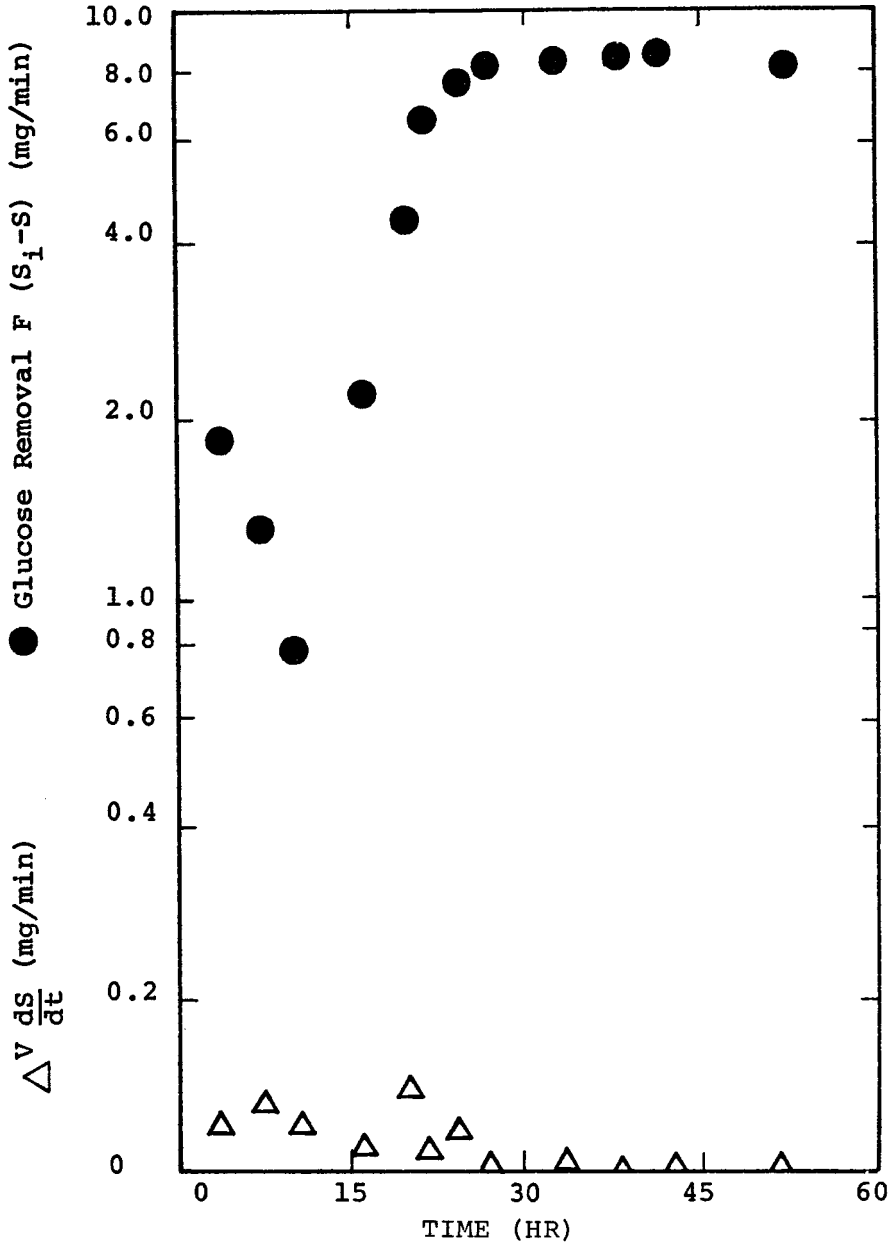

Figure 3-8. Glucose removal and the rate change in glucose mass as a function of time.

$$m_{tot} = X \cdot V + \rho_{Th} \cdot A \cdot Th \qquad (3\text{-}7)$$

$$\begin{bmatrix}\text{total}\\ \text{biomass}\end{bmatrix} = \begin{bmatrix}\text{suspended}\\ \text{biomass}\end{bmatrix} + \begin{bmatrix}\text{attached}\\ \text{biomass}\end{bmatrix}$$

where m_{tot} = total biomass in the reactor (m)

ρ_{Th} = biofilm dry mass density (m/L^3)

Th = biofilm thickness (L)

$\rho_{Th} \cdot A \cdot Th$ = biofilm mass (m)

The distribution of m_{tot} for a typical experiment in TFR3 is presented in Figure 3-9. Biomass production rate can be expressed as follows:

$$r = r_X + r_{Th} \qquad (3\text{-}8)$$

where r = rate of production of biomass (m/t)

r_X = rate of production of suspended biomass (m/t)

r_{Th} = rate of production of attached biofilm (m/t)

A material balance across the reactor for X results in the following:

$$V \cdot \frac{dX}{dt} = F \cdot (X_i - X) + r - r_{Th} \qquad (3\text{-}9)$$

Substituting from Eq. 3-6 and presuming $X_i = 0$,

$$V \cdot \frac{dX}{dt} = - F \cdot X + Y \cdot R'' \cdot A - r_{Th} \qquad (3\text{-}10)$$

Yield (Y) can then be determined for any time interval during an experiment by the following relationship:

$$Y = \left[V \cdot \frac{dX}{dt} + (F \cdot X) + r_{Th} \right] / R'' \cdot A \qquad (3\text{-}11)$$

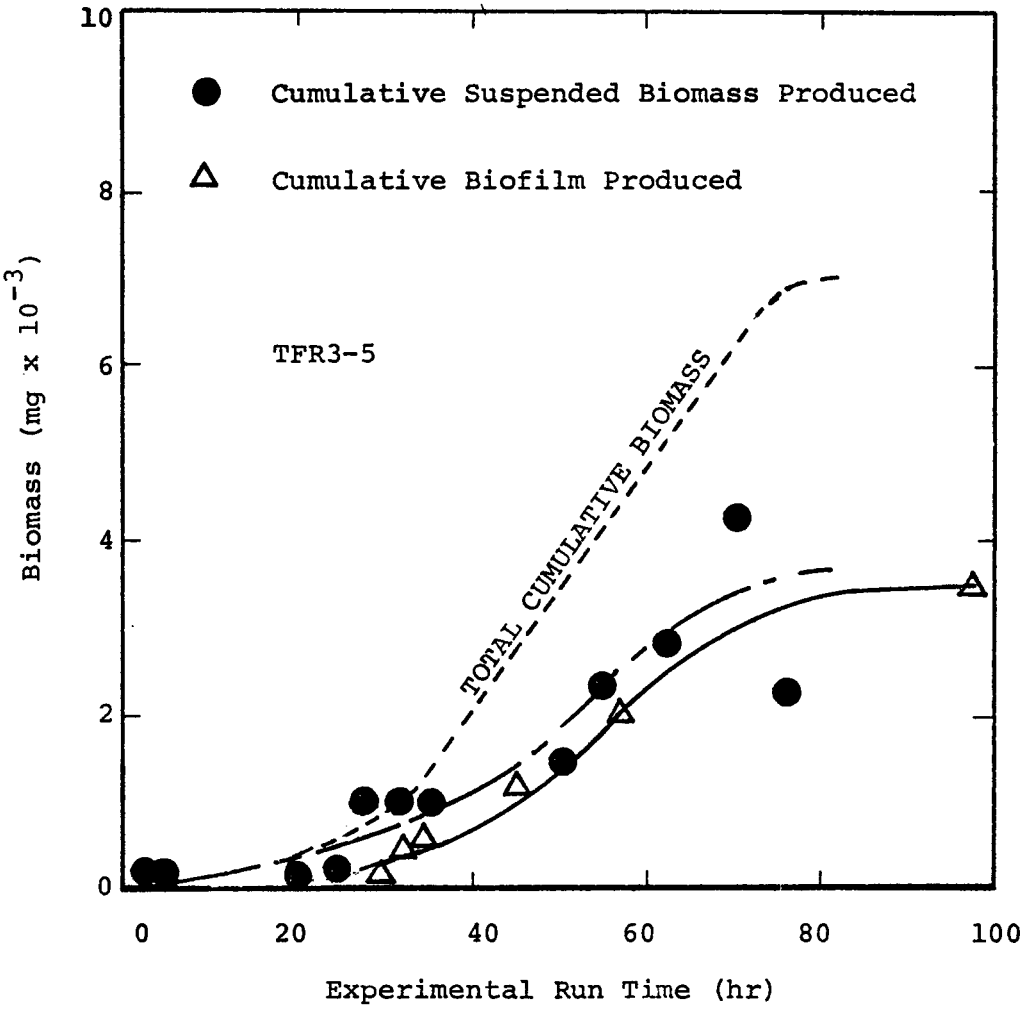

Figure 3-9. Cumulative total biomass production depicted as the sum of cumulative biofilm produced and cumulative suspended biomass produced.

In the experiments reported here, $V \cdot dX/dt$ is very small so that

$$Y = (F \cdot X + r_{Th})/R'' \cdot A \qquad (3\text{-}12)$$

At steady state, $r_{Th} = 0$ and $dX/dt = 0$ so that

$$Y = F \cdot X \,/\, R'' \cdot A \quad \text{(steady state)} \qquad (3\text{-}13)$$

Values for Y from TFR3, AFR and other investigators are presented in Table 3-5. Results from TFR3 and AFR are calculated from Eq. 3-11 or Eq. 3-12 at various time intervals throughout each experiment reported. Generally, yield was between 0.20 and 0.40. Results from TFR3-4 and TFR3-5 indicate that there is no significant difference in yield whether glucose plus mineral salts or glucose plus Trypticase Soy Broth is used.

Table 3-5

BIOMASS YIELDS IN BIOFILM PROCESSES

Source	Yield	Glucose Removal Rate, R" ($mg/m^2 \cdot min$)	Nutrient
TFR3-4	0.25 ± 0.08	3.8	glucose + TSB
TFR3-5	0.22 ± 0.06	18.3	glucose
AFR-5	0.32 ± 0.05 (5)	1.71	glucose + TSB
AFR-4	0.21 ± 0.07 (7)	0.71	glucose + TSB
AFR-6	0.27 ± 0.05 (6)	1.77	glucose + TSB
AFR-7	0.39 ± 0.14 (5)	2.23	glucose + TSB
AFR *	0.26 ± 0.04	30-86	glucose

* Kornegay and Andrews (2)

Sloughing rate (R_s) can be defined from Eq. 3-10 as follows:

$$r_X = Y \cdot R'' \cdot A - r_{Th} = V \cdot \frac{dX}{dt} + F \cdot X \qquad (3\text{-}14)$$

where r_X = sloughing rate (m/t).

For experiments reported here, $dX/dt << F \cdot X$ so that

$$r_X = Y \cdot R'' \cdot A - r_{Th} = F \cdot X \qquad (3\text{-}15)$$

r_x increases with increasing biofilm thickness (see Figure 3-10) and with time during the course of an experiment (see Figure 3-6).

Rate of Biofilm Development

Results from other biofilm research studies (2,12) indicate that glucose removal rate increases with increasing biofilm thickness up to some critical thickness, after which removal rate is constant. Assuming oxygen is present throughout the biofilm, the critical thickness represents the portion of the attached biomass actively removing glucose and represents the biofilm depth to which glucose penetrates before being completely reacted. Then,

$$R'' = R''_m \cdot \rho_{Th} \cdot Th \quad \text{for } Th < Th_A \qquad (3\text{-}16)$$

and $$R'' = R''_m \cdot \rho_{Th} \cdot Th_A \quad \text{for } Th \geq Th_A \qquad (3\text{-}17)$$

where

R''_m = glucose removal rate per unit mass in the active portion of the biofilm (m/L^2-m-t)

Th_A = active biofilm thickness (L)

Figure 3-11 illustrates how active biofilm thickness was determined. Results from the tubular and annular fouling reactors are consistent with previous research (2,12) and indicate that

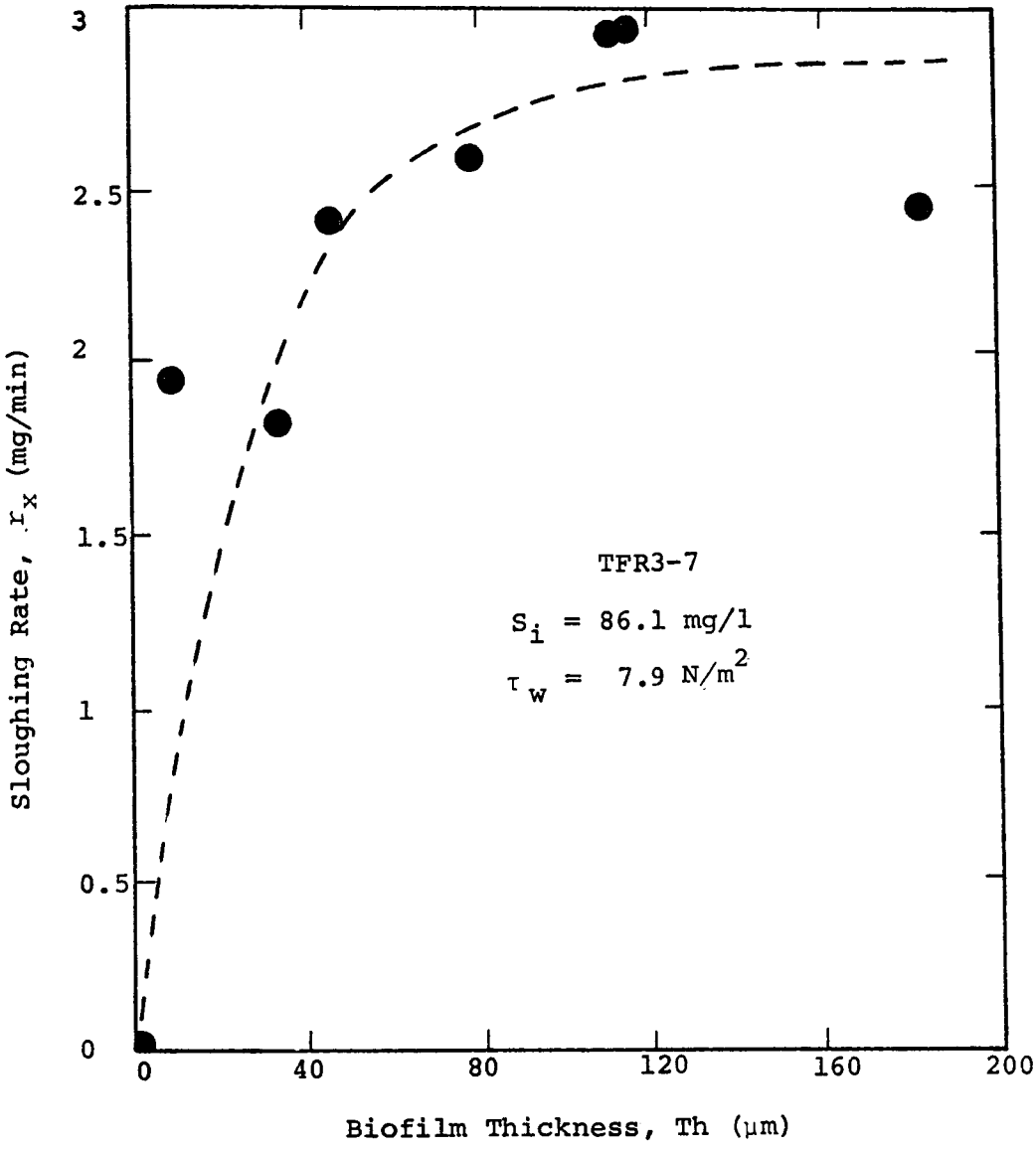

Figure 3-10. Sloughing rate as a function of biofilm thickness in the TFR3 system. Thickness is calculated from biofilm mass and density measurements.

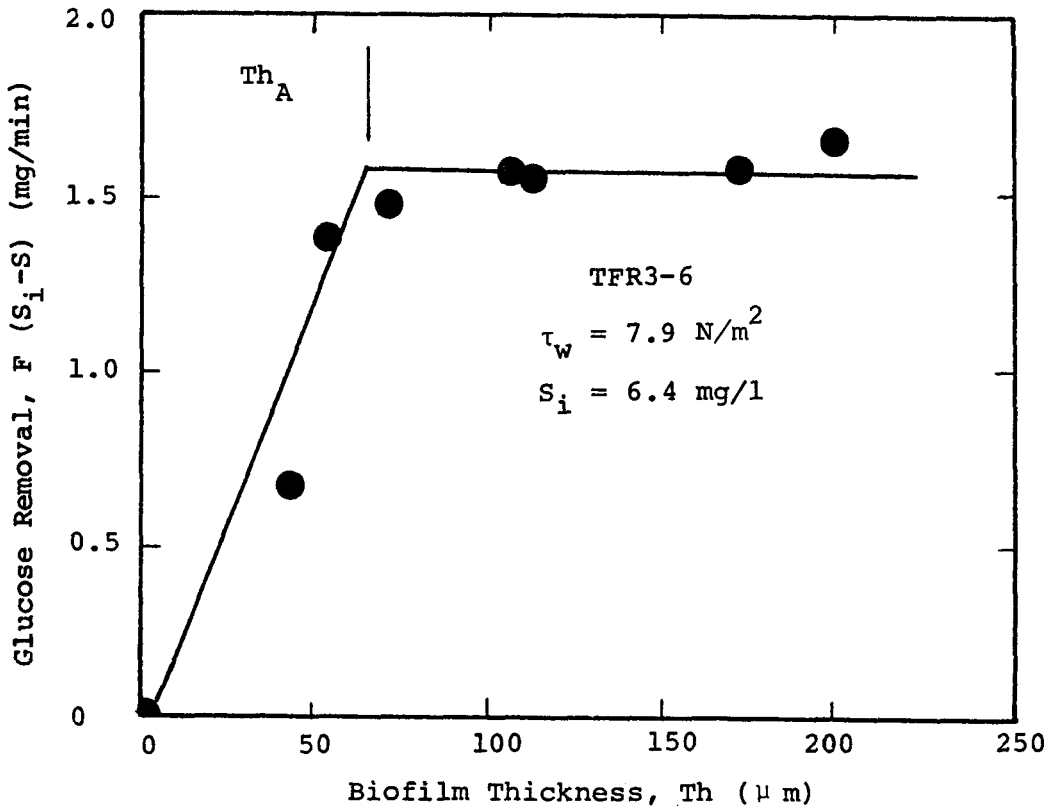

Figure 3-11. Glucose removal rate (R"·A) as a function of biofilm thickness. Thickness is calculated from biofilm mass and density measurements.

R''_m is constant within a given experiment (Figure 3-12). R''_m, however, is a function of the glucose loading rate for the experiment as indicated by Figure 3-13. Sufficient data are not available to determine the effect of wall fluid shear stress (τ_w) on R''_m at constant glucose loading rate. However, wall fluid shear stress determines the size of the viscous sublayer adjacent to the biofilm and, therefore, the mass transfer rate at the fluid-biofilm interface. As τ_w increases, the viscous sublayer decreases and reaction rate increases (Figure 3-14). Active thickness increases with increasing glucose loading rate (Figure 3-15).

The sloughing rate (r_X) of biomass from the biofilm surface increased with increasing biofilm thickness during a given experiment (Figure 3-10) which suggests r_X depends on shear stress at the biofilm surface. Sloughing rate, determined at steady state for each experiment (Eq. 3-15), is directly related to glucose loading rate (Figure 3-16) but insufficient data is available to determine the effect of shear stress. These data also suggest that yield increases with glucose loading rate up to some maximum yield.

Combining Eqs. 3-6, 3-8, 3-15, 3-16, 3-17, an expression for biofilm development rate is obtained:

$$r_{Th} = Y \cdot R''_m \cdot \rho_{Th} \cdot Th - F \cdot X \quad \text{for } Th < Th_A \tag{3-18}$$

$$r_{Th} = Y \cdot R''_m \cdot \rho_{Th} \cdot Th_A - F \cdot X \quad \text{for } Th \geq Th_A \tag{3-19}$$

A summary of the mathematical development leading to Eqs. 3-18 and 3-19 is presented in Table 3-6.

Analysis of the results on biofilm development indicated no significant effect due to bulk temperature in the range 30-40^{o}C. This is possibly due to the existence of a temperature optimum for biofilm development at approximately 35^{o}C. Results regarding the effect of wall temperature on biofilm development are presented with the heat transfer resistance results.

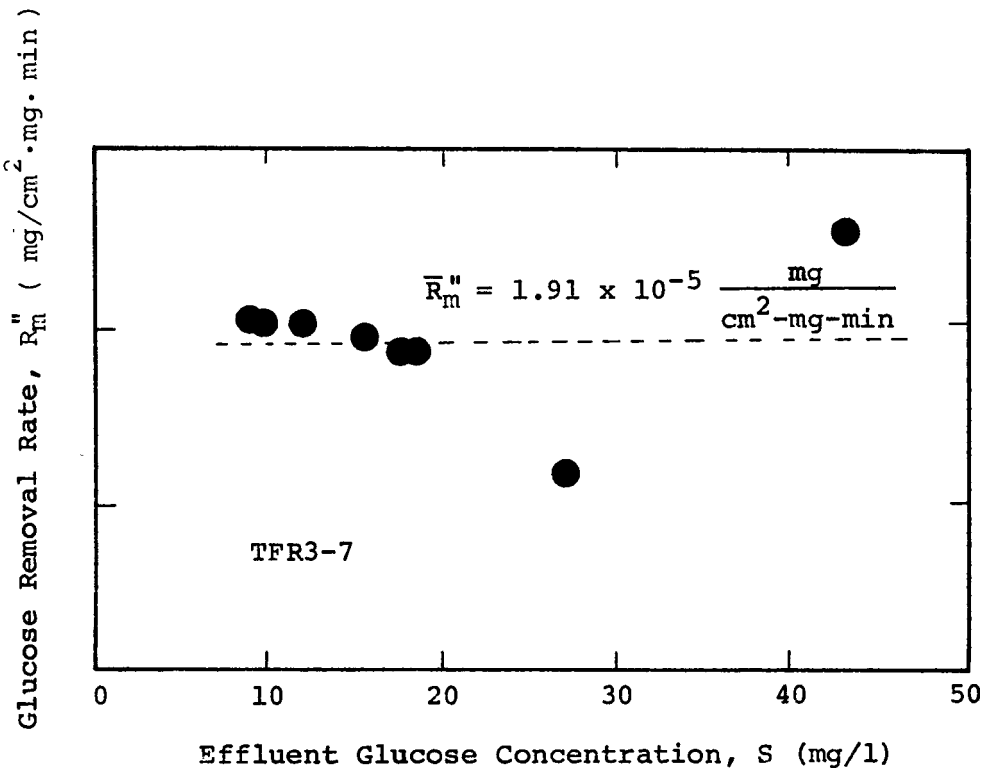

Figure 3-12. Glucose removal rate as a function of effluent concentration for a constant glucose loading rate of 69.5 mg/m^2-min.

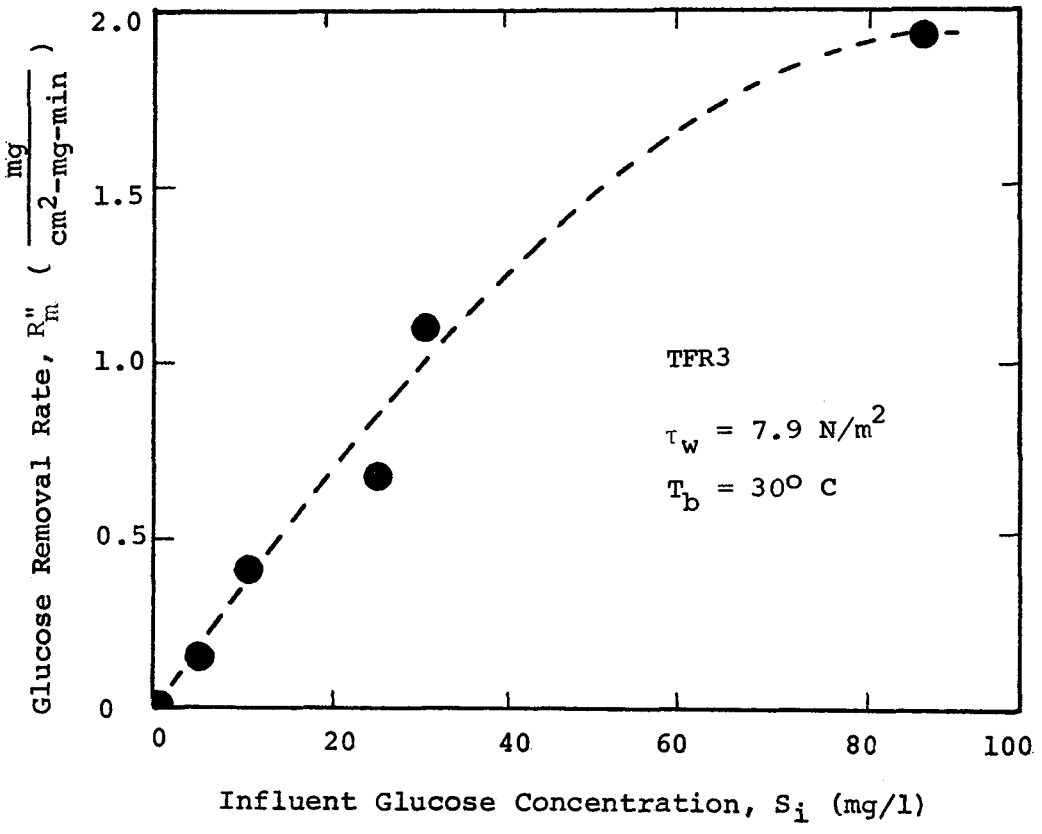

Figure 3-13. Glucose removal rate as a function of influent glucose concentration for six TFR3 experiments at the same wall shear stress and bulk temperature.

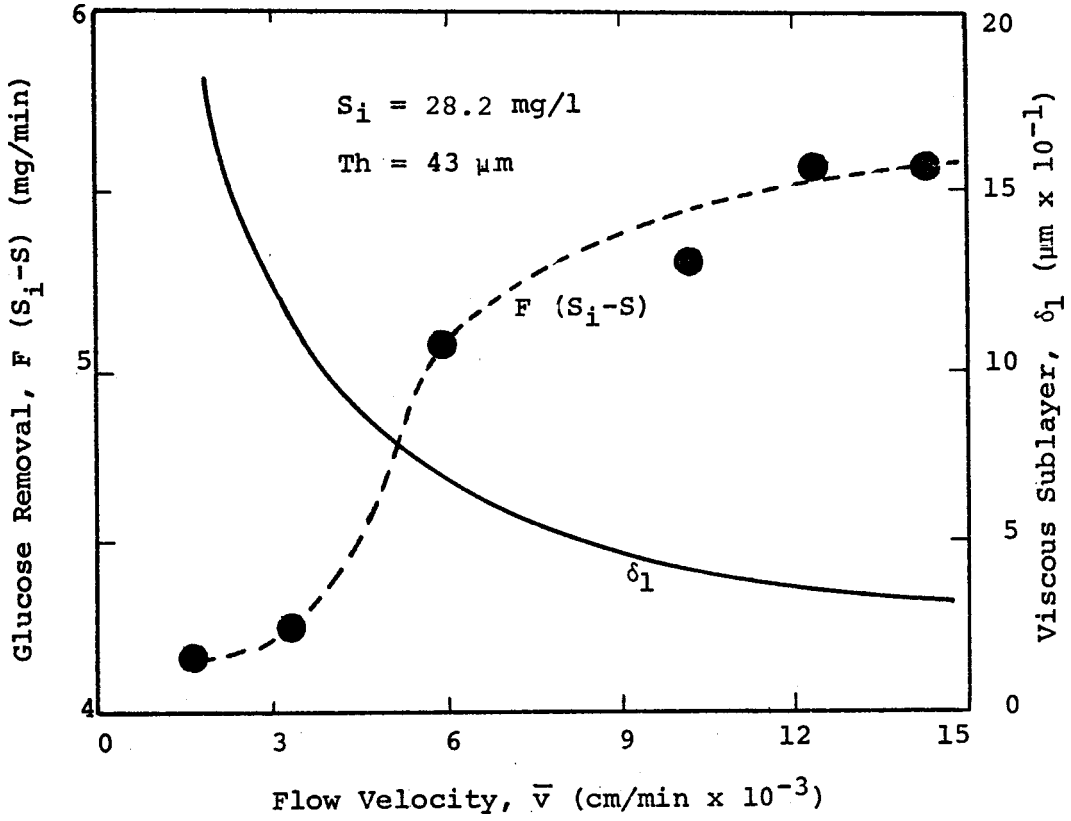

Figure 3-14. Glucose removal as a function of flow velocity in the TFR3 system. (TFR3-15)

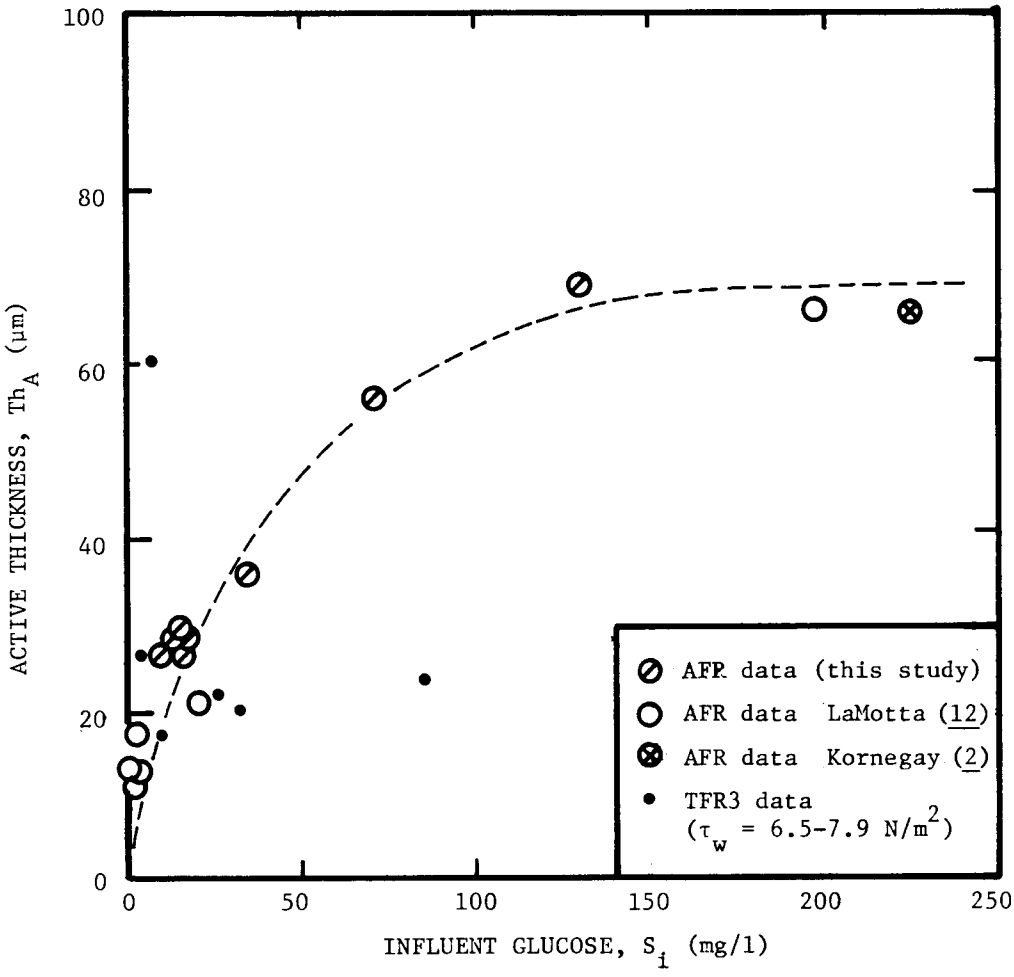

Figure 3-15. Active thickness as a function of influent glucose concentration.

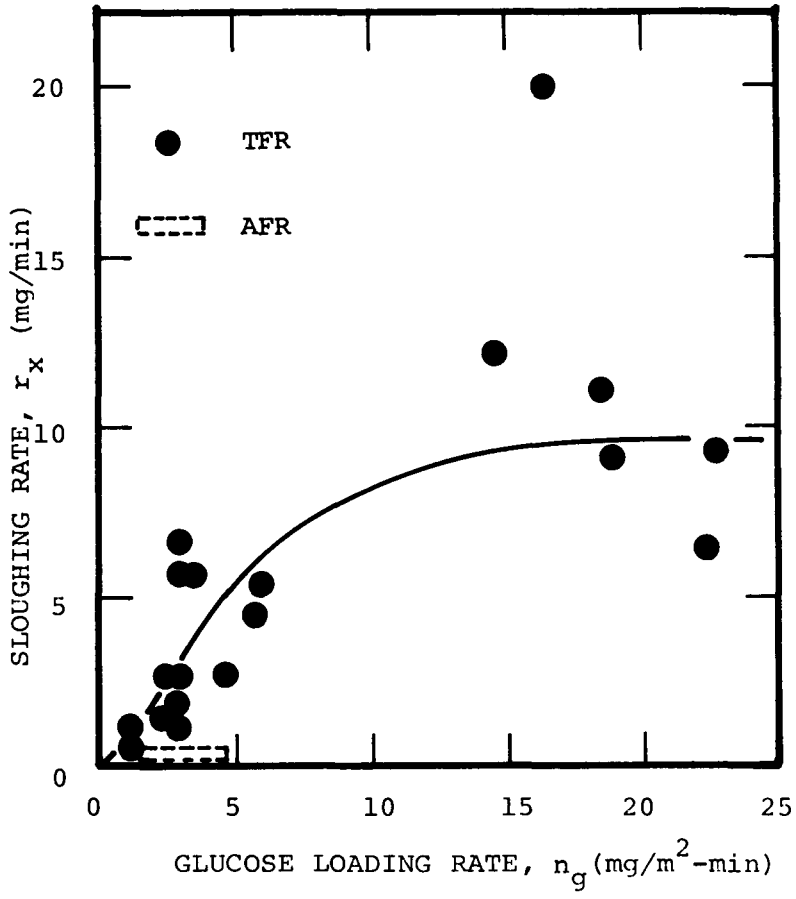

Figure 3-16. Effect of glucose loading rate on sloughing rate.

Table 3-6

SUMMARY OF MODEL FOR DESCRIBING BIOFILM DEVELOPMENT IN THE EXPERIMENTAL REACTORS

Rate of Biomass Production (Eqs. 3-6, 3-16, 3-17):

$$r = r_{Th} + r_X = Y \cdot R'' \cdot A$$
$$= Y \cdot R''_m \cdot A \cdot \rho_{Th} \quad \text{for } Th < Th_A$$
$$= Y \cdot R''_m \cdot A \cdot \rho_{Th} \cdot Th_A \quad \text{for } Th \geq Th_A$$

Rate of Sloughing (Eq. 3-15):

$$r_X = F \cdot X \quad \text{where } X = fc(Th)$$

Rate of Biofilm Development (Eqs. 3-18, 3-19):

$$r_{Th} = r - r_X = Y \cdot R''_m \cdot \rho_{Th} \cdot Th - F \cdot X \quad \text{for } Th < Th_A$$
$$= Y \cdot R''_m \cdot \rho_{Th} \cdot Th_A - F \cdot X \quad \text{for } Th \geq Th_A$$

where $R''_m = fc\ (n_g, \tau_w)$ Figures 3-13, 3-14

$\rho_{Th} = fc\ (n_g, \tau_w)$ Figures 3-1, 3-2, 3-3

* $r_X = fc\ (Th)$ Figure 3-10

$Th_A = fc\ (n_g)$ Figure 3-15

*note that at steady state, or when $r_{Th} = 0$, r_X is a function of glucose loading rate (Figure 3-16).

Extent of Biofilm Development

In the TFR1, TFR2 and AFR systems, experiments were not terminated until a steady biofilm thickness was attained. The steady biofilm thickness was approximately equal to the maximum biofilm thickness (Th_{MAX}) observed during the experiment.

The effect of shear stress on maximum biofilm thickness attained in the AFR is compared with other similar research (2) in Figure 3-17. Shear stress has a strong effect at the lower levels (<3 N/m^2). The data are not sufficient to determine if a significant effect of glucose loading exists. However, mean values for Th_{MAX} from TFR1, TFR2 and AFR experiments (for $\tau_w > 3.0$ N/m^2) indicates that glucose loading rate is important when shear stress at the wall is high (Table 3-7).

Table 3-7

EFFECT OF GLUCOSE LOADING RATE ON MAXIMUM THICKNESS*

Th_{MAX} (μm)	n_g (mg/m^2-min)
61 ± 11 (4)	< 2.3
142 ± 43 (9)	2.9 - 6.2
215 ± 114 (5)	14.8 - 22.9

*TFR1 and TFR2 experiments with $\tau_w > 3.0$ N/m^2

EFFECTS OF BIOFILM DEVELOPMENT ON FRICTIONAL RESISTANCE

The two relevant effects of biofilm development in this study were increased fluid frictional resistance and increased heat transfer resistance. Besides their obvious impact on power plant operation, the changes in fluid frictional resistance and heat transfer resistance can be used to indirectly monitor biofilm development. The data presented in this report will be helpful in assessing the feasibility of such monitoring devices for use in power plants.

Changes in fluid frictional resistance due to biofilm development were measured in all tubular fouling reactors (TFR), the annular

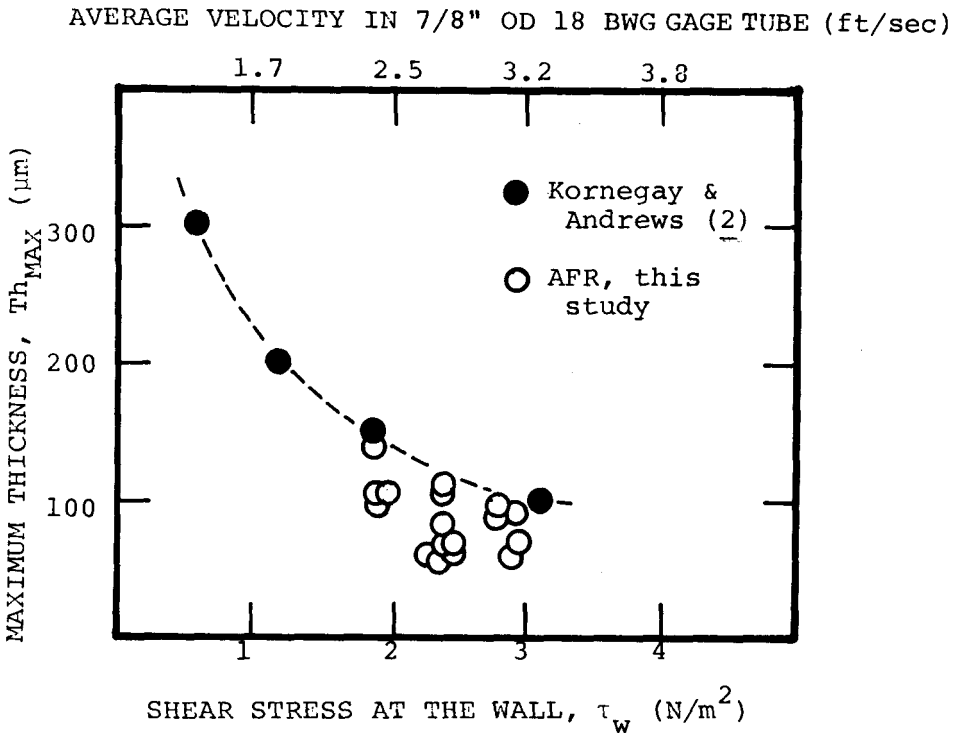

Figure 3-17. Effect of shear stress on maximum thickness attained in the AFR.

fouling reactor (AFR) and the field fouling reactor (FFR). The major portion of this discussion will be devoted to results from the tubular fouling reactors since the fluid dynamics in tubular geometries have been described in detail. The results from the AFR will be discussed in relation to the results from the tubular systems.

Frictional Resistance in the Tubular Reactor System

Frictional resistance due to microbial film accumulation during constant flow rate experiments (TFR1 and TFR2) causes an increase in pressure drop and more power is required for pumping (Figure 3-18).

Conversely, if pressure drop is held constant (TFR3), flow capacity is reduced. Figure 3-19 shows flow capacity was reduced to 42% of the original capacity in a 100-hour laboratory experiment.

Frictional resistance can be represented for both constant flow rate and constant pressure drop experiments by the following equation (13):

$$f = 2.0 \frac{d}{L} \frac{\Delta p}{\rho v_m^2} \qquad (3\text{-}20)$$

where f = friction factor

d = tube diameter (L)

ρ = fluid density (m/L^3)

v_m = mean fluid velocity (L/t)

Δp = pressure drop along length L ($m/m\text{-}t^2$)

The progression of friction factor with time for a TFR3 experiment is shown in Figure 3-20. The progression of film mass and film thickness with time from Figure 3-5 is shown also for comparison.

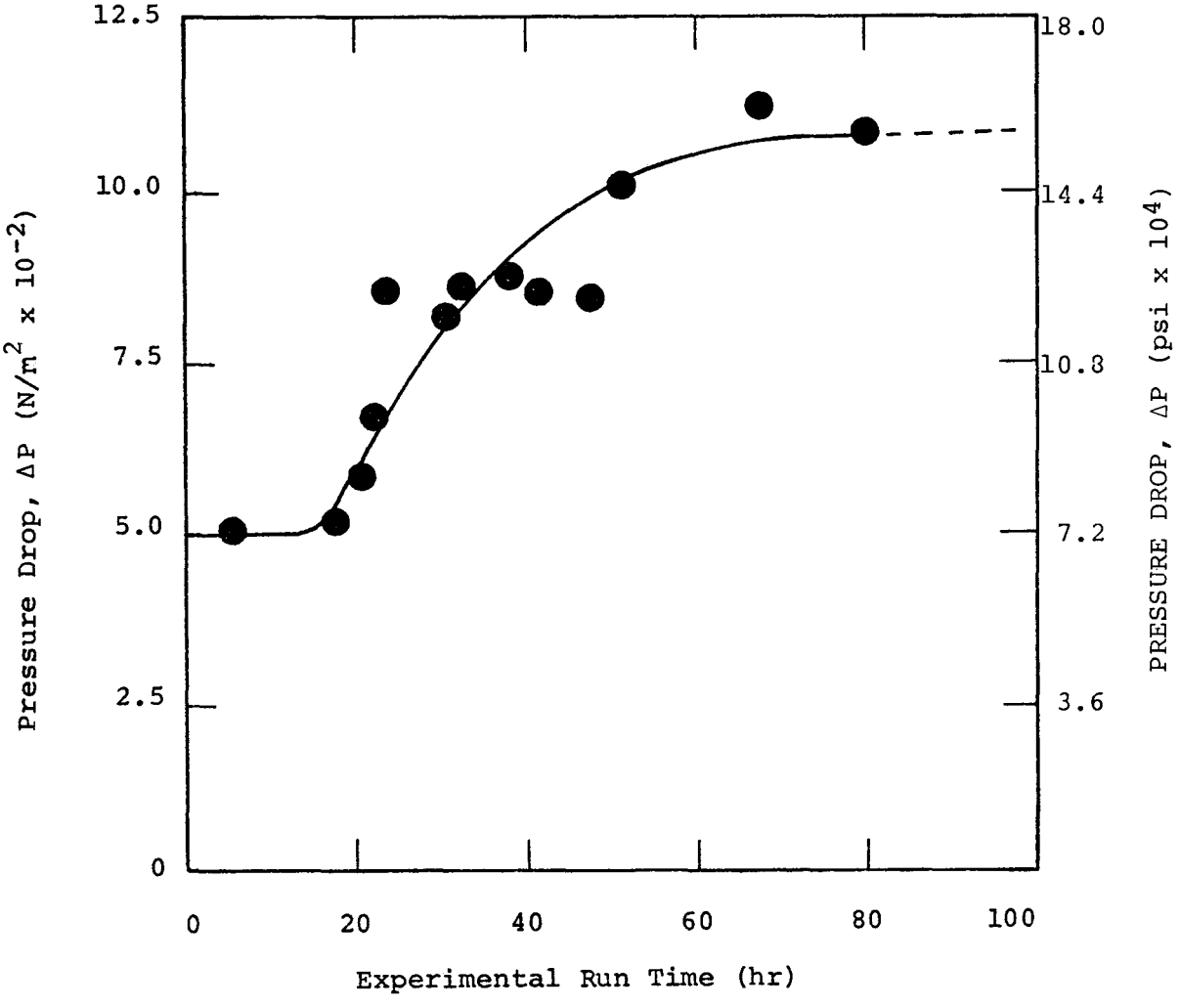

Figure 3-18. Change in pressure drop with time for a constant flow experiment (TFR1-12).

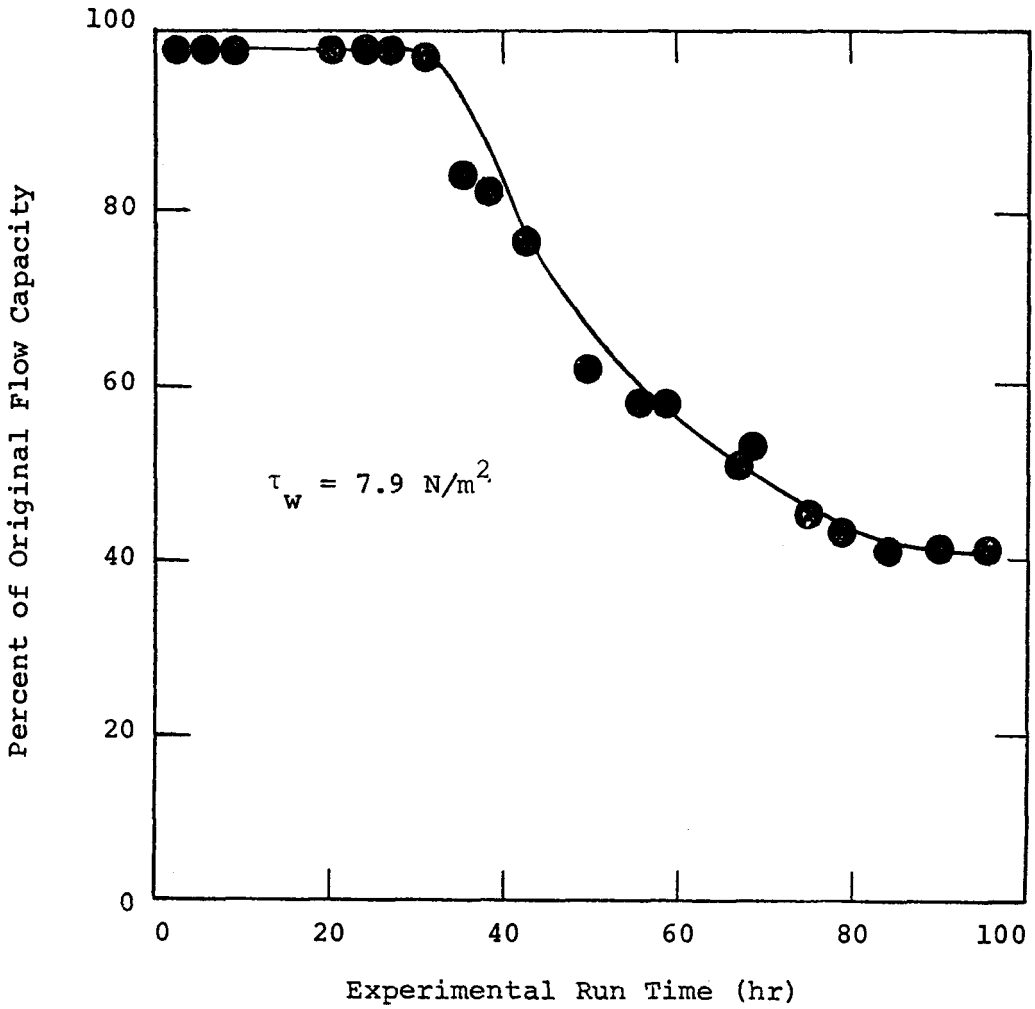

Figure 3-19. Change in flow capacity with time for a constant pressure drop experiment (TFR3-5).

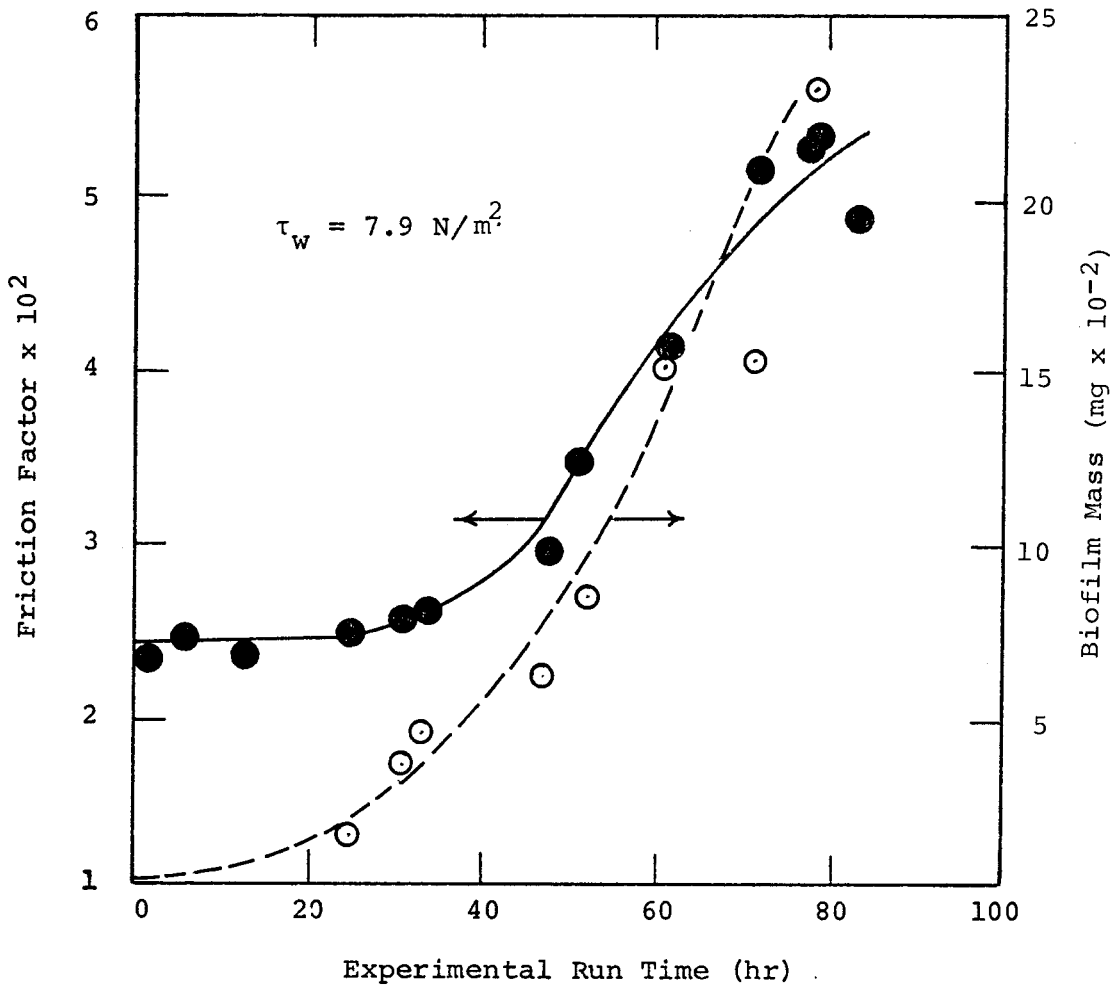

Figure 3-20. Change in friction factor and biomass with time for a constant pressure drop experiment (TFR3-7).

Equivalent Sand Roughness. The equivalent sand roughness (k_s) of the TFR tube surface can be calculated by the Colebrook and White equation as follows (13):

$$k_s = \frac{d}{2}\left[10^{(0.87 - 0.50/\sqrt{f})} - \frac{18.70}{Re\sqrt{f}}\right] \qquad (3\text{-}21)$$

The equation is derived from experiments by Nikuradse using circular pipes with sand grains immobilized on the inside surface. The relative roughness of the tube surface is expressed by the ratio of the size of the sand grain (k_s) to the internal radius of the tube (R). In Nikuradse's experiments, the relative roughness (k_s/R) varies from 0.002 to 0.0067, the pipe radius from 1.6 to 6.4 cm, and the water temperature from 12°C to 16°C (14).

In TFR experiments, k_s generally increases with time. Figure 3-21 shows the progression of k_s with time for one TFR3 experiment.

Figure 3-22 shows k_s is dependent on biofilm thickness for the range of shear stress investigated (6.5 - 7.9 N/m^2). Variation in the data cannot be attributed to changes in input glucose concentration (5-250 mg/l) or change in temperature (30-35°C).

Flow Regime Near the Pipe Wall. Determination of the flow regime depends on k_s and the relative size of the viscous sublayer, δ_l:

$$\delta_l = \frac{10\ d}{Re}\left[\frac{f}{2}\right]^{-0.5} \qquad (3\text{-}22)$$

where d = tube diameter (L)

$Re = \frac{v_m d}{\nu}$ = Reynolds Number

v_m = mean fluid velocity (L/t)

ν = kinematic viscosity (L^2/t)

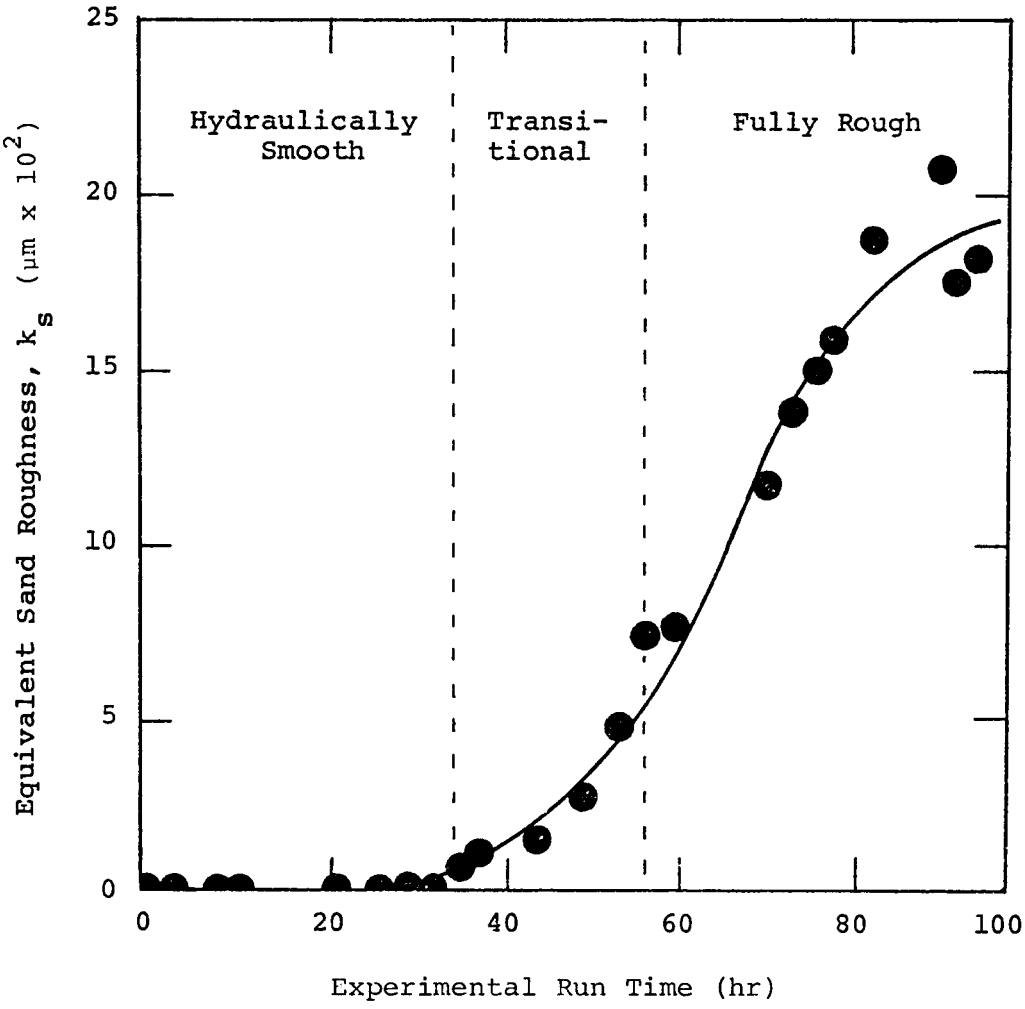

Figure 3-21. Change in equivalent sand roughness with time in a constant pressure drop experiment (TFR3-5).

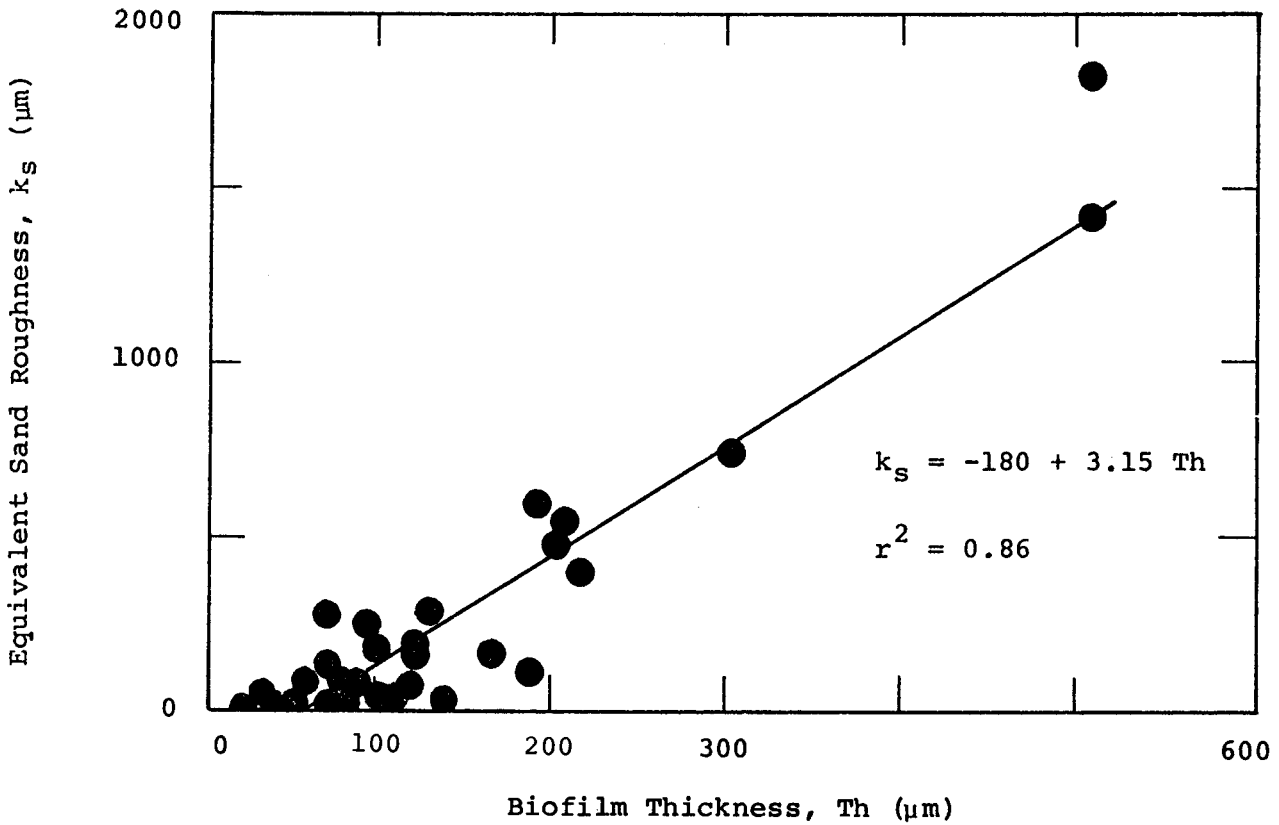

Figure 3-22. Change in the calculated equivalent sand roughness with biofilm thickness for all constant pressure drop experiments at a fluid shear stress of 6.5-7.9 N/m^2, with temperature at 30 to 35°C.

When $k_s < \delta_l$, the pipe is considered hydraulically smooth.
When 14 $\delta_l > k_s > \delta_l$, the flow is in the transitional regime.
When $k_s > 14\delta_l$, the flow is in the fully rough regime.

In all TFR experiments (except TFR3-11 which was a pre-roughened tube), the flow regime progresses from hydraulically smooth to transitional or fully rough. Increases in biofilm thickness precede changes in equivalent sand roughness (Figure 3-22) and friction factor (Figure 3-23).

Frictional Resistance in the Annular Reactor System

Increased frictional resistance is also observed in the AFR during biofilm development. However, the flow regime, consisting of the superimposition of axial flow (nutrients plus dilution water) through the reactor, centrifugal flow due to the rotating inner cylinder, and circulation induced by the impeller/draft tube arrangement, is too complex for detailed analysis. Fluid dynamic analysis of such a system has not been found in the literature. Some measured fluid dynamic characteristics of the clean AFR are presented in Figure 3-24.

In the AFR, friction factor has been defined as follows:

$$f_a = \frac{T_q}{\pi \rho R_i^3 (R_i + R_o) \Omega^2 H} \qquad (3\text{-}23)$$

where R_i = radius of inner cylinder (L)
R_o = radius of outer cylinder (L)
Ω = rotational velocity (t^{-1})
H = height of inner cylinder (L)
T_q = torque on inner cylinder ($m\text{-}L^2/t^2$)

The change in torque during biofilm development for a typical AFR experiment is presented in Figure 3-25. As in the TFR (Figure 3-23), biofilm thickness increases before frictional resistance.

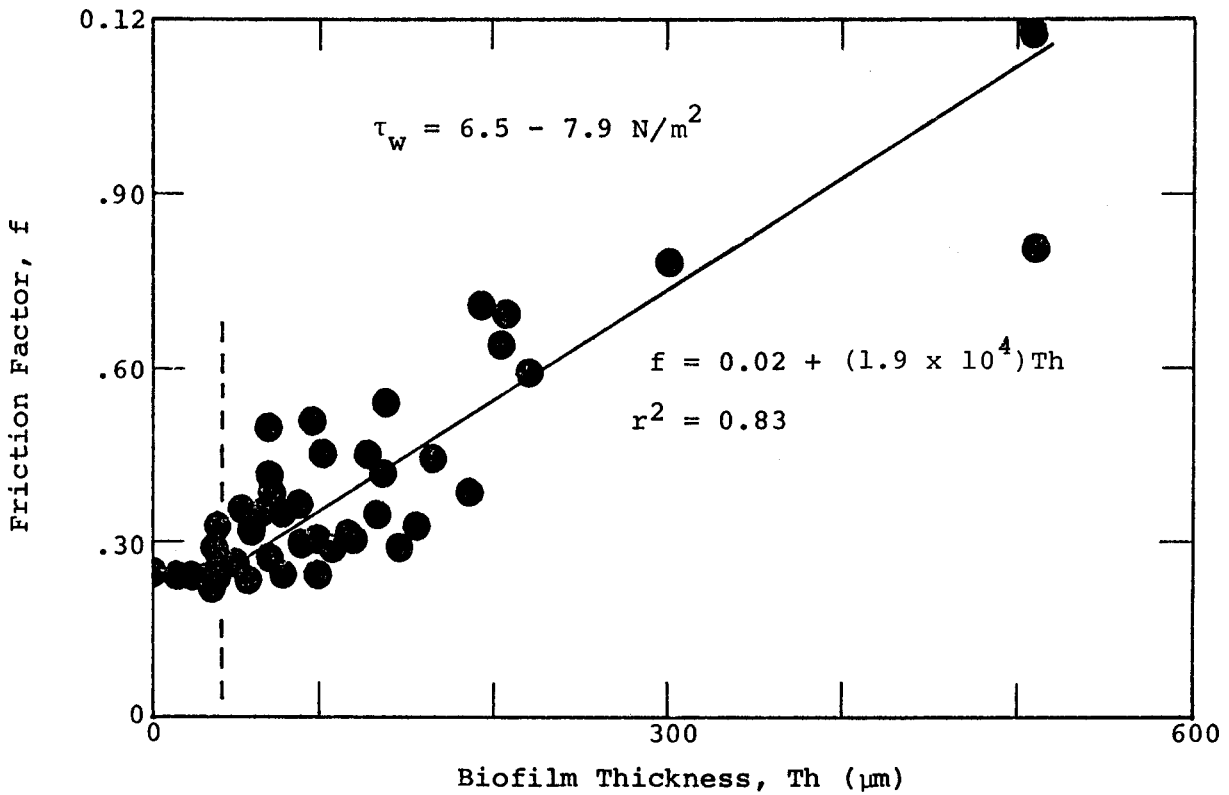

Figure 3-23. Change in friction factor with biofilm thickness in the constant pressure drop system (TFR3).

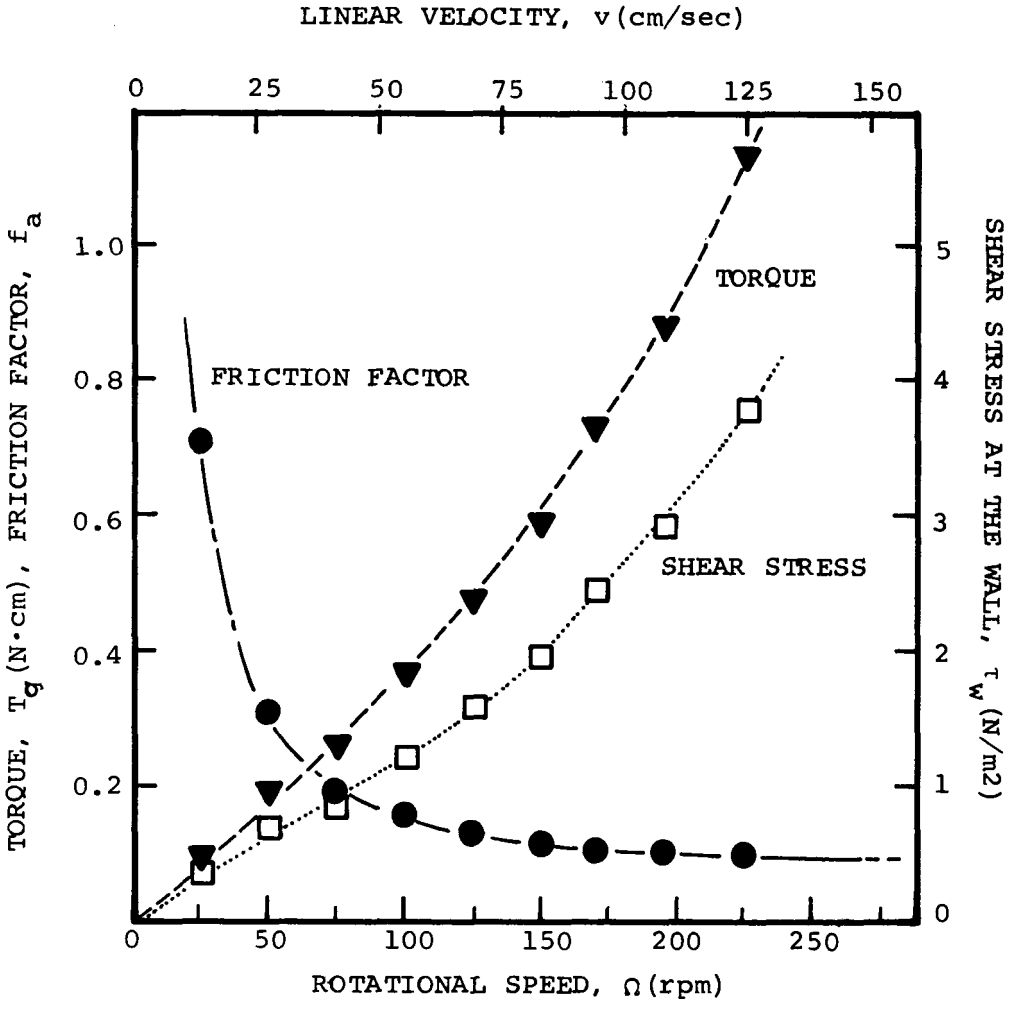

Figure 3-24. Relevant fluid dynamic characteristics of the clean AFR at 30°C.

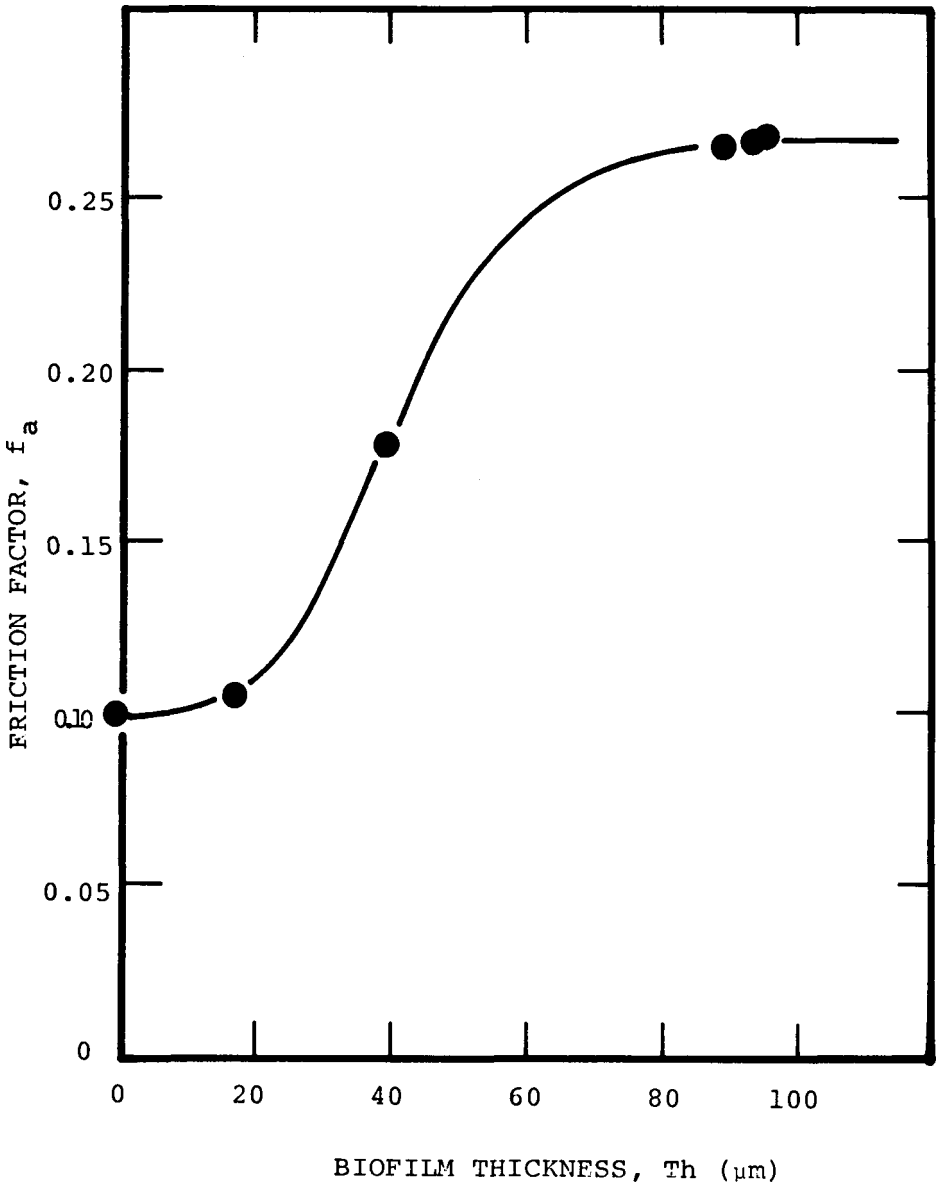

Figure 3-25. Change in friction factor with increasing biofilm thickness in a typical AFR experiment.

Rate of Biofouling

A logarithmic fouling rate (R*) is defined for the growth phase (see Figure 4-1) of biofouling. The growth phase represents the period of significant fouling as indicated by substantial biofilm accumulation and frictional resistance. Experimental results indicate the logarithm of the changes with time during this phase is essentially linear. Logarithmic fouling rates can refer to any of the following.

1. Frictional resistance (R_f^*)
2. Biofilm mass (R_{BM}^*)
3. Biofilm thickness (R_{Th}^*)

The slopes of R_f^*, R_{BM}^*, and R_{Th}^* are depicted in Figures 3-26, 3-27, and 3-28 for TFR3-2. Similar behavior was observed in the AFR. The rate of microbial fouling is dependent on the glucose loading rate (n_g).

Figures 3-29 to 3-31 indicate that R_f^*, R_{BM}^*, and R_{Th}^* increase with n_g. The data for R_{BM}^* (Figure 3-31) suggest that the dependence of fouling on n_g is described by a saturation function. This behavior has also been observed in other investigations of growth kinetics in biological film systems (12,22). Fouling rate (R_f^*) decreases with increasing shear stress (Figure 3-29).

Results from the AFR indicate similar behavior. Figure 3-32 illustrates the effect of glucose loading rate on R_f^*. The effect of bulk temperature on R_f^* was negligible in the AFR (Figure 3-33) and TFR systems. An optimal temperature for R_f^* at 35°C is suggested but more data would be needed for verification.

EFFECTS OF BIOFILM DEVELOPMENT ON HEAT TRANSFER

The effects of biofilm development on heat transfer were observed in TFR4. Experiments were performed so that heat transfer resistance, fluid frictional resistance and biofilm thickness were measured simultaneously. Overall heat transfer resistance is the sum of conductive and convective resistance and results indicate that both resistances can be significant in the biofouling process.

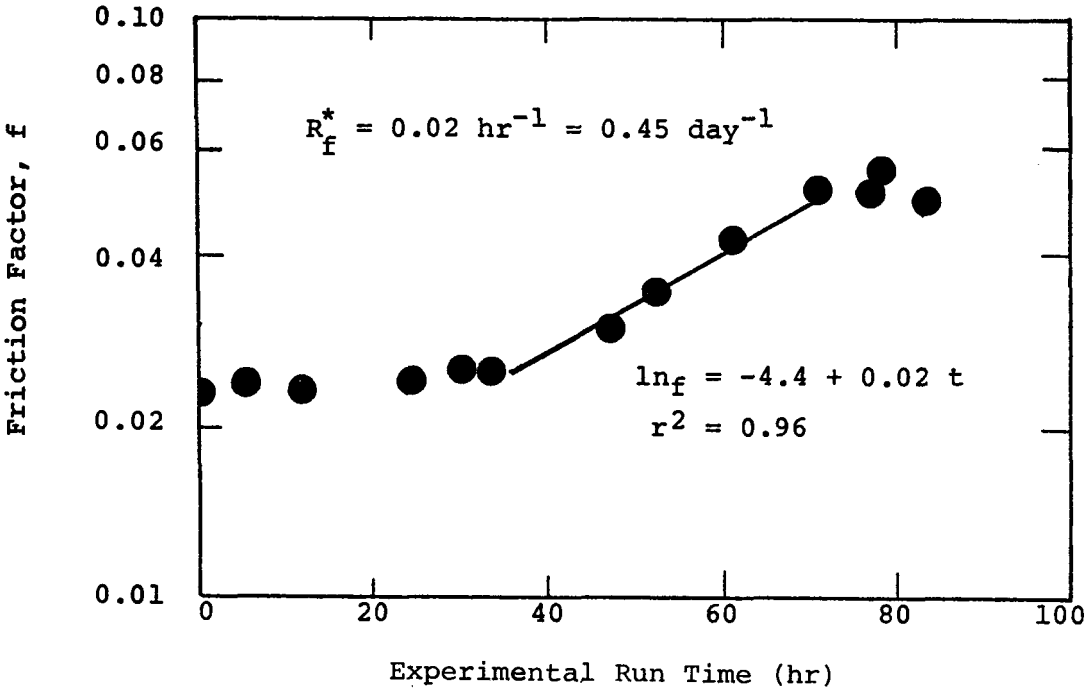

Figure 3-26. Determination of friction factor fouling rate for a constant pressure drop experiment (TFR3-7).

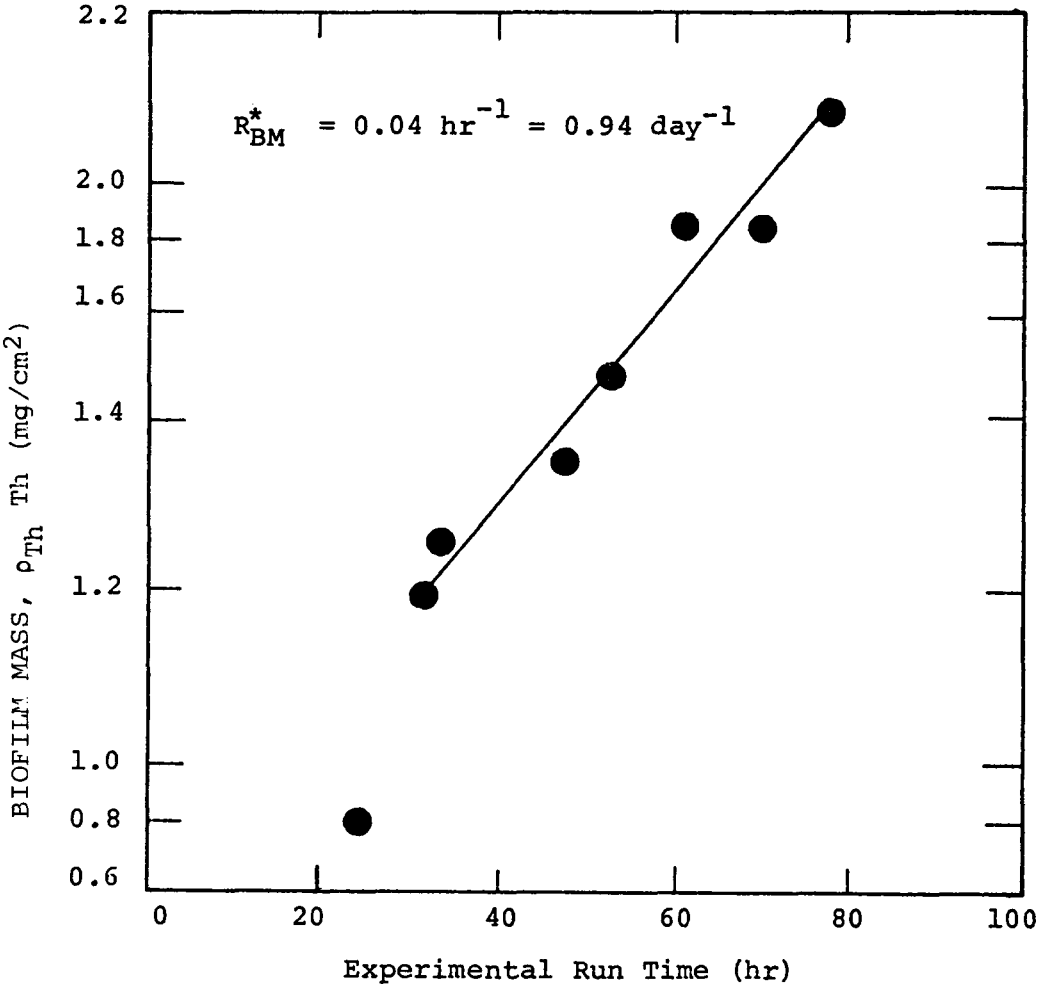

Figure 3-27. Determination of film mass fouling rate in a constant pressure drop experiment (TFR3-7).

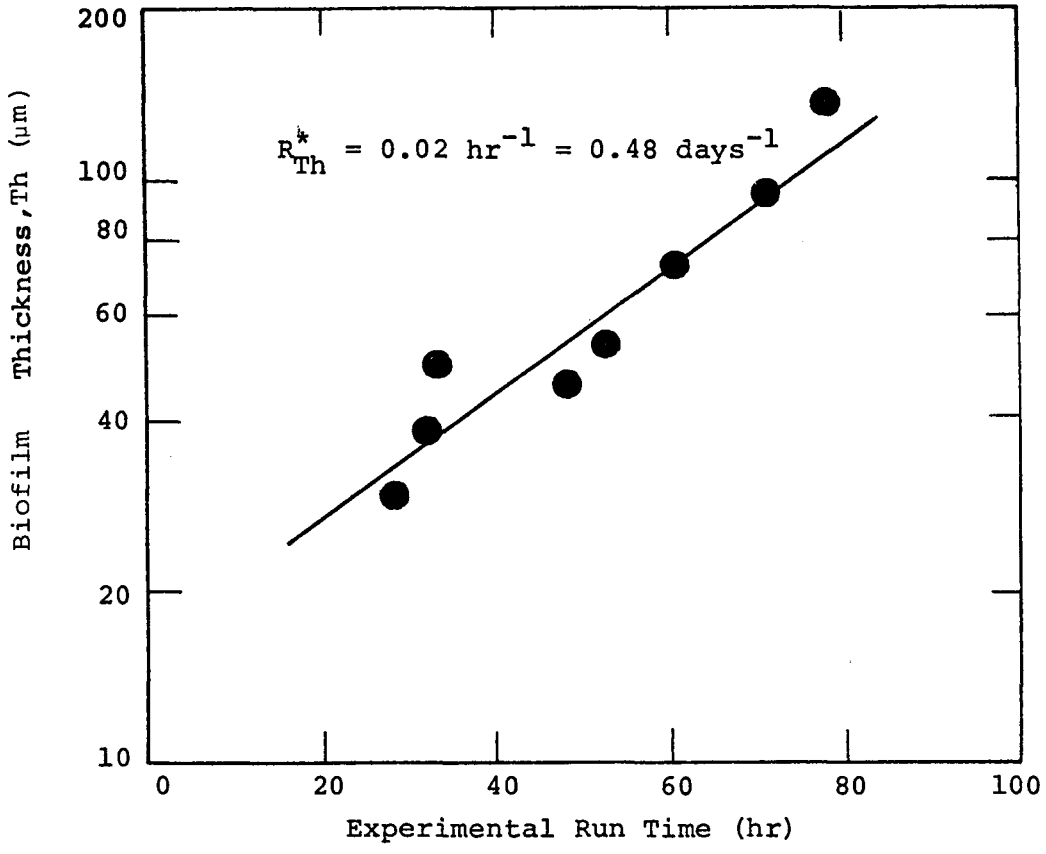

Figure 3-28. Determination of film thickness fouling rate in a constant pressure drop experiment (TFR3-7).

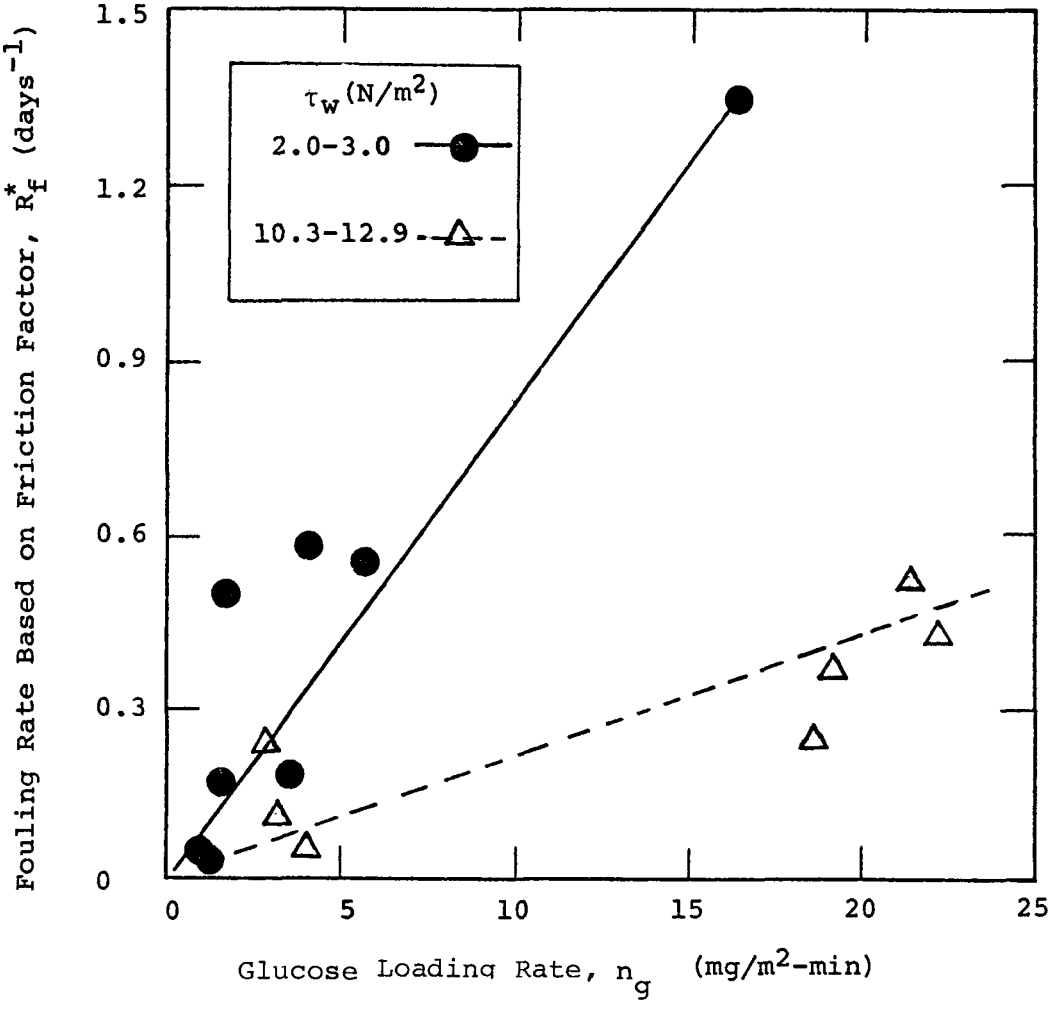

Figure 3-29. Influence of glucose loading rate on fouling rate based on friction factor in the constant flow rate system (TFR1 and TFR2).

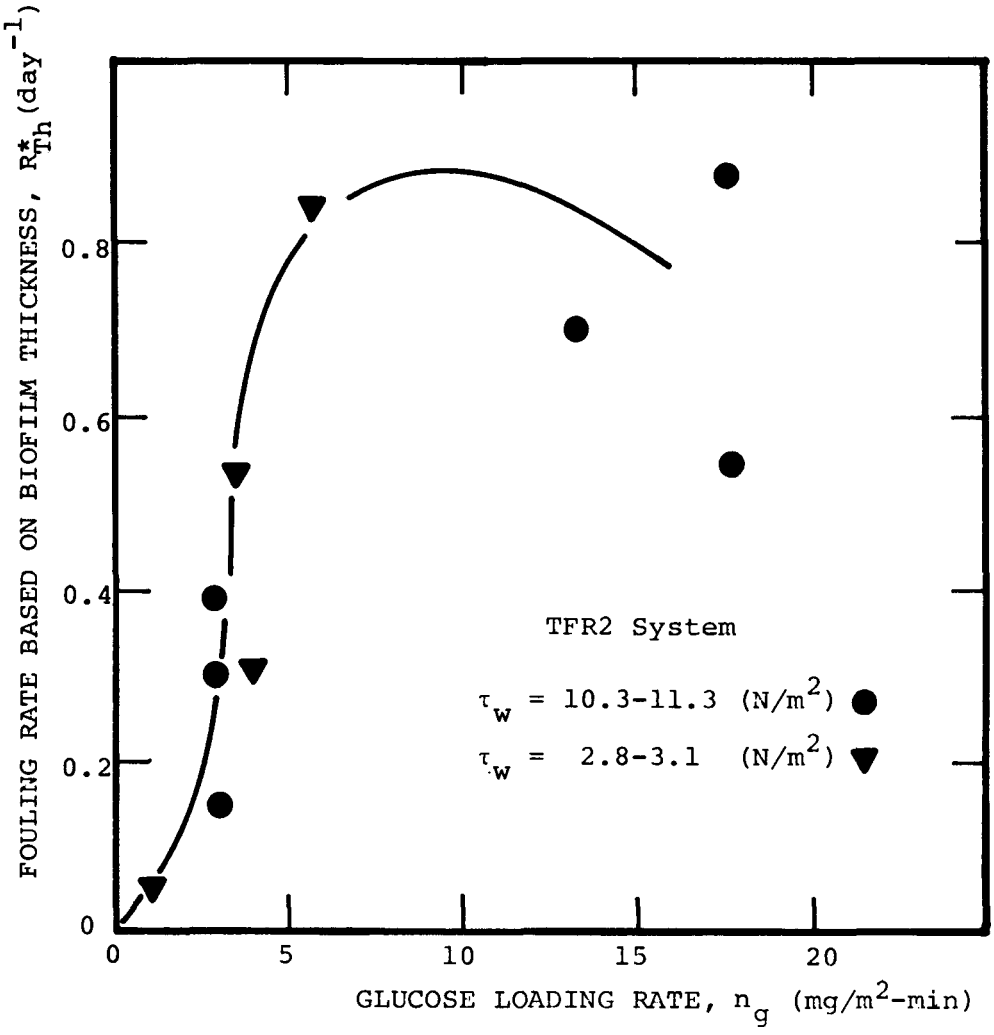

Figure 3-30. Effect of glucose loading rate on fouling rate (R^*_{Th}) in a constant flow rate system (TFR2).

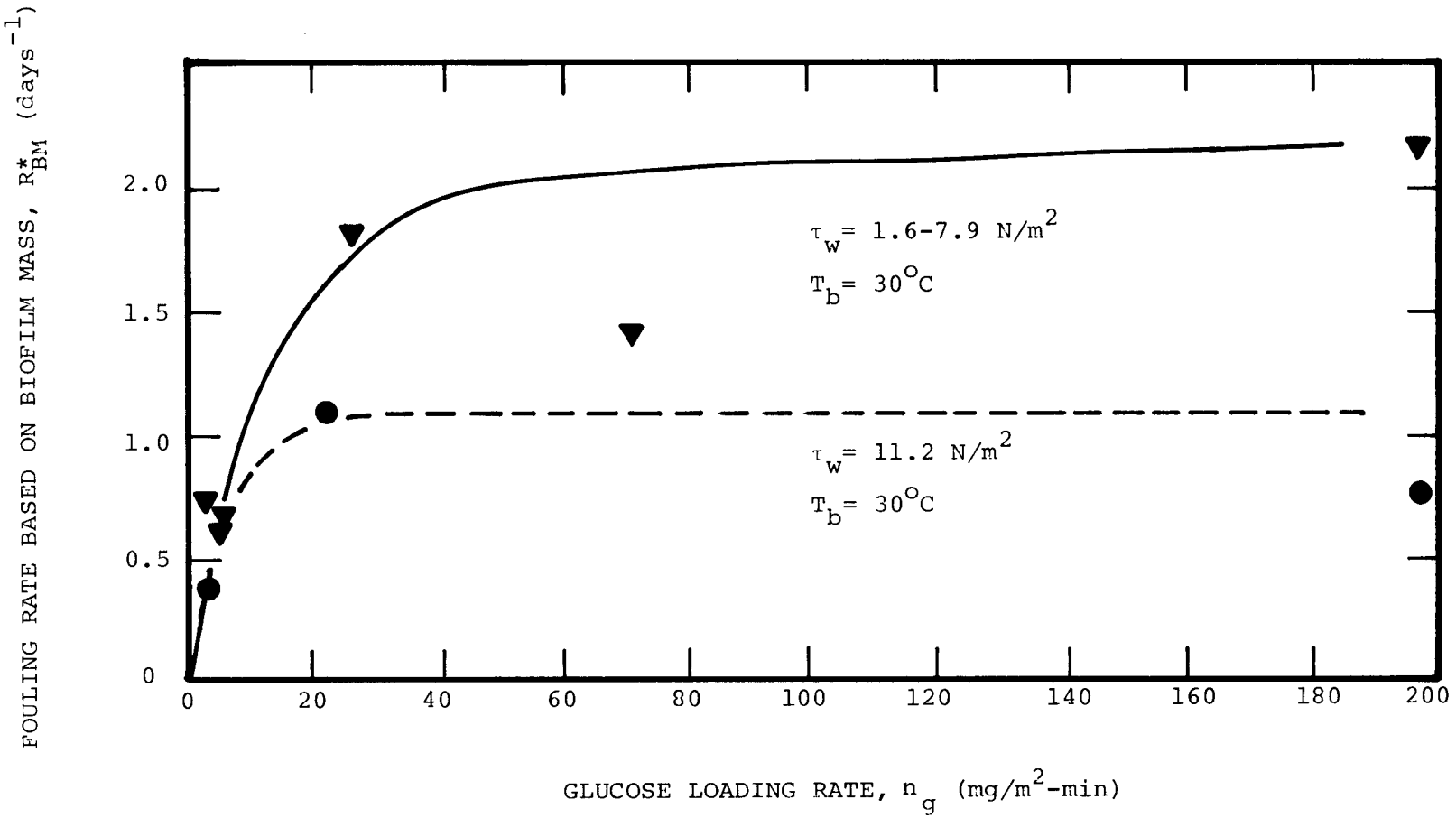

Figure 3-31. Effect of glucose loading rate on fouling rate based on biofilm mass in the constant flow system (TFR1).

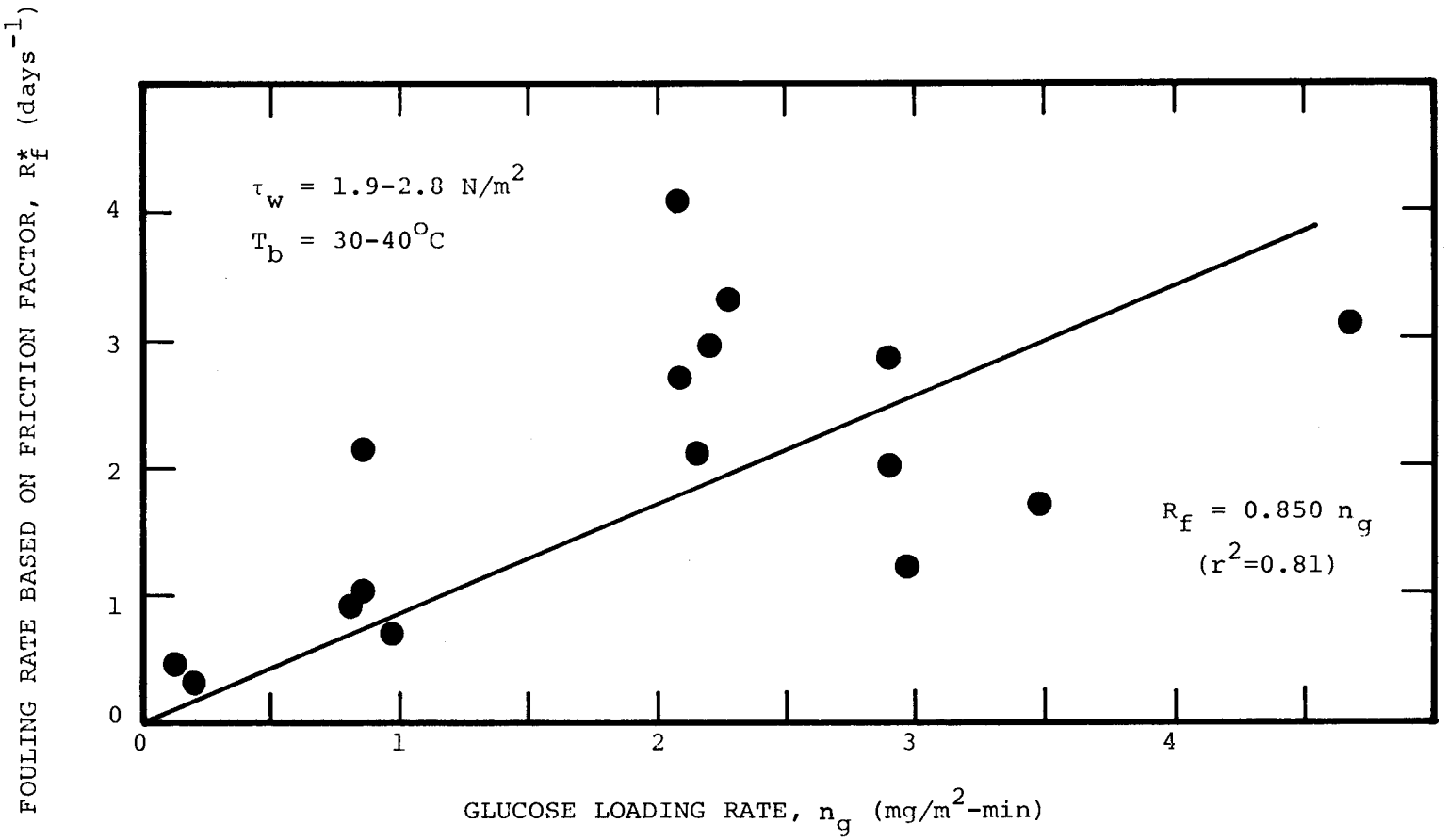

Figure 3-32. Effect of glucose loading rate on fouling rate based on friction factor in the AFR.

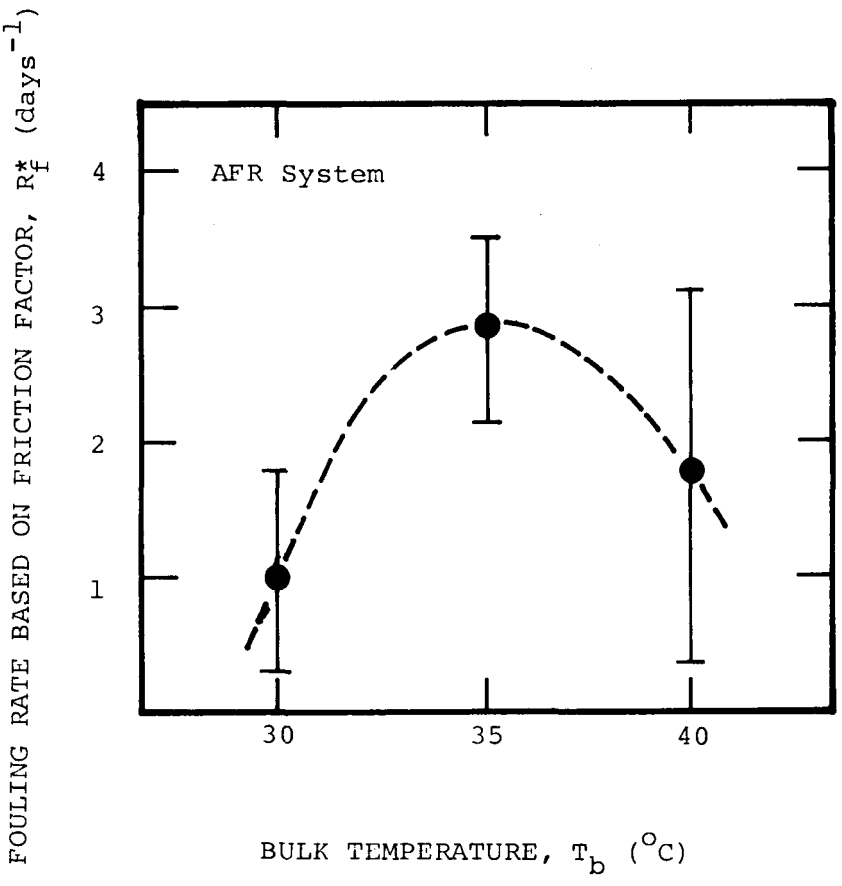

Figure 3-33. Effect of bulk temperature on fouling rate based on friction factor in the AFR.

Heat Transfer in the Test Heat Exchanger

Biofilm thermal conductivity was determined from temperature measurements in the bulk fluid (T_b) and temperatures in the aluminum test heat exchanger (THE) wall (T_i, T_{ii}). The following equations describe how the temperature measurements were used to calculate biofilm thermal conductivity and other quantities of interest. The notation is consistent with Figure 2-5.

The measured heat flux into the fluid is as follows:

$$q_o = (T_i - T_{ii}) \frac{k_A}{r_2} \frac{1}{\left[\ln r_i/r_{ii}\right]} \tag{3-24}$$

where q_o = heat flux through THE ($E/L^2 \cdot t$)

k_A = thermal conductivity of aluminum ($E/L \cdot T \cdot t$)

r_2, r_i, r_{ii} = radial distances from center of THE defined in Figure 2-5 (L)

T_i, T_{ii} = temperatures at r_i and r_{ii}, respectively (T)

The heat flow in the block is

$$Q = q_o A_o \tag{3-25}$$

where Q = heat flow to the THE (E/t)

$A_o = 2\pi r_2 L_T$ (L^2)

L_T = length of THE (L)

The measured overall heat transfer coefficient can be calculated as follows:

$$Q = UA_I (T_i - T_b) \tag{3-26}$$

where U = overall heat transfer coefficient ($E/L^2 \cdot T \cdot t$)

$A_I = 2\pi L_T r_I$ (L^2)

r_I = r_1 - Th, the radial distance to the biofilm-fluid interface (L)

r_1 = inner radius of THE (L)

T_b = bulk fluid temperature (T)

and

$$U = \left[\frac{1}{h} + \frac{r_I \ln(r_i/r_1)}{k_A} + \frac{r_I \ln(r_1/r_I)}{k_{Th}} \right]^{-1} \qquad (3\text{-}26a)$$

where h = heat transfer coefficient (E/L·T·t)

k_{Th} = thermal conductivity of biofilm (E/L·T·t)

A heat transfer coefficient can be calculated based on the wall temperature as follows:

$$Q = U_w A_w (T_w - T_b) \qquad (3\text{-}27)$$

where $$U_w = \left[\frac{1}{h} + \frac{r_I \ln(r_1/r_I)}{k_{Th}} \right]^{-1} \quad (E/L^2 \cdot T \cdot t) \qquad (3\text{-}28)$$

Overall heat transfer resistance within the tube is then

$$R_H = U_w^{-1} \qquad (3\text{-}29)$$

Heat transfer resistance due to convention is

$$R_{conv} = 1/h \qquad (3\text{-}30)$$

where $h = (f/8) \cdot C_p^{1/3} \cdot k_w^{2/3} \cdot \mu^{-2/3} \cdot \rho \cdot v_m$

f = friction factor (dimensionless)

C_p = heat capacity of water (E/m-T)

k_w = thermal conductivity of water (E/L·T·t)

μ = viscosity of water (m/L-t)

ρ = density of water (m/L^3)

v_m = velocity (L/t)

Heat transfer resistance due to conduction in the biofilm is as follows:

$$R_{cond} = \frac{r_I \ln(r_1/r_I)}{k_{Th}} \qquad (3\text{-}31)$$

The distribution of R_{cond} and R_{conv} is illustrated in Figure 3-34 for a typical experiment.

Biofilm Thermal Conductivity

Biofilm thermal conductivity, k_{Th}, was determined from measurements of friction factor, biofilm thickness and heat flow using Eqs. 3-26 and 3-26a. The results are presented in Table 3-8 and indicate that the k_{Th} is not significantly different from k_w.

Table 3-8

THERMAL CONDUCTIVITY OF BIOFILM

Expt. No.	T_b (°C)	Th (μm)	k_{Th} (watts/m·°C)	k_w (watts/m·°C)
TFR4-6	28.3	53	0.44	0.62
		106	0.59	
		113	0.62	
		141	1.07	
			0.68 ± 0.27	
TFR4-8	26.7	13	0.17	0.61
		100	1.06	
		257	1.08	
		99	0.47	
		164	0.74	
			0.71 ± 0.39	
TFR4-9	28.3	37	0.71	0.62
		112	0.57	
		128	0.60	
		118	0.53	
		118	0.44	
			0.57 ± 0.10	

mean fluid velocity = 80.7 cm/sec
glucose loading rate = 13.6 mg/m^2·min

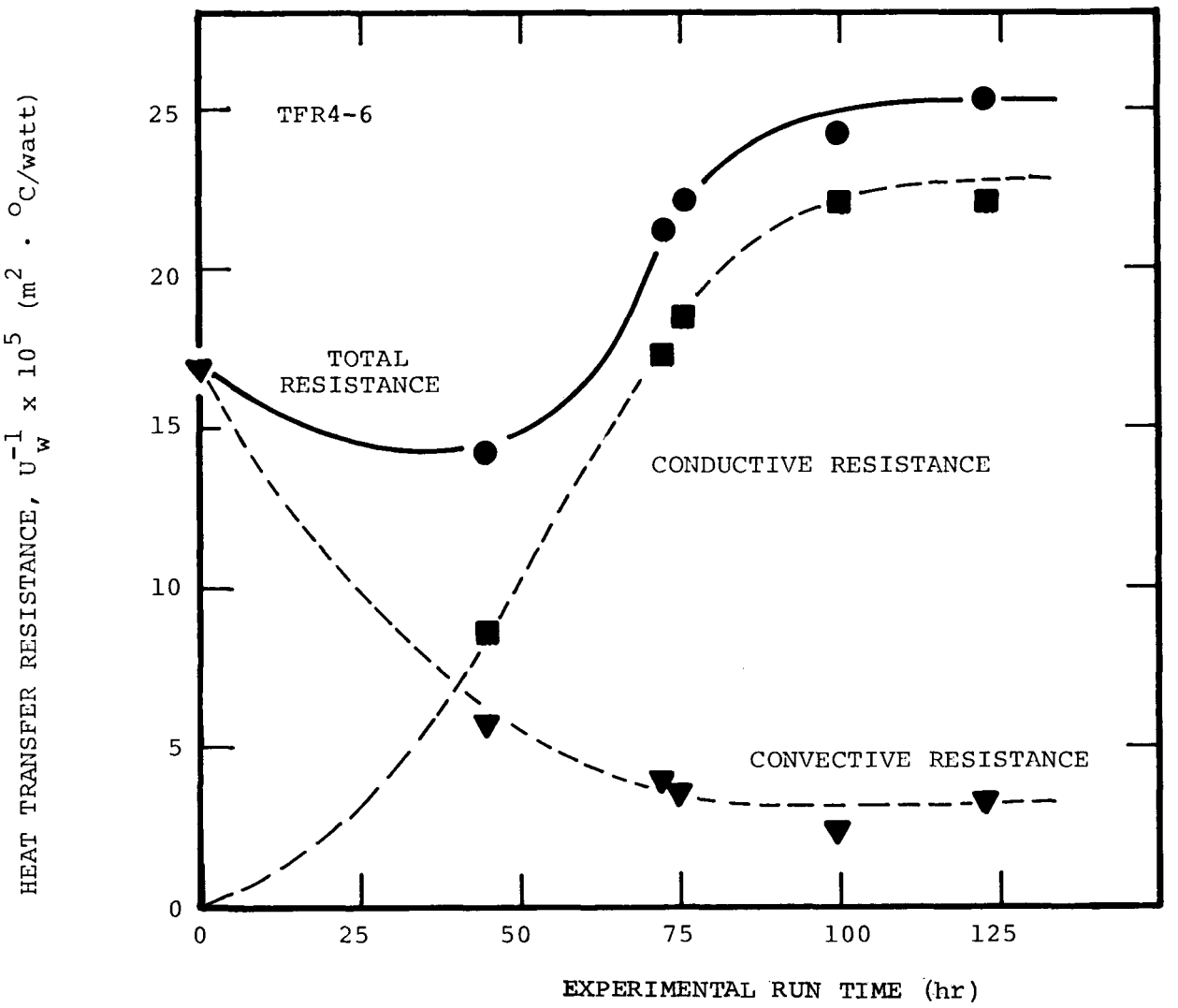

Figure 3-34. Change in heat transfer resistance due to biofilm development during a TFR4 experiment.

Effect of Wall Temperature on Biofilm Development

Experiments were conducted in TFR2 (T_b= 35°C) to determine the effect of wall temperature (T_w) on biofilm development rate (measured as R^*_{Th}) and extent of biofilm development (measured as Th_{MAX}). The results indicate that R^*_{Th} decreases significantly as T_w increases from 35°C to 49°C. The effect of T_w is greater when glucose loading rate is relatively high (Figure 3-35). Th_{MAX} also decreases with increasing wall temperature (Figure 3-36).

BIOFILM DESTRUCTION BY CHEMICAL METHODS

The destruction of biofilms by various chemical and physical techniques was studied in the TFR1, TFR2 and AFR systems. Physical methods of destruction were tested in TFR2 and included flow reversal, bulk temperature shock and surface temperature shock. Chemical destruction experiments with chlorine, chloramines, hydrogen peroxide and ozone were conducted in TFR1 and AFR. One chlorination experiment was conducted with a biofilm developed in the FTU at the P.H. Robinson field site.

Estimates of chemical consumption rates and film destruction rates were obtained. Chlorine demand (stoichiometric quantity) of biofilm was estimated by several techniques.

Chlorine

The reaction of chlorine with biofilm has been observed in laminar and turbulent flow in TFR1 and turbulent flow in the AFR. The rate processes observed are complex due to the variety of compounds present in the biofilm and mass transfer limitations in the biofilm. A summary of all the chlorination data is presented in Appendix P.

Rate of Chlorine Consumption by Biofilms. TFR1 was operated as a closed system for the turbulent flow experiments. For each experiment, chlorine was introduced as pulse injection, generally of equal magnitude. The reactor contents were recycled through the TFR1 at the same flow rate maintained during development of the biofilm; however, the fermenter was bypassed. This reactor configuration

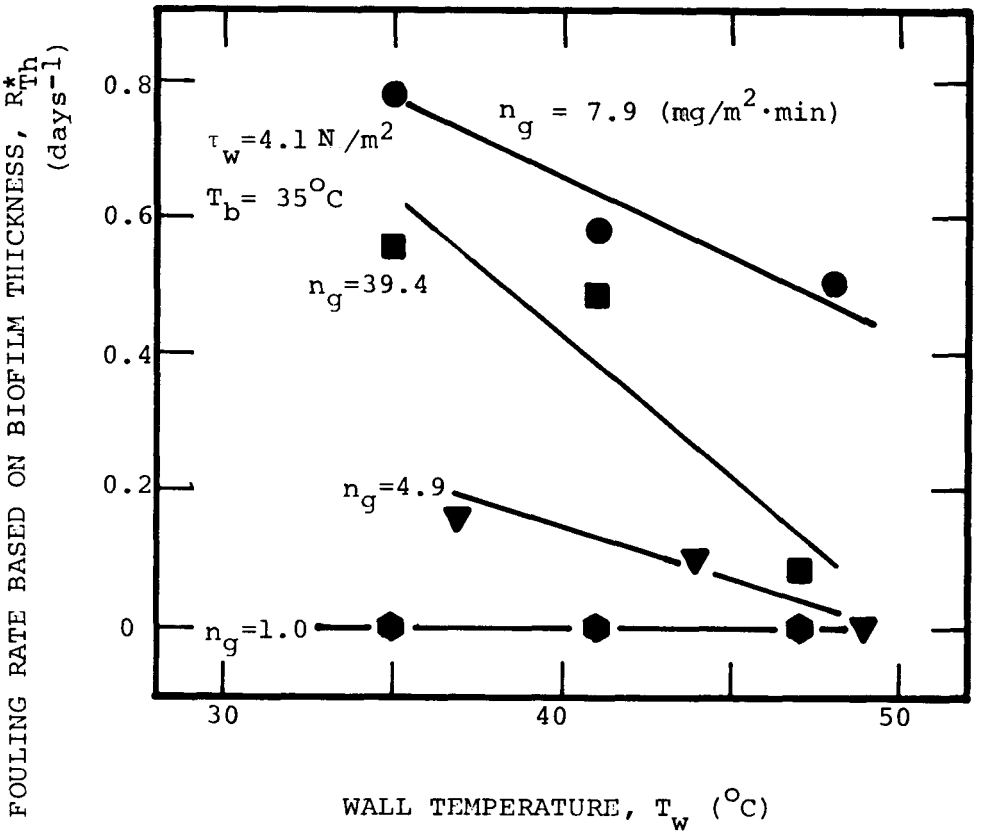

Figure 3-35. Effect of wall temperature and glucose loading rate on biofouling rate in TFR2.

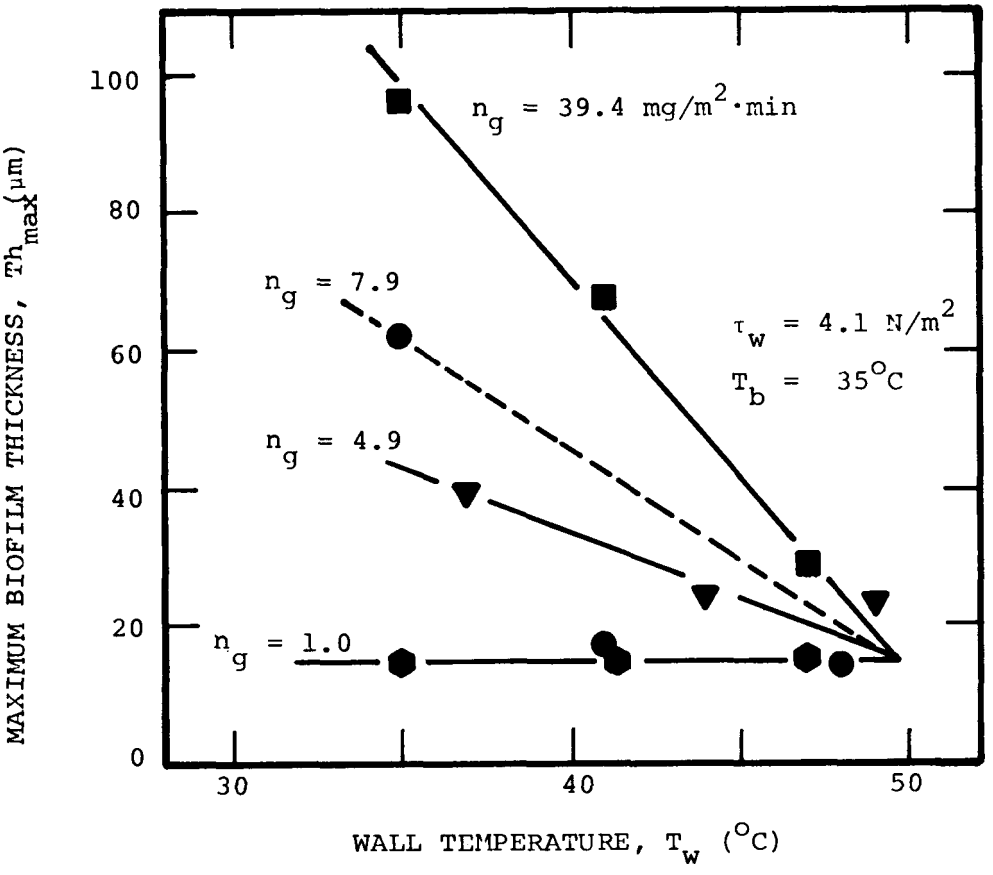

Figure 3-36. Effect of wall temperature and glucose loading rate on extent of fouling in TFR2.

is mathematically convenient because it is essentially a batch reactor.

Each input pulse resulted in a chlorine die-away characteristic of a first-order rate process (Figure 3-37). Therefore, chlorine consumption rate for each injection can be described by the following:

$$\frac{d\left[Cl_2\right]}{dt} = -K_c \left[Cl_2\right] \frac{A}{V} \qquad (3\text{-}32)$$

where Cl_2 = chlorine concentration (m/L^3)

K_c = first order rate constant (L/t)

V = reactor volume (L^3)

A = reactor surface area (L^3)

K_c has units of L/t, a surface reaction rate coefficient, because the consumption of chlorine is occurring at the reactor surfaces. Each successive injection during a given experiment resulted in a lower consumption rate, i.e., lower K_c. The "loss in reactivity" could provide information relating chlorine consumption and biofilm destruction. Since K_c was observed to decrease in a logarithmic manner with cumulative chlorine consumed by the biofilm (Figure 3-38),

$$K_c = K_o \exp\left[-K_d C_r\right] \qquad (3\text{-}33)$$

where C_r = cumulative chlorine reacted (m/L^2)

K_o = constant representing reactivity at $C_r = 0$ (L/t)

K_d = constant representing loss of reactivity (L^2/m)

Biofilm Destruction. The biofilm thickness measurement techniques used are not amenable for use during chlorination tests. Therefore, biofilm thickness data are restricted to before and after chlorination. However, biofilm destruction rates were indirectly monitored by pressure drop measurements in TFR experiments and by torque measurements in AFR tests. Figure 3-39 indicates the change in pressure drop in TFR1 as a function of chlorine reacted. Figure 3-40 illustrates the change in torque observed in the AFR as a function of

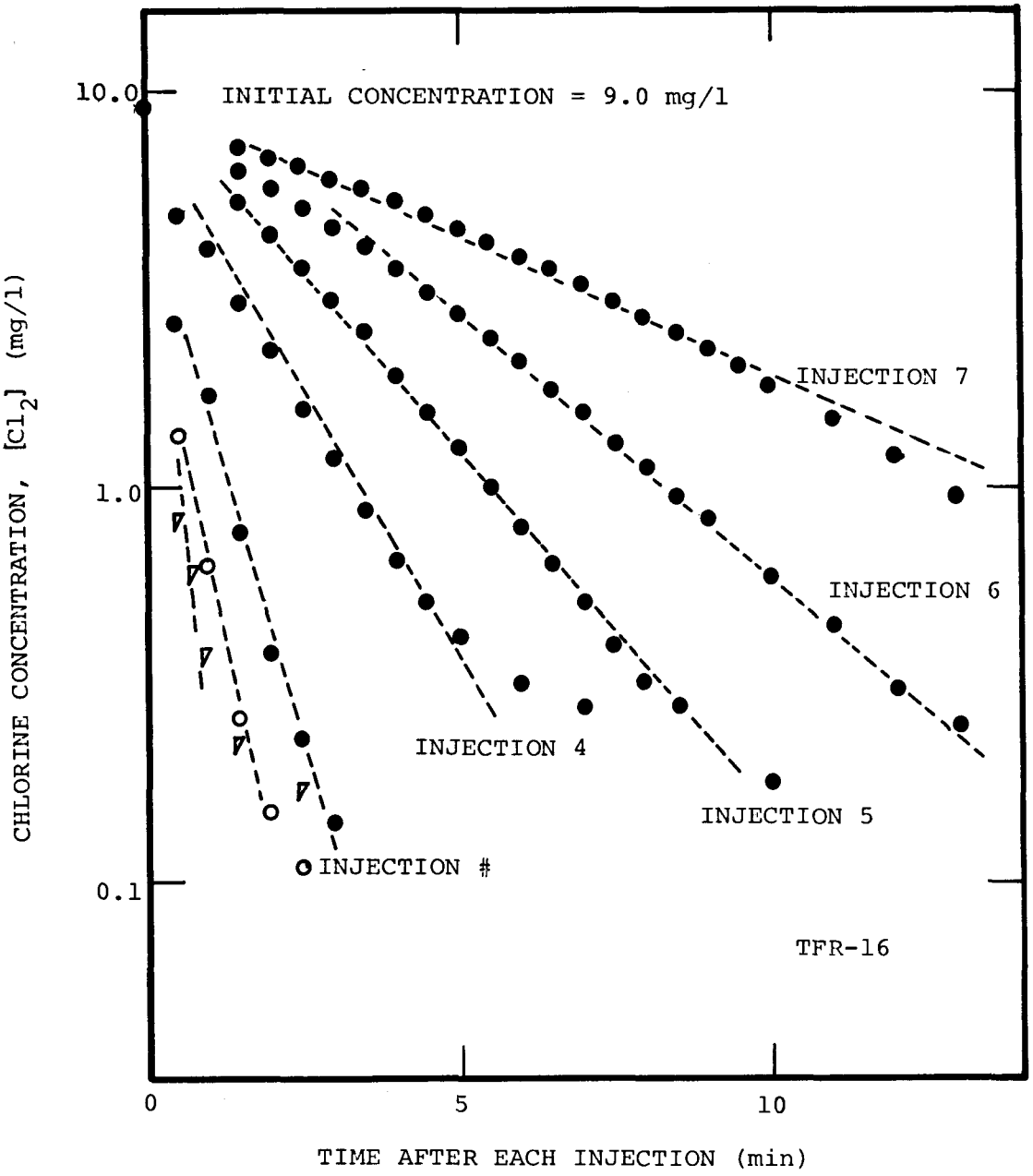

Figure 3-37. Chlorine decay for seven consecutive injections in TFR1-16.

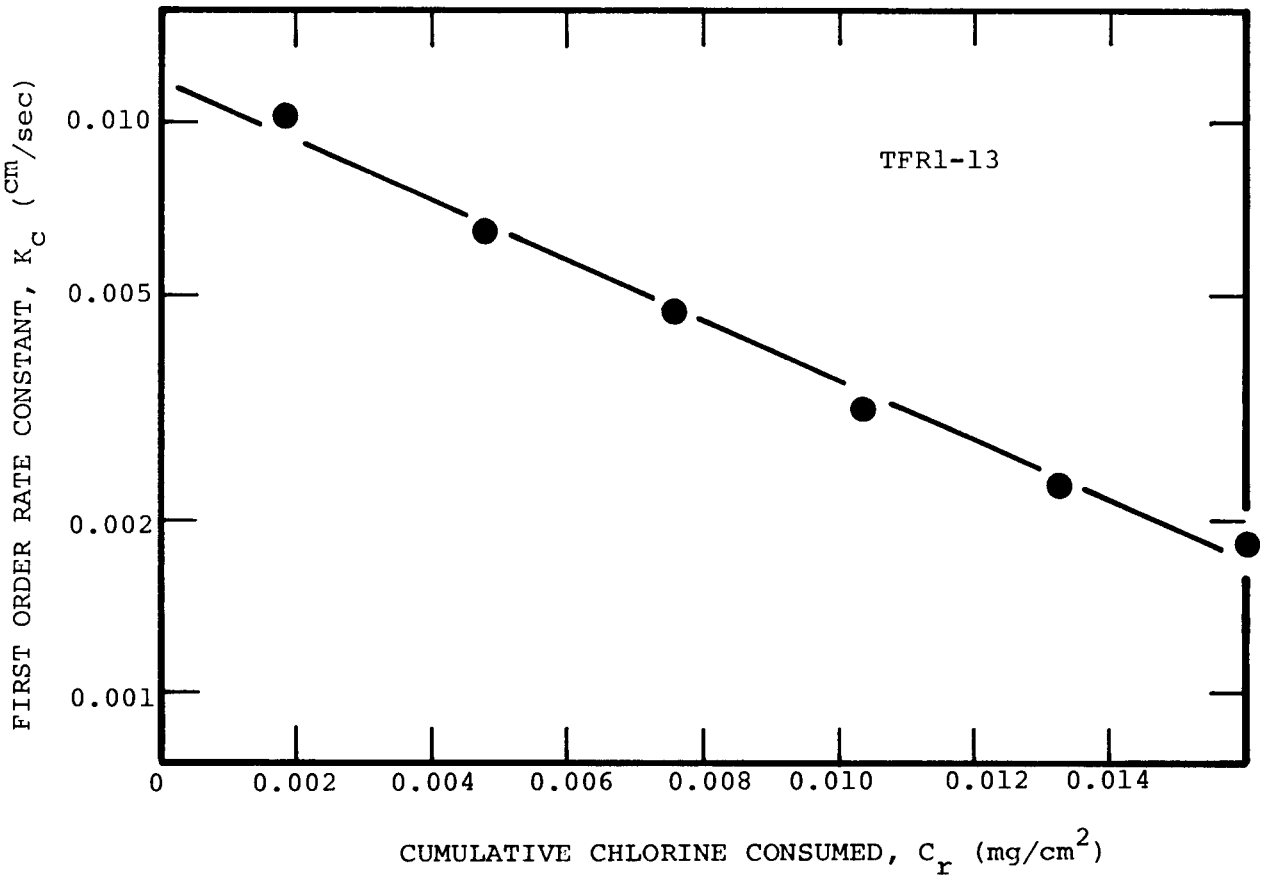

Figure 3-38. Decrease in the first order rate constant for chlorine decay (K_C) as a function of cumulative chlorine consumed by the biofilm (C_r).

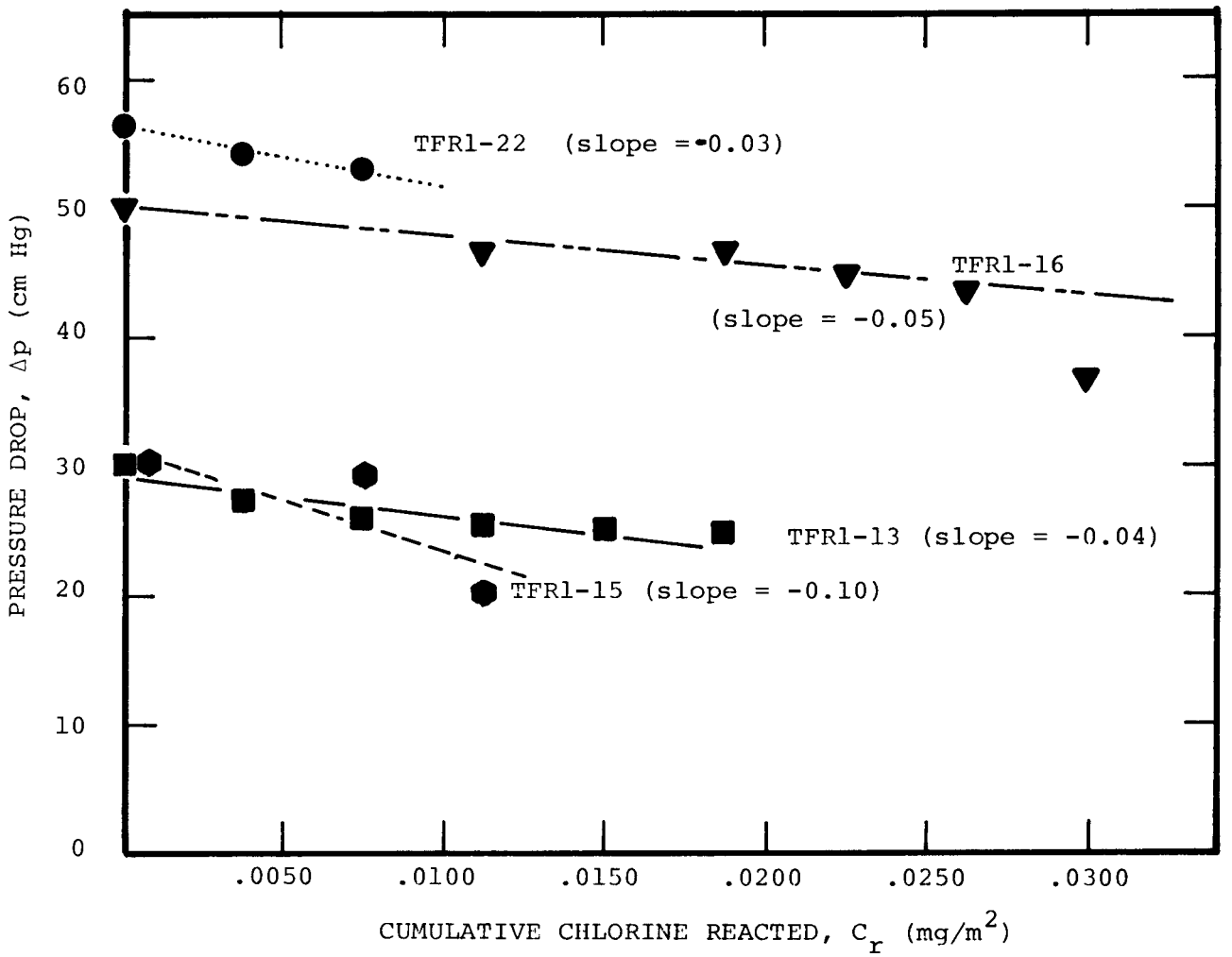

Figure 3-39. Change in pressure drop due to treatment of biofilm with chlorine in the TFR1. Slopes are calculated by regression and denote decrease in frictional resistance per unit chlorine reacted.

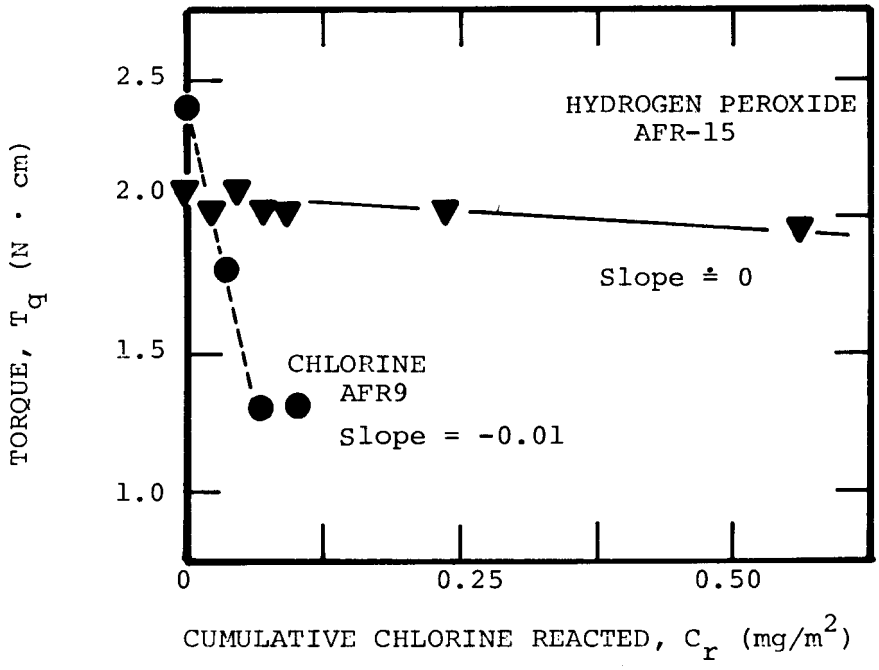

Figure 3-40. Change in torque due to treatment of biofilm with chlorine and hydrogen peroxide in the AFR. Slopes are calculated by linear regression and denote decrease in frictional resistance per unit oxidant reacted.

chlorine or hydrogen peroxide reacted.

Biofilm destruction due to chlorine addition is obviously occurring. Figure 3-41 illustrates the increase in organic carbon concentration in the AFR effluent subsequent to the addition of chlorine. Organic carbon increased from 1 mg/l prior to treatment to 6.5 mg/l before decreasing to 3 mg/l after approximately 45 minutes. Volumetric flow rate during this experiment was 57 cm^3/min. The increase in effluent organic carbon concentration reflects a removal of approximately 8.6 mg organic carbon or 45.3 mg of biofilm (based on a biofilm which is 19 wt% carbon). Similar results were obtained using effluent turbidity instead of effluent organic carbon concentration (Figure 3-42), indicating a change in suspended particulates as a result of chlorine addition. These results compare favorably with previous research efforts (15, 16).

Effectiveness of biofilm destruction can be evaluated by the difference in biofilm thickness before and after chlorination. The results indicate that biofilm thickness change due to chlorine addition is strongly dependent on the biofilm thickness prior to chlorine addition. These results compare favorably with other research (15) and are presented together in Figure 3-43.

Biofilm Regrowth Subsequent to Chlorination. Laboratory biofilms have been exposed to extremely severe treatments including combined strong acid, strong base and strong chlorine solutions. Microscope inspection subsequent to the treatments frequently indicates that some organic material and microbial cells remain attached to the surface. This is especially true when the film is of a filamentous nature. The remaining cellular material provides an inoculum for regrowth of the biofilm. Quantitative data regarding regrowth rates subsequent to chlorination were obtained by Norrman (15) and are presented in Table 3-9. It is hypothesized that the amount of remaining cellular material strongly influences regrowth rates but more data is necessary for corroboration.

Figure 4-14 indicates the increase in biofouling rate subsequent to chlorine treatment at the Deepwater field site.

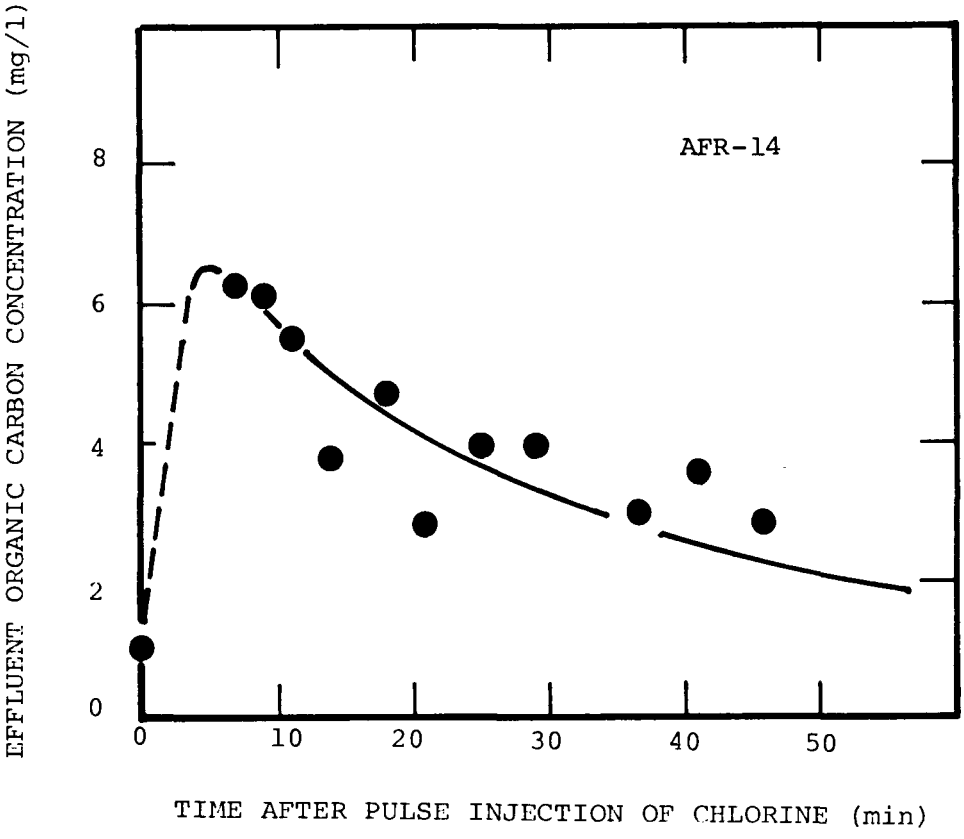

Figure 3-41. Increase in effluent organic carbon concentration due to biofilm sloughing subsequent to chlorine injection in the AFR.

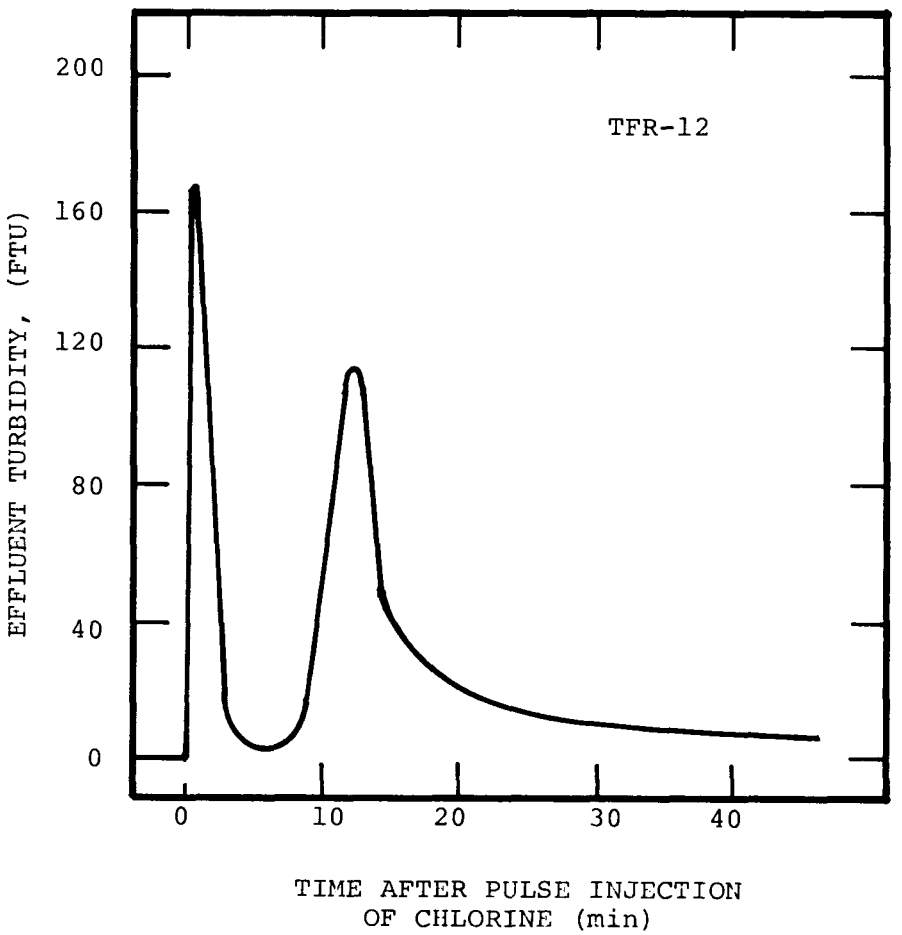

Figure 3-42. Change in effluent turbidity caused by a pulse injection in the TFR which contained a biofilm. The curve is reproduced from a recorder trace.

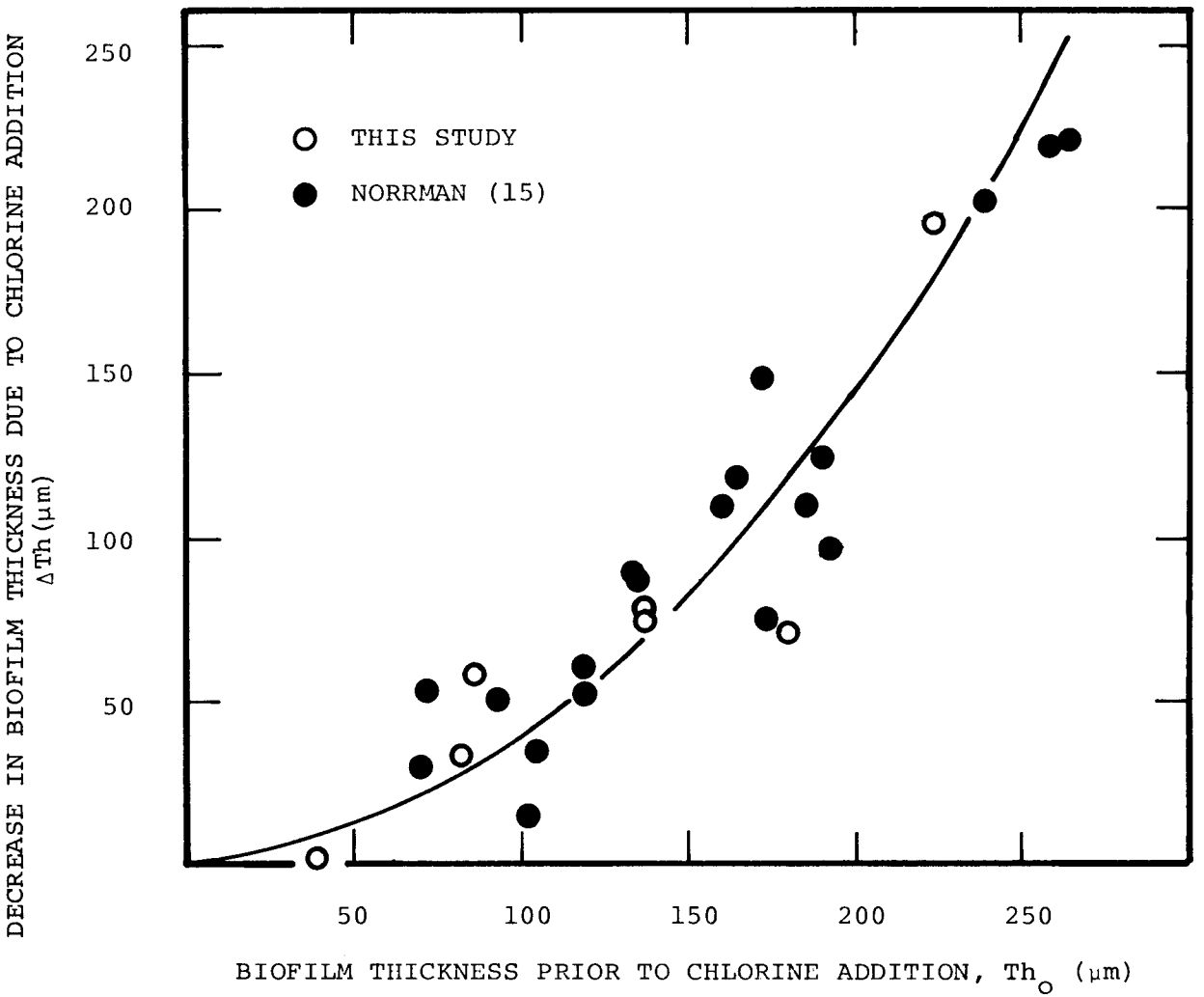

Figure 3-43. Effect of initial biofilm thickness on decrease in biofilm thickness during chlorine treatment.

Table 3-9

COMPARISON OF BIOFOULING FILM GROWTH RATES (R^*_{Th}) ON A CLEAN SURFACE AND AFTER REPEATED CHLORINE APPLICATIONS (15)

Expt. No.	τ_w (N/m^2)	Growth Rate, R^*_{Th} (days $^{-1}$)				Cl_2 (mg/l) [2]
		R^*_{Th} Initial Growth	R^*_{Th} after Chlorine Applications			
			First	Second	Third	
2	7.2	0.060	0.317	0.204	0.235	12.0
2	3.5	0.113	0.355	0.355	--	12.0
3	7.2	0.279	0.45[1]	0.65[1]	--	11.0

[1] Calculated from two measurements

[2] Feed concentration applied for 30 minutes

Table 3-10

STOICHIOMETRIC CHLORINE DEMAND OF BIOFILM

Expt. No.	C_r, Cumulative Chlorine consumed ($mg/cm^2 \times 10^4$)	ρ_{Th} Volumetric Film Density (mg/cm^3)	Initial Film Thickness (cm x 10^4)	Chlorine Demand (mg/mg)
TFR-12	170.4	19.4	137	0.06
TFR-22	223.9	13.9	138	0.12
Batch Test	--	--	--	0.31

Stoichiometric Chlorine Requirement of Biofilm. The chlorine demand of biofilm was determined in two ways. In the first, a sample of biofilm was scraped from a tube, blended and added to a chlorine solution of known concentration. The final steady chlorine concentration was used to determine the chlorine demand by the film material. The second method utilized the kinetic data from the multiple injection experiments. When the rate of chlorine decay for a particular injection became negligible, the cumulative chlorine consumed (C_r) equalled the chlorine demand of the biofilm. The calculation is as follows:

$$\text{Chlorine demand} = (C_r) \cdot (TH) / \rho_f \qquad (3\text{-}34)$$

Results indicate the chlorine demand lies between 0.06 and 0.31 mg chlorine/mg biofilm (Table 3.10). The chlorine demand will depend to a large extent on the composition of extracellular matrix and the organisms in the film.

Alternative Chemicals

Biofilm destruction tests were conducted using chloramines, hydrogen peroxide and ozone. The data summary for all experiments is presented in Appendix P. Oxidant consumption rates were measured the same way as chlorine consumption rates and resulted in similar oxidant decay functions but with different rate constants. Despite a very limited number of experiments, an attempt was made to evaluate the relative biofilm destruction efficiencies of the oxidants. Figures 3-44 and 3-45 illustrate the progression of experiments with chlorine and hydrogen peroxide, respectively. By plotting the pressure drop (TFR) or torque (AFR) versus cumulative oxidant consumed, a measure of the oxidant effectiveness can be determined (Figures 3-39 and 3-40). Table 3-11 lists the relative effectiveness for the oxidants tested.

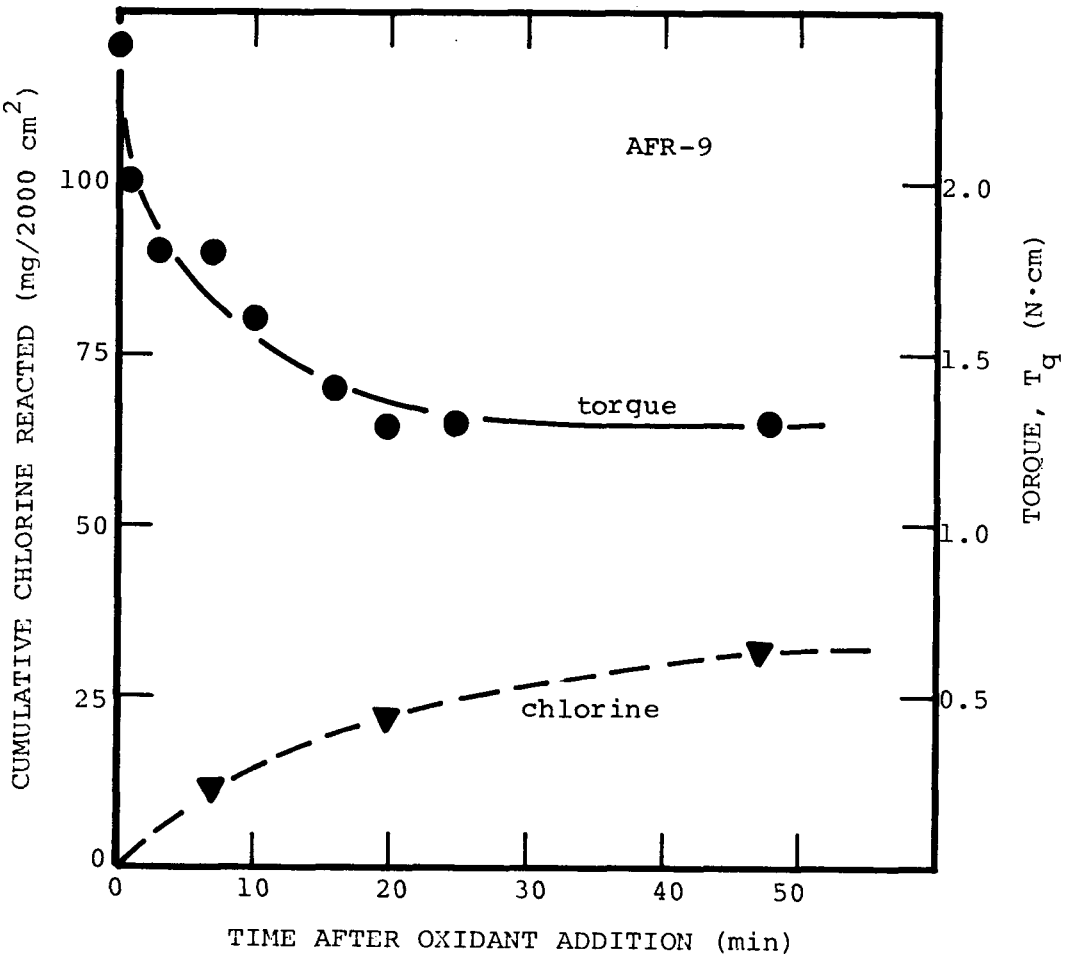

Figure 3-44. Biofilm destruction with chlorine in the AFR. Film thickness prior to chlorine addition was 70 μm.

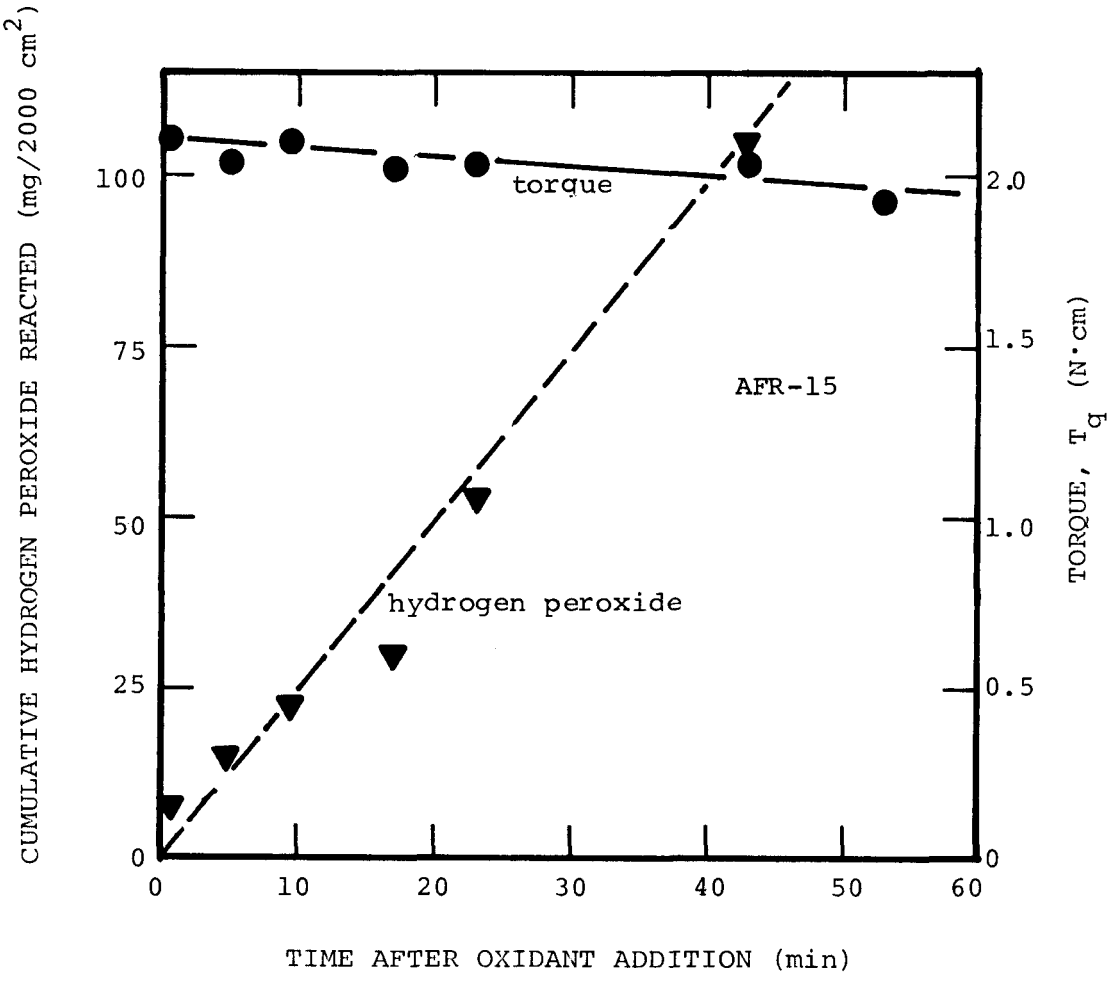

Figure 3-45. Biofilm destruction with hydrogen peroxide in the AFR. Film thickness prior to H_2O_2 addition was 60 μm.

Table 3-11

RELATIVE BIOFILM DESTRUCTION EFFECTIVENESS OF CHEMICAL OXIDANTS

Oxidant	Test System	Reduction in Frictional Resistance Per Unit Oxidant Consumed * (cm^2/g)
Chlorine	TFR1	20-80
Ozone	TFR1	
Chlorine	AFR	20
Hydrogen Peroxide	AFR	0.3

* See Figures 3-44 and 3-45

BIOFILM DESTRUCTION BY PHYSICAL METHODS

The physical stress experiments were conducted in TFR2. The apparatus provided for flow reversal, bulk temperature shock and surface temperature shock on biofilms.

Treatment Methods

Flow Reversal. During treatment periods, the fermenter contents of TFR2 were pumped only through the flow reversal loop and the other two tubular reactor sections were bypassed. Overall fluid frictional resistance decreased when using this procedure because overall tube length decreased. Therefore, flow rate in the flow reversal loop increased. The increase was from 6.5 - 8.2 ft/sec in low glucose loading experiments and 4.7 - 8.2 ft/sec in high glucose loading experiments.

Bulk Temperature Shock. Normal flow to this tubular reactor was stopped during treatment and hot tap water was passed through the tube at flow rates comparable to those prior to treatment. Bulk water temperature decreased linearly from an initial temperature of

60°C to 40°C in 20 minutes and then remained constant for the remaining time of treatment. The temperature decrease was due to the limited capacity of the water heater being used.

Surface Temperature Shock. Flow to this tubular reactor was stopped for treatment and the tube wall temperature was increased by means of heating tape. The surface temperature was controlled by a thermister located in the bulk fluid. After treatment, normal flow was resumed for five minutes and then pressure drop recorded. Flow was stopped again at this point to obtain samples for biofilm thickness measurement.

Biofilm Removal

The effect of such treatment application on biofilm removal was assessed by calculating percent removal, i.e., $(Th_o-Th)/Th_o \times 100)$. The data are presented in Table 3-12. It is important to note, however, that treatment effectiveness is strongly dependent on film thickness prior to treatment (Figure 3-46) as was observed with chlorine treatment. Using this criterion, bulk temperature shock was the most effective treatment within the range of our experimentation. Flow reversal ranked second, and surface temperature shock a distant third. No direct effect of glucose feed concentration was observed on bulk temperature shock treatment.

Flow reversal effectiveness was due primarily to disturbance of the biofilm by fluid shear stress. No enhancement of flow reversal treatment due to treatment duration was observed. The effect of substrate feed concentration, which directly influenced initial biofilm thickness (Th_o), was significant. Mean Th_o at 20 mg/l was 100 μm and between 272-427 μm at 100 mg/l. The effect of Th_o on treatment effectiveness has been noted in Figure 3-46.

Inhibition of Subsequent Biofilm Development

The effectiveness of each treatment was also evaluated by comparing the growth rate based on biofilm thickness before and after treatment. An illustration of the analysis is presented in Figures 3-47a and b for experiments TFR2-6b and TFR2-8b employing bulk temperature shock.

Table 3-12

THE EFFECT OF PHYSICAL STRESS TREATMENT ON BIOFOULING FILM THICKNESS
DATA INDICATE % DECREASE IN THICKNESS DUE TO TREATMENT OF VARYING DURATION ON BIOFILMS DEVELOPED AT 20 AND 100 MG/L SUBSTRATE FEED CONCENTRATIONS.

	% DECREASE IN BIOFILM THICKNESS			
Duration:	30 Minute Treatment		60 Minute	120 Minute
S_i:	20 mg/l	100 mg/l	100 mg/l	100 mg/l
Flow Reversal	4 ± 55 (4)*	69 ± 7 (3)	59 ± 32 (3)	47 ± 25 (3)
Bulk Temperature Shock	60 ± 25 (4)	77 ± 5 (3)	91 ± 5 (3)	89 ± 13 (3)
Surface Temperature	3	-12 ± 12 (2)	6 ± 66 (3)	15 ± 29 (3)

*mean value ± standard deviation (number of data points)

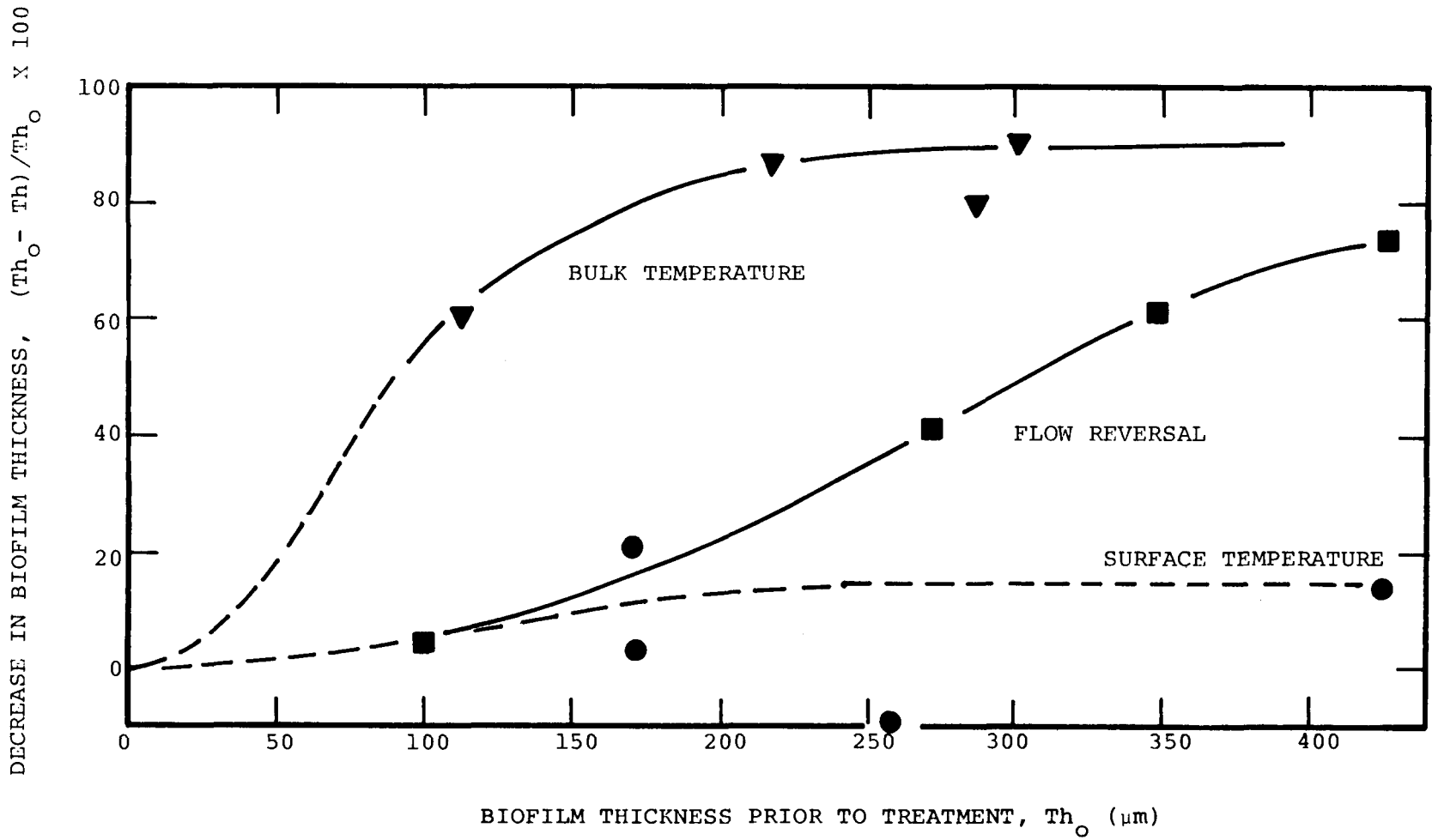

Figure 3-46. Effect of biofilm thickness prior to treatment on effectiveness of treatment.

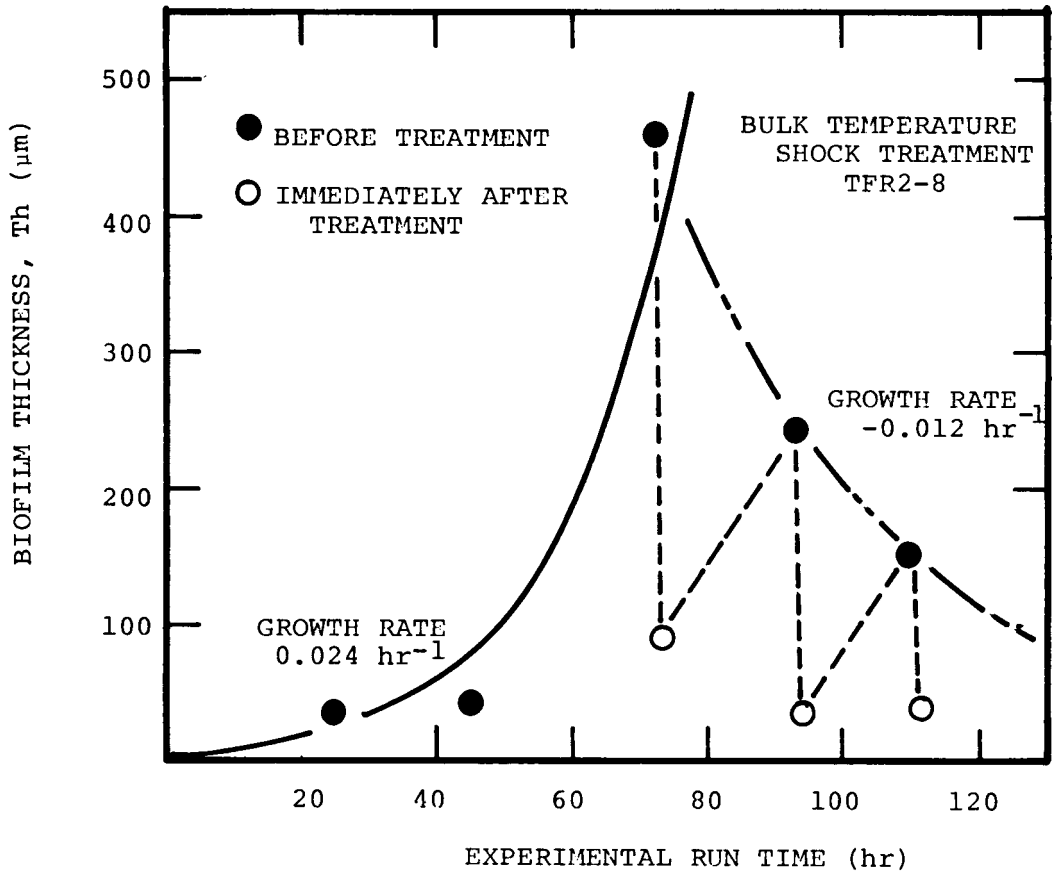

Figure 3-47a. The effect of bulk temperature shock on biofilm development rate.

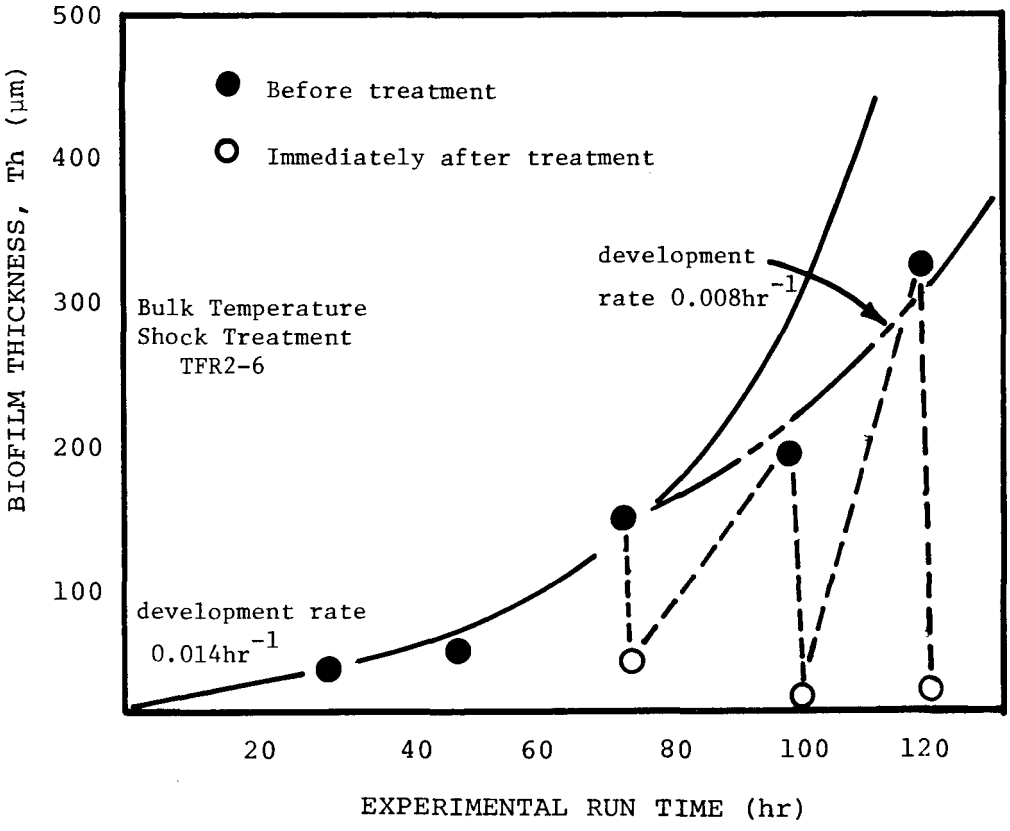

Figure 3-47b. Effect of bulk temperature shock on biofilm development rate.

Periodic treatment was initiated in TFR2-6b at 72 hours and TFR2-8b at 74 hours. The data indicate growth prior to treatment, projected growth rate for no treatment and growth rate after treatment. If there were no treatment, biofilm thickness would stabilize at approximately 300 and 500 μm for the 20 and 100 mg/l substrate experiments, respectively. The data for all experiments are summarized in Figure 3-48 and indicate that bulk temperature shock is the most effective treatment based on this criterion also.

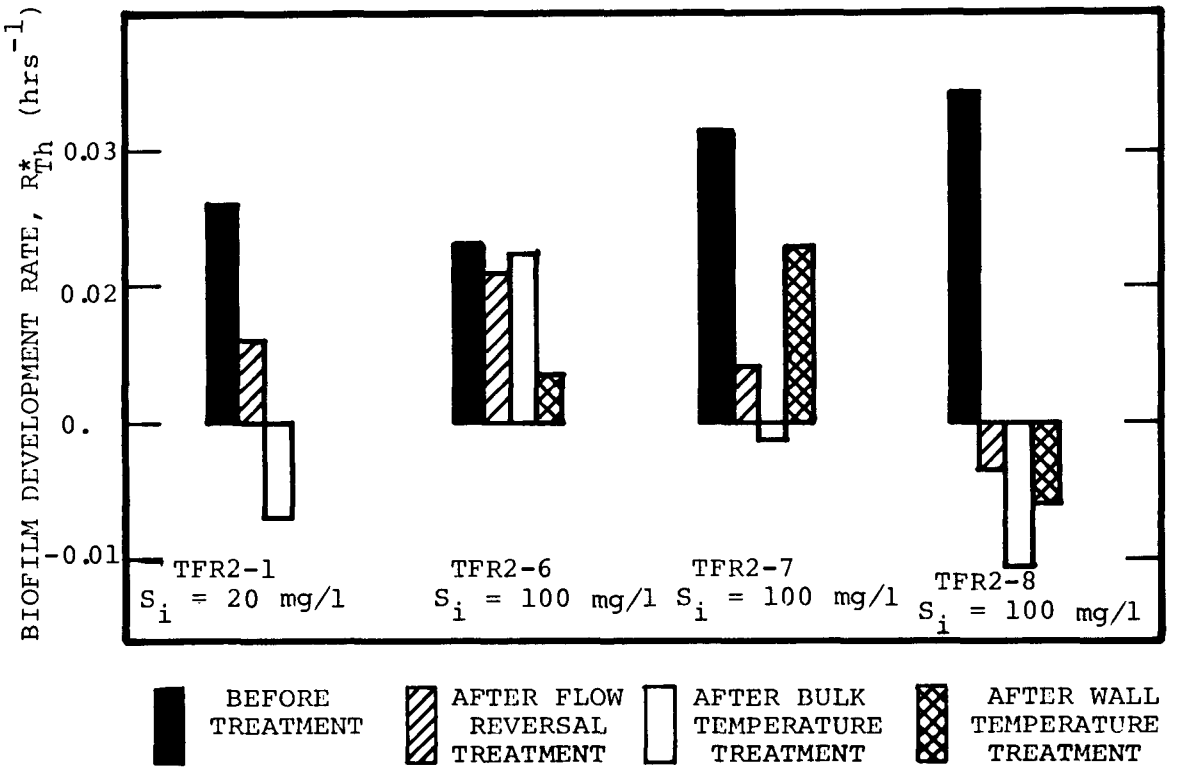

Figure 3-48. The effect of physical stress on biofilm development rate at different glucose loading rates.

Section 4

DISCUSSION

PROPERTIES OF BIOFILMS

Biofilm properties are a function of the microorganisms which colonize the surface and the microorganisms which are active in the film at any time. Biofilm characteristics are also dependent on the environment to which the attachment surface is exposed. Techniques for measurement of biofilm properties also vary between investigators and add to the variation in reported values.

Biofilm Dry Mass Density

Biofilm dry mass density (ρ_{Th})* is affected by shear stress (τ_w) at the wall and glucose loading rate. Indications from TFR experiments suggest that an increase in bulk temperature will also increase ρ_{Th}, but no conclusive data is available. The increase in ρ_{Th} with increasing τ_w suggests one of the following mechanisms:

1. selective attachment of only certain microbial species from the available population
2. microorganism response to environmental stress
3. pressure forces "squeeze" loosely bound water from the biofilm.

Chemical Properties

Inorganic composition of biofilms will undoubtedly vary with the chemical composition of the bulk water. Calcium, magnesium and iron affect intermolecular bonding of biofilm polymers which are partially responsible for the structural integrity of the deposit. For example, treatment with chelants (e.g., EDTA) has caused partial removal of biofilm (see Appendix W). In power plant condensers, corro-

*Notation and symbols are defined in the Notation Section

sion products and inert suspended solids which become embedded in the biofilm may influence the chemical composition of the deposit.

This research was accomplished with glucose as the sole energy source in a carbon-limited growth system. Changes in limiting nutrient, carbon source or energy source can significantly affect the microbial species distribution in the biofilm, as well as the extracellular polymer composition that is so important to the biofilm structure.

Biological Properties

The organisms which colonize the attachment surface will strongly influence biofilm development rate and biofilm properties. A standard inoculum was used in these studies to minimize effects of initial population diversity. However, organism-organism and organism-environment interactions undoubtedly shifted population distributions during an experiment. Of prime concern is the filamentous nature of the biofilm. At low τ_w and low glucose loading rate (n_g) the biofilm exhibited characteristic filaments which were not evident in experiments at high n_g (in the AFR). It is not known whether the organisms developed in a morphologically different manner, perhaps due to increased nutrient availability at higher n_g, or whether other organisms were dominant. The filamentous forms were also observed in field experiments conducted at the P. H. Robinson field site where flow velocities of 5-7 ft/sec were tested.

The observed change in morphology may be the determining factor influencing biofilm dry mass density which increases with increasing τ_w as indicated in Figures 3-1 and 3-2.

DEVELOPMENT OF BIOFILMS

The process of biofilm development on a glass surface due to consumption of a soluble nutrient is adequately described by a sigmoidal-shaped curve which is divided into three regions for convenience of analysis: (1) induction, (2) growth, and (3) plateau. This curve (Figure 4-1) describes the progression of frictional resistance and

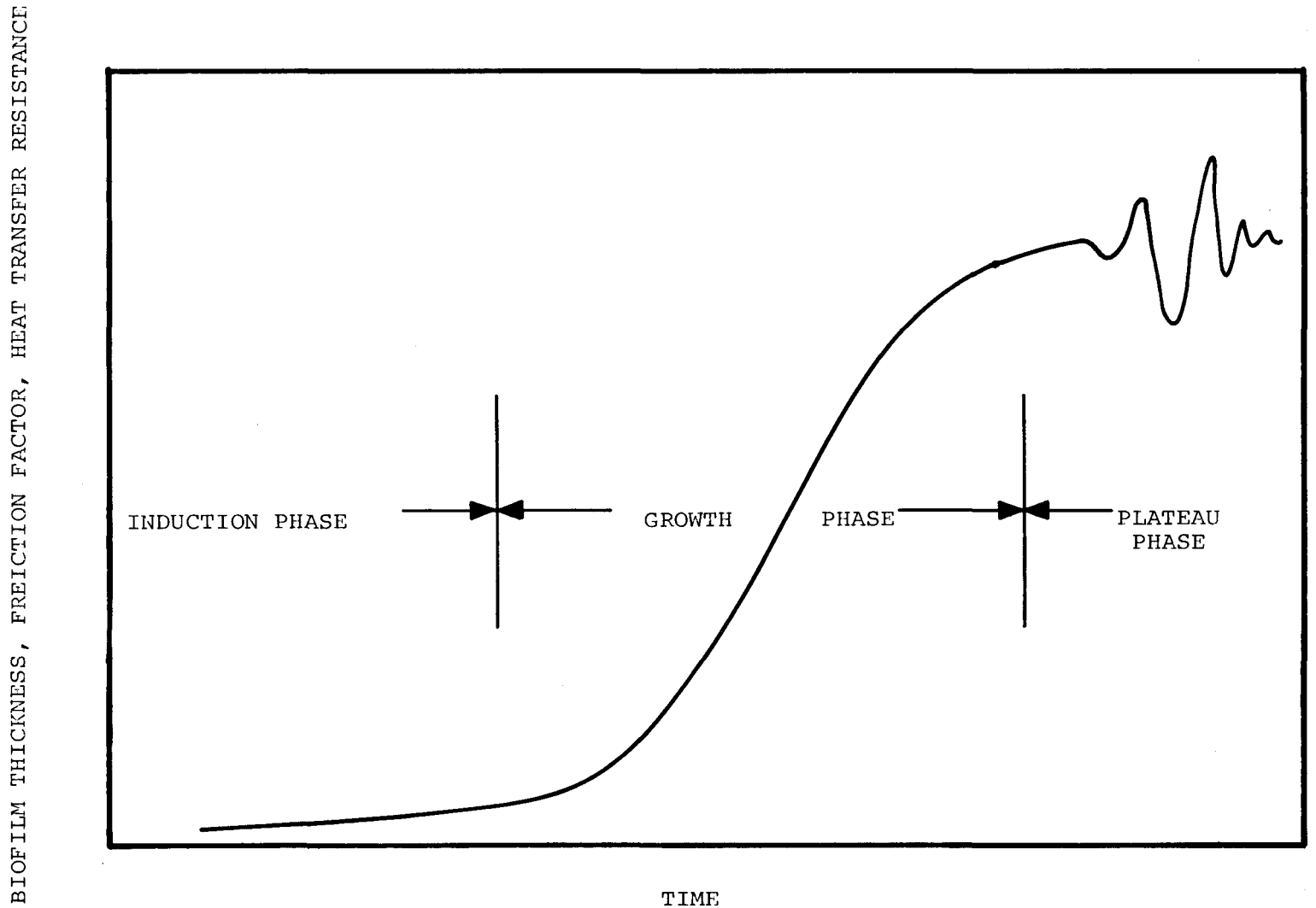

Figure 4-1. Progression of a Typical Biofouling Experiment

heat transfer resistance also. It is assumed that the only suspended solids present are those produced by microbial activity (i.e., volatile solids).

Induction Phase

Previous researchers have indicated that the length of the "induction" period is a function of the attachment surface roughness and composition (8). Quantitative observations of these effects were beyond the scope of this project. It has been noted, however, that the length of the induction period increases with decreasing nutrient loading rates. The accelerated surface activity at high nutrient loading rates could result from the chemical conditioning of the surface. Because of increased number of microbial particles (individual cells or flocs) resulting from high nutrient loading rate, the flux of particles to the attachment surface could also be enhanced. Proteinaceous material, such as found in the TSB portion of the nutrient, has a high surface activity and would be expected to adsorb rather quickly (23,24). The influence of the initial adsorbed films can differentially immobilize boundary layers of liquid approaching 100 μm (25) even on clean heat exchange surfaces. The influence of such a film would be to decrease convective heat transfer in the initial stages of exposure, an observation made during the THE experiments. The particle properties indicate that their transport to the attachment surface is by inertial deposition (26) and that transport rate increases with increasing particle concentration. Particle attachment, however, will be a function of the characteristics of the particle surface and the attachment surface, i.e., "stickiness."

Growth Phase

Biofilm Development. The rate of development in the growth phase (R^*_{Th}) can be dependent on glucose loading rate (n_g), wall surface temperature (T_w), bulk temperature (T_b), and wall shear stress (τ_w). The following have been observed in this study:

1. Logarithmic fouling rate based on biofilm thickness (R^*_{Th}) increases with glucose loading rate (n_g) up to

some saturating flux (approximately 65 mg/m^2-min). Glucose removal rate (R") also increases with increasing n_g up to some saturation value, as expected.

2. Increasing wall temperature (T_w) beyond 35°C decreases logarithmic fouling rate (R^*_{Th}).

3. No significant effect on R^*_{Th} was observed due to change in bulk temperature (T_b) (between 30-40°C). However, this result may be due to a suspected optimum temperature of 35°C for R^*_{Th} which made R^*_{Th} relatively insensitive in the temperature range studied. Bongers et al. (30) observed an increase in R^*_{BM} of 2.5x when temperature increased from 21 to 31°C during a field study at a power plant.

4. Increasing τ_w increases R" and therefore, increases total biomass production rate (r) which may increase R^*_{Th}. However, increasing τ_w can also increase sloughing rate which will decrease R^*_{Th}. A maximum fouling rate can be observed as illustrated in Figure 4-13.

Glucose Removal. The effects of biofilm thickness, mass transfer limitations and dissolved oxygen concentration on glucose removal have been investigated with the following results:

1. Glucose removal increases with biofilm thickness until an active thickness is reached during a given experiment.

2. Glucose removal decreases at low flow velocities past the biofilm surface.

3. Glucose removal is constant over a wide range of dissolved oxygen concentrations (2.5-15 mg/l).

Glucose removal has been shown to be diffusion-limited in biofilm reactor systems. Glucose removal is directly proportional to film thickness only up to an active thickness (Th_A) corresponding to the depth of glucose penetration into the biofilm (2,22,12). After an active thickness is reached, glucose removal becomes zero order with respect to biofilm thickness. Active thickness increases with influent glucose concentration, a result also observed by others (12).

Glucose removal in this study has been shown to be dependent on the rate of flow past the biofilm surface. Other work (2,27) also indicates that glucose removal increases with rotational or mixing speed

in a fixed biofilm, continuous flow, annular reactor. The mass transfer limitation at the reduced flow velocities is due to an increase in the viscous sublayer (δ_1) with the consequent reduction in the concentration gradient necessary for diffusion of substrate.

Glucose removal has been shown to be independent of dissolved oxygen concentration (2.5-15 mg/l) in experiments conducted by others in a continuous flow annular reactor (2). Other investigations of the effect of oxygen concentration on biofilm systems also indicate dissolved oxygen is not a rate limiting factor (28). Results from TFR3 indicate glucose removal is zero order with respect to dissolved oxygen concentration between 2.5 and 15 mg/l (see Appendix Q).

Model for Biofilm Development. The development of a model describing biofilm development has been summarized in Table 3-6 and is based on fundamental material balances for glucose and biomass in the reactors. Results based on the model are compared to experimental results in Figure 4-2. The model for biofilm production does not include the effects of temperature or shear stress. All parameters used in developing the model came from TFR3 experiments conducted between 30-35°C with a fluid shear stress of 6.5 to 7.9 N/m^2.

The model results would be greatly improved by more data on sloughing rates during an experiment. In addition, better predictions of Th_{MAX} are necessary to improve the accuracy of the model.

Plateau Phase

The plateau phase has been characterized by the maximum biofilm thickness (Th_{MAX}). Th_{MAX} is strongly dependent on shear stress and glucose loading rate to a lesser extent in low shear stress (τ_w < 3.0 N/m^2) experiments. Th_{MAX} is strongly dependent on glucose loading rate and less dependent on shear stress when τ_w > 3.0 N/m^2. Shear stress equal to 3.0 N/m^2 corresponds to an average flow velocity of 3 ft/sec. Consequently, in condensers with higher flow velocities the maximum thickness would be dependent primarily on nutrient loading rate.

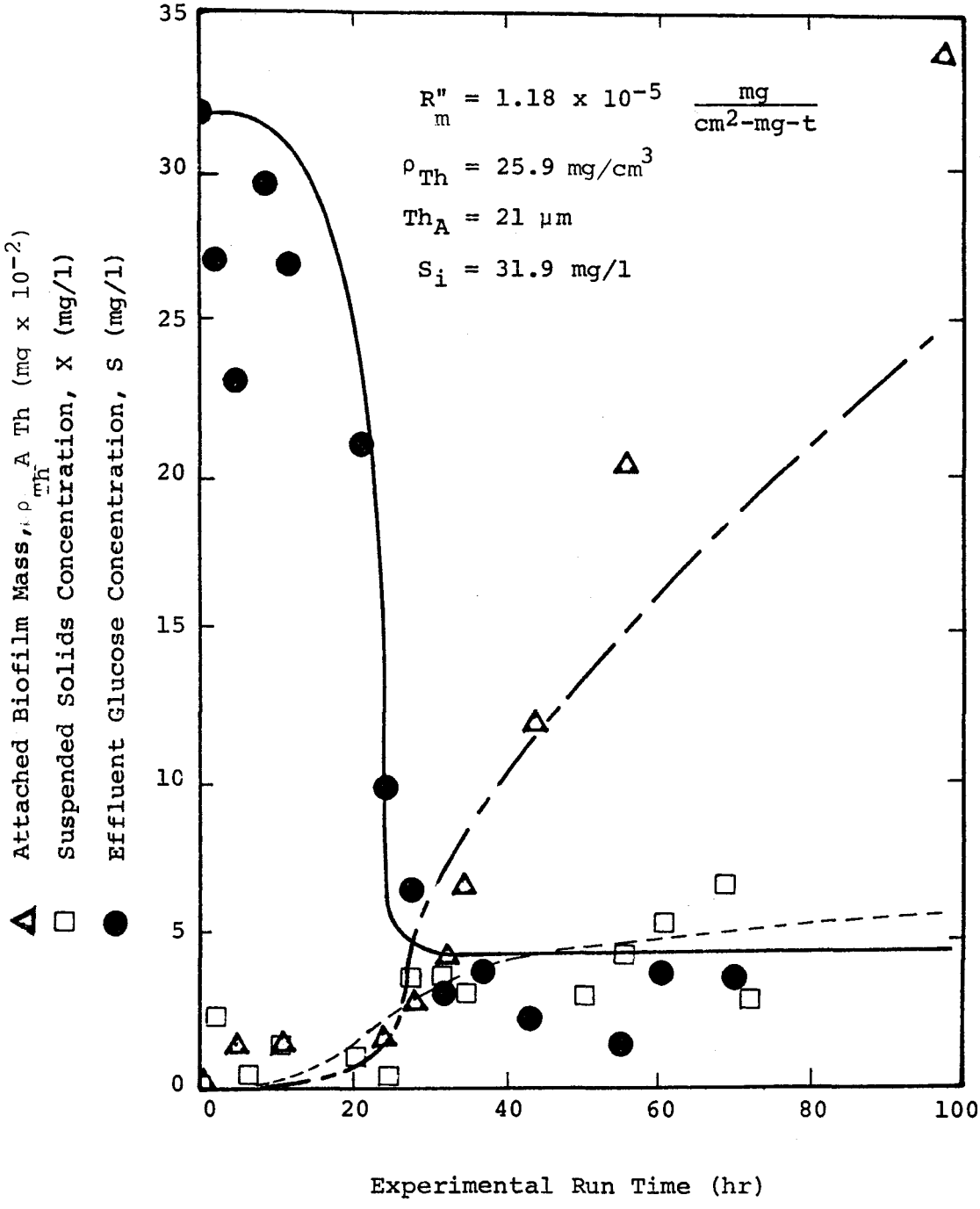

Figure 4-2. Biofilm production model and experimental data from TFR3-5.

The plateau is not necessarily a stable phase. Changes in the biofilm caused by sloughing or changes in morphology (e.g., predominance of filamentous organisms) caused oscillations in biofilm thickness at plateau.

FRICTIONAL RESISTANCE

The results indicate frictional resistance due to biofilm accumulation can be substantial; the following mechanisms explaining this pronounced frictional resistance have been investigated:

1. A constriction in the tube due to biofilm accumulation.
2. An increase in fluid viscosity.
3. Transport of biofilm in the direction of flow.
4. An increase in roughness of the tube surface due to biofilm accumulation.
5. Energy dissipation in the biofilm due to its viscoelastic nature.
6. Energy dissipation due to the presence of filaments in the biofilm.

Pressure Drop Due to Tube Constriction

Constriction of the tube due to biofilm accumulation cannot, alone, account for the increase in frictional resistance as illustrated in Figure 4-3. The following are indicated in Figure 4-3:

1. The increase in pressure drop and biofilm thickness with time for TFR1-12.
2. The increase in pressure drop for a decrease in radius equivalent to the measured biofilm thickness as calculated from the Blasius equation for a smooth tube:

$$f = \frac{0.316}{(dv_m/\nu)^{0.25}} \qquad (4\text{-}1)$$

Constriction of the tube accounts for an approximate 10% increase in pressure drop whereas pressure drop due to biofilm accumulation increases approximately 110%. Clearly, the effect of a reduction in tube diameter by biofilm accumulation is minimal.

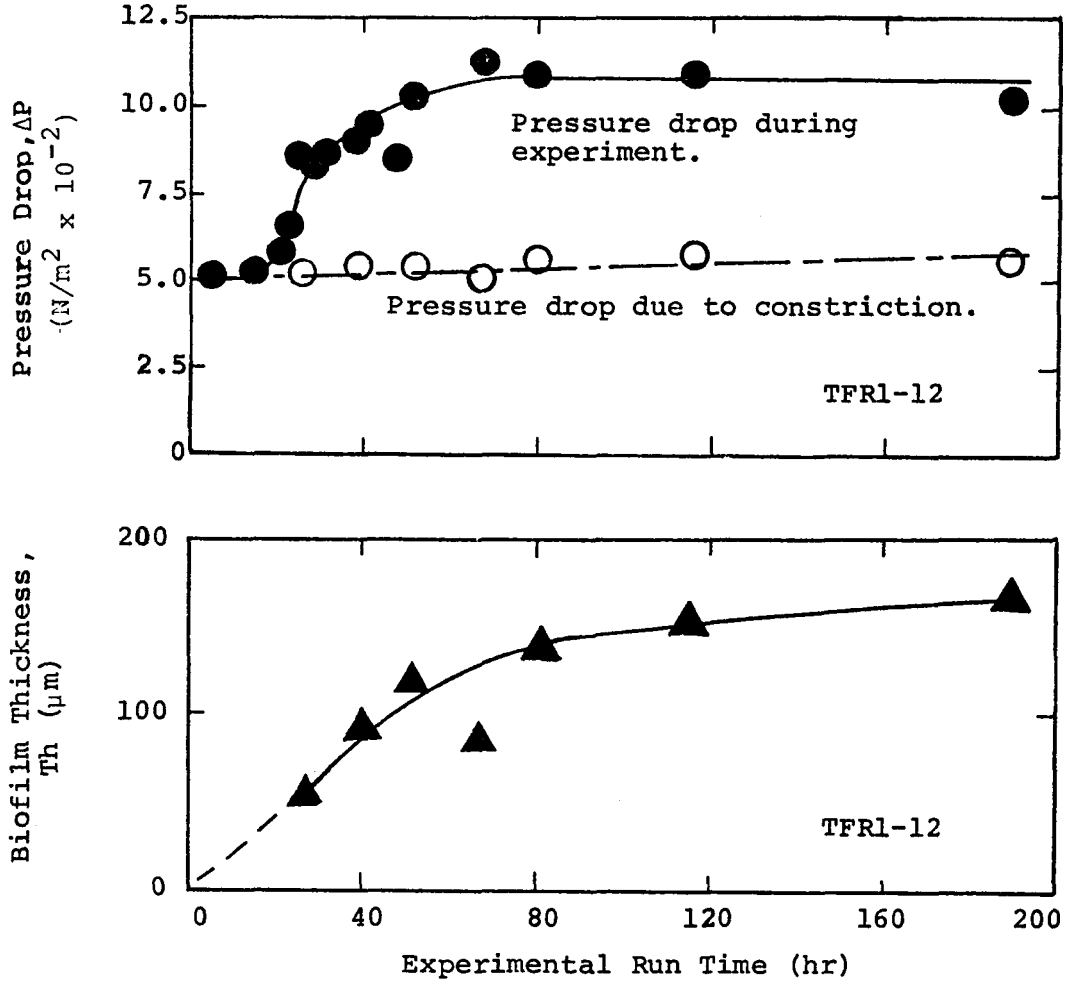

Figure 4-3. Pressure drop progression in a TFR1 experiment compared to the calculated pressure drop due to a decrease in tube radius equal to the biofilm thickness.

Fluid Viscosity

Fluid viscosity does not change during a TFR experiment. Fluid viscosity from TFR experiments under different conditions was measured using a capillary viscometer. Fluid viscosity never varied more than 2.0% from water viscosity during an experiment (Appendix R).

Transport of Biofilm in the Direction of Flow

Brauer (31) performed experiments on form stability of the interior of asphalt-lined pipes as a function of temperature of the flowing water. At higher temperatures, the asphalt coating assumed a rippled surface structure which was accompanied by an unusual increase in frictional resistance. Brauer explained the phenomenon as an actual flow of the coating under the action of shear stresses. Energy is dissipated by the asphalt being dragged along the pipe surface.

Transport of biofilm in the TFR system seems an unlikely explanation for the high frictional resistance in the fouled TFR system for the following reasons:

1. The biofilm coating always appeared uniform throughout the system; biofilm transport would require a steady supply of film or else the wall coating would disappear.

2. There was no evidence of an accumulation of biofilm in pipe bends or other areas where film could collect; biofilm transport would result in accumulation of film as film flowed to the downstream end of a tube.

Biofilm as a Rigid Rough Surface

Frictional resistance of biofilms grown under constant pressure drop (TFR3) have been compared to the frictional resistance of pipes with a rigid roughness of immobilized sand grains. The following are indicated:

1. Frictional resistance due to biofilm shows a similar dependency on Reynolds number as frictional resistance due to a rigid rough surface of immobilized sand grains.

2. Frictional resistance is dependent on biofilm thickness.

3. Frictional resistance does not increase above the hydraulically smooth conditions until a critical film thickness is obtained.

The Blasius-Stanton or Moody diagram (32) can be used to compare frictional resistance by a biofilm with frictional resistance of a rigid rough surface. The Blasius-Stanton diagram is a plot of friction factor vs Reynolds number for a series of pipes with different sized sand grains immobilized on the surface (Figure 4-4); the friction factor in a pipe with a rigid rough surface depends on both the relative roughness and the Reynolds number.

The relationship between friction factor and Reynolds number for the fouled TFR3 system is presented in Figure 4-5. This figure shows the dependency of friction factor on Reynolds number is the same as for a tube with a rigid rough surface between the range of Reynolds numbers investigated (5,000-48,000). This data was obtained by reducing the shear stress in increments from the initial shear stress in a given experiment and calculating friction factor and Reynolds number at each incremental shear stress. Sloughing of film during the experiment was minimized by always reducing shear stress from the initial condition rather than increasing it.

Figure 4-6 shows friction factor vs Reynolds number for a TFR3 experiment at different stages of film development; friction factor increases with biofilm thickness. The relationship between film thickness and friction factor for all experiments at τ_w = 6.5 to 7.9 N/m^2 is shown in Figure 4-7. Friction factor is dependent on film thickness after a critical thickness (Th_{crit}), approximately equal to the viscous sublayer, is attained.

The critical film thickness can be explained as the stage of biofilm development when surface irregularities protrude through the viscous sublayer. Until this stage, the roughness peaks are less than the viscous sublayer ($k_s < \delta_1$) and friction factor does not increase (the tube is hydraulically smooth). For a shear stress of 6.5 - 7.9 N/m^2 the viscous sublayer is approximately equal to 40 μm; this corresponds well with the observed Th_{crit} (30-35 μm) for the same shear stress range (Figure 4-8).

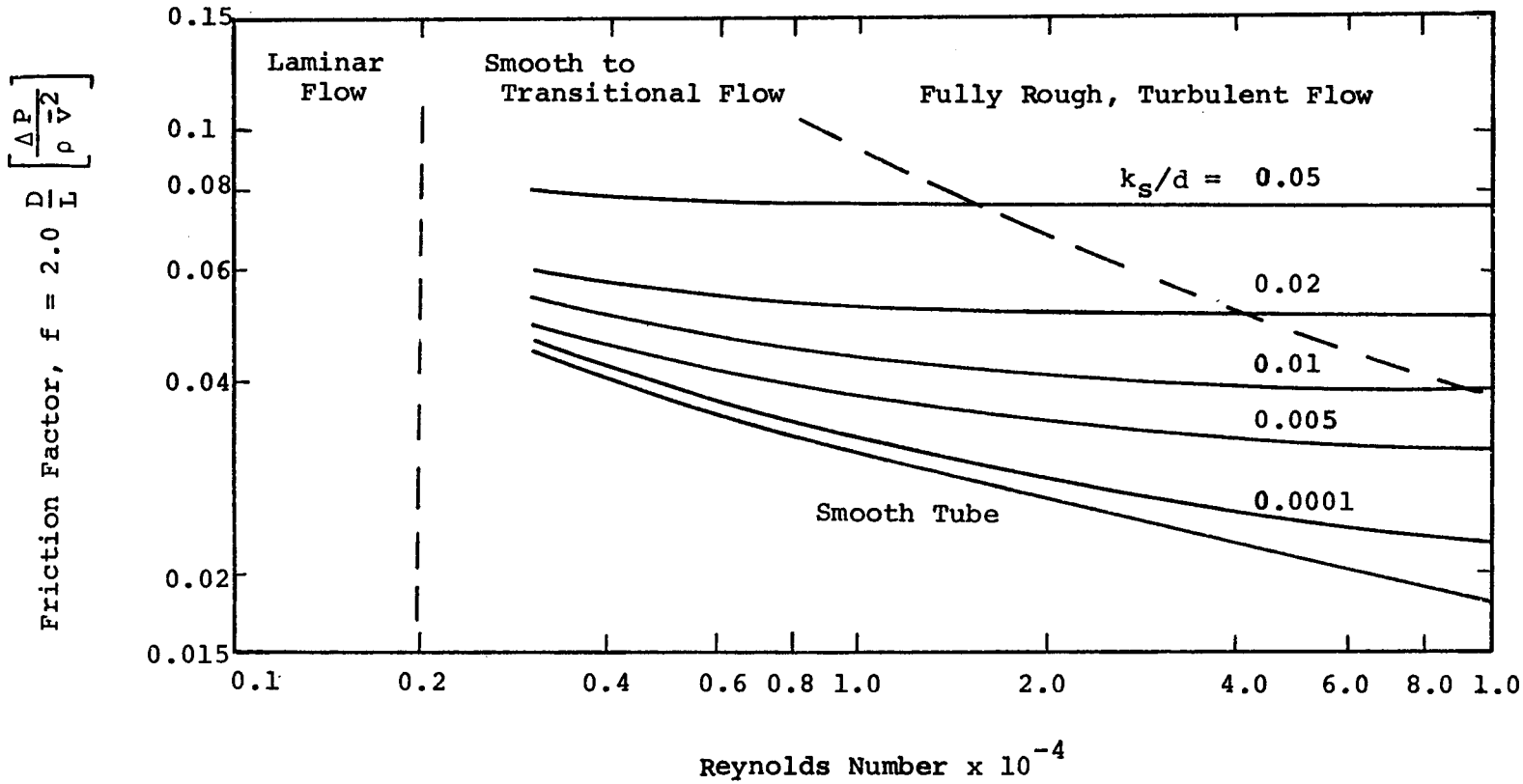

Figure 4-4. Blasius-Stanton Diagram for friction factors for pipes of different sand roughness (32).

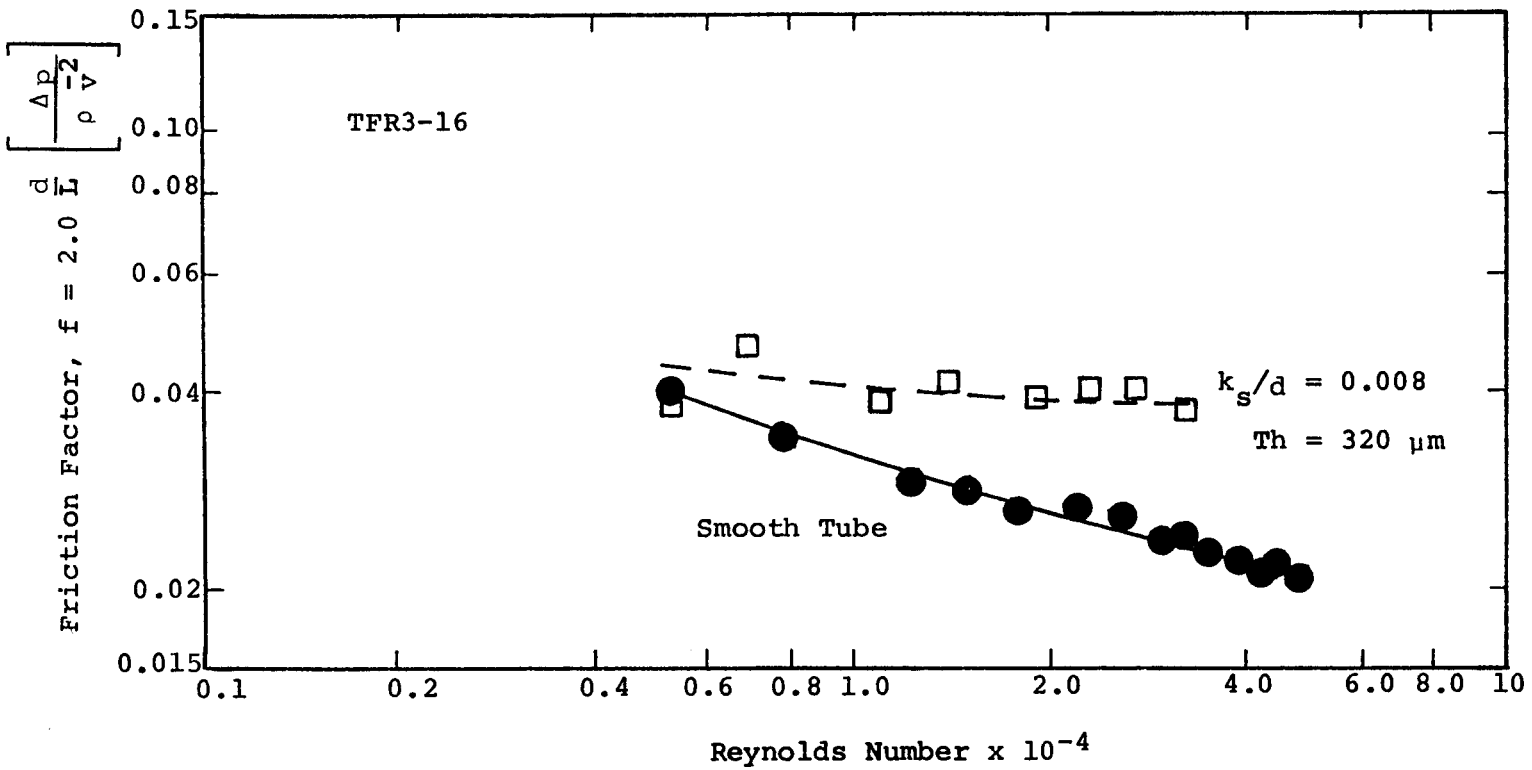

Figure 4-5. Change in friction factor with Reynolds number for the fouled constant pressure drop system (TFR3).

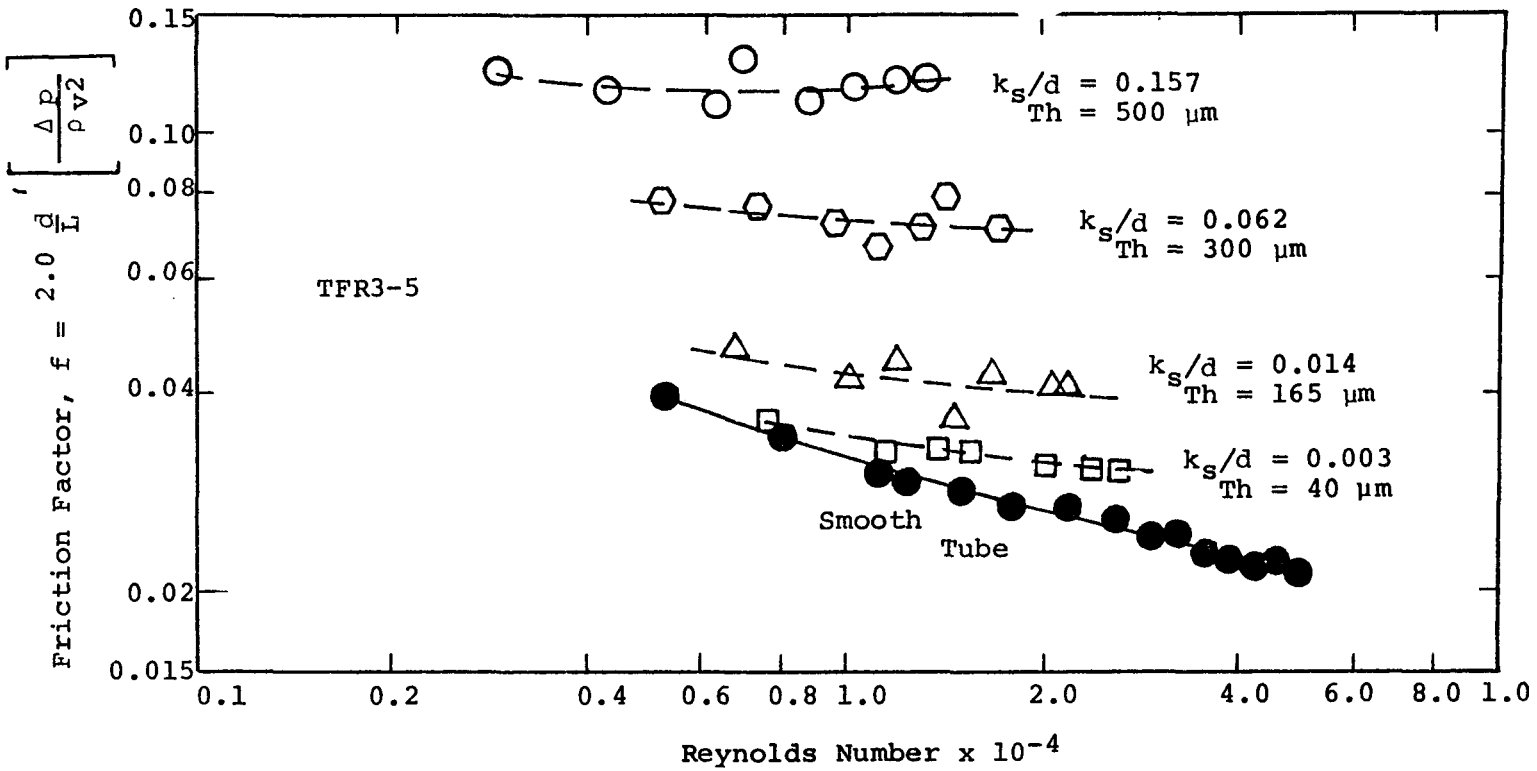

Figure 4-6. Change in friction factor with Reynolds number for the fouled constant pressure drop system (TFR3).

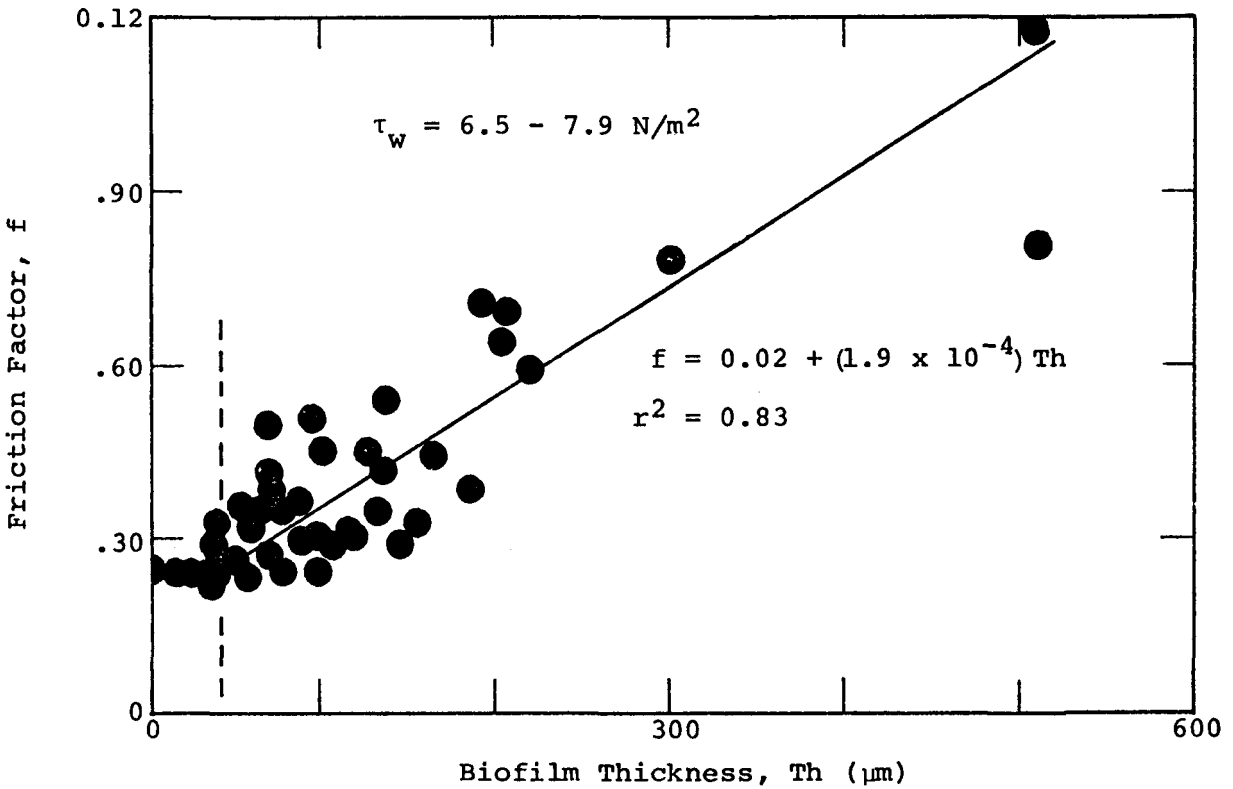

Figure 4-7. Change in friction factor with biofilm thickness in the constant pressure drop system (TFR3).

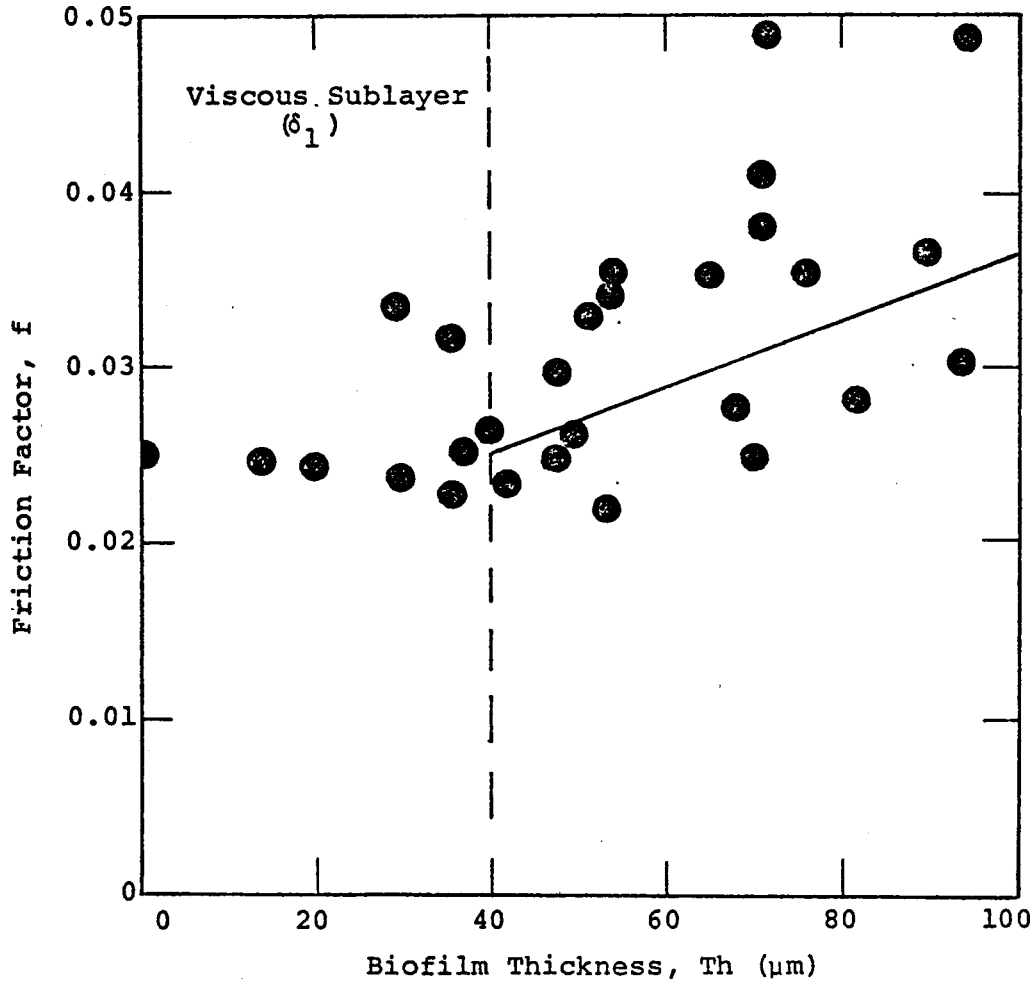

Figure 4-8. Change in friction factor with biofilm thickness in the constant pressure drop system (TFR3). The critical film thickness (TH_{crit}) is observed to be approximately 30-35 μm.

If the biofilm increases the effective roughness of the tube wall, a dependency of calculated equivalent sand roughness (k_s) on biofilm thickness would be expected. The equivalent sand roughness for a given pipe flow frictional resistance corresponds to the diameter of sand grains which, when immobilized on the inside surface, would produce the same resistance. Therefore, it is implied that k_s is a calculation of the heights of the roughness peaks causing the frictional resistance.

Figure 3-22 (k_s vs biofilm thickness) shows that the equivalent sand roughness is dependent on biofilm thickness for all TFR3 experiments at a fluid shear stress of 6.5 N/m^2 to 7.9 N/m^2. The data implies that the equivalent sand roughness of the biofilm can be greater than the actual film thickness ($k_s \doteq 3.15\ Th - 180$). Furthermore, scatter in the k_s data cannot be attributed to change in feed glucose flux (2.4 - 65 mg/m^2-min) or change in temperature (30 to 35°C). The difficulty in determining the dependency of k_s on biofilm thickness may be due to one or all of the following reasons:

1. The biofilm thickness measurement is an average thickness measurement and does not measure actual height of peaks. The average film thickness would always be less than any roughness peaks of the film.

2. Drainage of the sample tube prior to the biofilm thickness measurement may decrease the film volume and thus decrease the film thickness; the effective film thickness may be greater with the sample tube in situ and the film saturated with water.

3. It is sometimes impossible to fit commercially rough surfaces into the scale of sand roughness. Schlichting (13) cites an example of a rib-like deposit in a pipe giving an effective roughness 20-50 times the height of the actual roughness peaks. Other studies show k_s values of up to 1.64 times the mean sand grain diameter when Nikuradse's work was repeated (33).

Effect of Surface Roughness on Biofouling

Figure 4-9 compares two TFR3 experiments with identical conditions except for the inner tube surface. The surface of TFR3-6 is hydraulically smooth ($k_s/\delta_1 = 0.20$) and for TFR3-11 the surface is

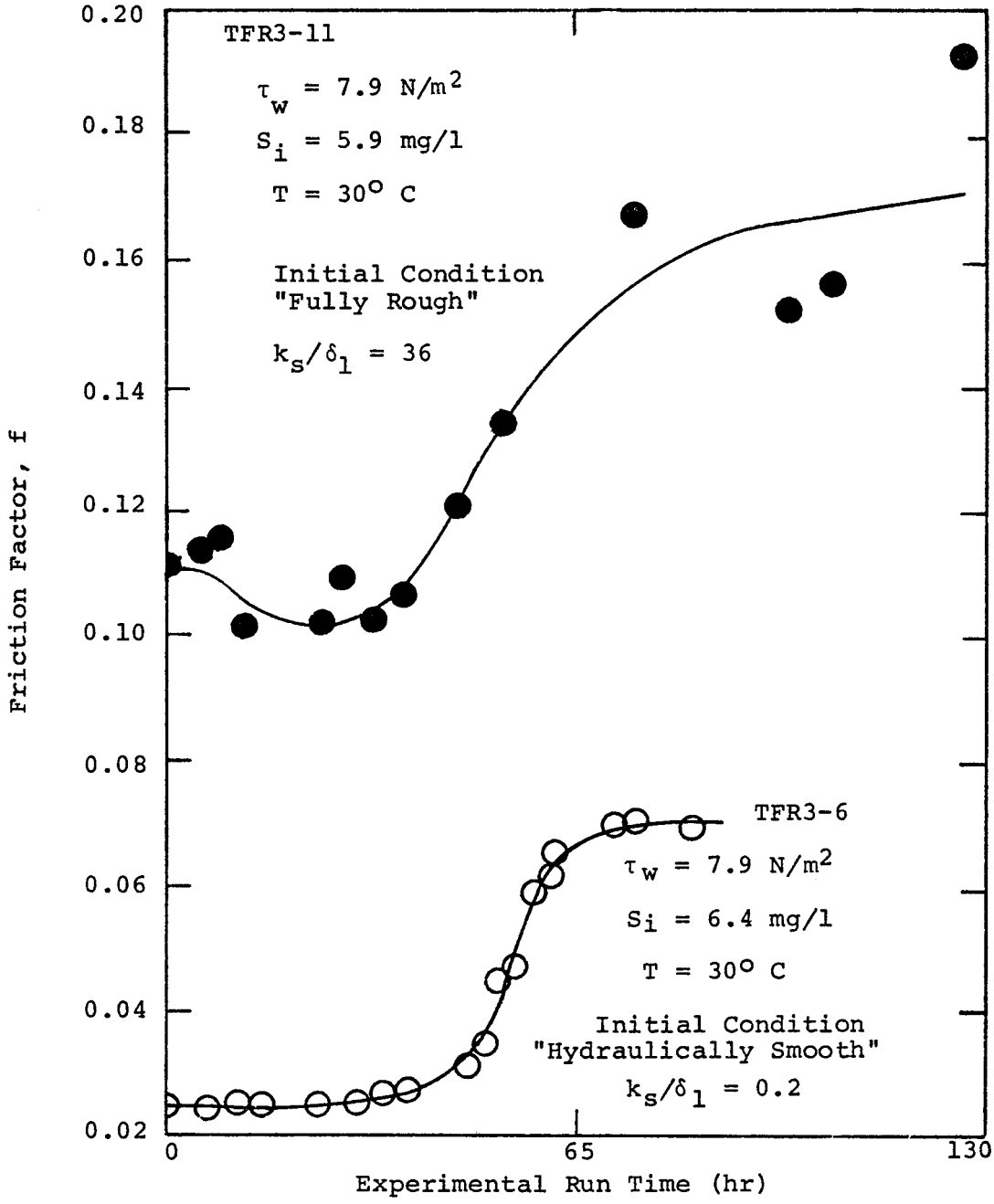

Figure 4-9. Comparison of friction factor progression in a pre-roughened tube (TFR3-11) with friction factor progression in a smooth tube (TFR3-6).

fully rough (k_s/δ_1 = 36); the fully rough condition is due to sand grains (mean diameter = 0.022 cm) immobilized on the inside surface. The following results are evident:

1. Initial friction factor is greater in the rough tube and frictional resistance remains greater at all times.

2. Frictional resistance is reduced slightly during the first 30 hours in the rough tube.

The relative friction factors ($f-f_o$) are superimposed in Figure 4-10 and indicate little difference. The pronounced frictional resistance in the pre-roughened tube indicates that the effect of the biofilm on frictional resistance is not due to a simple increasing of surface roughness. It appears that the biofilm begins to grow on the sand grains and thereby exerts a greater frictional resistance than that observed in the smooth tube. The decrease in frictional resistance at the beginning of TFR3-11 indicates the film grew between the sand grains and provided a less rough surface up to approximately 30 hours.

Energy Dissipation Within the Biofilm Due to its Viscoelastic Nature

Schuster (33) studied the interaction between turbulent shear flow and a compliant gel-like wall layer, directing his efforts toward explaining the unusually high losses in carrying capacities of conduits with slime deposits on the walls. The experimental system consisted of a rectangular duct test section with a 5000 μm wall layer of GE silicon Gel RTV-619 forming the lower horizontal boundary of the test section. The cured silicon gel formed a mirror-like gel surface of high compliancy.

Schuster's results indicate that friction factor increases dramatically when flow past the compliant boundary reaches a Reynolds number of 75,000 (Figure 4-11). The increase in friction factor was associated with an observed onset of rippling in the gel wall. The phenomenon occurred without overall transport of the compliant boundary in the direction of flow. Schuster concludes that some correlation exists between the changes in the turbulent energy spectrum of the flow and the dynamic mechanical properties (viscoelastic properties) of the compliant gel boundary.

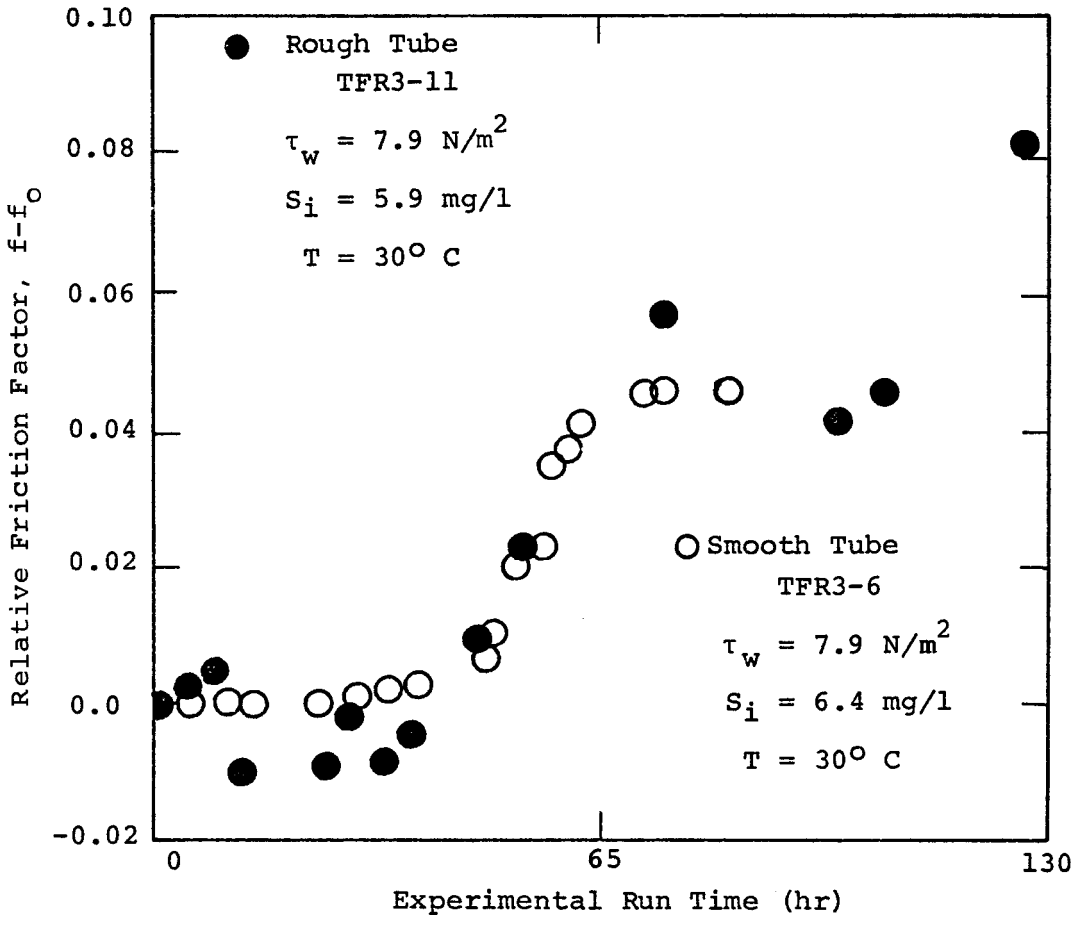

Figure 4-10. Relative friction factor progression ($f-f_o$) in a pre-roughened tube (TFR3-11) and in a smooth tube (TFR3-6).

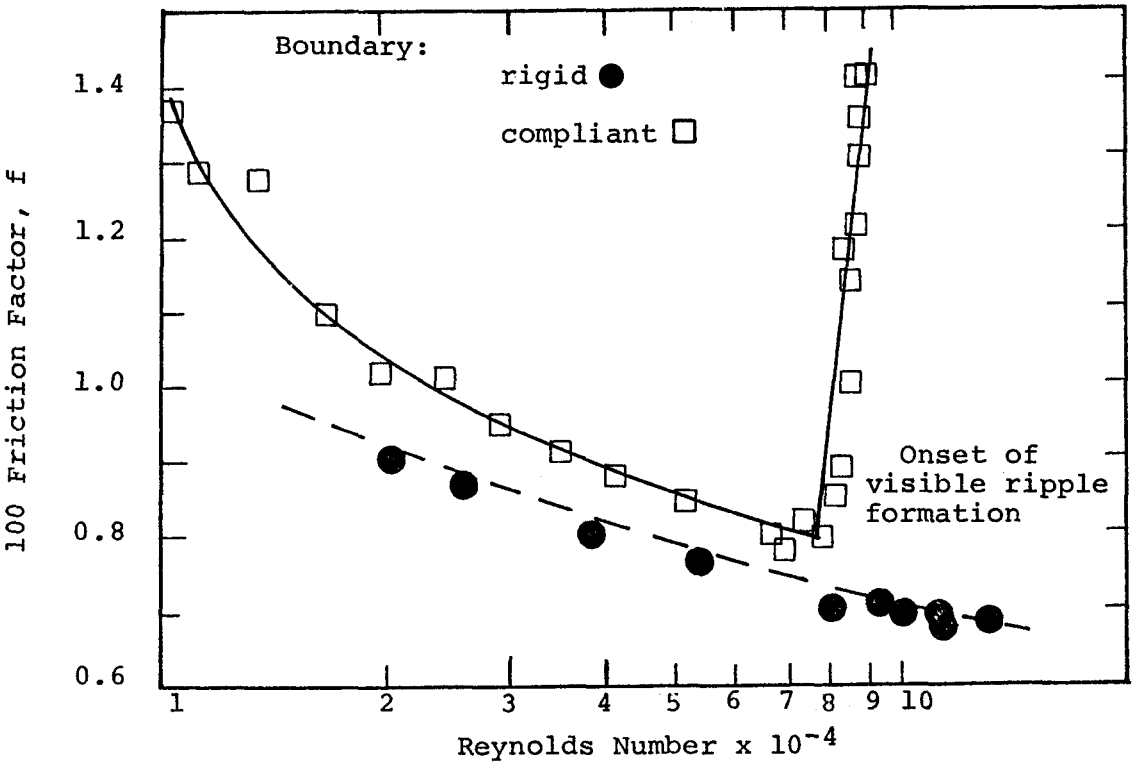

Figure 4-11. Change in friction factor with Reynolds number for flow in a rectangular duct past a compliant gel (33).

No dramatic increase in friction factor occurred in the TFR system at or below the maximum Reynolds number attainable (50,000). It is likely the sudden increase in friction Schuster observed at Re = 75,000 would be observed in the TFR system if higher Reynolds numbers were tested.

Note that flow past the silicon gel prior to the onset of visible ripple formation (Re = 75,000) behaved the same as flow past a rigid rough surface (Figure 4-5) or flow past the microbial film (Figures 4-6 and 4-7). The effect of a compliant boundary appears to increase frictional resistance at all Reynolds numbers and may be a contributing cause of the high frictional resistance in the TFR systems.

Energy Dissipation Due to Presence of Filaments in the Biofilm

The filaments in the biofilm were observed to resonate or "flutter." Figure 4-12 depicts the response of the filaments to normal flow, reversed flow, and no flow. The frequency of the filaments appears to be a direct function of the flow velocity past the surface.

Benjamin (34,35) describes a type of flow disturbance caused by a flexible or compliant boundary which is similar to the formation of waves by wind over a water surface. This instability is essentially a resonance effect which can be stabilized by damping in the wall; it is scarcely affected by the viscosity of the fluid since the "wall friction layer" is largely cancelled.

The high frictional resistance caused by the increased surface area of the filamentous microbial film is analogous to drag in a stream due to bottom vegetation.

Frictional resistance is observed to increase with increasing filament length which supports the assertion that the filaments play a role in causing frictional resistance.

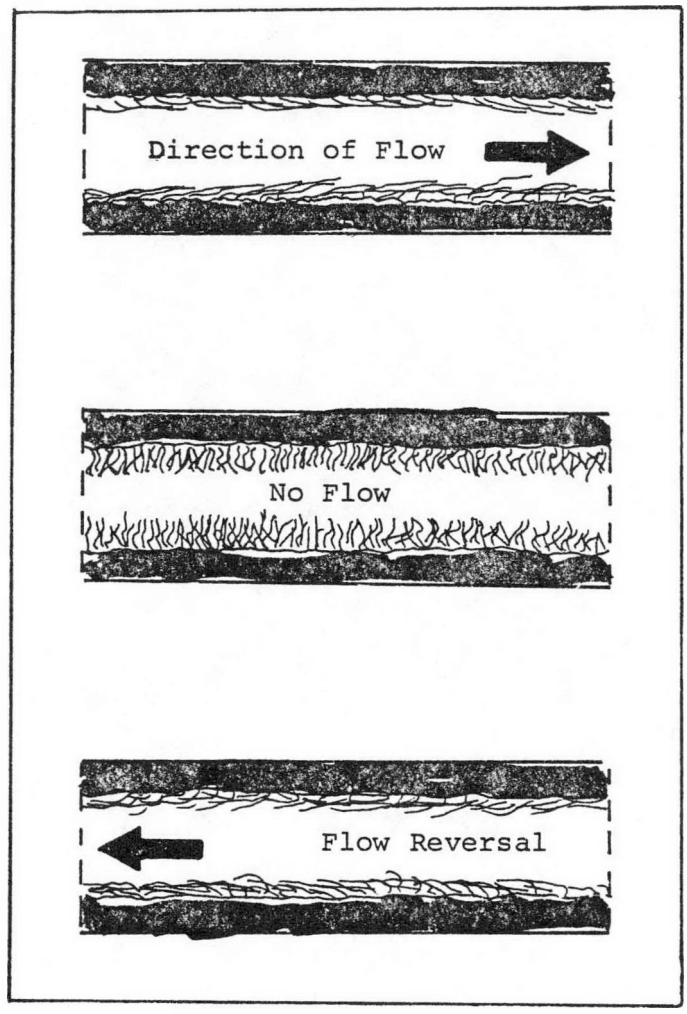

Figure 4-12. Effect of flow on filaments of the biofilm layer.

HEAT TRANSFER RESISTANCE

Biofilm development and resulting increased frictional resistance have been discussed in some detail. Changes in heat transfer resistance arise from the combined effects of increased biofilm thickness (conductive heat transfer) and increased frictional resistance (convective heat transfer). Changes in heat transfer resistance due to biofouling film development were observed in the TFR4 system. Initially, heat transfer decreases for a short period, as expected, due to the insulating effect of the biofilm against conductive heat transfer. Further biofilm development increases hydraulic roughness (as indicated by increasing friction factor) causing higher rates of convective heat transfer. Consequently, the rate of increase in heat transfer resistance is not simply related to changes in conductive heat transfer arising from biofilm development.

Biofilm Thermal Conductivity

Results indicate that biofilm thermal conductivity is essentially the same as water. This is not a surprising result since biofilm is 90-98% water. It is important to remember that there were no inert suspended solids in the feed to the experimental systems. However, an important observation was made when activated carbon particles leaked into the TFR system. During these experiments, carbon particles were observed in the film matrix and dramatic increases in heat transfer resistance were measured from the beginning and persisted throughout the run. Estimating the thermal conductivity of the carbon particles to be close to that of charcoal flakes (0.088 watts/m^2-C as compared to 0.598 for water), an equivalent layer of carbon 5 μm thick would account for observed decreases in heat transfer, even when accounting for enhancement of convective heat transfer due to a 50 μm biofilm. A reasonable hypothesis is that particulate matter entrapped in highly adsorbent biofilm may contribute significantly to the reduced heat transfer in fouled heat exchangers. The degree would depend upon the particle volumetric concentration and thermal conductivity. More experimentation is needed to verify this hypothesis.

Heat Transfer Resistance and Biofilm Development

The effect of glucose loading rate and shear stress at the wall on heat transfer resistance can be calculated from the following relationship (derived in the RESULTS section, Eq. 3-28):

$$U_w = \left[\frac{1}{h} + \frac{r_1 \ln(r_1/r_I)}{k_{Th}} \right]^{-1}$$

k_{Th} is known and h is a function of Reynolds number, friction factor, and the properties of water. The biofilm development rate can be determined from equations in Table 3-6. The increase in friction factor as biofilm develops can be determined from data such as illustrated in Figures 3-20 and 3-23. Therefore, based on knowledge of biofilm thickness and friction factor, the effect of biofilm development on rate of increase in heat transfer resistance can be calculated. An example of such a calculation is presented in Figure 3-34.

FOULING MEASUREMENT TECHNIQUES

Table 4-1 lists the fouling measurement techniques tested and their potential for use in power plants. All techniques listed can be used on a sidestream of a power plant condenser. In the table, reliability refers to maintenance requirements while sensitivity refers to limits of detection.

Only the TFR system has been tested in the field and has provided consistent, maintenance-free operation. However, based on laboratory experience, the AFR frictional resistance technique is the most promising for use in an operating power plant. Some of its advantages are as follows:

1. Compact
2. Sensitive (i.e., can detect biofilm at relatively small thicknesses)
3. Flexibility - shear stress, hydraulic retention time and surface temperature can be varied independently. As a result, this sidestream device could be operated to maximize fouling rate in a given cooling water rather than simulating the processes occurring in a condenser. In this way, the monitor would provide an early warning of biofouling in the actual condenser.

Table 4-1

COMPARISON OF THE TECHNIQUES TESTED FOR MEASUREMENT OF BIOFOULING**

Measurement	Reliable	Sensitivity	Non-Destructive	Continuous	Installed in a Condenser
Biofilm Volume	2*	2*	no	no	no
Optical Microscope	2	2	yes	no	no
Biofilm Mass	1	3	no	no	no
Frictional Resistance (TFR)	1	2	yes	yes	yes
Frictional Resistance (AFR)	1	1	yes	yes	no
Heat Transfer Resistance	3	2	yes	yes	yes

** Evaluations are based on the level of fouling that has occurred in the experimental systems over a maximum period of 7 days.

* 1 ∿ excellent

2 ∿ good

3 ∿ fair

4 ∿ poor

5 ∿ useless

4. Low maintenance

5. Dependable analog signal for recording and/or controlling

Wall temperature (T_w) was not varied concurrently with bulk temperature, shear stress, and nutrient loading rate in the laboratory AFR studies. Results presented in Figures 3-35 and 3-36 indicate that T_w may be a significant influence on biofilm development. However, based on present experience, wall temperature of the outside cylinder could be used to simulate T_w in the power plant condenser. Maintenance of a constant heat flux over the entire outside reactor wall would be convenient in the AFR but not the TFR. The heat transfer coefficient could be determined by inlet and outlet fluid temperatures and measurement of input heat flux.

Variation of the reactor dimensions in the AFR and TFR may change sensitivity and accuracy of the two systems. For example, more experiments are necessary to determine the effect of gap width on sensitivity in the AFR.

Frictional resistance appears superior to heat transfer resistance as a fouling indicator in the ranges tested. When the biofilm thickness is less than the viscous sublayer thickness, no change in frictional resistance is observed. Any decrease in heat transfer resistance during this period, due to reduction in conductive heat transfer, was barely detectable. As the film grows further, a significant change in frictional resistance is observed due to the increase in hydraulic "roughness" caused by the film. Heat transfer resistance, however, is not as sensitive in this period due to increase in convective heat transfer resulting from the increased "roughness." Although heat transfer resistance will eventually increase above the starting conditions, the fouling deposit will be affecting plant efficiency significantly and will be difficult to remove. Consequently, frictional resistance does not provide an indication of the onset of fouling. The sensitivity of the frictional resistance measurement will depend on the viscous sublayer thickness which can be directly related to Reynolds number in a circular tube geometry. This must be tested in actual plant conditions.

There are several strategies that should be considered for using these techniques in a sidestream of the cooling water, besides attempting to simulate the actual condenser:

1. The adjustable variables for the monitoring device (annular fouling reactor) can be set to provide optimum conditions for biofilm development. For example, the heat flux, bulk water temperature, rotational speed and hydraulic residence time of the AFR could be adjusted to promote biofilm growth. In this way, the AFR would serve as an early warning against the onset of biofouling in the condenser with its "harsher" environment.

2. Frictional resistance cannot be detected until the biofilm develops through the viscous sublayer. At this point, the extent of biofouling may be too much for control procedures to be effective. The sensitivity of the AFR could be increased by operating primarily at the velocity characteristic of the condenser. However, periodically the rotational velocity can be increased, thus decreasing the viscous sublayer thickness. Comparison of the friction factor at this elevated velocity with that in the clean AFR will indicate if any biofouling film has developed.

SOME LIMITATIONS OF THE EXPERIMENTAL SYSTEMS

The studies reported herein were conducted to develop a better understanding of fouling biofilm development as it occurs in power plant condenser tubes. The experimental systems, however, differ significantly from power plant condenser tubes. Consequently, several fundamental features which may be limitations must be considered when relating experimental results obtained here to biofouling in operating power plants:

1. Glass or plastic surfaces were used to eliminate corrosion so that observed effects could be attributed solely to the presence of fouling biofilms. Power plant condensers are composed of a variety of metals or metal alloys which can significantly influence the fouling process observed in the field.

2. A soluble substrate (glucose) was used as the sole energy source for microbial growth in this research. Natural waters serve as cooling waters for power plants and the carbon and energy source for microbial growth will vary with plant location and other environmental factors, but in all likelihood are not glucose.

3. The microbial inoculum for all laboratory experiments was composed of a variety of microbial species. Use of a single substrate, however, essentially precludes the maintenance of a stable mixed population. Therefore, as an experiment progressed, the microbial population was probably dominated by a very few species which could compete better for the available nutrients under the imposed experimental conditions. However, microbial populations entering power plant condensers will probably also decrease in diversity due to the change in environment. Entering populations will also probably vary with location, water quality, and many other environmental factors.

4. The feed water to the laboratory experimental reactors used in this research contained less than 1 mg/l suspended solids. Although biofouling may enhance and in fact is essential for the adsorption of inert suspended solids to condenser surfaces in operating power plants, suspended solids were not an influence on fouling in the reported laboratory experiments.

5. Concentration of other water quality parameters, besides the limiting nutrient, were not considered in this research. Biofouling in operating power plants is probably affected by other soluble and collodial components of the cooling water such as calcium, magnesium, silica, and iron compounds.

More field work is necessary to test the validity of the laboratory models. Ideally, several laboratory model systems would be operated in parallel with an operating condenser which is instrumented to provide the same, or similar, data as the laboratory models. Such investigations would determine the relative effect of the above limitations.

COMPARISON OF FIELD AND LABORATORY RESULTS

Field tests were conducted at two locations in the Houston area:

1. Deepwater Plant, Houston, Texas
   (cooling water from the Houston Ship Channel)

2. P. H. Robinson Plant, Thompson's Corners, Texas
   (cooling water from a freshwater lake)

The data from the field tests are summarized in Appendix S.

Water Quality

A summary of the water quality data in the field locations is compared to the laboratory feed stream in Table 4-2. More water quality data from Deepwater is in Appendix T.

Table 4-2

WATER QUALITY DATA FOR BIOFILM EXPERIMENTS*

	Bulk Temp. (°C)	Bact. Nos. $\log_{10}$ (#/ml)	pH	SOC (mg/l)	BOD (mg/l)	SS (mg/l)
Houston Ship Channel	16	3	6.4	33	19	100
Lake at Thompson's Corners	12	3	9.0	21	4	--
Laboratory Tap Water	--	--	7.0	8.6	0	0
C_{s_o} = 5 mg/l	30-40	4.3	7.0	--	2.5**	--
12.5 mg/l	30-40	6.8	7.0	--	6.2**	--
20 mg/l	30-40	6.9	7.0	18.0	10**	--
100 mg/l	30-40	7.2	7.0	54.8	50**	--

*data from other power plant locations are presented in Appendix V.

**estimated value

There are obvious differences between the soluble organic carbon (SOC) biodegradability (as evidenced by the SOC/BOD ratio) in the laboratory and in the field caused by differences in composition and presence of toxic materials. Biochemical oxygen demand (BOD) tests with undiluted samples were conducted to determine relative rates of degradation.

In the laboratory experiments, microbial growth is carbon-limited since nitrogen, phosphorous and other nutritional requirements are

satisfied by the TSB fraction. In the field, microbial growth is often limited by an inorganic nutrient (e.g., nitrogen or phosphorous). Generally, inorganic nutrient-limited growth is slower and chemical composition of the biomass is different from that due to carbon-limited growth. A high C/N ratio (i.e., nitrogen-limited growth), for example, increases extracellular polysaccharide production, an important constituent of biofouling films (16).

The laboratory feed contained no inorganic particulates, a potentially important factor in overall fouling at many field sites. The effect of particulates on fouling was not tested in this research. In summary, there is no one convenient method of assessing the relative effect of water quality in the field relative to the laboratory situations tested in this work. Futher work in both situations will be required to develop this knowledge.

Rate of Biofouling Based on Frictional Resistance

The rate of biofouling based on frictional resistance can be used conveniently to compare the laboratory and field systems. TFR1 and TFR2 experiments conducted under the following conditions were chosen for the comparison:

1. low glucose loading rates (2.0 to 4.1 mg/m^2-min) which corresponded to approximately 2-5 mg SOC/m^2-min
2. bulk temperature 30°C (lowest temperature tested).

Fouling rates (R_f^*) are compared in Figure 4-13. Bulk temperature at Deepwater was 16°C and at P. H. Robinson was 12°C so the R_f^* values were adjusted using the data from Bongers *et al.* (30), which indicate that fouling rates increase by 2.5 between 21 and 31°C. The data comparison is satisfactory despite any differences which may exist in water quality at the three locations considered.

The progression of fouling based on the logarithmic fouling rate based on mass (R_{BM}^*) appears quite similar to that observed in the laboratory (Figure 3-5) as indicated in Figure 4-14. The field data are compared with an experiment in TFR1 (expt. TFR1-23). Note that the induction period in the laboratory system is quite short in com-

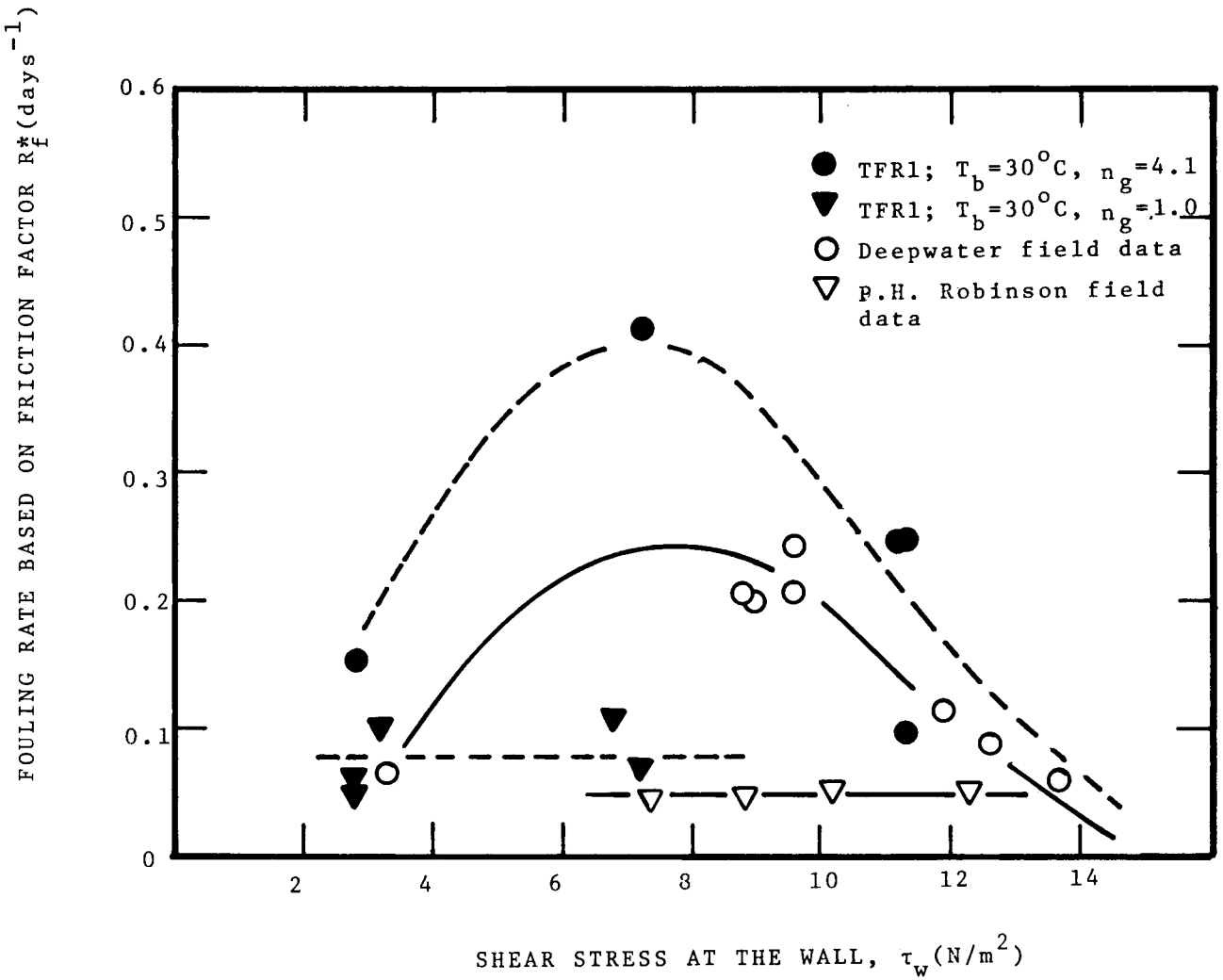

Figure 4-13. Comparison of fouling rates measured in the field and in laboratory experiments. Fouling rates measured in the field have been adjusted to 30°C by using a temperature factor determined in the field by others (30).

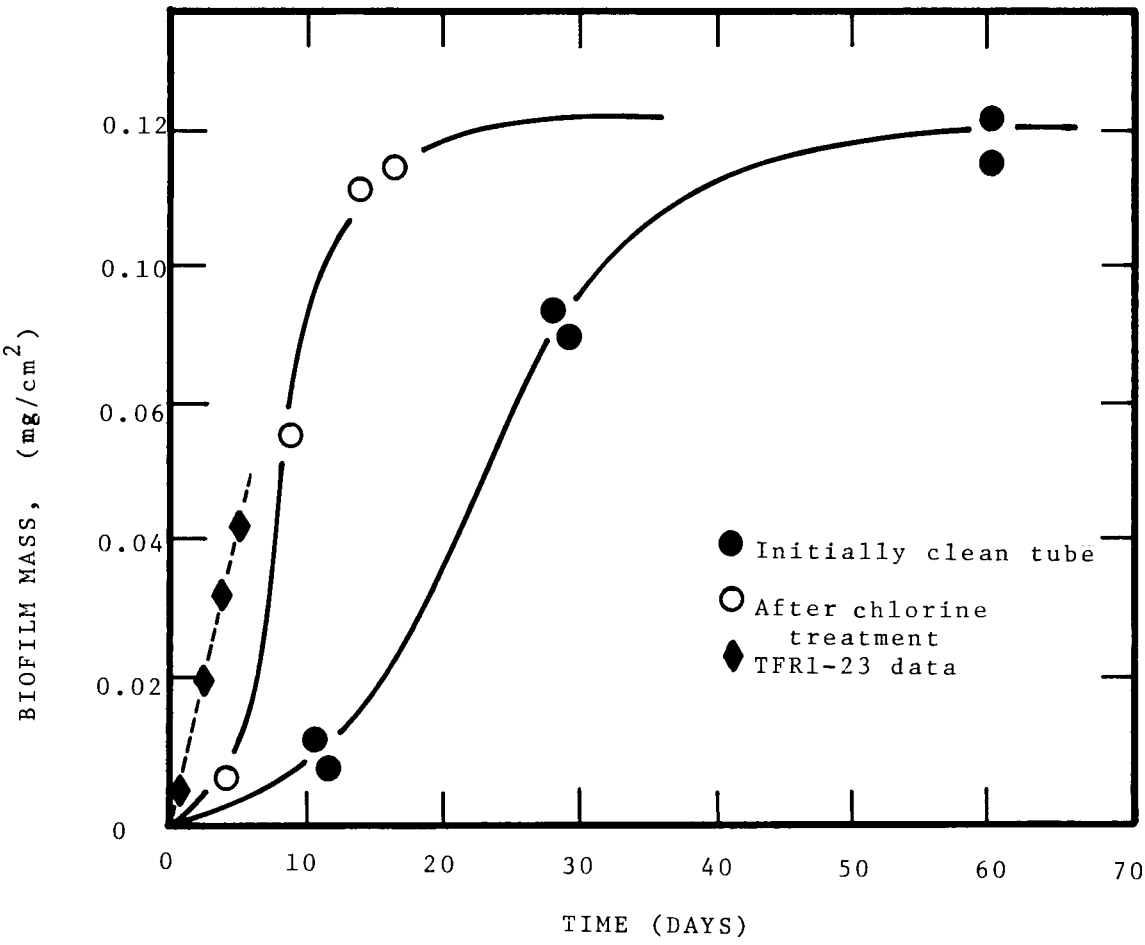

Figure 4-14. Fouling rates at the Deepwater field site comparing fouling rates in a clean tube and a tube treated with chlorine. TFR1 data is presented for comparison with laboratory data.

parison. This short induction period was quite intentional in the TFR system. After 12 days, the tube from the field unit was chlorinated until it appeared clean (by visual inspection). After the chlorine treatment, condenser water began flowing through the tube again. The difference in the induction period and the fouling rate is quite significant and probably results from incomplete removal of the fouling deposit. More effort must be directed in the area of the induction phase, especially as it effects biofouling after repeated chlorination. The effect of the oxidant treatment on the subsequent induction growth phases may be critical in determining which oxidant to use and how it is to be applied.

Extent of Fouling

Biofilm thickness measurements for the field fouling reactor (FFR) were difficult to obtain, so extent of fouling was evaluated by using the maximum friction factor attained at the plateau and defined as f_{MAX}. These data were also available for the TFR experiments. f_{MAX} for TFR laboratory experiments employing low glucose loading rates (n_g<4.1 mg/m^2-min) at temperatures ranging from 28-40^{o}C were plotted versus shear stress and curve-fitted to an exponential function. The result was as follows:

$$f_{MAX} = 0.0034 \exp (3.5 \tau_w^{-0.5}) \qquad (4\text{-}2)$$
$$(r^2 = 0.74)$$

Field data (FFR) were not used in determining the curve-fit. In Figure 4-15, both TFR data and FFR data are plotted and compared to Eq. 4-2. The comparison clearly indicates no difference between the laboratory and field results on the extent of fouling.

Maximum mass in the TFR ranges from 0.04-1.80 mg/cm^2 and is significantly affected by glucose loading rate. Table 4-3 compares the biofilm mass at plateau in the laboratory and field experiments and suggests that the extent of fouling at Deepwater is similar to that in the TFR at low loadings.

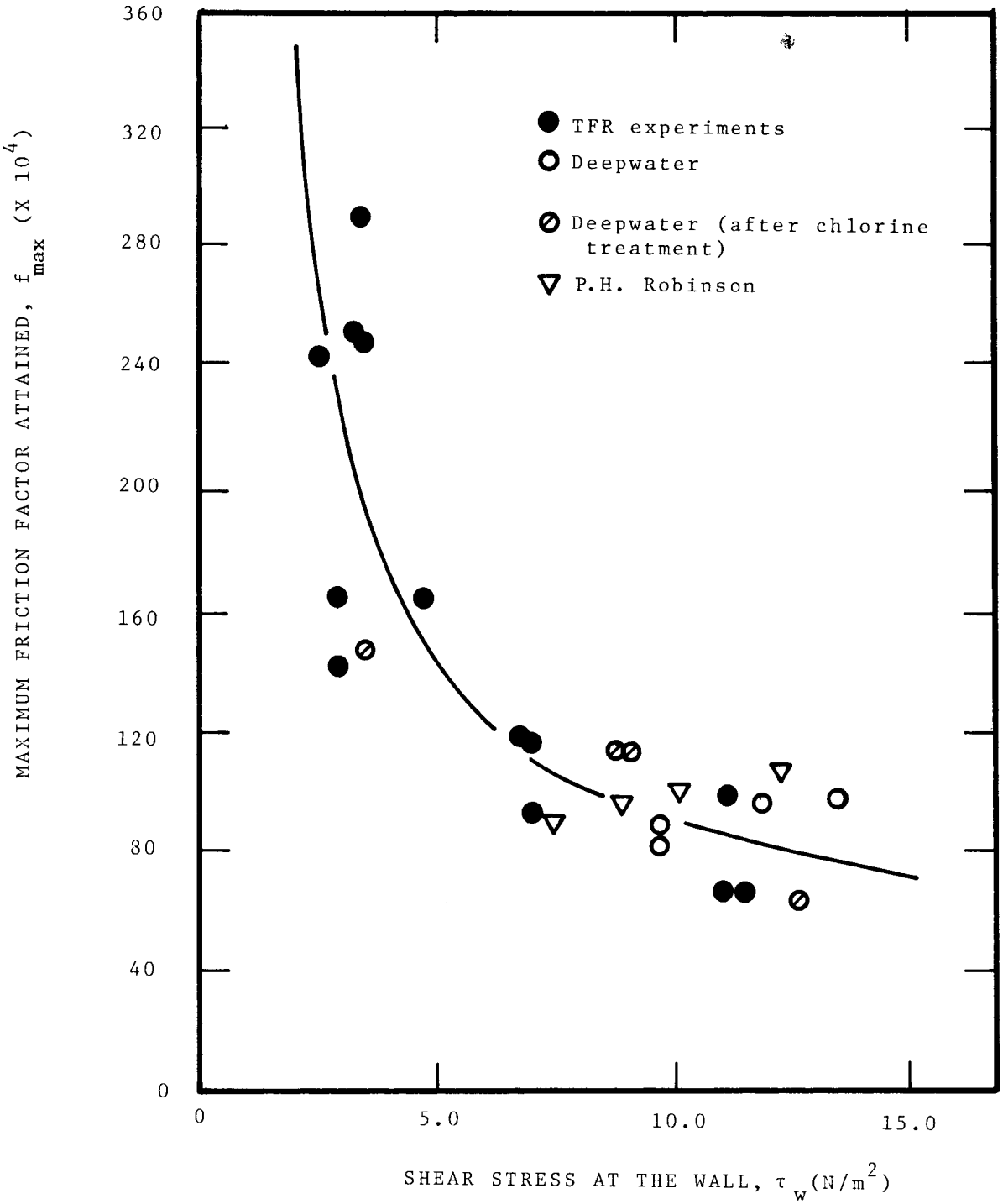

Figure 4-15. Comparison of extent of fouling measured in the laboratory and in the field.

Table 4-3

EXTENT OF FOULING IN FIELD AND LABORATORY TESTS
AS DETERMINED BY ATTACHED MASS MEASUREMENTS

	Glucose Loading Rate (mg/m^2-min)	MAXIMUM ATTACHED MASS (mg/cm^2)
TFR1 and TFR2	4.1	0.35 ± 0.20 (7)
	2.5	0.16 ± 0.06 (4)
	1.0	0.07 ± 0.04 (4)
Deepwater	---	0.09 (3)

BIOFILM DESTRUCTION BY CHEMICAL METHODS

Oxidant Decay Rate

The disappearance of oxidants with time corresponds to a first order rate process with respect to oxidant concentration. The first order rate expression can be indicative of a first order reaction or a mass transfer limitation occurring in the bulk fluid or within the biofilm. As an illustration, consider the relative values of the diffusional resistance and the experimentally determined first order rate constant (K_c). If Th_f is the biofilm thickness following chlorination and $D_{Cl_2} = 1.25 \times 10^{-5}$ cm^2/sec is the diffusivity of chlorine in biofilm (0.9 x D_{Cl_2} in water), then the diffusional rate can be represented by D_{Cl_2}/Th_f. Table 4-4 compares the diffusion rate to the first order rate constant and indicates that the first order rate constant is comparable to the estimated diffusion rate of chlorine in biofilm. Therefore, it appears that chlorine decay is diffusion-controlled in the biofilm. Consequently, extent of biofilm removal by chemical oxidants probably reflects their depth of penetration in the biofilm.

More effective biofouling control strategies can be chosen in view of these results. Since the overall reaction rate is diffusion-controlled, the reaction rate will be increased by higher concentrations in the bulk fluid (i.e., larger concentration gradient). For those power plants which periodically add oxidant for biofouling control, a pulse injection at relatively high concentration will be more effective than low level continuous chlorination for biofilm destruction. As an illustration, consider the following application schedules which may occur once a day:

	Schedule 1	Schedule 2
velocity	6 ft/sec	6 ft/sec
flow rate*	33.6 liters/min	33.6 liters/min
inlet oxidant	0.5 mg/l	1.0 mg/l
time of treatment	30 min	5 min (repeated 3 times after 5 min intervals with no oxidant)
total oxidant used	500 mg	500 mg

*for one condenser tube

Schedule 2 would be expected to provide more effective treatment because of the higher concentration utilized. The intervals without oxidant feed are considered necessary for enhanced removal of the weakened biofilm from the wall by the fluid shear forces (see below).

Table 4-4

COMPARISON OF CHLORINE DIFFUSION RATE AND DECAY RATE IN BIOFILM

Expt. No.	D_{Cl_2}/Th_f (cm/min)	K_C (cm/min)
TFR1-12	0.12	0.01
TFR1-13	0.28	0.06
TFR1-14	0.20	0.12
TFR1-15	0.07	0.19

Oxidant Effect on the Biofilm

Maximum penetration of oxidant for a given concentration gradient, will occur in a thick film with a relatively low mass density.

Biofilm removal by chemical oxidation, based on decrease in biofilm thickness, is strongly dependent on initial biofilm thickness (Figure 3-43). This effect may result from a combination of two factors:

1. deeper biofilm penetration by the oxidant
2. higher shear forces at the interface of the thicker biofilms.

Chemical oxidizers attack the biofilm matrix causing partial sloughing as indicated by turbidity and organic carbon measurements during chlorination (16). Continued sloughing of biofilm is frequently observed for some time after all oxidant is dissipated indicating the role of wall shear stress following chlorination. Norrman et al. (17) also recorded the enhanced effect of increased τ_w on biofilm removal by chlorination. These results suggest the following:

1. Oxidant penetrates deep into thick biofilm of low density and weakens the polymer matrix responsible for the biofilm structure.
2. The high shear stress at the thick biofilm interface tears portions of biomass away from the surface.
3. The chemically-induced sloughing exposes unreacted biofilm surfaces nearer the tube wall and further chemical attack is promoted.

Concomitant changes in pressure drop also occur with increasing amounts of chlorine reacted (Figure 4-16).

Comparison of Oxidant Effectiveness

A thorough comparative evaluation of oxidant effectiveness was not within the scope of this project because of the many factors which can influence oxidant biofouling film destruction effectiveness. Based on limited testing, however, chlorine and chloramines were equally effective in destroying biofilms. Hydrogen peroxide was not as effective when compared to chlorine on a mass basis (i.e., equal

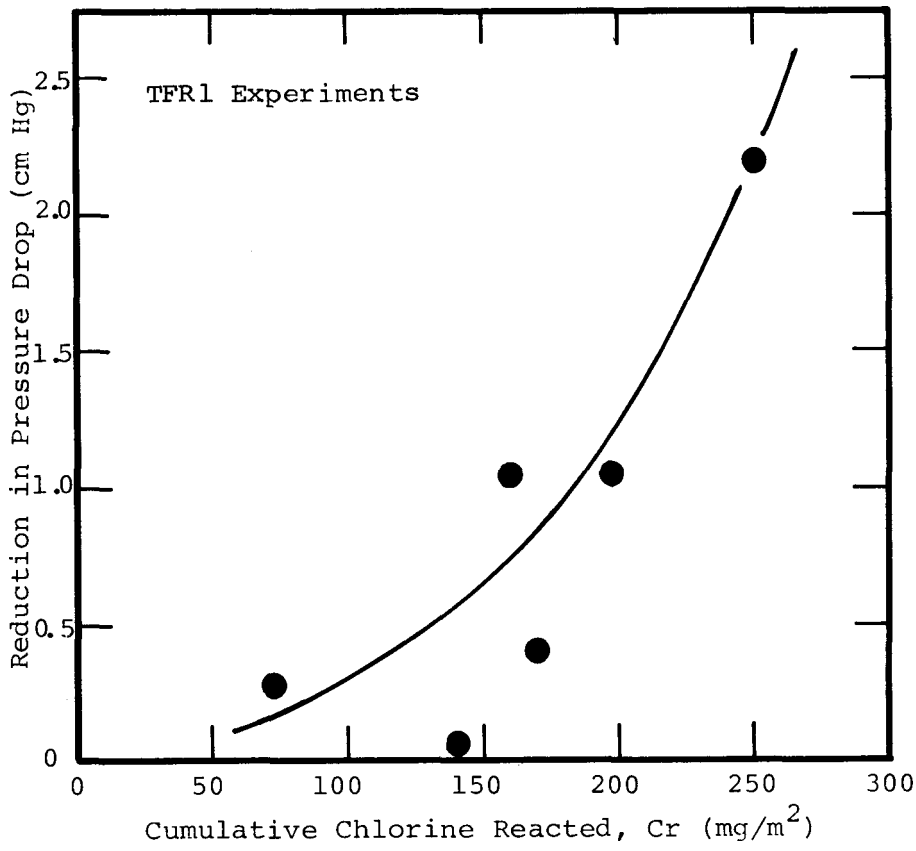

Figure 4-16. Reduction in pressure drop as a function of chlorine reacted by the biofilm in TFR1.

mass dosage). Ozone was the most effective in cleaning the surface but the dosage could not be determined with great certainty. In all treatments, aside from ozone, there always remained a residual deposit of biofilm or filaments which were observable under magnification (430x).

It cannot be overemphasized that the relative "ranking" of the oxidants may change with certain environmental variables, the most important being pH. Chlorination serves as an excellent illustration of the potential pH effects. Disinfection (i.e., inactivation of microorganisms) with chlorine is known to be more effective at lower pH (6.0-6.5) where the HOCl species dominates (36). Supposedly, the uncharged HOCl species can penetrate the cell easier than the larger, charged OCl^- species. Oxidation of polysaccharides with chlorine is more effectual at somewhat higher pH (7.0-7.5) as reported from studies with starch (37). Consequently, the optimal pH for biofouling film destruction may be different from that for disinfection since OCl^- may be the active oxidizing agent. More testing under controlled conditions is necessary to evaluate the effect of pH on the performance of oxidants.

BIOFILM DESTRUCTION BY PHYSICAL METHODS

Results of experiments using physical stress treatment indicate that a step increase in bulk temperature removes a significant amount of biofilm. Step increases in surface temperature and flow reversal had relatively little effect on biofilms under the conditions tested. Flow reversal would be expected to have less effect on thin biofilms of high density, i.e., biofilms developed at high shear stress. All physical stress treatments exhibited increased biofilm removals when applied to thicker biofilms.

Section 5

REFERENCES

1. Ritter, R. B., and Suitor, J. W. "Fouling Research on Copper and Its Alloys -- Seawater Studies." Progress Report to International Copper Research Assoc., Inc., Heat Transfer Research, Inc., Alhambra, California, 1976.

2. Kornegay, B.H. and Andrews, J. F. "Characteristics and Kinetics of Biological Film Reactors," Federal Water Pollution Control Administration Final Report. Research grant WP-01181, Dept. of Environmental Systems Engineering, Clemson University, 1967.

3. Sanders, W. M. "Oxygen Utilization by Slime Organisms in Continuous Culture," Int. J. Air Wat. Pollut., Vol. 10, 1966, pp. 253-276.

4. Difco Manual. 9th ed. Detroit: Difco Laboratories, Inc., 1966, p. 265.

5. American Public Health Association. Standard Methods for the Examination of Water and Wastewater. 14th ed., Washington, D.C.: APHA, 1976.

6. Anderson, M. R. Vaccarro R. F. and Toner, R. C. "A New Concept in Power Plant Operation to Control Slime Bacteria in Steam Electric Condenser Cooling Systems." Presented at the Symposium on Biological Fouling Power Plants, Johns Hopkins University, 1976.

7. Gunsalus, I. C. and Stanier, R. Y. The Bacteria. Vol. 1, New York: Academic Press, 1960, Chapter 1.

8. Characklis, W. G. "Attached Microbial Growths. I. Attachment and Growth." Water Research, Vol. 7, 1973a, pp. 1113-1128.

9. Characklis, W. G. Attached Microbial Growths. II. Frictional Resistance Due to Microbial Slimes." Water Research, Vol. 7, 1973b, pp. 1249-1259.

10. Glover, C. J., McIntire, L. V., Brown, C. H. III, and Naterlson, E. A. "Rheological Properties of Fibrin Clots, Effects of Fibrinogen Concentration, Factor XIII Deficiency, and Factor XIII Inihibition," Journal of Laboratory and Clinical Medicine.

11. Kirkpatrick, J. P., McIntire, L. V. and Characklis, W. G. "Mass and Heat Transfer in a Circular Tube with Biofouling." Accepted for publication, Water Research, 1979.

12. LaMotta, E. J. "Kinetics of Growth and Substrate Uptake in a Biological Film System," Applied and Environmental Microbiology, February 1976a, pp. 765-769.

13. Schlichting, H. Boundary Layer Theory, McGraw-Hill Book Co., New York, 1968.

14. Gieseche, F. E. and Hopper, S. S. "Frictional Heads of Water Flowing in Six Such Pipes and the Effects of Pipe Surface Roughness and Water Temperature on Frictional Heads," Bulletin of the Agricultural and Mechanical College of Texas, College Station, Texas, Vol. 14, No. 9, 1943.

15. Norrman, G. "Control of Microbial Fouling in Circular Tubes with Chlorine," M. S. Thesis, Rice University, Department of Environmental Science and Engineering, 1976.

16. Characklis, W. G. and Dydek, S. T. "The Influence of Carbon to Nitrogen Ratio on the Chlorination of Microbial Aggregates," Water Research, No. 10, 1976, pp. 515-522.

17. Norrman, G., Characklis, W. G. and Bryers, J. D. "Control of Microbial Fouling in Circular Tubes with Chlorine," Dev. Ind. Microbiol., Vol. 18, 1977, pp. 581-590.

18. Bryers, J. D. and Characklis, W. G. "A Mathematical Simulation of Microbial Fouling in Water Supply Systems," Paper presented at National AWWA Meeting, Anaheim, California. May 1977.

19. Characklis, W. G. "Oxygen Transfer through Biological Slimes," M.S. Thesis, Univeristy of Toledo, 1967.

20. Hartman, L. "Influence of Turbulence on the Activity of Bacterial Slimes," Journal of Water Pollution Control Federation, Vol. 39, No. 6, 1967, pp. 958-964.

21. Heukelekian, H. "Slime Formation in Polluted Waters, II. Factors Affecting Slime Growth," Sewage and Industrial Wastes, Vol. 28, 1956, pp. 78-92.

22. Atkinson. Biochemical Reactors. London: Pion Limited, 1974.

23. Loeb, G. I. and R. A. Neihof. "Marine Conditioning Films." Applied Chemistry at Protein Interfaces (R.E. Baier, ed.) Washington, D.C. American Chemical Society, 1975, pp. 319-335.

24. Baier, R. E. "Influence of the Initial Surface Condition on Bioadhesion," Proc. 3rd International Congress on Marine Corrosion and Biofouling, National Bureau of Standards, Gaithersburg, Maryland, October 2-6, 1972.

25. Henniker, J. C. "Depth on Surface Zone of a Liquid." Reviews Modern Physics, Vol. 21, No. 2, April 1949, pp. 322-341.

26. Friedlander, S. K. Smoke, Dust and Haze. New York: Wiley, 1977.

27. LaMotta, E. J. "External Mass Transfer in a Biological Film Reactor," Biotechnology and Bioengineering, Vol. 18, 1976c, pp. 1359-1370.

28. Bungay, J. R. III, Whalen, W. J., and Sanders, W. M. III "Microprobe Techniques for Determining Diffusivities and Respiration Rates in Microbial Slime Systems," Biotechnology and Bioengineering, Vol. II, 1969, pp. 765-772.

29. LaMotta, E. J. "Internal Diffusion and Reaction in Biological Films" Env. Sci. & Tech, Vol. 10, No. 8, 1976, pp. 765-769.

30. Bongers, L. H. and T. P. O'Connor. Bromide Chloride-An Alternative to Chlorine for Fouling Control in Condenser Cooling Systems. U.S. Environmental Protection Agency, Contract No. 68-02-2158, EPA-600/7-77-053, May 1977.

31. Brauer, H. "Flow Resistence in Pipes with Ripple Roughness," Chemische Zeitung, Vol. 87, 1963, p. 199.

32. Moody, L. F. "Friction Factors for Pipe Flow." Trans. Amer. Soc. Mech. Eng., Vol. 66, 1944, p. 671.

33. Schuster, H. "Fluid Friction in the Presence of Non-Rigid Boundaries," Ph.D. Thesis, Johns Hopkins University, Baltimore, Maryland, 1971.

34. Benjamin, B. T. "Effects of a Flexible Boundary on Hydrodynamic Stability," Journal of Fluid Mechanics, Vol. 9, 1960, pp. 513-532.

35. Benjamin, B. T. "The Threefold Classification of Unistable Disturbances in Flexible Surfaces Bounding Inviscid Flows," Journal of Fluid Mechanics, Vol. 16, 1963, pp. 736-450.

36. White, G. C. Handbook of Chlorination. New York: Van Nostrand Reinhold Co., 1972.

37. Whistler, R. L. and Schweiger, K. "Oxidation of Amylopectin with Hypochlorite at Different Hydrogen Ion Concentration," Journal of American Chemical Society, Vol. 79, No. 24, 1957, pp. 6460-6464.

38. Black, A. P. and Whittle, G. P. "New Methods for the Colorimetric Determination of Chlorine Residuals," J. Am. Wat. Works Assn., Vol. 59, pp. 607-619.

39. Dukes, E. K. and Hyder, M. L. "Determination of Peroxide by Automatic Colorimetry," Anal. Chem., Vol. 36, 1964, pp. 1689-1690.

40. Thomson, B. M. personal communication, 1977.

Section 6

NOTATION

Symbol	Special Symbol	Description	Units	Defined By Equation
A		wetted surface area	L^2	
	A_I	$2\pi L_T r_I$	L^2	
	A_o	$2\pi r_2 L_T$	L^2	
AFR		Annular Fouling Reactor System		
BOD		Biochemical Oxygen Demand	ML^{-3}	
C_p		heat capacity of water	$EM^{-1}T^{-1}$	
C_r		cumulative chlorine reacted per unit surface area	ML^{-2}	
d		diameter	L	
D		diffusion coefficient	L^2t^{-1}	
	D_{Cl_2}	diffusion coefficient of chlorine in biofilm	L^2t^{-1}	
f		friction factor (for tubular reactors)		3-20
	f_a	friction factor for AFR		3-23
	f_{max}	maximum friction factor		
	f_o	initial friction factor		
F		volumetric flow rate of dilution water	L^3t^{-1}	
	F_r	volumetric flow rate in recycle line	L^3t^{-1}	
FFR		Field Fouling Reactor		
G'		biofilm elastic (storage) modulus	$ML^{-1}t^{-2}$	

Symbol	Special Symbol	Description	Units	Defined By Equation
G"		biofilm viscous (loss) modulus	$ML^{-1}t^{-2}$	
h		individual heat transfer coefficient	$EL^{-1}T^{-1}t^{-1}$	3-30
H		height of inner AFR cylinder	L	
k		thermal conductivity	$EL^{-1}T^{-1}t^{-1}$	
	k_A	thermal conductivity of aluminum	$EL^{-1}T^{-1}t^{-1}$	
	k_{Th}	thermal conductivity of biofilm	$EL^{-1}T^{-1}t^{-1}$	
	k_w	thermal conductivity of water	$EL^{-1}T^{-1}t^{-1}$	
k_s		equivalent sand roughness	L	3-21
K_c		first order rate constant	Lt^{-1}	3-32
K_d		loss of reactivity	L^2M^{-1}	3-33
K_o		rate constant	Lt^{-1}	3-33
L		length	L	
	L_T	length of THE	L	
m_{tot}		total biomass	M	3-7
n		mass loading rate	$ML^{-2}t^{-1}$	
	n_g	glucose loading rate	$ML^{-2}t^{-1}$	
p		pressure	$ML^{-1}t^{-2}$	
q_o		heat flux through THE	$EL^{-2}t^{-1}$	3-24
Q		heat flow to THE	Et^{-1}	3-25
r		biomass production rate	Mt^{-1}	3-8
	r_x	suspended biomass production rate (also sloughing rate)	Mt^{-1}	
	r_{Th}	attached biomass production rate	Mt^{-1}	

Symbol	Special Symbol	Description	Units	Defined By Equation
r_1		inner radius of THE	L	
r_2		radial distance from center of THE to the heat source	L	Fig. 2-5
r_i		radial distance from center of THE to thermistor i	L	Fig. 2-5
r_{ii}		radial distance from center of THE to thermistor ii	L	Fig. 2-5
r_I		r_1 - Th	L	
R		radius	L	
	R_o	radius of AFR outer cylinder	L	
	R_i	radius of AFR inner cylinder	L	
R*		logarithmic fouling rate	t^{-1}	
	R^*_{BM}	R* based on biofilm mass	t^{-1}	
	R^*_f	R* based on f	t^{-1}	
	R^*_{Th}	R* based on Th	t^{-1}	
R_{cond}		conductive heat transfer resistance	$LTtE^{-1}$	3-31
R_{conv}		convective heat transfer resistance	$LTtE^{-1}$	3-30
R_H		overall heat transfer resistance	$LTtE^{-1}$	3-29
R_v		glucose removal rate	Mt^{-1}	3-1
	R'	glucose removal rate per unit X	t^{-1}	3-2
	R"	glucose removal rate per unit A	$ML^{-2}t^{-1}$	3-2
	R''_m	glucose removal rate per unit active biomass in biofilm	$L^{-2}t^{-1}$	3-16
Re		Reynolds Number (dv/ν)		
S		limiting nutrient concentration (glucose)	ML^{-3}	

Symbol	Special Symbol	Description	Units	Defined By Equation
	S_i	limiting nutrient concentration in inlet	ML^{-3}	
SS		suspended solids	ML^{-3}	
T		temperature	T	
	T_b	bulk fluid temperature	T	
	T_i	temperature at r_i in THE	T	
	T_{ii}	temperature at r_{ii} in THE	T	
	T_w	wall temperature	T	
T_q		torque on inner cylinder in AFR	ML^2t^{-2}	
TFR		Tubular Fouling Reactor System		
	TFR1	Tubular Fouling Reactor One		
	TFR2	Tubular Fouling Reactor Two		
	TFR3	Tubular Fouling Reactor Three		
	TFR4	Tubular Fouling Reactor Four		
Th		biofilm thickness	L	
	Th_A	active biofilm thickness	L	3-16,17
	Th_{crit}	biofilm thickness above which hydraulic deterioration is observed	L	
	Th_f	biofilm thickness following chlorination	L	
	Th_{max}	maximum biofilm thickness	L	
	Th_o	biofilm thickness prior to chlorination	L	
THE		Test Heat Exchanger		
TOC		Total Organic Carbon	ML^{-3}	
TSB		Trypticase Soy Broth		
U		overall heat transfer coefficient	$EL^{-2}T^{-1}t^{-1}$	3-26

Symbol	Special Symbol	Description	Units	Defined By Equation
	U_w	overall heat transfer coefficient based on T_w	$EL^{-2}T^{-1}t^{-1}$	3-26
v		velocity	Lt^{-1}	
	v_m	mean fluid velocity	Lt^{-1}	
V		reactor volume	L^3	
X		biomass concentration in bulk fluid	ML^{-3}	
Y		yield (biomass produced per unit mass glucose consumed)		3-6

Greek Letters

δ_l	viscous sub-layer thickness	L	3-22
Δp	pressure drop across length L	$ML^{-1}t^{-2}$	
Θ	mean hydraulic residence time	t	
μ	viscosity	$ML^{-1}t^{-1}$	
ν	kinematic viscosity	L^2t^{-1}	
ρ	density	ML^{-3}	
ρ_{Th}	biofilm dry mass density	ML^{-3}	
τ_w	wall shear stress	$ML^{-1}t^{-2}$	
Ω	rotational velocity	t^{-1}	

Dimensions

E	energy	ML^2t^{-2}
L	length	L
M	mass	M
t	time	t
T	temperature	T

Appendix A

EXPERIMENTAL REACTOR CLEANING PROCEDURES

Standard cleaning procedures subsequent to a fouling experiment have been established to ensure relatively uniform surface conditions for initial attachment and growth.

The following cleaning procedure has been established for TFR1:

1. Set valves A and B to by-pass the Fermenter (Figure 2-2).
2. Pump cleaning solution into system at Port A by means of peristaltic pump.
3. Open discharge valve, C, to direct flow into cleaning solution bottle.
4. Flush with tap water (10-15 min).
5. Recycle 6N NaOH (30 min).
6. Flush with tap water (10-15 min).
7. Recycle 6N HCl (30 min).
8. Flush with tap water (10-15 min).
9. Recycle 0.1N $NaHCO_3$ (30 min).
10. Flush with tap water (60 min) including pressure measurement system.

All fluids are circulated by a peristaltic pump (Model WZ1RO31, Cole-Parmer Co., Chicago, Ill.) because of their corrosivity to the screw pump.

Cleaning procedures for the TFR2 system consists of the same chemicals as TFR1. However, the solutions are introduced into the system through the fermenter and circulated with the screw pump.

A mechanical cleaning procedure, without the chemical wash, was established for the TFR3 system:

1. Drain system and clean tubes with a nylon brush. Approximately 80% of the tubing length is accessible with the nylon brush including the pressure port section and test section.

2. Remove test section and sample tubes and clean the inside of the test section with a nylon brush.

3. Run the TFR system with a 0.25% sodium hypochlorite concentration for one hour.

4. Drain the system and refill with dilution water.

5. Run the system with dilution water for 2 hours to remove all residual chlorine in the system.

6. Check the pressure drop and velocity to ensure the system has returned to original conditions.

The AFR cleaning procedure differed from the TFR systems due to the accessibility of the reactor surfaces in the AFR. The procedure was as follows:

1. Operate in the batch mode at 150 rpm and room temperature for 10 min. with an initial chlorine concentration of 1750 mg/l.

2. Disassemble the reactor and scrub all surfaces with a soft bristle brush under a stream of warm water.

3. Assemble the reactor and repeat step 1.

4. Flush the reactor three times in a fill-and-draw manner and then flush continuously with dilution water for 30 - 40 minutes.

Appendix B

PROTOCOL FOR BATCH INDUCTION PERIOD OPERATION

An initial period of batch operation is necessary to minimize the induction period, i.e., period of initial attachment. The following steps are followed subsequent to cleaning the reactor:

1. Set temperature and flow rate to experimental conditions.
2. Shut off the dilution water flow.
3. Fill the reactor with an initial nutrient solution as follows:

   TFR1 and TFR2 - 100 mg/l glucose + 100 mg/l trypticase soy broth.

   TFR3-1 to TFR3-4 - 50 mg/l glucose + 50 mg/l trypticase soy broth.

   TFR3-5 to TFR3-16 - 50 mg/l glucose + micronutrient mixture.
4. Add one vial of standard inoculum (10 cm^3).
5. Operate the reactor for approximately 10 hours.

At the end of batch operation, initial attachment, and perhaps some initial growth, has occurred. Occasionally experiments at low inlet substrate concentration (5 mg/l) in TFR2 required two or more inoculations before significant growth was observed. Note that TFR2 dilution water is untreated tap water with no pH adjustment.

In the AFR, the following procedure occurred subsequent to cleaning the reactor:

1. Set rotational speed to 150 rpm.
2. Fill the reactor with an initial nutrient solution as follows:

   50 mg/l glucose + 50 mg/l trypticase soy broth

3. Add one vial of standard inoculum (10 cm^3)

4. Operate the reactor for approximately 8 hrs.

Appendix C

ANALYTICAL PROCEDURES

BIOFILM DEVELOPMENT EXPERIMENTS

Suspended Solids Concentration

Suspended solids are determined by filtering a specified sample volume through a Nuclepore membrane (Nuclepore Corp., Pleasanton, Calif., No. 111107; average pore size 0.45 μm). The samples are stirred before filtering to provide a more uniform sample. Samples are stored no longer than 24 hrs before analysis. An adequate sample volume is 100 mg/l.

Glucose

Glucose concentration is determined by the Glucostat semimicro procedure (Worthington Biochemical Co., Freehold, N.J). The calibration curves consistently exhibit linear behavior in the desired concentration range.

Soluble Organic Carbon

The direct injection module of a Total Carbon System (Oceanography International Corp., College Station, Texas) is used for soluble organic carbon (SOC) determinations. Inorganic carbon (IC) is determined by injection into acid in a standardization ampule on the main circuit of the system. Precision is ± 2.0 mg/l for samples measured.

Bulk Fluid Viscosity

A water bath maintains a temperature of 37.8°C for viscosity measurements with a capillary viscometer. A calibration curve supplied by the manufacturer (Fisher Scientific, Fair Lawn, N.J.) provides a coefficient for converting time of efflux (in seconds) to viscosity in centistokes (± 1.0%).

Bacterial Number Density in Biofilms

After a biofilm volume measurement is completed with a TFR test section, the biofilm is scraped and rinsed from the test section to a beaker. The suspension is transferred to a volumetric flask and diluted to 500 ml with deionized water. The resulting suspension is blended for six seconds, diluted using a Millipore 1:10,000 dilution kit, and sample with a Millipore Biocount Sampler. After 24-48 hours, the sampler is counted. A density is obtained from the count by dividing with the measured biofilm volume.

OXIDIZING BIOCIDE EXPERIMENTS

Continuous Oxidant Monitor

The Autoanalyzer II (Technicon Instruments Corp., Tarrytown, N.Y.) provides continuous, on-line analysis of oxidant in the biofouling film destruction experiments. The interface of the TFRI system with the AAII is presented in Figure C-1a. Pressure drop across the by-pass tube section resulted in a flow with a residence time of less than 5 seconds when fluid velocity in the TFRI is 90 cm/sec, the lowest fluid velocity employed. The interface of the AAII with the AFR is presented in Figure C-1b. Residence time in the by-pass is less than 5 seconds.

Analytical Methods

Free Chlorine. Free chlorine is determined by a modification of the leuco crystal violet method (Black and Whittle, 1967) for use in the AAII. The AAII tubing schematic is shown in Figure C-2. Reagents are prepared as follows:

1. Leuco crystal violet. Leuco crystal violet (1.5 g) is added to 500 ml demineralized water followed by 3.5 ml perchloric acid (70%). The resulting clear solution is stored in an amber bottle.

2. Buffer. pH 4.0 buffer (Fisher Scientific Co., Fair Lawn, N.J.) consisting of 0.05 M potassium acid phthalate is diluted 10 times.

Chlorine solutions are prepared from sodium hypochlorite solutions ("Clorox" 5.25% Cl wt/V) in the range 0-10 mg/l and standardized on an amperometric titrator (Wallace and Tiernan, Bellville, N.J., Model No. A790013). A calibration curve for the colorimetric analysis is presented in Figure C-3. Figure C-4 indicates the response of the AAII to a step input of chlorine.

Combined Chlorine. Chloramines are determined by a modification of the method for free chlorine described above. Potassium iodide (1.5 g) is added to the buffer reagent (200 ml). A calibration curve is presented in Figure C-5.

Hydrogen Peroxide. Hydrogen peroxide is determined by the method of Dukes and Hyder (39). Reduced phenolphthalein reacts with hydrogen peroxide in the presence of cupric ion and base to form the red anionic form of phenolphthalein. The AAII tubing schematic is presented in Figure C-6. The reagents are prepared in the following manner:

1. Leuco phenolphthalein. Reflux the following for two hours or until colorless; 10 g phenolphthalein, 100 g sodium hydroxide, 50 g zinc dust, and 200 ml demineralized water. Filter through glass wool, dilute to two liters and store in a dark bottle. The reagent is diluted 5X before use.

2. Copper sulfate reagent (0.05 M). Dissolve 0.4 g $CuSO_4 \cdot 5H_2O$ in one liter demineralized water. The reagent is diluted 5X before use.

Ozone. Ozone is determined by a modification of the leuco crystal violet method (Black and Whittle, 1967). The modification was developed by Thomson (1977) as a manual method and further modified for autoanalyzer use during this project. The buffer employed for chlorine analysis is replaced by the following:

> Buffer. Glacial acetic acid is added to 1 liter of water containing sodium acetate (8.2 g) and manganous sulfate (1.66 g) until pH 4.0 is attained.

A calibration curve for the colorimetric analysis is presented in Figure C-7.

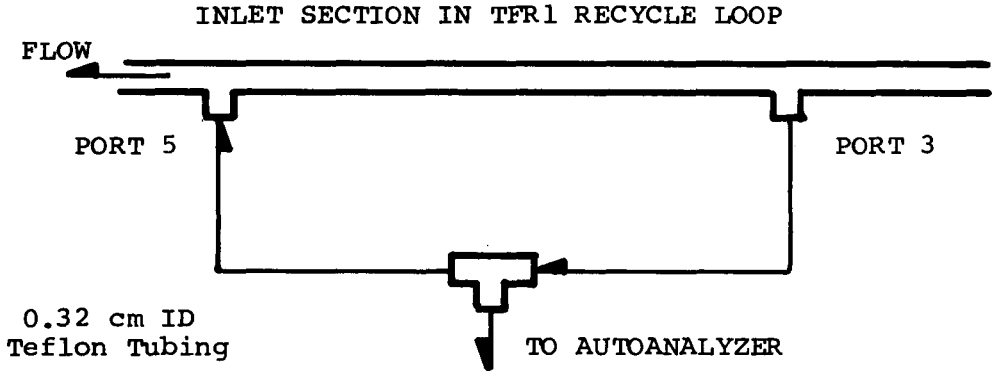

Figure C-1a. Schematic diagram of the interface between TFR1 and the oxidant monitor.

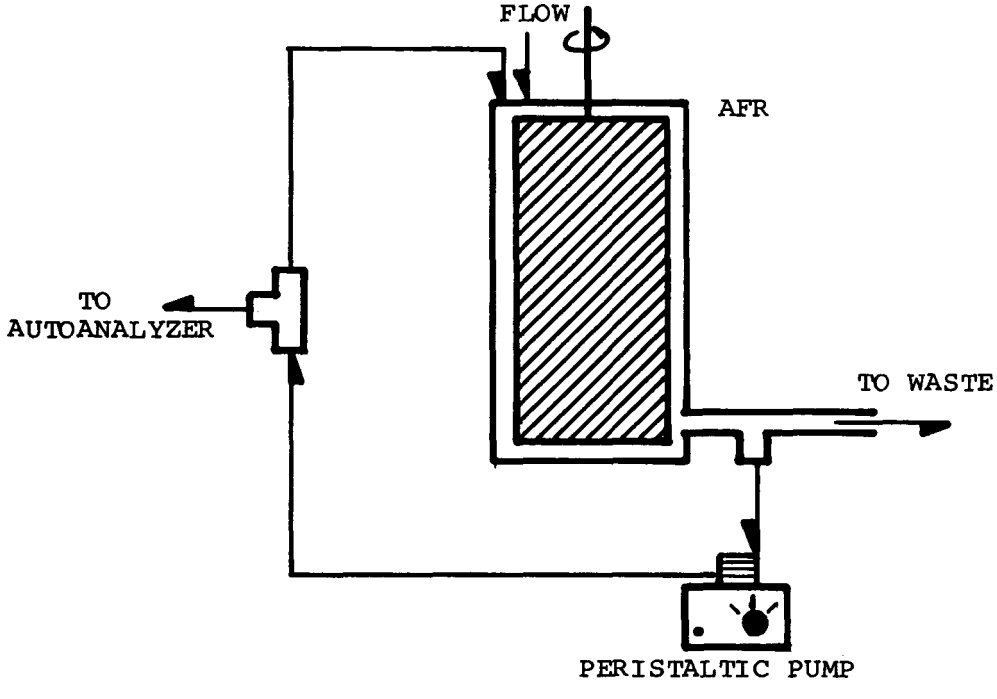

Figure C-1b. Schematic diagram of the interface between AFR and the oxidant monitor.

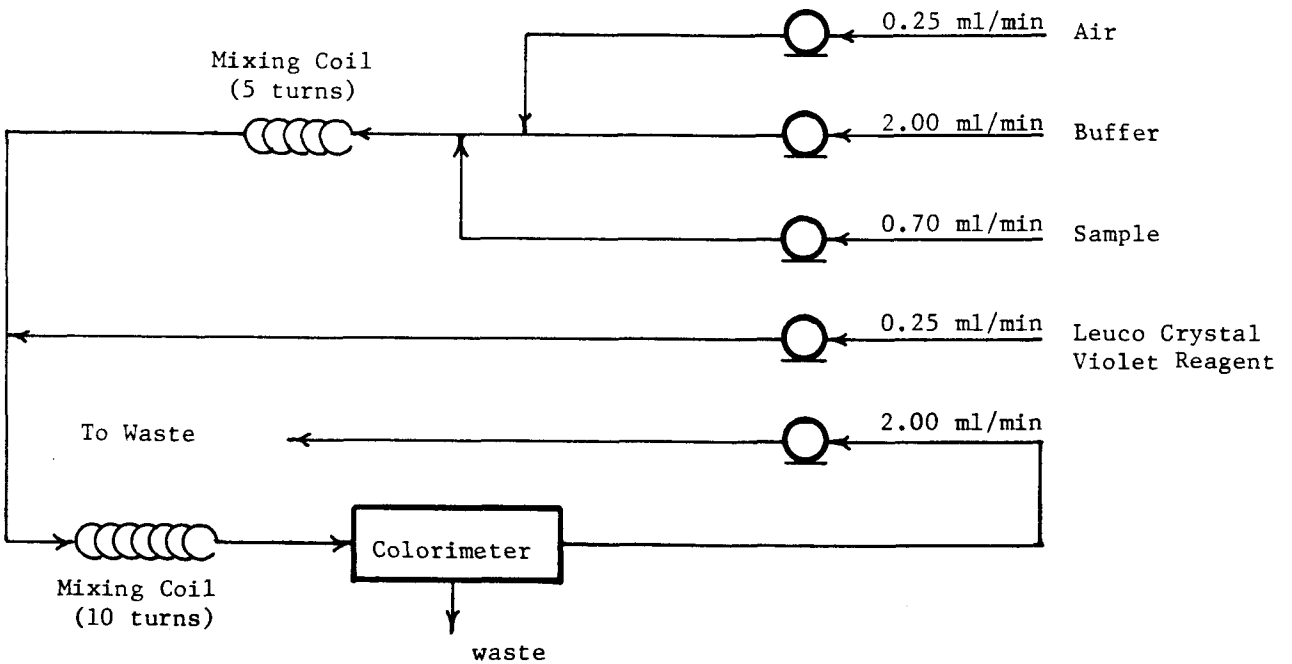

Figure C-2. AAII tubing schematic for free chlorine analysis by modified leuco crystal violet method. Colorimeter is set at 630 nm.

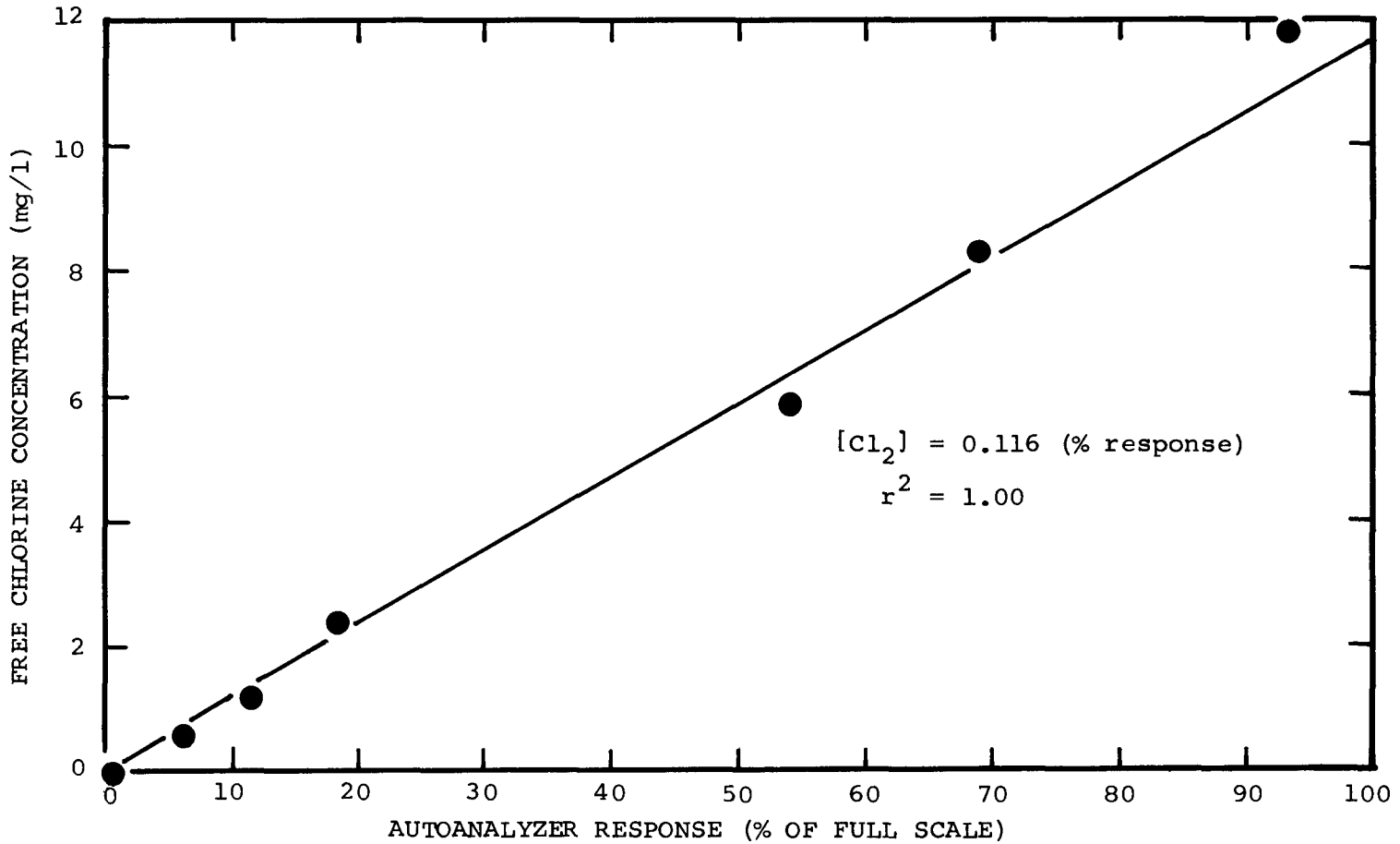

Figure C-3. Calibration curve for free chlorine analysis by AAII leuco crystal violet method.

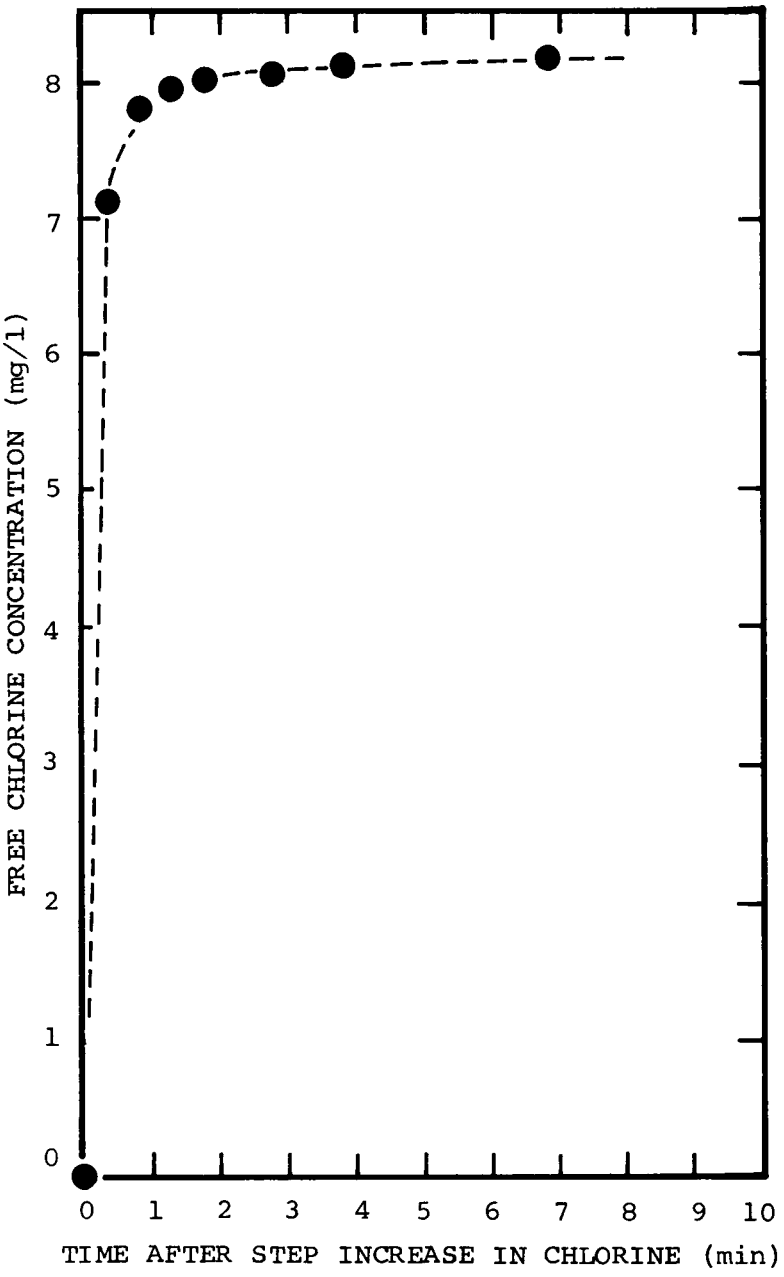

Figure C-4. Response of AAII leuco crystal violet method to a step increase in free chlorine concentration (8 mg/l).

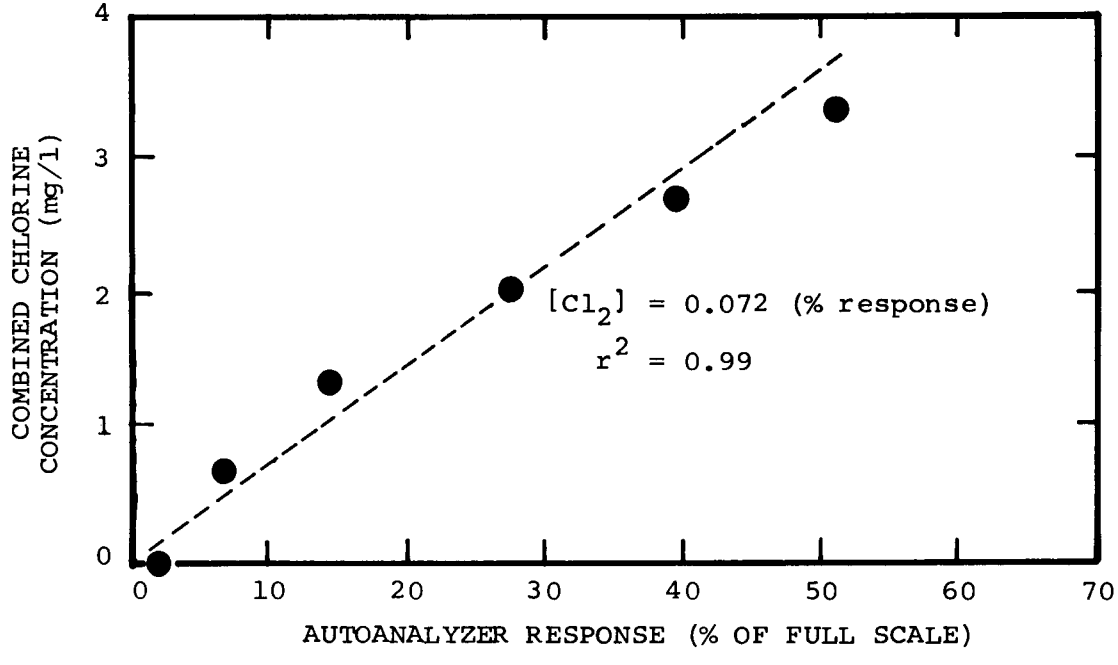

Figure C-5. Calibration curve for chloramine analysis by AAII method. Chloramines were prepared by adding NaOCl to an excess of ammonium sulfate.

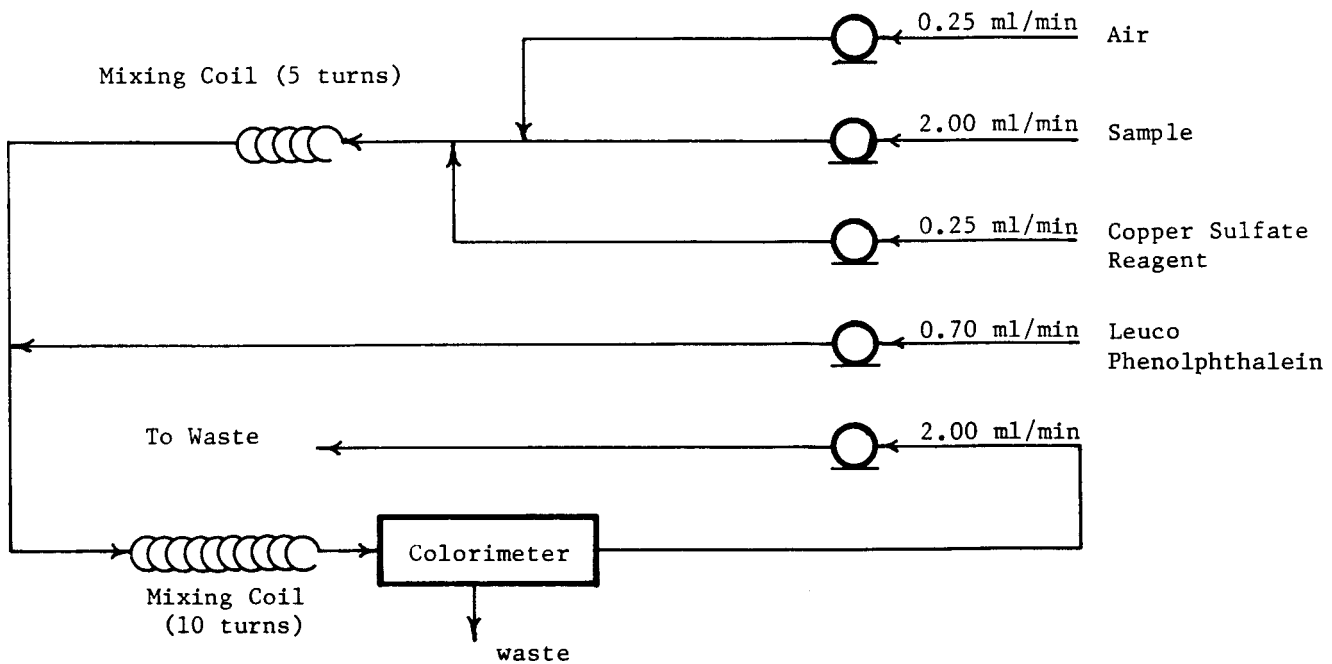

Figure C-6. AAII tubing schematic for hydrogen peroxide analysis by method of Dukes and Hyder (39). Colorimeter is set at 520 nm.

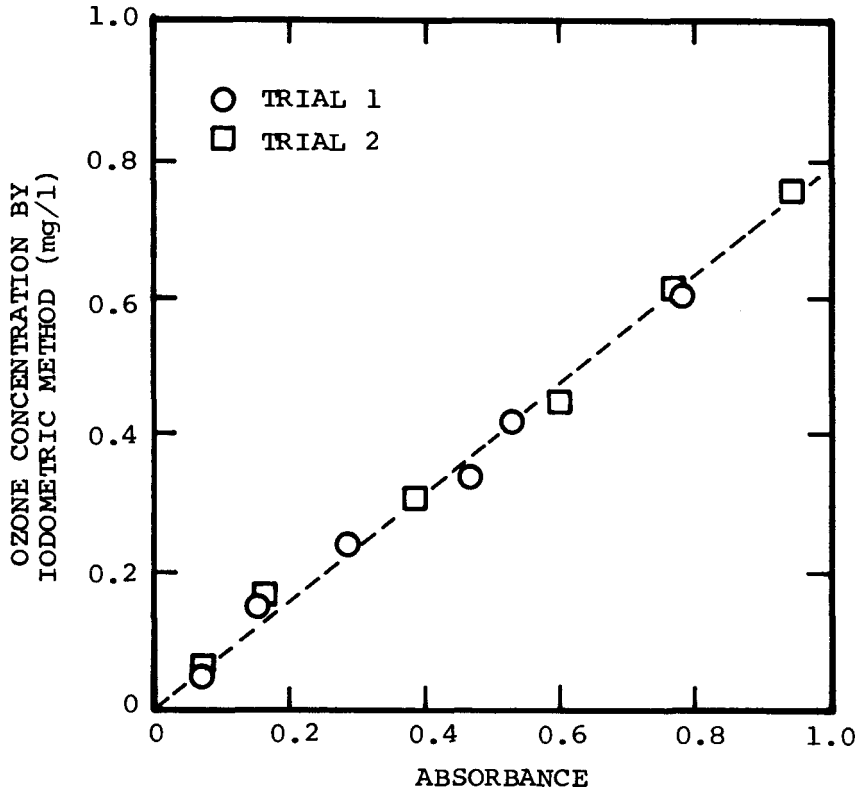

Figure C-7. Manual calibration curve for ozone analysis by modified leuco crystal violet method.

Appendix D

EFFECT OF DRAIN TIME ON MEASURED BIOFILM VOLUME

Biofilm thickness is calculated from biofilm volume by dividing by sample tube surface area. Repeated measurements of a fouled sample tube from TFR3-14.

DRAIN TIME (min)	THICKNESS (μm)
0.0	70
0.0	84
0.0	100
2.5	80
2.5	74
10.0	57
10.0	61

Appendix E

WEIGHT AND DISPLACEMENT OF SAMPLE TUBES
USED IN BIOFILM VOLUME DETERMINATION

Change in Liquid Level (cm ÷ 2.54)	Clean Sample Tube Mass (mg)
0.7068	17.6676
0.6875	17.2115
0.6982	17.4564
0.6906	17.2915
0.6859	17.1589
0.6975	17.4442
0.6901	17.2639
0.6825	17.0897
0.6812	17.0346
0.6980	17.4343
0.6921	17.2804
0.6888	17.2079
0.6867	17.1573
0.6979	17.4261
0.6905	17.2460

$$\frac{\text{Clean Sample Tube Mass}}{\text{Change in Liquid Level}} = 25.0028 \pm 0.02401 \text{ mg/in}$$

$$= 9.844 \pm 0.0095 \text{ mg/cm}$$

Appendix F

VARIANCE IN BIOFILM THICKNESS DETERMINED FROM BIOFILM VOLUME MEASUREMENT IN TFR3-1 AT 105 HR

FILM MASS (mg)	FILM THICKNESS (μm)	BIOFILM DENSITY (mg/cm^3)
2.2	112	9.85
7.8	111	35.22
3.5	96	18.27
-	115	-
4.6	103	22.39
4.8	103	23.36
4.1	97	21.19
5.1	97	21.19
5.1	97	26.36
3.9	85	23.00
3.8	-	-
3.4	109	15.64
4.3	88	24.49
4.6	98	23.53
4.2	95	22.16
5.2	-	-
6.3	-	-
Average:		
4.5 ± 1.3 (16)	100 ± 9.0 (14)	22.05 ± 5.8 (13)

Appendix G

CALIBRATION CURVE FOR FILM THICKNESS MEASUREMENT
USING THE OPTICAL MICROSCOPE TECHNIQUE

Each point is a measurement on a solid material (e.g., metal shims) with actual thickness being the average of repeated measurements with a Vernier micrometer.

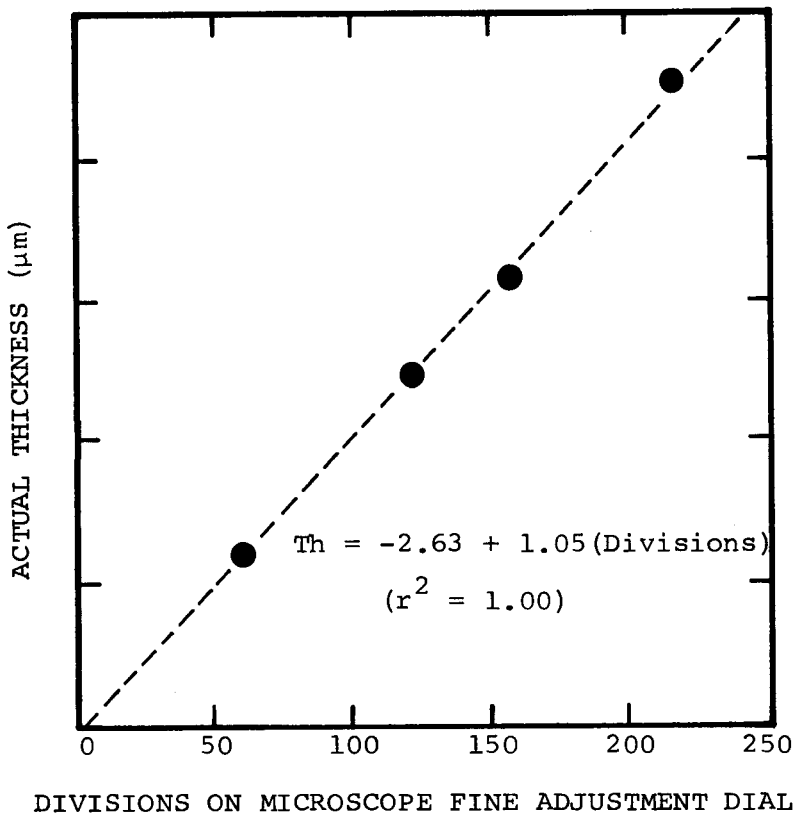

Appendix H

VARIANCE IN BIOFILM THICKNESS DETERMINATION
USING THE OPTICAL MICROSCOPE (AFR)

Determinations of biofilm thickness are made at four or five predetermined locations on the plastic removable slide at each observation time. The five determinations are averaged to yield the biofilm thickness at that observation time. The table below lists the mean and standard deviation for all thickness measurements in 15 AFR experiments. The mean standard deviation is 11.9 $\pm$ 8.9 μm.

Expt. No.	Elapsed Time (hr)	Mean Biofilm Thickness (μm)	Standard Deviation (μm)	Determinations
1	16	36.1	4.2	5
	23	47.8	5.0	4
	37	71.4	11.6	5
	47	88.9	5.8	4
	62	103.3	13.2	4
	72	103.8	15.5	4
2	18	11.4	7.9	5
	25	83.2	10.4	5
	42	93.9	24.0	5
	47	67.6	5.0	5
	61	71.8	8.6	5
3	16	35.9	7.1	5
	24	67.7	8.1	5
	37	108.9	29.9	5
	41	136.3	24.7	5
	60	112.8	14.6	5
4	18.5	17.5	6.1	5
	26.9	40.0	10.6	5
	38.2	95.5	20.3	5
	62.0	93.6	7.9	5
	68.5	89.2	5.7	5

Expt. No.	Elapsed Time (hr)	Mean Biofilm Thickness (μm)	Standard Deviation (μm)	Determinations
5	12.6	36.2	4.7	5
	16.1	75.0	10.4	5
	21.5	96.3	15.9	5
	37.6	113.3	44.4	5
	45.8	110.0	37.1	5
	59.7	106.2	34.2	5
6	14.2	25.2	6.9	5
	18.6	49.4	9.9	5
	22.3	84.4	10.5	5
	35.2	93.2	26.4	5
	41.4	91.3	24.3	5
	59.6	105.1	38.1	5
7	15.2	44.4	8.5	5
	23.4	91.9	29.9	5
	39.4	76.4	14.4	5
	59.8	87.5	24.6	5
8	23.8	32.9	9.0	5
	34.1	57.8	12.4	5
	41.8	82.8	5.0	5
	61.3	95.9	10.5	5
	86.0	102.6	12.7	5
9	22.3	26.0	4.6	5
	37.4	50.2	4.6	5
	48.3	45.9	4.7	5
	60.3	67.5	14.7	5
	66.0	62.8	7.8	5
10	25.0	35.9	7.7	5
	42.6	85.7	17.2	5
	48.4	92.4	22.5	5
11	13.0	31.7	2.9	5
	17.8	62.9	7.5	5
	37.8	79.2	14.1	5
	58.7	73.9	15.8	5
12	11.9	34.0	6.6	5
	20.9	56.6	6.0	5
	35.0	34.6	7.0	5
13	11.9	23.5	4.5	5
	18.1	49.1	8.2	5
	23.8	59.7	14.9	5
	36.1	46.5	12.2	5
	41.5	42.6	3.3	5
	60.1	33.4	2.3	5

Expt. No.	Elapsed Time (hr)	Mean Biofilm Thickness (μm)	Standard Deviation (μm)	Determinations
14	11.5	30.2	3.4	5
	22.8	53.9	4.2	5
	40.7	58.5	7.2	5
	66.1	52.6	7.8	5
15	16.2	34.6	6.9	5
	24.9	58.9	10.6	5
	37.4	53.4	7.5	5
	51.7	43.0	3.7	5
	60.5	55.1	7.4	5
	77.9	44.7	4.1	5

Appendix I

SUMMARY OF ALL TFR1 AND TFR2 EXPERIMENTS EXCLUDING THOSE WITH VARYING T_s

TFR # Expt.	S_j (mg/l)	T_b (°C)	τ_w (N/m²)	$\bar{v}$ (cm/sec)	R_f^* (days^{-1})	R_{th}^* (days^{-1})	f_{max}	TH_{max} (μm)	$\bar{\rho}_f$ (mg/cm³)	n_g (mg/m²-min)	F_D (l/min)	$S_i - \bar{S}$ (mg/l)	R" (mg/m²-min)
1-1		28	4.3	111	0.579		0.0320				0.50		
1-2	9.8	28	3.1	92	0.547	0.837	0.0600	135		5.8**	0.50	9.3	5.1
1-3	2.8*	28	3.1	92	0.166		0.0363	75		1.5**	0.50		
1-4	9.8*	35	3.0	92	0.566	0.303	0.0302	150		4.2**	0.36		
1-5	3.9	30	3.0	92	0.497		0.0255			1.7	0.36	3.5	1.4
1-6	47.1	30	12.9	210	0.238		0.0190	200		18.4	0.36	42.1	16.5
1-7	42.2	35	3.0	92	1.351	0.329	0.0500	950	14.2	16.5	0.36	34.8	13.6
1-8	37.7	40	6.9	151	0.214	.114	0.0230	100	32.9	14.8	0.36	36.2	14.2
1-10	12.9	40	2.8	90	0.430	0.213	0.0203	150	10.2	6.2	0.44	12.3	5.9
1-11	6.6	35	4.7	120	0.060	0.069	0.0215	139	15.2	3.2	0.44	5.6	2.7
1-12	10.0	40	6.8	150	0.360	0.374	0.0142	175	19.4	4.8	0.44	9.9	4.7
1-13	2.0	40	6.8	150	0.106	0.498	0.0115	64	20.0	1.0	0.44		
1-14	12.4	30	7.2	150	0.413	0.571	0.0175	105	15.5	5.9	0.44	11.1	5.3
1-15	7.7	30	2.9	90	0.151	0.535	0.0285	470	10.1	3.7	0.44	6.6	3.2
1-16	6.4	35	4.7	120	0.065	0.224	0.0165	125	11.8	3.1	0.44	5.8	2.8
1-17	2.3	30	2.9	90	0.060	0.060	0.0175	55	10.5	1.1	0.44	1.7	0.8
1-21	6.0**	35	4.7	120	0.048	0.572	0.0087	60	12.3	2.9**	0.44		
1-22	5.2	35	4.7	120	0.271	1.087	0.0139	138	13.9	2.5	0.44		
1-23	3.0	35	7.2	150	0.067	0.571	0.0085	50	10.4	1.4	0.44	1.9	0.9
1-24	2.8**	40	2.8	90	0.046	0.112	0.0090	48	7.5	1.3**	0.44	2.0	1.0
2-1	9.8**	30	11.2	194	0.247	0.382	0.0080	200	27.5	3.1**	0.44	8.3	3.2
2-2	8.0	30	11.3	195	0.249	0.300	0.0120	60	23.6	3.2	0.44	7.1	2.8
2-3	7.6	30	11.3	195	0.094	0.154	0.0080	185	33.2	3.0	0.44	6.9	2.7
2-6	58.0	30	10.5	187	0.522	0.538	0.0325	170	38.0	22.9	0.44	54.0	21.2
2-7	47.0	30	10.4	186	0.250	0.690	0.0205	201	36.7	18.6	0.44	36.3	14.2
2-8	57.0	30	10.3	185	0.338	0.859	0.0390	406	22.0	22.5	0.44	55.0	21.6
TAFRI	5.6	30	2.0	72	0.151		0.0184	79		2.1	0.48	4.0	

**calculated values (see Appendix U)

First number identifies the apparatus and the second number identifies the experiment. For example, 1-14 identifies the 14th experiment with TFR1.

R" refers to plateau or steady state value.

Appendix J

SUMMARY OF ALL AFR EXPERIMENTS

AFR Expt.#	S_i (mg/l)	T_b (°C)	τ_w (N/m²)	$\bar{v}$ (cm/sec)	R_f^* ($days^{-1}$)	R_{th}^* ($days^{-1}$)	f_{max}	TH_{max} (μm)	$\bar{\rho}_f$ (mg/cm³)	n_q (mg/m²-min)	F_D (l/min)	$S_i - \bar{S}$ (mg/l)	R" (mg/m²-min)
1	2.6	30	1.9	82.5	0.71	0.30	0.385	103		0.82	0.057	1.6	0.46
2	9.4	30	2.9	104.5	1.14	2.76	0.353	93		2.98	0.057	8	2.28
3	9.2	40	1.9	82.5	2.00	0.52	0.390	136		2.92	0.057	5	1.43
4	2.7	40	2.8	104.5	1.01	0.89	0.278	96	13.8	0.86	0.057	2.5	0.71
5	6.6	35	2.4	93.5	2.84	2.16	0.475	113	25.5	2.09	0.057	6	1.71
6	6.8	35	2.4	93.5	2.11	1.56	0.439	105	41.6	2.16	0.057	6.2	1.77
7	9.2	40	2.8	104.5	3.59	0.92	0.344	92	18.4	2.92	0.057	7.8	2.23
8	3.1	40	1.9	82.5	0.43	0.54	0.410	103	23.8	0.98	0.057	1.3	0.37
9	0.4	30	2.9	104.5	0.20	0.45	0.252	68	39.4	0.13	0.057	0	0
10	11.0	30	1.9	82.5	1.70	0.52	0.487	92	48.5	3.49	0.057	9	2.57
11	7.2	35	2.4	93.5	2.75	1.49	0.344	79	10.7	2.28	0.057	6	1.71
12	6.6	35	2.4	93.5	4.07	0.59	0.365	57		2.09	0.057	5.6	1.60
13	7.0	35	2.4	93.5	2.39	1.24	0.356	60	34.4	2.22	0.057	5.8	1.66
14	2.7	30	2.9	104.5	2.11	1.23	0.322	58	45.5	0.86	0.057	1.5	0.43
15	14.8	35	2.4	93.5	2.91	1.56	0.298	59	59.5	4.69	0.057	13.4	3.83
HT (16)		30**	2.4	93.5	1.93	0.42	0.436	58	14.4	2.16	0.057	--	--
TAFRI (17)	5.6	30	2.4	93.5	0.18	0.58	0.202	63		1.78	0.057	4	1.53

** Inlet bulk temperature

R" refers to plateau or steady state value.

Appendix K

DATA SUMMARY FOR TFR3 EXPERIMENTS

EXPT. #	S_i (mg/l)	T_b (°C)	τ_w (N/m^2)	F_D (cm^3/min)	$\bar{v}$ (cm/min)	R_f^* ($days^{-1}$)	R_{BM}^* ($days^{-1}$)	$\bar{\rho}_{Th}$ (mg/cm^3)	n_g (mg/m^2-min)
1	4.0	35	9.8	140	12500	0.062	--	19.7	1.57
2	6.5	35	6.5	140	9780	0.172	0.499	22.1	2.55
3	10.6	35	6.5	140	10000	0.067	0.551	16.4	4.15
4	26.3	35	6.5	140	10000	0.292	--	20.2	10.30
5	31.9	30	7.9	280	11100	0.398	1.79	25.9	25.76
6	6.4	30	7.9	280	10800	0.236	0.657	17.1	5.17
7	86.1	30	7.9	280	10800	0.163	1.39	36.7	69.48
8	248.6	30	7.9	280	10800	0.164	2.14	44.4	200.60
9	--	30	7.9	280	11100	--	--	31.0	201.70
10	0.	30	7.9	280	11100	0.0	0.0	--	0.0
11	5.9	30	2.0	280	5160	0.125	0.585	9.4	4.76
12	4.2	30	1.6	280	4800	0.147	0.687	8.1	3.43
14	5.5	30	14.2	280	15700	0.141	0.392	20.1	4.44
15	28.2	30	14.2	280	15200	0.083	1.10	38.5	22.80
16	--	30	14.2	280	15200	0.100	0.758	37.3	201.70

Appendix L

SUMMARY OF TFR4 EXPERIMENTS

Expt. #	S_i (mg/l)	T_b (°C)	Initial τ_w (N/m^2)	$\bar{v}$ (cm/sec)	R_f^* ($days^{-1}$)	R_U^* ($days^{-1}$)	R_{Th}^* ($days^{-1}$)	f_{max}	U_{min} (watt/m^2 C)	Th_{max} (μm)	ρ_f (mg/cm^3)	n_g (mg/m^2-min)	F_D (l/min)	R^* (mg/m^2-min)	k_{Th} (watt/m-°C)	Water in Biofilm (%)
1	200	31.9	2.20	80.9	0.26	-0.31	0.58	0.067	3161[1]	245	39.9	68.2	0.474	-	0.73	98.1
2	20	31.5	2.28	80.7	0.24	-0.10	0.23	0.092	4717	94	18.3	6.82	0.474	-	0.73	98.6
3	10	31.5	2.28	80.5	0.09	-0.01	0.16	0.037	5796	94	14.4	3.41	0.474	2.9	-	98.9
4	50	31.5	2.28	80.8	0.74	-0.05[2]	0.38	0.197	5044	302	21.6	17.1	0.474	16.7	-	98.6
5	50	31.5	2.32	80.5	1.06	-0.04[2]	0.30	0.182	0122	223	15.3	17.1	0.474	16.8	-	99.0
6	20	28.3	2.28	80.7	0.62	-0.17	0.41	0.208	3915	141	16.2	6.8	0.474	6.2	0.69	98.9
7	50	26.7	2.30	80.7	1.82	-0.55	0.65	0.154	3088	259	28.0	17.1	0.474	16.4	0.64	98.1
8	20	26.7	2.28	80.8	0.60	-0.18	0.55	0.212	3115	232	23.6	6.8	0.474	-	0.80	98.5
9	20	28.3	2.28	80.7	0.53	-0.11	0.51	0.202	3464	128	24.0	6.8	0.474	-	0.57	98.2
10	0	31.5	2.28	80.8	0.00	-0.01	0	0.030	6091	0	0	0	0.474	-	-	-

[1] non-uniform biofouling in THE

[2] placeau not reached; premature nutrient depletion

Appendix M

ANALYSIS OF INORGANIC DEPOSIT FROM TFR3 ACCOMPLISHED WITH AN ETEC AUTOPROBE IN THE DEPARTMENT OF GEOLOGY, RICE UNIVERSITY

Stage Coordinates: Discolored - 665 510 8858
Clear - 455 510 8870

Elements examined: Al,Si,P,S,K,Ca,Ti,V,Cr,Mn,Fe,Co,Ni,Cu,Zn

Elements found: Al,Si,Ca,Fe,Cu,Zn

100 sec counts:-

Specimen	Al	Ca	Fe	Cu	Zn
Discolored	C 016867	D 008320	E 037739	E 005511	E 004447
Clear	C 017813	D 000983	E 000872	E 001486	E 001662
Offsets (On Clear Spec.)	C 002520 C 003261	D 000090 D 000155	E 000083 E 000095	E 001574 E 001262	

The specimens were mounted on an Al disc. Although the disc was well below the plane of focus of the spectrometers, this might account for the high Al count observed in both specimens.

The Offsets are the backgrounds. The average of the two numbers in each offset should be subtracted from the numbers reported for the specimens.

Results suggest the following approximate composition:

74% Fe 15% Ca 6% Zn 5% Cu

Appendix N

IN SITU RHEOLOGICAL TESTS ON BIOFILM

Excitation Frequency (Hz)	Elastic (Storage) Modulus, G' (N/m^2)	Viscous (Loss) Modulus, G" (N/m^2)
3.00	54.5	76.2
4.32	51.7	88.7
5.27	53.6	98.4
6.00	59.5	118
7.93	76.4	142
9.80	117	182
12.00	299	368

Reactor T_b was maintained at 40^{o} C and initial shear stress (τ_w) was 5 N/m^2. Substrate Input (S_i) consisted of 10 mg/l Trypticase Soy Broth. The viscoelastic measurements were conducted on a Weissenberg Rheogoniometer.

Appendix O

VIABLE CELL NUMBERS IN BIOFILM
AND IN THE BULK FLUID FOR EXPERIMENTAL REACTORS

Experiment	Biofilm Bacterial Number Density* (#/cm^3 biofilm)		
TFR1-10	3.9×10^6	$\pm$ 3.1×10^6	(2)
TFR1-11	2.7×10^7	$\pm$ 3.1×10^8	(2)
TFR1-12	7.8×10^8	--	(1)
TFR1-13	2.0×10^8	--	
	Suspended Bacterial Number Density* (#/cm^3)		
TFR1-2	9.3×10^5	$\pm$ 6.1×10^5	(3)
TFR1-3			
run time (hr)			
12	1.2×10^6		
44	1.0×10^6		
52	1.3×10^6		
78	1.3×10^6		
82	7.9×10^5		
95	2.5×10^6		
102	1.6×10^6		
123	2.5×10^5		
136	2.5×10^3		
140	3.9×10^5		
Average	1.0×10^6	$\pm$ 7.3×10^5	(10)
TFR1-4	3.1×10^5	--	(2)
TFR1-7	1.6×10^5	--	(1)
TFR1-8	1.9×10^7	$\pm$ 1.0×10^7	(3)
TFR1-10	5.4×10^6	$\pm$ --	(2)
TFR1-11	6.7×10^6	$\pm$ --	(2)
TFR1-12	2.3×10^6	$\pm$ --	(1)
TFR1-13	2.0×10^6	$\pm$ --	(1)

* Mean values $\pm$ standard deviation (number of determinations)

Appendix P

SUMMARY OF OXIDANT PULSE INJECTION EXPERIMENTS

EXPT. NO. / Inject No.	TREATMENT	TEMP. (°C)	pH	REACTOR SURFACE (cm^2)	REACTOR VOLUME (cm^3)	INITIAL α_f (mg/cm^2)	INITIAL ρ_f (mg/cm^3)	INITIAL THICKNESS (μm)	FINAL THICKNESS (μm)	INITIAL ΔP (mmHg)	FINAL ΔP (mmHg)	K_c RATE COEFFICIENT ($cm/sec \times 10^3$)	K_d (cm^2/mg)	$C_r \times 10^4$ (mg/cm^2)
TFR-11	chlorine	23.5	7.4	13200	4180	0.21	15.2	81	48	42	39			
1														7.7
2												2.43		15.4
3												1.01		92.7
4												1.66		170.0
5												2.79		195.6
6														272.9
TFR-12	chlorine	25	8.0	13200	4180	0.34	19.4	137	62	81	59		162	
1												3.85		
2												1.69		28.4
3												1.16		56.8
4												0.83		85.2
5												0.58		113.6
6												0.45		142.0
7												0.16		170.4
														251.5
TFR-13	chlorine	25	7.0	13200	4180	0.13	20.0	85	27	65.5	61.5		119	
1												5.40		
2												4.24		28.4
3												3.08		56.8
4												2.15		85.2
5												1.58		113.6
6												0.99		142.0
														170.4
TFR-14	chlorine	25	7.9	13200	4180	0.16	15.5	40	38	55.5	55.0		86	
1												4.64		
2												5.19		28.4
3												3.27		56.8
4												2.34		85.2
5												2.03		113.6
														142.0

EXPT. NO.	TREATMENT	TEMP. (°C)	pH	REACTOR SURFACE (cm^2)	REACTOR VOLUME (cm^3)	INITIAL α_f (mg/cm^2)	INITIAL ρ_f (mg/cm^3)	INITIAL THICKNESS (μm)	FINAL THICKNESS (μm)	INITIAL ΔP (mmHg)	FINAL ΔP (mmHg)	K_C RATE COEFFICIENT ($cm/sec \times 10^3$)	K_d (cm^2/mg)	C_r (mg/cm^2)
Inject No.														
TFR-15	chlorine	25.5	8.3	13200	4180	0.47	10.1	180	109	44.8	34.5			
1												6.46		
2												3.12		81.1
3														162.1
TFR-16	chlorine	40	7.0	13200	4180	0.15	11.8	223	26	51.0	40.5		133	
1												7.32		
2												8.88		28.4
3												6.54		56.8
4												2.68		85.2
5												2.18		113.6
6												1.50		142.0
7												1.01		170.4
														198.9
TFR-22	chlorine	27	8.2	6700	2130	0.19	13.9	139	56.5/75				111	
1												2.42		
2												0.77		56.0
3												0.55		111.9
4												0.34		167.9
														223.9
TFR-24	H_2O_2		8.3	6700	2130		7.5	48						
1												0.28		
2												0.25		22.4
														44.8
TFR-clean	chlorine			6700	2130			0	0					
												0.03		
														56.0

EXPT. NO.	TREATMENT	TEMP. (°C)	pH	REACTOR SURFACE (cm^2)	REACTOR VOLUME (cm^3)	INITIAL α_f (mg/cm^2)	INITIAL ρ_f (mg/cm^3)	INITIAL THICKNESS (μm)	FINAL THICKNESS (μm)	INITIAL ΔP (mmHg)	FINAL ΔP (mmHg)	K_c RATE COEFFICIENT ($cm/sec \times 10^3$)	K_d (cm^2/mg)	C_r (mg/cm^2)
Inject No.														
TXXPO	H_2O_2	28.5	8.3	6700	2130			85	67	82.5	81.3			
1												1.82		22.4
2												1.92		67.2
3												1.74		156.7
AFR-7	chlorine	40		1800	571	0.17	18.4	92					-0.0610	
1												2.51		59.4
2												1.31		118.9
3												0.68		178.3
AFR-8	chlorine	40		1800	571	0.24	23.8	103					-0.0756	
1												8.07		59.4
2												4.15		118.9
3												1.60		178.3
AFR-9	chlorine	30		1800	571	0.27	39.4	68		2.4	1.3		-0.0696	
1												5.06		59.4
2												2.30		118.9
3												1.14		178.3
AFR-15	H_2O_2	35		1800	571	0.35	59.5	59		2.1	1.96			
1												6.72		41.7
2												6.77		83.3
3												6.96		125.0
4												6.52		166.7
5												6.64		208.3
6												6.42		291.7
7												4.86		458.3
8												5.48		

EXPT. NO.	TREATMENT	TEMP. (°C)	pH	REACTOR SURFACE (cm^2)	REACTOR VOLUME (cm^3)	INITIAL α_f (mg/cm^2)	INITIAL ρ_f (mg/cm^3)	INITIAL THICKNESS (μm)	FINAL THICKNESS (μm)	INITIAL ΔP (mmHg)	FINAL ΔP (mmHg)	K_c RATE COEFFICIENT ($cm/sec \times 10^3$)	K_d (cm^2/mg)	C_r (mg/cm^2)
TXX03	ozone	27.1	--	6700	2130			153	0	26.5	14.2	48.9		1300
T03 clean	ozone	24.1	7.8	13200	4180			--	--			4.75		
TPO clean	H_2O_2	24.9	8.0	13200	4180			--	--			0.03		
TNCl clean	NCl_x	24.6	8.0	13200	4180			--	--			0		
TFTU	chlorine	23.6	8.0	973	4180			<25	<25			1.1		
TXXNCL	NCl_x	26.8	7.8	13200	4180			73	43	80	61	0.0003		28

Appendix Q

EFFECT OF DISSOLVED OXYGEN CONCENTRATION ON GLUCOSE REMOVAL IN TFR3

Experimental Run Time (hr)	Dissolved Oxygen Concentration (mg/l)	Glucose Removal (mg/min)
65.3	15.0	7.0
66.2	2.5	6.6
67.7	11.0	6.8
68.3	15.0	7.0

This investigation was conducted on a 43 μm biofilm produced in experiment TFR3-15. Influent glucose concentration was 28.1 mg/l.

Appendix R

CHANGES IN BULK FLUID VISCOSITY DURING TFR EXPERIMENTS

Experiment Number	% Difference From Distilled H_2O
TFR1-4	2.05
TFR1-4	0.42
TFR1-5	0.80
TFR1-5	0.28
TFR1-6	0.23
TFR1-6	0.13
TFR1-7	3.35
TFR1-7	2.03
TFR3-2	0.60

Measurements were made using a capillary viscometer in a water bath set to the same temperatures as the experimental conditions.

Appendix S

DATA SUMMARY FOR FFR FIELD TESTS

Location	Expt. No.	τ_w (N/m^2)	$\bar{v}$ (cm/sec)	R_f^* ($days^{-1}$)	f_{max}	R_{BM}^* ($days^{-1}$)
Deepwater	1	11.9	191	0.045	0.012	0.045
	2	9.6	168	0.083	0.011	
	3	13.5	205	0.024	0.012	0.056
	4	9.6	168	0.096	0.011	
	1A	9.0	163	0.080	0.014	
	2A	8.8	160	0.083	0.014	
	3A	12.6	197	0.035	0.008	
	4A	3.3	92	0.025	0.018	0.197
P.H. Robinson	1	12.3	198	0.012	0.013	
	2	10.2	178	0.009	0.012	
	3	8.8	163	0.005	0.012	
	4	7.4	148	0.002	0.011	

Appendix T

WATER QUALITY DATA FOR THE FIELD TESTING UNIT AT THE DEEPWATER PLANT

Date	Bulk Temp. (C)	Bacteria (#/ml)	pH	Suspended Solids (mg/l)	Total Carbon (mg/l)	Total Inorganic Carbon (mg/l)
2/14	15.5	$\leq 10^3$	6.3	16	68	19
2/25	15.9	$\leq 10^3$	6.5	150	46	31
3/2	16.1	$\leq 10^3$	6.5	180	45	24
3/17	16.5	$\leq 10^3$	6.4	56	69	32

Date	Total Organic Carbon (mg/l)	Total Kjeldahl N (mg/l)	Total Phosphorous (mg/l)	Specific Conductance (micromhos/cm)
2/14	49	3.5	1.8	650
2/25	25	3.3	1.8	650
3/2	21	3.8	2.1	500
3/17	37	4.2	3.2	1100

Appendix U

VARIATION IN MEASURED INLET GLUCOSE CONCENTRATIONS

	INLET GLUCOSE CONCENTRATION (mg/l)		
	Desired	Measured*	Relative Error (measured values)
TUBULAR FOULING REACTORS 1 and 2	2.5	2.8 ± 0.8 (5)	0.30
	6.25	6.0 ± 0.7 (4)	0.11
	10.0	9.8 ± 2.4 (6)	0.25
	50.0	48.2 ± 8.0 (6)	0.17
ANNULAR FOULING REACTOR	2.5	2.3 ± 1.1 (4)	0.47
	6.25	6.8 ± 0.3 (5)	0.04
	10.0	9.7 ± 0.9 (4)	0.09
	12.5	14.8 (1)	--
TUBULAR FOULING REACTOR 3	5.0	5.6 ± 1.0 (15)	0.2
	10.0	10.6 ± 0.0 (4)	0.1
	25.0	28.6 ± 3.1 (9)	0.12
	100.0	86.3 ± 4.8 (8)	0.05
	250.0	294 ±79.5 (5)	0.32

* mean values ± standard deviation (number of determinations)

Appendix V

ORGANIC CARBON CONTENT OF SOME POWER PLANT COOLING WATER
(MEASURED AT THE INLET)

Power Plant	Water Source	TOC (mg/l) Range	Average
*Wisconsin Electric Valley Power Station Milwaukee, Wis.	Menomonee River	3-20	10
*Wisconsin Electric North Oak Creek Power Station Milwaukee County, Wis.	Lake Michigan	1-9	3
*Duquesne Light Co. Phillips Power Station Pittsburgh, Pa.	Ohio River	3-4	4
*Connecticut Light and Power Co. Devon Power Station Bridgeport, Conn.	Long Island Sound	3-6	4.5
*Houston Lighting and Power Co. Deepwater Power Station Houston, Tx.	Houston Ship Channel	21-40**	33**
*Houston Lighting and Power Co. P.H. Robinson Power Station Thompsons Corners, Tx.	Cooling Lake	14-25**	21**

*Data obtained from personal communication from David Bour, NUS Corp., Pittsburgh, Pa.

**after filtration with 0.45 μm pore size filters

Appendix W

EFFECT OF EDTA ON AN EXISTING BIOFILM IN THE AFR.

Time (min)	Effluent Suspended Solids (mg/l)	Torque (N-cm)	Reactor EDTA (mg/l)
-5	3.5	-	0
0	3.5	0.19	0
1	-	-	50
15	3.5	-	50
25	4.0	0.16	50
35	4.5	-	50
36	-	-	0
45	5.5	0.12	0

Increase in effluent suspended solids indicates biofilm removal as does a decrease in frictional resistance (measured as torque).

Appendix X

Raw Data

TUBULAR FOULING REACTOR 1

Time	=	Experimental Run Time (hr)
Velocity	=	Average Fluid Velocity (cm/sec)
DP	=	Pressure Drop (N/m^2)
MTH	=	Attached Biofilm Mass (mg)
TH	=	Biofilm Thickness (μm)
X	=	Suspended Biomass Concentration (mg/l)
S	=	Glucose Concentration (mg/l)
OBS	=	Observation Number

TUBULAR FOULING REACTOR 1

EXPNUMB=1

OBS	TIME	DP	MTH	TH	X	S
1	6	2252.77	.	.	.	.
2	8	2372.74	.	.	.	.
3	12	3052.57	.	.	.	.
4	15	3265.85	.	.	.	.
5	16	3585.77	.	.	.	.
6	18	4118.97	.	.	.	.
7	20	4718.82	.	.	.	.
8	22	5678.58	.	.	.	.
9	24	5678.58	.	.	.	.
10	30	6225.11	.	.	.	.
11	35	5678.58	.	.	.	.

TUBULAR FOULING REACTOR 1

EXPNUMB=2

OBS	TIME	DP	MTH	TH	X	S
12	0.0	7864.7	.	.	.	.
13	8.0	7864.7	.	.	.	.
14	18.0	7864.7	.	.	10	9.0
15	23.0	7864.7	.	.	10	8.5
16	25.0	8664.5	.	.	.	.
17	27.0	8797.8	.	25	1	3.5
18	31.2	13729.9	.	.	.	.
19	32.2	17595.6	.	.	.	.
20	34.2	18662.0	.	.	5	3.5
21	43.0	25593.6	.	.	.	.
22	45.0	26793.3	.	.	.	.
23	47.0	27459.8	.	.	.	.
24	48.0	27593.1	.	130	3	.
25	50.0	28392.9	.	.	6	2.0
26	53.5	33991.5	.	.	25	0.5
27	67.5	25193.7	.	.	7	.
28	70.0	25993.5	.	.	.	.
29	80.0	.	.	.	.	0.5
30	96.0	.	.	.	.	0.5
31	120.0	.	.	85	.	0.5
32	140.0	.	.	.	.	.
33	142.0	.	.	28	.	.
34	192.0	.	.	45	.	.

TUBULAR FOULING REACTOR 1

EXPNUMB=3

OBS	TIME	DP	MTH	TH	X	S
35	0.00	4905.4	.	.	.	.
36	7.00	4425.6	.	.	.	1.0
37	14.00	4212.3	.	.	.	.
38	22.50	4212.3	.	.	.	.
39	31.25	4212.3	.	.	.	.
40	37.50	5038.7	.	.	.	.
41	45.75	5785.2	.	.	3	1.0
42	49.50	7464.8	.	55.0	3	1.0
43	51.50	7464.8	.	.	.	1.0
44	56.00	8771.1	.	10.0	1	.
45	60.50	7278.2	.	45.0	3	0.0
46	62.00	.	.	.	.	0.0
47	66.00	.	.	35.0	.	0.0
48	68.00	.	.	.	.	0.0
49	69.50	8024.7	.	.	.	.
50	72.00	8118.0	.	40.0	.	0.0
51	74.00	8491.2	.	.	20	.
52	78.00	8864.4	.	12.5	.	.
53	82.00	9424.3	.	.	2	.
54	94.50	8864.4	.	.	1	1.5
55	98.20	12223.6	.	13.0	.	1.0
56	102.00	.	.	.	.	0.5
57	104.00	.	.	.	.	0.5
58	106.00	.	.	.	.	0.5
59	108.00	11757.1	.	.	.	0.5
60	112.00	.	.	.	.	0.5
61	115.00	13063.4	.	.	.	0.5
62	118.00	13063.4	.	.	5	0.5
63	123.50	.	.	8.0	.	0.5
64	131.00	13383.3	.	.	.	.
65	140.00	13330.0	.	.	3	0.7
66	190.00	.	.	5.0	.	.

TUBULAR FOULING REACTOR 1

EXPNUMB=4

OBS	TIME	DP	MTH	TH	X	S
67	0	1426.31	.	.	.	.
68	15	1959.51	.	.	6.0	.
69	19	2972.59	.	.	.	.
70	27	4398.90	.	.	11.5	.
71	30	5411.98	.	5	.	.
72	32	6078.48	.	.	.	.
73	36	5665.25	.	.	.	.
74	40	6078.48	.	10	.	.
75	44	5665.25	.	.	.	.
76	48	5798.55	.	.	.	.
77	52	5665.25	.	.	9.5	.
78	57	5665.25	.	.	.	.
79	61	5545.28	.	.	7.0	.
80	68	.	.	60	.	.
81	72	.	.	.	12.0	.
82	82	5292.01	.	.	.	.
83	88	4718.82	.	.	.	.
84	90	.	.	.	12.0	.
85	96	.	.	.	7.0	.
86	102	.	.	.	7.0	.
87	103	.	.	.	9.0	.
88	108	.	.	.	.	.
89	115	.	.	.	.	.
90	118	.	.	.	.	.
91	122	.	.	220	.	.
92	174	.	.	350	.	.

TUBULAR FOULING REACTOR 1

EXPNUMB=5

OBS	TIME	DP	MTH	TH	X	S
93	0.0	2266.10	.	.	.	2.0
94	19.0	2266.10	.	.	.	1.5
95	28.0	3132.55	.	.	1	1.0
96	32.0	3732.40	.	.	1	1.0
97	36.0	4665.50	.	.	2	0.4
98	40.0	5598.60	.	.	.	0.6
99	44.0	5332.00	.	.	4	.
100	48.0	4665.50	.	19	4	.
101	54.3	3465.80	.	.	.	0.4
102	58.3	4798.80	.	.	.	.
103	62.3	7598.10	.	.	.	0.6
104	67.0	7598.10	.	.	.	0.3
105	68.0	7998.00	.	8	.	.
106	70.3	7998.00	.	.	.	0.4
107	78.0	5332.00	.	.	9	0.0
108	82.0	5332.00	.	.	11	.
109	86.0	5598.60	.	.	1	1.3
110	90.0	5998.50	.	.	0	.
111	96.0	7131.55	.	16	.	.
112	105.0	9464.30	.	.	.	.
113	113.0	9864.20	.	.	.	.

TUBULAR FOULING REACTOR 1

EXPNUMB=6

OBS	TIME	DP	MTH	TH	X	S
114	0.0	10330.8	.	.	.	.
115	4.9	10330.8	.	.	.	.
116	9.3	10997.3	.	.	8.7	4.9
117	20.5	10504.0	.	.	16.0	.
118	22.0	11063.9	.	.	21.3	19.2
119	24.1	11330.5	.	.	2.0	.
120	25.0	11330.5	.	.	.	18.1
121	28.1	12157.0	.	200	12.0	14.1
122	32.1	11997.0	.	.	10.0	11.1
123	36.1	11837.0	.	.	28.0	9.4
124	40.1	11997.0	.	.	34.0	8.3
125	42.1	13596.6	.	21	.	.
126	44.0	13996.5	.	.	.	9.3
127	44.1	13996.5	.	.	32.0	.
128	48.0	14796.3	.	.	.	9.3
129	48.1	15196.2	.	.	30.0	.
130	55.9	15862.7	.	45	.	.
131	56.8	15862.7	.	.	28.0	10.2
132	60.0	16662.5	.	.	.	8.1
133	60.8	16662.5	.	.	38.0	.
134	64.8	19728.4	.	.	44.0	5.9
135	68.8	25327.0	.	.	44.0	5.0
136	72.8	26393.4	.	.	42.0	4.2
137	78.6	27459.8	.	.	104.0	0.3
138	83.1	28126.3	.	.	20.0	.
139	87.1	29992.5	.	.	.	4.7
140	91.1	30125.8	.	.	38.0	5.0

TUBULAR FOULING REACTOR 1

EXPNUMB=7

OBS	TIME	DP	MTH	TH	X	S
141	0.0	1732.9	.	.	.	.
142	1.6	1732.9	.	.	.	.
143	8.1	1732.9	.	.	.	.
144	20.0	2666.0	.	.	.	.
145	20.2	1866.2	.	.	.	.
146	22.0	2399.4	.	.	.	.
147	25.0	4265.6	.	.	50	6.0
148	29.0	6931.6	.	.	.	7.3
149	31.4	9197.7	.	.	58	8.6
150	33.0	.	.	.	.	.
151	37.0	9730.9	.	.	52	7.3
152	41.0	11597.1	.	.	63	8.8
153	43.0	9864.2	2499.61	155.0	.	.
154	45.0	11597.1	.	.	55	5.0
155	47.4	.	2464.13	165.5	.	.
156	48.5	10664.0	.	.	.	.
157	55.1	11597.1	.	.	.	.
158	66.1	13729.9	4381.03	255.5	.	.
159	70.0	13729.9	.	.	.	.
160	74.0	13729.9	.	.	.	9.0
161	78.0	.	.	.	.	7.6
162	80.0	15596.1	.	.	.	.
163	80.2	.	7667.61	587.0	.	.
164	82.0	.	.	.	.	7.5
165	90.0	13330.0	.	.	.	.
166	95.0	14396.4	.	.	.	.
167	100.0	14929.6	.	.	.	.
168	104.0	13330.0	.	949.5	.	.

TUBULAR FOULING REACTOR 1

EXPNUMB=8

OBS	TIME	DP	MTH	TH	X	S
169	4.0	.	.	.	18	91.0
170	8.0	6131.8	.	.	35	85.0
171	12.0	6265.1	.	.	.	.
172	20.0	8797.8	.	.	81	30.0
173	21.8	.	1910.45	52.5	.	.
174	24.7	8931.1	.	.	.	.
175	35.8	11463.8	2615.72	65.5	.	.
176	41.0	11730.4	2110.42	71.0	44	1.5
177	43.6	11997.0	.	.	.	.
178	44.3	.	.	.	147	.
179	45.8	.	.	.	36	2.6
180	49.8	.	.	.	31	2.3
181	53.8	.	.	.	26	3.4
182	56.9	9730.9	.	.	.	.
183	57.8	.	.	.	45	2.1
184	65.8	.	.	.	16	2.0
185	66.5	9464.3	.	.	.	.
186	69.8	.	.	.	20	.
187	70.2	.	.	.	20	1.5
188	71.3	8531.2	.	99.0	.	.
189	74.2	.	.	.	22	1.7
190	78.2	.	.	.	46	1.3
191	82.2	.	.	.	10	1.6
192	83.0	9730.9	.	.	.	.
193	86.2	.	.	.	20	1.6
194	87.1	9730.9	.	.	.	.
195	88.4	10130.8	.	.	.	.
196	90.9	.	1665.33	88.0	.	.
197	104.7	11063.9	.	.	.	.
198	110.7	6665.0	.	.	.	.
199	116.0	17995.5	.	.	.	.
200	117.1	19461.8	.	.	.	.
201	126.6	17995.5	.	.	.	.

TUBULAR FOULING REACTOR 1

EXPNUMB=10

OBS	TIME	DP	MTH	TH	X	S
202	0.3	2466.05	.	.	.	.
203	4.9	2266.10	.	.	.	.
204	5.7	2399.40	.	.	.	.
205	7.9	.	.	.	8	3.3
206	8.0	.	.	.	.	.
207	8.1	2399.40	.	.	.	.
208	10.1	2399.40	.	.	.	.
209	11.9	.	.	.	8	3.6
210	15.9	.	.	.	6	2.4
211	19.9	.	.	.	5	1.8
212	22.9	.	.	116	.	.
213	22.9	.	1129.93	148	.	.
214	23.8	4332.25	.	.	.	.
215	23.9	.	.	.	8	1.9
216	27.6	5531.95	.	.	.	.
217	27.8	.	.	.	.	.
218	27.9	.	1659.95	143	15	1.5
219	27.9	.	1179.38	129	.	.
220	31.9	.	.	.	26	1.7
221	32.6	5465.30	.	.	.	.
222	35.9	5598.60	.	.	.	.
223	35.9	.	.	.	29	1.9
224	36.1	5598.60	.	.	.	.
225	39.9	.	.	.	9	2.9
226	40.5	5332.00	.	.	.	.
227	40.6	.	1027.80	105	.	.
228	40.6	.	1242.82	91	.	.
229	43.9	.	.	.	12	3.1
230	45.6	.	.	.	.	.
231	46.0	4865.45	.	.	.	.
232	46.5	.	.	.	.	.
233	47.9	.	.	.	7	2.1
234	50.5	.	.	.	.	.
235	50.5	.	922.44	66	.	.
236	50.5	.	.	77	.	.
237	50.9	.	.	.	.	.
238	51.9	.	. .	23	0.3	
239	52.2	.	. .	.	.	
240	55.9	.	. .	16	1.4	
241	59.9	.	. .	7	0.6	
242	60.0	6665.0	. .	.	.	
243	64.4	.	. .	6	0.6	
244	67.9	.	. .	14	0.5	
245	78.4	5598.6	. .	.	.	
246	95.5	4265.6	. .	.	.	
247	96.0	.	. .	.	.	

TUBULAR FOULING REACTOR 1

EXPNUMB=11

OBS	TIME	DP	MTH	TH	X	S
248	0.0	3865.70	.	.	.	.
249	0.0	.	.	.	6	.
250	2.5	3865.70	.	.	.	.
251	4.0	3865.70	.	.	.	.
252	4.0	.	.	.	4	4.9
253	8.0	.	.	.	.	.
254	8.0	.	.	.	4	2.5
255	12.0	.	.	.	.	.
256	12.0	.	.	.	2	1.3
257	16.0	.	.	.	4	1.0
258	20.0	.	.	.	.	1.1
259	20.2	3865.70	.	.	.	.
260	20.7	4332.25	.	.	.	.
261	21.4	4132.30	.	.	.	.
262	24.0	.	.	.	10	1.0
263	25.4	4332.25	.	.	.	.
264	27.3	4398.90	.	.	.	.
265	28.0	.	1072.95	43	10	0.5
266	28.0	.	483.79	57	.	.
267	29.1	4398.90	.	.	.	.
268	32.0	.	.	.	7	.
269	35.8	4665.50	.	.	.	.
270	36.0	.	.	.	5	1.1
271	40.0	.	.	.	9	0.7
272	44.0	.	.	.	1	0.7
273	45.8	4665.50	.	.	.	.
274	48.0	.	.	.	4	0.1
275	50.4	4598.85	.	.	.	.
276	50.8	4532.20	.	.	.	.
277	51.4	4598.85	.	.	.	.
278	52.0	.	.	.	.	.
279	52.0	.	.	.	6	0.9
280	52.6	3999.00	.	.	.	.
281	55.0	4265.60	.	.	.	.
282	56.0	.	907.38	35	.	.
283	56.0	.	1026.72	43	.	.

TUBULAR FOULING REACTOR 1

EXPNUMB=11

OBS	TIME	DP	MTH	TH	X	S
284	57.1	4265.60	.	.	.	.
285	57.9	4398.90	.	.	.	.
286	60.0	.	.	.	4	0.1
287	64.0	.	.	.	6	0.6
288	68.0	.	.	.	3	.
289	70.3	4398.90	.	.	.	.
290	72.0	.	.	.	7	.
291	73.8	4532.20	.	.	.	.
292	76.0	.	.	.	5	.
293	76.8	4798.80	.	.	.	.
294	77.6	4798.80	.	.	.	.
295	79.9	4865.45	.	.	.	.
296	80.0	.	.	.	2	.
297	84.0	.	.	.	0	.
298	88.0	.	.	.	5	.
299	92.0	.	.	.	6	.
300	92.2	4865.45	.	.	.	.
301	100.3	5731.90	.	.	.	.
302	105.8	4398.90	.	.	.	.
303	106.0	.	898.784	43	6	.
304	106.0	.	.	54	.	.
305	107.0	.	.	.	.	.
306	110.0	.	.	.	6	.
307	114.0	.	.	.	3	0.3
308	118.0	.	.	.	5	0.4
309	118.4	4798.80	.	.	.	.
310	122.0	.	.	.	7	0.7
311	126.0	.	.	.	7	0.3
312	127.2	4732.15	.	.	.	.
313	127.7	4665.50	.	.	.	.
314	129.6	4865.45	.	.	.	.
315	134.0	.	.	.	9	.
316	138.0	.	.	.	7	.
317	140.2	5332.00	.	.	.	.
318	142.0	.	.	.	8	.
319	144.0	5332.00	.	.	.	.

TUBULAR FOULING REACTOR 1

EXPNUMB=11

OBS	TIME	DP	MTH	TH	X	S
320	146.0	.	.	.	9	.
321	150.0	.	.	.	8	.
322	152.9	5598.60	.	.	.	.
323	154.0	.	405.31	61	10	.
324	154.0	.	1294.42	83	.	.
325	158.0	.	.	.	6	.
326	162.0	.	.	.	7	.
327	163.9	5998.50	.	.	.	.
328	166.0	.	.	.	6	1.1
329	169.9	5598.60	.	.	.	.
330	170.0	.	.	.	6	.
331	171.2	5598.60	.	.	.	.
332	174.0	.	.	.	3	.
333	175.0	5598.60	.	.	.	.
334	178.0	.	.	.	6	.
335	182.0	.	.	.	5	1.5
336	186.0	.	.	.	2	.
337	190.0	.	.	.	7	.
338	191.1	6665.00	.	.	.	.
339	193.0	.	.	.	.	.
340	194.0	.	.	88	7	.
341	195.3	5798.55	.	.	.	.
342	198.0	.	.	.	6	.
343	202.0	.	.	.	6	.
344	206.0	.	.	.	9	.
345	210.0	.	.	.	9	1.7
346	214.0	.	1824.44	101	7	.
347	214.0	.	1778.22	119	.	.
348	215.1	5598.60	.	.	.	.
349	218.0	.	.	.	6	.
350	222.0	.	.	.	6	.
351	222.1	5798.55	.	.	.	.
352	222.5	.	.	.	.	.
353	224.4	6065.15	.	.	.	.
354	225.6	6065.15	.	.	.	.
355	226.0	.	.	.	8	.

TUBULAR FOULING REACTOR 1

EXPNUMB=11

OBS	TIME	DP	MTH	TH	X	S
356	230.0	.	.	.	6	.
357	234.0	.	.	.	5	1.1
358	237.1	7198.2	.	.	.	.
359	238.0	.	.	.	10	.
360	241.2	7731.4	.	.	.	.
361	242.0	.	.	.	5	.
362	242.5	.	.	.	.	.
363	246.0	.	.	.	5	.
364	248.3	9730.9	.	.	.	.
365	249.1	9730.9	.	.	.	.
366	249.7	9730.9	.	.	.	.
367	254.0	.	.	.	5	.
368	258.0	.	.	.	6	.
369	258.0	.	.	.	5	1.1
370	261.8	11197.2	.	.	.	.
371	262.0	.	1851.32	70	6	.
372	263.4	10597.3	.	.	.	.
373	266.0	.	.	.	7	.
374	270.0	.	.	.	8	.
375	272.6	10530.7	.	.	.	.
376	273.4	10464.0	.	.	.	.
377	274.0	.	.	.	7	.
378	278.0	.	.	.	5	.
379	282.0	.	.	.	6	1.0
380	282.6	9730.9	.	.	.	.
381	290.0	.	.	.	3	.
382	291.6	9730.9	.	.	.	.
383	296.2	8731.1	.	.	.	.
384	298.0	.	.	.	5	.
385	302.0	.	.	.	6	.
386	306.0	.	.	.	5	1.0
387	310.0	.	.	.	6	.
388	314.0	.	.	.	3	.
389	318.0	.	.	.	7	.
390	322.0	.	.	.	3	.
391	326.0	.	.	.	3	.

TUBULAR FOULING REACTOR 1

EXPNUMB=11

OBS	TIME	DP	MTH	TH	X	S
392	330.0	.	.	.	6	1.0
393	331.2	7798.05	.	.	.	.
394	332.4	7598.10	.	.	.	.
395	333.0	7598.10	.	.	.	.
396	334.0	.	.	.	6	.
397	338.0	.	.	.	6	.
398	342.0	.	.	.	4	.
399	346.0	7064.90	.	.	.	.
400	346.0	.	.	.	13	.
401	350.0	.	.	.	6	.
402	354.0	.	.	.	5	1.1
403	356.4	5332.00	.	.	.	.
404	356.9	6265.10	.	.	.	.
405	358.0	.	.	.	6	.
406	360.2	4665.50	.	.	.	.
407	360.6	4532.20	.	.	.	.
408	362.0	.	.	.	3	.
409	366.0	.	.	.	5	.
410	370.0	.	.	.	5	.
411	374.0	.	.	.	4	.
412	377.7	6198.45	.	.	.	.
413	378.0	.	.	.	6	0.9
414	378.7	6131.80	.	.	.	.
415	382.0	.	.	.	6	.
416	384.5	.	.	.	.	.
417	385.0	.	.	.	.	.
418	402.8	4798.80	.	.	.	.
419	405.3	5465.30	.	.	.	.
420	405.5	.	.	.	.	.
421	406.2	5665.25	.	.	.	.
422	413.7	.	771.922	100	.	.
423	413.7	.	700.965	110	.	.
424	413.8	5731.90	.	.	.	.

TUBULAR FOULING REACTOR 1

EXPNUMB=12

OBS	TIME	DP	MTH	TH	X	S
425	4.0	.	.	.	15	0.6
426	5.9	5398.6	.	.	.	.
427	6.1	.	.	.	.	.
428	8.0	.	.	.	10	0.6
429	12.0	.	.	.	5	0.4
430	16.0	5598.6	.	.	9	0.3
431	20.4	.	.	.	2	0.4
432	21.0	6065.1	.	.	.	.
433	23.5	7131.5	.	.	.	.
434	24.4	.	.	.	12	0.8
435	26.0	9064.4	.	.	.	.
436	28.0	.	.	.	6	.
437	28.2	8664.5	.	.	.	.
438	29.4	.	1347.10	55	.	.
439	29.4	.	1454.61	49	.	.
440	32.4	9197.7	.	.	.	.
441	38.3	9464.3	.	.	.	.
442	40.0	.	2209.33	89	12	1.1
443	40.6	9064.4	.	.	.	.
444	44.0	.	.	.	5	.
445	47.8	8931.1	.	.	.	.
446	48.0	.	.	.	5	.
447	51.4	10797.3	.	.	.	.
448	52.0	.	2585.62	114	5	1.2
449	58.1	.	.	.	3	0.7
450	67.8	11930.3	.	.	.	.
451	67.8	.	1616.95	85	.	.
452	70.1	.	.	.	2	.
453	77.9	.	.	.	0	.
454	80.2	11597.1	.	.	.	.
455	81.0	.	1616.95	133	.	.
456	116.5	11463.8	.	.	.	.
457	116.5	.	.	150	.	.
458	189.4	10797.3	.	.	.	.
459	189.4	.	2203.95	164	.	.

TUBULAR FOULING REACTOR 1

EXPNUMB=13

OBS	TIME	DP	MTH	TH	X	S
460	0.8	5598.60	.	.	.	.
461	1.1	.	.	.	22.0	.
462	10.6	5731.90	.	.	.	.
463	22.3	.	.	.	4.1	.
464	22.8	5731.90	.	.	.	.
465	25.2	5598.60	.	.	.	.
466	25.3	.	.	.	12.0	1.8
467	34.3	5465.30	.	.	.	.
468	34.3	.	538.63	36	.	.
469	44.8	5531.95	.	.	.	.
470	44.8	.	.	.	.	.
471	45.7	.	.	.	5.0	0.0
472	46.2	5731.90	.	.	.	.
473	46.3	.	754.72	47	.	.
474	46.4	5865.20	.	.	.	.
475	49.2	.	.	.	4.0	.
476	51.6	.	862.23	48	.	.
477	51.8	6131.80	.	.	.	.
478	54.7	6265.10	.	.	.	.
479	57.9	6465.05	.	.	.	.
480	67.0	7731.40	.	.	.	.
481	71.7	.	1325.60	19	.	.
482	71.8	7731.40	.	.	.	.
483	76.0	.	1347.10	32	.	.
484	76.1	7731.40	.	.	.	.
485	78.8	7931.35	.	.	.	.
486	81.5	8264.60	.	.	.	.
487	81.5	.	1023.50	41	.	.
488	81.5	.	808.48	43	.	.
489	82.6	.	.	.	.	.
490	86.6	8664.50	.	.	.	.
491	93.7	9597.60	.	.	.	.
492	95.2	.	.	.	1.0	0.7
493	95.3	.	1616.95	64	.	.
494	95.3	.	1078.33	44	.	.
495	95.3	.	808.48	32	.	.
496	100.2	9197.7	.	.	.	.

TUBULAR FOULING REACTOR 1

EXPNUMB=14

OBS	TIME	DP	MTH	TH	X	S
497	0	5598.6	.	.	48	5.1
498	9	5332.0	.	.	9	1.9
499	19	5731.9	.	.	12	.
500	25	6065.1	.	.	13	1.3
501	26	6398.4	.	.	.	.
502	29	6531.7	.	.	7	0.9
503	33	6265.1	.	.	10	0.9
504	41	6398.4	.	.	.	.
505	42	5998.5	.	53	.	.
506	49	6598.3	.	.	4	2.4
507	49	6598.3	.	.	.	.
508	50	7598.1	.	.	.	.
509	55	12263.6	862.23	108	14	.
510	62	12090.3	866.53	90	13	1.4
511	66	11930.3	.	.	.	.
512	66	11930.3	.	.	.	.
513	67	11397.1	.	.	11	.
514	70	10797.3	.	.	4	1.2
515	70	10464.0	.	.	.	.
516	75	9331.0	592.38	31	.	.
517	89	12996.8	1078.33	47	8	2.5
518	89	12996.8	1135.31	33	.	.
519	89	12996.8	.	.	.	.
520	89	12996.8	.	.	.	.
521	92	14263.1	.	.	.	.
522	111	20261.6	.	.	.	.
523	111	20261.6	.	.	.	.
524	111	20261.6	.	.	.	.

TUBULAR FOULING REACTOR 1

EXPNUMB=15

OBS	TIME	DP	MTH	TH	X	S
525	1.8	2532.70	.	.	.	5.6
526	2.3	2532.70	.	.	.	.
527	3.6	2532.70	.	.	2	5.8
528	5.4	2599.35	.	.	.	4.0
529	6.8	2599.35	.	.	.	.
530	7.2	2599.35	.	.	4	3.5
531	9.0	2799.30	.	.	.	5.3
532	19.9	3065.90	.	.	.	.
533	26.0	3732.40	.	.	3	1.8
534	26.5	3732.40	647.21	81	.	.
535	26.7	3732.40	.	.	.	.
536	26.9	3732.40	.	.	.	.
537	30.4	3665.75	1994.31	188	5	2.6
538	41.2	3799.05	2910.30	294	.	.
539	44.1	3865.70	.	.	.	.
540	47.3	3732.40	.	.	.	1.4
541	54.7	6131.80	.	.	.	1.1
542	54.8	6131.80	.	.	.	.
543	54.9	6131.80	.	.	.	.
544	56.2	5998.50	4634.76	461	.	.
545	59.0	5931.85	.	.	1	.
546	67.0	5065.40	5173.38	432	.	.
547	72.2	4998.75	.	.	.	.
548	72.3	4998.75	.	.	.	.
549	72.4	4998.75	.	.	.	.
550	72.7	5198.70	.	.	11	1.4
551	77.0	4598.85	.	.	19	2.0
552	77.2	4598.85	.	.	.	.
553	79.5	4598.85	3502.68	243	.	.
554	91.1	7931.35	1778.22	158	.	.
555	95.2	7931.35	.	.	38	2.8
556	95.3	7931.35	.	.	.	.
557	95.5	7931.35	.	.	.	.
558	95.9	8531.20	.	.	.	.
559	96.0	7664.75	.	.	.	.
560	102.4	7598.10	.	196	.	.
561	116.1	8797.8	.	.	.	.
562	116.2	8797.8	.	.	.	.
563	116.5	8797.8	.	.	.	.

TUBULAR FOULING REACTOR 1

EXPNUMB=16

OBS	TIME	DP	MTH	TH	X	S
564	3.0	.	.	.	.	.
565	5.3	.	.	.	.	.
566	5.3	.	.	.	.	.
567	5.3	.	.	.	.	.
568	8.9	4066	.	.	4.0	0.4
569	21.7	5199	1670.71	106.0	4.0	0.6
570	22.4	5599	.	.	.	.
571	22.7	5532	.	.	.	.
572	22.7	.	.	.	.	.
573	22.7	.	.	.	.	.
574	22.7	.	.	.	.	.
575	23.3	.	.	.	.	.
576	23.4	5132	.	.	.	.
577	23.4	5132	.	.	.	.
578	23.4	5132	.	.	.	.
579	30.1	5332	729.99	93.0	.	.
580	35.4	5665	.	.	.	.
581	46.7	6265	539.70	76.5	.	0.2
582	50.9	6465	863.31	110.0	.	.
583	59.1	5999	1023.50	85.0	1.5	1.0
584	72.2	6532	1153.58	62.0	2.0	1.0
585	73.9	6798	.	.	.	.
586	78.5	7332	1239.59	90.0	1.0	0.5
587	94.5	8465	.	.	.	.
588	94.7	123969	1672.86	114.0	.	.

TUBULAR FOULING REACTOR 1

EXPNUMB=17

OBS	TIME	DP	MTH	TH	X	S
589	-10.5	1466.30	.	.	.	.
590	0.0	2332.75	.	.	16.0	0.7
591	6.4	2732.65	.	.	7.0	.
592	8.2	2332.75	.	.	.	.
593	12.4	2466.05	.	.	.	1.2
594	16.2	2399.40	.	79.0	4.0	1.3
595	20.8	2532.70	.	.	7.0	0.5
596	26.3	3199.20	.	.	6.0	1.2
597	26.3	3199.20	.	.	.	.
598	26.3	3199.20	.	.	.	.
599	26.6	2999.25	.	.	1.5	.
600	28.4	3199.20	.	75.0	.	.
601	28.6	3199.20	.	.	.	.
602	28.7	2999.25	.	.	3.0	3.7
603	33.4	3132.55	.	.	14.0	.
604	35.5	3332.50	.	.	.	.
605	38.2	2666.00	.	.	.	.
606	47.8	2399.40	.	.	7.5	.
607	52.7	2799.30	.	.	.	.
608	53.3	2266.10	.	.	.	.
609	53.8	2399.40	.	.	.	.
610	57.8	2399.40	.	.	3.5	0.7
611	65.0	3465.80	.	.	.	2.1
612	78.8	3399.15	.	.	.	.
613	79.0	3532.45	524.649	46.5	7.5	0.5
614	86.8	.	.	.	22.0	.
615	97.5	3865.70	.	.	4.0	0.5
616	97.5	3865.70	.	.	4.0	.
617	98.0	3865.70	431.115	51.0	.	.
618	98.0	3865.70	.	.	.	.
619	102.6	4332.25	.	.	1.5	0.5
620	109.7	5065.40	700.965	55.0	8.0	.
621	119.0	4798.80	647.210	50.0	7.0	.
622	121.1	4932.10	.	.	.	.
623	126.2	5198.70	.	.	.	.
624	126.2	5198.70	.	.	.	.
625	126.6	5065.4	.	.	.	.

TUBULAR FOULING REACTOR 1

EXPNUMB=21

OBS	TIME	DP	MTH	TH	X	S
626	0.0	4198.95	395.637	3.5	6	.
627	3.0	4198.95	.	.	.	.
628	8.0	3665.75	.	.	.	.
629	23.2	3865.70	.	.	4	2.1
630	25.2	4065.65	.	.	.	.
631	33.4	4198.95	.	.	3	5.7
632	50.3	4332.25	537.550	50.0	4	1.6
633	56.3	.	483.795	31.0	.	.
634	57.1	4532.20	484.870	13.0	0	1.7
635	73.3	3999.00	.	.	.	.

TUBULAR FOULING REACTOR 1

EXPNUMB=22

OBS	TIME	DP	MTH	TH	X	S
636	0.0	3932.35	.	.	.	.
637	6.8	3999.00	.	.	0	6.5
638	14.6	3865.70	.	.	4	2.4
639	26.5	4932.10	142.99	9.5	0	1.4
640	29.7	5798.55	.	.	.	.
641	34.0	6531.70	450.47	30.0	2	1.0
642	39.4	7464.80	704.19	43.5	6	1.0
643	50.0	7198.20	1289.04	108.0	7	0.3
644	71.9	6531.70	.	.	.	.
645	71.9	6531.70	.	.	.	.

TUBULAR FOULING REACTOR 1

EXPNUMB=23

OBS	TIME	DP	MTH	TH	X	S
646	0.0	5665.25	238.672	5.5	0	.
647	4.7	5665.25	.	.	.	3.0
648	9.4	5598.60	.	.	1	2.4
649	21.6	5598.60	.	.	0	2.5
650	23.0	5731.90	.	.	.	.
651	28.4	5798.55	275.226	5.0	1	1.9
652	47.6	6265.10	269.850	18.5	1	1.7
653	50.9	6598.35	.	.	.	.
654	57.9	6864.95	.	.	3	0.9
655	58.4	6931.60	296.728	31.0	.	.
656	70.7	6531.70	.	50.0	.	.
657	80.9	6398.40	.	.	.	1.3

TUBULAR FOULING REACTOR 1

EXPNUMB=24

OBS	TIME	DP	MTH	TH	X	S
658	0.0	2532.70	162.340	24	.	.
659	3.0	2466.05	.	.	2	6.0
660	6.0	2399.40	.	.	.	.
661	16.6	2332.75	.	.	2	2.0
662	18.9	2399.40	.	.	.	.
663	22.0	2399.40	.	.	.	.
664	31.8	2532.70	.	.	.	.
665	46.6	2666.00	182.767	40	.	.
666	47.8	2532.70	.	.	4	1.8
667	67.0	2532.70	384.886	49	3	0.8
668	72.7	2399.40	.	.	.	.
669	90.0	2399.40	.	.	.	.
670	97.0	2399.40	381.660	29	2	1.4

TUBULAR FOULING REACTOR 2

Time	=	Experimental Run Time (hr)
Velocity	=	Average Fluid Velocity (cm/sec)
DP	=	Pressure Drop (N/m^2)
MTH	=	Attached Biofilm Mass (mg)
TH	=	Biofilm Thickness (μm)
X	=	Suspended Biomass Concentration (mg/l)
S	=	Glucose Concentration (mg/l)
OBS	=	Observation Number

TUBULAR FOULING REACTOR 2

EXPNUMB=1

OBS	TIME	S	X	TH	MTH	P
1	0	.	.	.	.	11277.6
2	18	.	.	.	.	11540.3
3	19	7.5	.	.	.	11277.6
4	25	.	.	.	.	9166.8
5	32	.	.	.	.	10285.3
6	49	.	.	.	.	11020.9
7	68	3.0	.	.	.	9166.8
8	91	2.4	.	.	.	10524.9
9	121	2.4	.	.	.	10770.0
10	141	4.0	.	.	.	11020.9
11	163	.	.	.	.	11540.3
12	168	4.2	16	11	175.56	9380.3
13	170	.	.	.	.	10770.0
14	176	.	.	.	.	8754.2
15	187	1.8	.	.	.	10051.2
16	188	.	.	.	.	11540.3
17	190	.	.	78	.	10285.3
18	192	.	16	.	.	.
19	193	.	.	.	.	.
20	194	.	.	82	1620.32	.
21	196	2.2	6	.	.	.
22	199	1.6	2	.	.	.
23	201	.	16	.	.	.
24	204	1.8	14	.	.	.
25	208	1.2	8	.	.	.
26	210	.	.	.	.	.
27	212	0.6	2	.	.	.
28	213	0.6	.	.	.	.
29	216	.	.	91	3388.84	.
30	220	2.6	20	.	.	.
31	221	.	20	.	.	12365.6
32	230	1.8	.	.	.	.
33	234	1.4	.	.	.	10285.3
34	236	.	.	200	2128.00	.
35	238	1.6	.	.	.	.
36	241	.	.	.	.	10524.9
37	242	2.2	.	.	.	10051.2
38	244	.	.	.	.	11020.9
39	250	0.8	36	.	.	.
40	251	.	.	.	.	10524.9
41	259	.	.	.	.	10051.2
42	263	.	.	.	.	11020.9
43	264	.	.	78.5	.	11020.9

TUBULAR FOULING REACTOR 2

EXPNUMB=2

OBS	TIME	S	X	TH	MTH	P
44	0	.	.	.	.	8554.931
45	13	.	.	.	.	1.32500E+13
46	18	.	20	.	.	8554.931
47	19	8.2	6	.	.	.
48	22	.	.	.	.	8554.931
49	24	3.4	4	.	.	.
50	30	2.4	10	.	.	.
51	33	.	.	.	.	8169.896
52	36	1.6	12	.	.	.
53	42	0.2	12	26.0	.	8554.931
54	47	.	.	.	.	8554.931
55	49	0.8	20	.	.	.
56	55	0.2	12	.	.	.
57	61	1.2	10	.	.	.
58	65	1.0	10	.	.	.
59	66	.	.	52.0	.	9598.791
60	71	0.8	14	.	.	.
61	77	0.2	12	.	.	.
62	83	1.0	12	.	.	.
63	89	0.9	18	49.0	.	9822.376
64	96	.	.	.	.	9380.296
65	97	1.0	44	.	.	.
66	102	.	.	.	.	9598.791
67	103	0.8	32	.	.	.
68	109	0.2	24	.	.	.
69	113	.	.	.	.	9822.376
70	119	.	.	.	.	9822.376
71	121	0.8	10	.	.	.
72	127	0.2	8	.	.	.
73	133	1.0	10	.	.	.
74	137	0.9	8	.	.	.
75	138	.	.	57.5	.	15930.03

TUBULAR FOULING REACTOR 2

EXPNUMB=3

OBS	TIME	S	X	TH	MTH	P
76	0	.	.	.	.	8554.93
77	1	.	.	.	.	8360.20
78	5	.	.	.	.	8360.20
79	11	.	.	.	.	8554.93
80	17	.	.	.	.	8554.93
81	20	.	.	.	.	8360.20
82	22	.	.	.	.	8169.90
83	23	.	12	.	.	.
84	28	.	.	15	558.60	.
85	29	.	2	.	.	8754.20
86	30	.	.	.	.	.
87	32	.	4	.	.	.
88	46	.	.	.	.	8554.93
89	52	1.4	18	.	.	.
90	53	.	.	62	1130.88	.
91	54	.	.	.	.	8754.20
92	56	0.7	4	.	.	.
93	59	.	.	.	.	.
94	61	.	.	.	.	.
95	67	.	.	.	.	.
96	70	.	.	.	.	8754.20
97	71	0.5	2	.	.	.
98	72	.	.	73	1608.92	.
99	75	0.6	4	.	.	.
100	77	.	.	.	.	.
101	78	.	.	.	.	.
102	80	.	.	.	.	.
103	82	.	.	.	.	.
104	85	.	.	.	.	.
105	91	.	.	.	.	.
106	94	1.5	2	.	.	8554.93
107	99	1.0	6	.	.	.
108	100	.	.	.	.	8958.11
109	104	.	.	.	.	.
110	105	0.3	4	.	.	.
111	110	0.6	4	.	.	.

TUBULAR FOULING REACTOR 2

EXPNUMB=3

OBS	TIME	S	X	TH	MTH	P
112	116	.	.	.	.	.
113	118	.	.	.	.	.
114	120	0.9	8	.	.	8754.20
115	121	.	.	88	2742.08	.
116	124	.	.	.	.	.
117	129	.	.	.	.	.
118	133	0.3	4	.	.	.
119	141	.	.	.	.	.
120	144	.	.	157	.	.
121	145	.	.	.	.	9822.38
122	148	0.6	6	.	.	.
123	150	.	.	.	.	.
124	152	0.3	8	.	.	.
125	154	.	.	.	.	.
126	158	0.0	12	.	.	.
127	159	.	.	.	.	.
128	160	.	.	.	.	.
129	162	.	.	.	.	.
130	164	2.2	8	.	.	.
131	165	.	.	.	.	.

TUBULAR FOULING REACTOR 2

EXPNUMB=6

OBS	TIME	S	X	TH	MTH	P
132	0	.	.	.	.	8754.2
133	8	55.00	0.7	.	.	.
134	14	38.50	0.7	.	.	.
135	20	22.30	20.0	.	.	.
136	23	.	.	.	.	8958.1
137	25	21.40	12.0	.	.	.
138	27	.	.	.	.	9166.8
139	30	21.40	36.0	35	1223.60	9822.4
140	39	0.25	88.0	.	.	10051.2
141	46	.	.	.	.	11277.6
142	48	20.70	14.0	.	.	.
143	49	.	.	47	1643.12	.
144	51	.	.	.	.	17873.8
145	56	5.30	3.0	.	.	.
146	57	.	.	.	.	30354.0
147	62	1.50	1.0	.	.	.
148	68	5.00	16.0	.	.	.
149	74	.	.	171	2859.12	42876.2

TUBULAR FOULING REACTOR 2

EXPNUMB=7

OBS	TIME	S	X	TH	MTH	P
150	0	.	.	.	.	8360.2
151	5	.	.	.	.	7983.9
152	6	.	.	.	.	7983.9
153	8	50.0	1	.	.	.
154	14	43.0	7	.	.	.
155	20	20.3	13	.	.	.
156	23	.	.	.	.	9380.3
157	25	16.6	21	21.000	1021.44	.
158	27	.	22	.	.	9822.4
159	30	.	.	.	.	10524.9
160	32	12.2	29	.	.	.
161	38	13.5	36	.	.	.
162	43	.	.	.	.	11540.3
163	44	14.7	43	.	.	.
164	47	.	.	.	.	14197.7
165	49	7.2	26	.	.	15567.4
166	52	.	.	49.000	968.24	16680.8
167	53	.	.	.	.	15930.0
168	56	7.1	29	.	.	.
169	59	.	.	.	.	17873.8
170	62	.	37	.	.	.
171	63	.	.	.	.	20521.9
172	67	.	.	.	.	24111.1
173	68	2.2	33	.	.	.
174	69	.	.	.	.	25835.5
175	72	.	.	.	.	27683.2
176	73	.	16	196.667	2989.33	27053.1

TUBULAR FOULING REACTOR 2

EXPNUMB=8

OBS	TIME	S	X	TH	MTH	P
177	0	.	.	.	.	8169.9
178	5	52.00	1	.	.	8360.2
179	11	41.80	7	.	.	.
180	17	17.00	10	.	.	.
181	21	.	.	.	.	10051.2
182	23	10.50	16	.	.	.
183	25	.	.	37.000	646.76	13558.7
184	29	1.50	25	.	.	.
185	31	.	.	.	.	.
186	35	2.50	24	.	.	.
187	37	.	.	.	.	.
188	41	.	19	.	.	.
189	45	.	.	43.000	751.64	19598.2
190	46	.	.	.	.	.
191	48	0.82	14	.	.	.
192	49	.	.	.	.	39103.6
193	53	2.70	11	.	.	.
194	59	2.40	5	.	.	.
195	65	2.00	15	.	.	.
196	72	.	.	398.333	6054.67	51548.6

TUBULAR FOULING REACTOR 3

Time	=	Experimental Run Time (hr)
Velocity	=	Average Fluid Velocity (cm/sec)
DP	=	Pressure Drop (N/m^2)
MTH	=	Attached Biofilm Mass (mg)
TH	=	Biofilm Thickness (μm)
X	=	Suspended Biomass Concentration (mg/l)
S	=	Glucose Concentration (mg/l)
OBS	=	Observation Number

TUBULAR FOULING REACTOR 3

EXPNUMB=1

OBS	TIME	VELOCITY	MTH	TH	X	S
2	0.00	208.19	.	.	2.4	48.0
3	2.80	205.99	.	.	1.0	14.9
4	8.20	205.90	.	.	2.0	4.7
5	13.40	207.51	.	.	3.0	3.1
6	25.10	205.89	.	.	5.0	1.3
7	32.00	203.09	.	.	3.0	0.5
8	38.30	198.45	.	.	6.0	0.6
9	48.40	201.72	.	.	.	0.7
10	53.70	199.56	.	.	7.0	0.7
11	57.70	196.18	.	.	1.0	0.7
12	61.20	194.36	.	.	.	0.2
13	72.30	195.76	.	.	.	8.0
14	80.90	192.11	.	.	3.0	0.7
15	85.00	188.95	.	.	8.0	1.2
16	96.70	186.59	.	.	6.0	0.4
17	105.00	186.59	382.27	112	10.0	2.4
18	105.01	186.59	1355.11	111	10.0	2.4
19	105.02	186.59	607.89	96	10.0	2.4
20	105.03	186.59	.	115	10.0	2.4
21	105.04	186.59	799.20	103	10.0	2.4
22	105.05	186.59	833.86	103	10.0	2.4
23	105.06	186.59	712.21	97	10.0	2.4
24	105.07	186.59	886.19	97	10.0	2.4
25	105.08	186.59	677.56	85	10.0	2.4
26	105.09	186.59	660.23	273	10.0	2.4
27	105.10	186.59	590.57	109	10.0	2.4
28	105.11	186.59	746.87	88	10.0	2.4
29	105.12	186.59	799.20	98	10.0	2.4
30	105.13	186.59	729.54	95	10.0	2.4
31	105.14	186.59	1007.50	266	10.0	2.4
32	105.15	186.59	1094.49	259	10.0	2.4

TUBULAR FOULING REACTOR 3

EXPNUMB=2

OBS	TIME	VELOCITY	MTH	TH	X	S
33	0.00	163.81	.	.	0	.
34	3.10	160.50	.	.	1	17.3
35	9.00	162.25	.	.	1	1.3
36	22.70	165.86	156.306	8	3	4.4
37	30.50	165.86	.	.	0	1.4
38	35.90	165.86	.	.	0	2.1
39	50.40	155.17	573.237	67	6	1.6
40	50.41	155.17	555.908	58	6	1.6
41	50.42	155.17	503.922	80	1	1.6
42	53.60	150.78	.	.	1	5.0
43	56.70	144.22	.	.	4	1.8
44	59.30	132.57	.	.	.	.
45	61.00	124.91	920.852	142	4	.
46	61.01	124.91	764.547	124	4	.
47	71.90	122.08	.	.	6	5.0
48	72.60	122.08	694.885	121	.	.
49	72.61	122.08	764.547	169	.	.
50	72.62	122.08	851.191	114	.	.
51	72.63	122.08	694.885	100	.	.
52	75.70	126.77	.	.	.	.
53	78.40	122.65	.	.	.	.
54	80.90	127.15	.	.	.	.

TUBULAR FOULING REACTOR 3

EXPNUMB=3

OBS	TIME	VELOCITY	MTH	TH	X	S
55	0.00	163.67	.	.	.	.
56	9.90	164.48	.	.	0.0	9.3
57	15.00	164.12	.	.	0.8	7.4
58	20.70	164.57	.	.	9.5	2.0
59	36.10	166.04	86.991	19	4.4	1.8
60	36.11	166.04	69.662	8	4.4	1.8
61	43.40	163.85	86.991	205	7.0	1.2
62	43.41	163.85	121.648	60	7.0	1.2
63	48.70	161.55	.	28	6.0	1.4
64	48.71	161.55	121.648	30	6.0	1.4
65	51.40	158.63	121.648	63	6.0	0.9
66	51.41	158.63	190.963	44	6.0	0.9
67	58.00	157.79	156.306	63	4.0	1.0
68	58.01	157.79	156.306	60	4.0	1.0
69	65.50	161.46	.	.	10.0	1.0
70	68.80	160.07	295.283	51	0.0	1.0
71	82.00	156.83	.	.	10.0	0.8
72	87.60	153.33	277.954	77	10.0	0.8
73	87.61	153.33	295.283	81	10.0	0.8
74	91.40	153.49	.	.	8.0	0.6
75	103.10	144.08	208.639	34	7.0	0.9
76	103.11	144.08	312.612	33	7.0	0.3
77	111.00	143.12	312.612	52	4.0	1.3
78	111.01	143.12	312.612	52	4.0	1.3
79	118.50	134.59	.	.	7.0	.
80	132.30	132.68	364.945	72	6.0	0.6
81	132.31	132.68	503.922	87	6.0	0.6
82	132.32	132.68	434.260	81	6.0	0.6

TUBULAR FOULING REACTOR 3

EXPNUMB=4

OBS	TIME	VELOCITY	MTH	TH	X	S
83	0.00	166.67	.	.	.	.
84	5.20	166.89	.	.	1.4	26.5
85	8.20	168.42	.	.	2.0	22.0
86	10.20	.	.	.	1.3	19.9
87	11.40	169.14	.	.	3.0	14.6
88	13.60	168.67	.	.	2.0	12.4
89	20.40	150.00	17.329	98	.	.
90	20.41	150.00	347.616	62	.	.
91	20.42	150.00	121.648	44	.	.
92	20.43	150.00	295.283	107	.	.
93	24.40	143.70	.	.	2.0	4.6
94	25.20	140.07	.	.	.	.
95	28.20	135.43	468.917	.	4.0	0.5
96	28.21	135.43	364.945	108	4.0	0.5
97	28.22	135.43	416.931	69	4.0	0.5
98	32.10	137.49	382.273	.	7.0	0.8
99	32.11	137.49	625.570	89	7.0	0.8
100	32.12	137.49	468.917	63	7.0	0.8
101	34.30	138.95	.	.	3.3	0.4
102	36.50	137.22	260.625	41	7.3	0.5
103	36.51	137.22	642.898	64	7.3	0.5
104	36.52	137.22	416.931	58	7.3	0.5
105	46.50	144.49	173.635	32	8.0	0.7
106	46.51	144.49	451.589	33	8.0	0.7
107	46.52	144.49	538.579	42	8.0	0.7
108	46.53	144.49	277.954	193	8.0	0.7
109	46.54	144.49	329.940	35	8.0	0.7
110	74.70	113.43	660.227	.	.	.
111	74.71	113.43	573.237	233	.	.
112	74.73	113.43	486.593	89	.	.
113	74.74	113.43	886.195	93	.	.

TUBULAR FOULING REACTOR 3

EXPNUMB=5

OBS	TIME	VELOCITY	MTH	TH	X	S
114	0.00	184.00	.	.	.	.
115	2.20	180.96	.	.	2.8	27.5
116	5.00	181.15	69.66	.	0.2	23.4
117	5.01	181.15	69.66	.	0.2	23.4
118	8.90	178.77	.	.	1.2	30.2
119	11.40	177.74	121.65	.	0.0	26.8
120	11.40	177.74	121.65	.	0.0	26.8
121	21.00	181.15	69.66	.	1.6	21.2
122	21.01	181.15	69.66	.	1.6	21.0
123	25.80	180.60	104.32	.	0.8	10.6
124	25.81	180.60	138.98	.	0.8	10.6
125	28.50	181.45	.	.	4.0	7.1
126	32.10	174.73	416.93	41	3.6	3.5
127	32.11	174.73	468.92	37	3.6	3.5
128	35.20	151.29	538.58	52	3.0	4.0
129	35.21	151.29	712.21	78	3.0	4.0
130	37.10	145.49	.	.	.	.
131	44.60	137.45	1233.46	181	.	1.9
132	44.61	137.45	1146.47	150	.	1.9
133	50.40	124.59	.	.	3.3	2.5
134	53.40	113.00	.	.	.	.
135	55.90	101.53	1737.39	233	4.7	1.4
136	55.91	101.53	2327.95	366	4.7	1.4
137	59.90	101.51	.	.	5.3	4.6
138	69.20	90.88	.	.	7.3	3.6
139	73.50	86.41	.	.	.	.
140	76.00	84.81	.	.	3.3	.
141	77.70	83.20	.	.	.	.
142	82.30	79.74	.	.	.	.
143	91.50	91.50	.	.	.	.
144	94.30	80.56	.	.	.	.
145	97.30	79.92	3474.77	530	.	.
146	97.31	79.92	3648.41	480	.	.

TUBULAR FOULING REACTOR 3

EXPNUMB=6

OBS	TIME	VELOCITY	MTH	TH	X	S
147	0.00	177.70	.	.	.	.
148	2.00	177.70	.	.	.	6.3
149	5.70	177.60	.	.	.	4.9
150	8.20	177.39	.	.	.	.
151	10.90	177.02	.	.	.	.
152	14.10	177.61	.	.	.	4.0
153	23.40	180.06	243.30	.	.	1.5
154	29.50	177.17	312.61	.	.	1.1
155	33.20	172.57	399.60	.	.	0.8
156	34.90	173.46	.	.	.	0.8
157	37.40	171.77	607.89	.	.	0.8
158	47.00	161.55	851.19	126	1.6	0.8
159	47.01	161.55	781.88	99	1.6	0.8
160	49.30	150.64	642.90	138	1.2	.
161	49.31	150.64	712.21	121	1.2	.
162	52.70	133.99	764.55	126	0.8	0.4
163	52.71	133.99	712.21	177	0.8	0.4
164	54.70	130.82	.	.	.	.
165	58.10	117.17	868.52	202	0.4	.
166	58.11	117.17	990.17	233	0.4	.
167	60.30	114.14	.	.	1.6	.
168	61.70	111.48	1111.82	185	1.0	0.4
169	61.71	111.48	938.18	220	1.0	0.4
170	70.70	107.10	1216.14	179	0.0	0.4
171	70.71	107.10	1164.15	202	0.0	0.4
172	73.40	106.75	.	.	.	.
173	83.10	108.17	1285.45	150	.	.
174	83.11	108.17	1667.72	267	.	.

TUBULAR FOULING REACTOR 3

EXPNUMB=7

OBS	TIME	VELOCITY	MTH	TH	X	S
175	0.00	184.97	.	.	.	.
176	5.70	183.85	.	.	.	90.5
177	12.30	185.39	.	.	.	87.7
178	24.20	183.66	86.99	12	9.2	43.3
179	24.21	183.66	138.98	34	9.2	43.3
180	24.22	183.66	190.96	41	9.2	43.3
181	30.40	179.58	312.61	38	.	.
182	30.41	179.58	364.94	.	.	.
183	33.30	178.14	416.93	119	7.2	27.1
184	33.31	178.14	416.93	48	7.2	27.1
185	33.32	178.14	434.26	49	7.2	27.1
186	47.50	.	521.25	49	10.8	18.0
187	47.51	.	555.91	40	10.8	18.0
188	47.52	.	642.90	43	10.8	18.0
189	52.20	154.20	781.88	42	7.2	15.7
190	52.21	154.20	1285.45	65	7.2	15.7
191	60.80	140.44	1789.37	81	6.4	9.9
192	60.81	140.44	1129.14	61	6.4	9.9
193	70.90	125.86	972.84	67	5.2	9.2
194	70.91	125.86	1980.68	123	5.2	9.2
195	77.00	124.21	.	.	.	.
196	78.10	123.78	1407.10	103	2.0	18.8
197	78.11	123.78	1563.40	52	2.0	18.8
198	78.12	123.78	3161.81	186	2.0	18.8
199	78.13	123.78	3179.14	207	2.0	18.8
200	83.00	129.79	.	.	8.0	12.0

TUBULAR FOULING REACTOR 3

EXPNUMB=8

OBS	TIME	VELOCITY	MTH	TH	X	S
201	0.00	183.79	.	.	.	.
202	4.30	186.41	0.00	.	.	377.8
203	4.31	186.41	0.00	.	.	377.8
204	13.10	185.75	.	.	.	320.3
205	22.80	188.49	86.99	57	.	178.1
206	22.81	188.49	86.99	14	.	178.1
207	25.80	187.47	.	.	.	.
208	29.90	184.47	538.58	42	.	146.4
209	29.91	184.47	486.59	66	.	146.4
210	33.30	180.89	1164.15	67	8.0	136.0
211	33.31	180.89	799.20	74	8.0	136.0
212	37.30	166.24	1407.10	114	2.4	164.8
213	37.31	166.24	1407.10	92	2.4	164.8
214	46.00	163.54	1285.45	104	8.0	178.6
215	46.01	163.54	1129.14	68	8.0	178.6
216	46.02	163.54	1355.11	109	8.0	178.6
217	52.30	158.80	1546.08	60	13.6	216.6
218	52.31	158.80	1372.44	252	13.6	216.6
219	56.40	161.78	2136.99	143	34.0	216.6
220	56.41	161.78	2136.99	143	34.0	216.6
221	60.40	156.47	1928.35	114	0.8	208.0
222	60.41	156.47	1772.04	118	0.8	208.0
223	71.10	147.42	6740.56	276	10.4	205.1
224	71.11	147.42	3387.78	164	10.4	205.1
225	71.11	147.42	1459.43	119	10.4	205.1
226	76.50	.	.	.	.	.

TUBULAR FOULING REACTOR 3

EXPNUMB=9

OBS	TIME	VELOCITY	MTH	TH	X	S
227	0.00	185.52	.	.	.	.
228	14.80	186.38	.	.	2.8	.
229	20.10	185.51	.	.	.	.
230	39.20	186.89	.	.	.	.
231	40.60	185.43	173.63	33	.	.
232	40.61	185.43	121.65	50	.	.
233	44.30	185.43	.	.	3.2	.
234	49.70	180.93	1181.48	73	2.4	.
235	49.71	180.93	642.90	135	.	.
236	60.70	167.83	1459.43	136	.	.
237	60.71	167.83	1685.05	155	.	.
238	63.00	163.78	.	.	.	.
239	65.90	161.55	.	.	4.4	.
240	67.70	162.41	.	.	2.4	.
241	86.30	.	3943.69	310	22.8	.
242	86.31	.	4864.54	367	.	.
243	92.10	135.39	.	.	.	.
244	94.70	124.69	.	.	.	.
245	97.40	115.43	5125.17	387	35.5	.
246	97.41	115.43	5802.72	457	.	.
247	100.00	107.28	.	.	.	.
248	112.00	85.67	4516.93	506	.	.
249	112.01	85.67	4899.20	466	.	.
250	120.70	.	5576.75	658	.	.
251	120.71	.	5507.09	648	.	.

TUBULAR FOULING REACTOR 3

EXPNUMB=10

OBS	TIME	VELOCITY	MTH	TH	X	S
252	0.00	184.58	69.662	.	.	.
253	0.01	184.58	104.319	.	.	.
254	0.02	184.58	69.662	.	.	.
255	20.61	188.95	0.000	.	.	.
256	20.80	188.95	86.991	.	.	.
257	34.30	187.17	36.390	.	.	.
258	34.31	187.17	34.658	.	.	.
259	53.10	184.28	225.968	.	.	.
260	53.11	184.28	0.000	.	.	.
261	67.60	185.38	138.977	.	.	.
262	67.61	185.38	104.319	.	.	.

TUBULAR FOULING REACTOR 3

EXPNUMB=11

OBS	TIME	VELOCITY	MTH	TH	X	S
263	0.00	85.30	.	.	.	.
264	5.40	83.86	.	.	.	7.8
265	7.40	83.31	312.61	.	4.5	3.8
266	7.41	83.31	295.28	.	4.5	3.8
267	12.60	88.77	312.61	.	2.0	1.6
268	23.10	88.36	694.88	.	0.0	2.0
269	23.11	88.36	138.98	.	0.0	2.0
270	27.00	85.97	2779.54	.	0.7	0.3
271	32.10	88.17	208.64	.	1.3	0.6
272	32.11	88.17	329.94	.	1.3	0.6
273	37.10	87.00	295.28	82	1.2	0.4
274	37.11	87.00	329.94	95	1.2	0.4
275	46.70	81.64	538.58	.	1.5	0.4
276	46.71	81.64	625.57	.	1.5	0.4
277	53.20	77.34	434.26	113	2.5	0.2
278	53.21	77.34	434.26	138	2.5	0.2
279	74.00	69.63	521.25	149	6.5	0.0
280	74.01	69.63	781.88	201	6.5	0.0
281	81.60	.	364.94	153	.	.
282	81.61	.	607.89	151	.	.
283	98.60	72.81	260.63	180	3.3	0.4
284	98.61	72.81	295.28	186	3.3	0.4
285	106.10	71.85	.	.	4.0	0.4
286	118.80	64.53	329.94	203	1.3	1.0
287	140.00	.	156.31	116	.	.

TUBULAR FOULING REACTOR 3

EXPNUMB=12

OBS	TIME	VELOCITY	MTH	TH	X	S
288	0.00	79.61	17.329	.	.	.
289	3.40	81.56	.	.	2.0	3.0
290	3.41	81.56	34.658	.	2.0	3.0
291	16.10	.	86.991	.	1.2	2.6
292	16.11	.	0.000	.	1.2	2.6
293	21.00	79.61	69.662	.	.	.
294	21.01	79.61	86.991	.	.	.
295	26.40	79.31	156.306	.	2.0	1.4
296	26.41	79.31	138.977	.	2.0	1.4
297	38.20	80.19	121.648	.	0.8	0.3
298	38.21	80.19	173.635	87	0.8	0.3
299	41.90	73.81	364.945	81	1.6	0.4
300	41.91	73.81	208.639	91	1.6	0.4
301	50.70	70.19	382.273	102	2.4	0.3
302	50.71	70.19	347.616	107	2.4	0.3
303	68.60	63.32	86.991	90	.	.
304	68.61	63.32	121.648	109	.	.
305	87.70	70.10	.	.	.	.

TUBULAR FOULING REACTOR 3

EXPNUMB=14

OBS	TIME	VELOCITY	MTH	TH	X	S
306	0.00	251.03	.	.	.	.
307	14.80	257.36	138.98	.	2.4	2.2
308	14.81	251.03	104.32	.	2.4	2.2
309	24.00	255.89	190.96	.	2.4	0.7
310	24.01	255.89	173.63	.	2.4	0.7
311	36.40	236.94	329.94	.	2.0	0.9
312	36.41	236.94	364.94	.	2.0	0.9
313	41.40	239.98	364.94	50	3.2	0.3
314	41.41	239.98	295.28	67	3.2	0.3
315	48.50	228.96	486.59	82	2.4	0.2
316	48.51	228.96	451.59	82	2.4	0.2
317	51.90	214.00	573.24	103	1.6	0.6
318	51.91	214.00	521.25	68	1.6	0.6
319	60.80	201.22	781.88	121	.	0.5
320	60.81	201.22	729.54	134	.	0.5
321	72.00	186.97	1042.50	105	.	0.4
322	72.01	186.97	1146.47	111	.	0.4
323	83.50	179.84	.	.	0.0	.
324	90.10	197.27	468.92	64	.	.
325	90.11	197.27	521.25	65	.	.

TUBULAR FOULING REACTOR 3

EXPNUMB=15

OBS	TIME	VELOCITY	MTH	TH	X	S
326	0.00	251.72	34.658	.	.	.
327	0.01	251.72	17.329	.	.	.
328	1.60	.	34.658	.	.	.
329	9.80	259.15	86.991	.	0.4	27.5
330	9.81	259.15	69.662	.	.	27.5
331	11.80	.	.	.	.	.
332	12.90	.	69.662	.	0.0	28.1
333	12.91	.	86.991	.	0.0	28.1
334	19.00	254.00	51.986	.	.	25.9
335	19.01	254.00	20.448	.	.	25.9
336	26.70	256.65	121.648	.	.	5.4
337	26.71	256.65	138.977	.	.	5.4
338	34.70	257.80	.	.	.	1.5
339	39.70	.	284.885	.	.	.
340	39.71	.	208.639	.	.	.
341	42.50	251.66	.	.	.	2.9
342	45.80	245.96	.	.	.	0.7

TUBULAR FOULING REACTOR 3

EXPNUMB=16

OBS	TIME	VELOCITY	MTH	TH	X	S
343	0.00	253.36	.	.	.	.
344	1.50	250.30	17.33	.	.	.
345	1.51	250.30	0.00	.	.	.
346	12.30	254.07	104.32	.	.	.
347	12.31	254.07	34.66	.	.	.
348	16.60	252.81	69.66	.	.	.
349	20.10	251.65	104.32	.	.	.
350	34.80	253.54	173.63	.	.	.
351	34.81	253.54	156.31	.	.	.
352	40.90	.	.	.	.	.
353	51.20	252.14	190.96	.	.	.
354	60.80	254.96	121.65	.	.	.
355	60.81	254.96	277.95	.	.	.
356	68.20	260.05	.	.	.	.
357	79.60	.	781.88	.	.	.
358	93.70	230.82	1963.01	.	.	.
359	108.20	252.78	.	.	.	.
360	111.70	238.41	.	.	.	.
361	154.00	198.59	.	.	.	.

TUBULAR FOULING REACTOR 4

Time = Experimental Run Time (hr)

F_r = Volumetric Recycle Flow Rate (gpm)

ΔP = Pressure Drop (in Hg)

T_b = Bulk Temperature (°C)

T_i = Thermistor Temperature in THE (°C)

T_{ii} = Thermistor Temperature in THE (°C)

Thermal Power (watts)

Thickness (μm)

Experiment 1 Tubular Fouling Reactor 4

Time	F_r	ΔP	T_{bulk}	T_i	T_{ii}	Thermal Power	Thickness
0	2.75	0.56	31.80	43.21	47.00	316	0
7.1	2.76	0.62	32.03	43.03	47.00	331	
18.0	2.76	0.69	31.85	43.81	47.62	317	
23.0	2.77	0.75	31.80	45.75	49.50	312	31.4
27.5	2.77	0.89	32.12	47.59	51.25	305	
39.4	2.79	1.20	31.74	48.99	52.9	326	
40.4	2.75	1.15	31.90	49.55	53.2	304	
45.3	2.76	1.05	31.79	49.79	53.2	301	
45.8	2.79	1.10	33.2	51.9	55.9	333	132
54.4	2.73	1.30	31.70	50.40	54.2	317	
65.8	2.73	1.30	31.13	47.62	51.3	306	
66.4	2.74	1.38	31.75	48.19	52.0	317	
69.9	2.75	1.35	31.83	48.25	52.1	321	241, 242, 141

Experiment 2 Tubular Fouling Reactor 4

Time	F_r	ΔP	T_{bulk}	T_i	T_{ii}	Thermal Power	Thickness
0	2.74	0.58	31.72	40.82	45.05	352.3	0
9.6	2.74	0.59	31.50	41.01	45.57	379.8	-
18.2	2.79	0.58	31.50	40.39	44.72	360.6	-
19.6	2.76	0.58	31.50	40.58	44.91	360.6	-
27.9	2.75	0.58	31.50	40.68	45.09	367.3	-
31.7	2.78	0.58	31.50	40.82	45.38	379.8	-
40.7	2.74	0.58	31.50	40.94	45.35	367.3	-
55.9	2.72	0.61	31.50	42.50	47.00	374.8	-
66.9	2.69	0.84	31.50	42.62	47.20	381.4	-
68.3	2.76	0.94	31.50	42.79	47.30	375.6	-
70.2	2.76	0.85	31.50	42.63	47.21	381.4	36.1, 24.5
72.6	2.78	0.84	31.50	42.23	46.59	363.1	-
73.6	2.75	0.85	31.50	42.18	46.38	349.8	-
89.3	2.76	1.19	31.50	42.22	46.37	345.6	-
94.3	2.75	1.16	31.50	43.96	48.01	337.3	-
102.2	2.74	1.09	31.50	43.40	47.65	353.9	38.3, 40.2
113.7	2.76	1.65	31.50	44.20	48.39	348.9	-
116.4	2.77	1.65	31.50	44.38	48.52	344.8	-
136.9	2.73	1.74	31.50	44.60	48.82	351.4	-
140.4	2.77	1.80	31.50	44.80	48.99	348.9	-
148.2	2.75	1.77	31.50	45.56	49.81	353.9	-
150.0	2.74	1.66	31.50	45.01	49.30	357.3	-
166.1	2.73	1.34	31.50	44.59	48.65	338.1	-
167.2	2.77	1.87	31.50	45.00	49.20	349.8	-
186.9	2.75	1.79	31.50	44.62	48.90	356.4	94.8, 84.7
187.4	2.75	1.82	31.50	44.42	48.65	352.3	92.4, 84.4

Experiment 3 Tubular Fouling Reactor 4

Time	F_r	ΔP	T_{bulk}	T_i	T_{ii}	Thermal Power	Thickness
0	2.72	0.58	31.50	41.01	45.25	353.1	0
6.42	2.75	0.58	31.50	41.03	45.41	364.8	-
7.6	2.76	0.58	31.50	41.00	45.30	358.1	-
21.3	2.74	0.58	31.50	40.98	45.22	353.1	-
25.7	2.72	0.58	31.50	41.10	45.40	358.1	-
43.3	2.77	0.58	31.50	41.42	45.61	348.9	11.61
46.3	2.75	0.60	31.50	41.60	45.81	350.6	-
49.5	2.74	0.61	31.50	41.63	45.92	357.3	-
53.9	2.75	0.61	31.50	41.49	45.68	348.9	-
67.3	2.73	0.61	31.50	41.15	45.37	351.4	-
70.7	2.76	0.61	31.50	41.27	45.51	353.1	-
73.3	2.75	0.62	31.50	41.48	45.73	353.9	-
93.7	2.73	0.70	31.50	42.40	46.61	350.6	-
104.7	2.73	0.76	31.50	43.21	47.59	364.8	-
104.9	2.76	0.77	31.50	42.79	46.99	349.8	55.22
117.8	2.76	0.67	31.50	41.19	45.23	336.5	-
118.8	2.73	0.64	31.50	41.62	45.80	348.1	-
137.2	2.74	0.68	31.50	41.62	45.79	347.3	-
138.4	2.75	0.65	31.50	42.05	46.30	353.9	-
140.8	2.74	0.67	31.50	41.97	46.18	350.6	51.3
144.4	2.74	0.68	31.50	42.04	46.29	352.3	-
161.4	2.73	0.61	31.50	42.30	46.52	351.4	-
164.9	2.73	0.65	31.50	42.64	46.97	360.6	-
165.2	2.77	0.65	31.50	42.58	46.79	350.6	94.3
169.8	2.75	0.68	31.50	42.41	46.62	350.6	-
175.5	2.76	0.70	31.50	42.81	47.05	353.1	-
185.4	2.73	0.70	31.50	41.60	45.80	349.8	-
187.3	2.73	0.65	31.50	41.57	45.64	339.0	-
189.6	2.74	0.63	31.50	41,99	46,21	351.4	64.9
198.3	2.76	0.68	31.50	42.60	46.82	351.4	-
210.5	2.75	0.74	31.50	42.80	46.97	347.3	-
212.5	2.77	0.75	31.50	43.15	47.25	341.5	-
216.0	2.74	0.71	31.50	43.99	48.20	350.6	-
234.5	2.75	0.70	31.50	42.59	46.78	348.9	54.9, 57.3
243.8	2.75	0.70	31.50	42.81	47.01	349.8	-
256.5	2.78	0.70	31.50	42.09	46.35	354.8	-

Experiment 4 Tubular Fouling Reactor 4

Time	F_r	ΔP	T_{bulk}	T_i	T_{ii}	Thermal Power	Thickness
0	2.76	0.58	31.50	41.56	45.77	350.6	0
.7	2.79	0.61	31.50	41.38	45.59	350.6	-
8.5	2.72	0.61	31.50	41.10	45.30	349.8	-
10.7	2.77	0.61	31.50	41.03	45.24	350.6	-
14.7	2.73	0.61	31.50	41.10	45.38	356.4	-
21.5	2.76	0.61	31.50	42.60	46.83	352.3	-
21.8	2.73	0.62	31.50	42.58	46.81	352.3	-
24.8	2.80	0.63	31.50	43.49	47.80	358.9	-
32.7	2.74	0.63	31.50	41.90	46.02	343.1	-
32.9	2.72	0.61	31.50	42.22	46.44	351.4	-
33.1	2.74	0.61	31.50	42.32	46.58	354.8	-
35.0	2.75	0.61	31.50	42.03	46.20	347.3	30.5
58.9	2.77	0.80	31.50	41.18	45.38	349.8	-
61.1	2.81	0.82	31.50	42.20	46.38	348.1	-
62.4	2.75	0.87	31.50	43.42	47.59	347.3	-
63.5	2.76	0.94	31.50	44.17	48.36	348.9	148.5
72.5	2.75	1.65	31.50	43.80	48.00	349.8	100.9
82.8	2.76	2.32	31.50	44.25	48.40	345.6	-
93.9	2.75	2.93	31.50	44.80	49.03	352.3	-
95.1	2.76	3.10	31.50	44.41	48.63	351.4	212.1
103.8	2.78	3.95	31.50	43.79	47.97	348.1	-
106.9	2.73	3.90	31.50	43.82	47.98	346.4	-
109.3	2.78	4.15	31.50	44.60	48.70	341.4	-
115.7	2.73	4.00	31.50	45.30	49.79	373.9	-
116.2	2.77	4.15	31.50	43.85	48.00	345.6	-
116.4	2.75	4.05	31.50	43.97	48.21	353.1	301.5
131.3	2.78	3.72	31.50	43.50	47.72	351.4	-
143.7	2.73	4.00	31.50	43.18	47.38	349.8	209.8
154.3	2.62	4.00	31.50	43.53	47.38	320.6	333.6

Experiment 5 Tubular Fouling Reactor 4

Time	F_r	ΔP	T_{bulk}	T_i	T_{ii}	Thermal Power	Thickness
0	2.76	0.59	31.50	40.79	45.02	351.4	0
0.8	2.76	0.58	31.50	40.78	45.00	351.4	-
8.8	2.72	0.61	31.50	40.83	45.21	364.8	-
9.7	2.75	0.61	31.50	40.43	44.65	351.2	-
23.0	2.76	0.61	31.50	40.50	44.63	343.9	-
23.2	2.73	0.59	31.50	40.61	44.80	348.9	-
25.4	2.77	0.61	31.50	40.75	44.99	353.1	-
31.3	2.74	0.61	31.50	40.85	45.17	359.7	-
52.1	2.76	0.94	31.50	41.17	45.37	349.8	78.5
55.1	2.75	1.04	31.50	40.79	44.97	348.1	-
60.7	2.72	1.39	31.50	41.79	46.04	353.9	-
61.1	2.90	1.57	31.50	41.23	45.56	360.6	-
61.3	2.76	1.51	31.50	41.23	45.55	359.8	-
62.0	2.75	1.50	31.50	41.04	45.21	347.3	-
73.1	2.78	3.83	31.50	40.00	44.15	345.6	-
74.5	2.72	3.67	31.50	40.30	44.58	356.4	-
75.2	2.77	3.80	31.50	40.19	44.41	351.4	228.7
95.2	2.76	3.52	31.50	39.63	43.95	359.8	-
95.6	2.74	3.50	31.50	39.55	43.77	351.4	176.5
101.6	2.72	3.02	31.50	39.68	43.93	353.9	-
109.8	2.74	3.04	31.50	39.83	44.18	362.3	-
110.0	2.73	2.94	31.50	39.65	43.82	347.3	-
116.6	2.73	2.75	31.50	39.78	43.99	350.6	240.3, 205.3

Experiment 6 Tubular Fouling Reactor 4

Time	F_r	ΔP	T_i	T_{ii}	Thermal Power	Thickness	Ca^{++} (mg/l)	Mg^{++} (mg/l)
0	2.76	0.58	38.72	42.91	348.9	0	13.6	5.4
1.7	2.75	0.58	38.42	42.59	347.3	-	-	-
9.4	2.74	0.62	38.21	42.48	355.6	-	-	-
11.7	2.76	0.61	38.23	42.50	355.6	-	-	-
21.0	2.74	0.61	38.19	42.40	350.6	-	-	-
27.8	2.73	0.60	38.52	42.80	356.4	-	-	-
45.1	2.75	1.69	40.97	45.16	348.9	52.6	-	-
47.6	2.77	1.50	40.00	44.22	351.4	-	11.2	9.3
50.5	2.76	1.40	40.96	45.14	348.1	-	-	-
52.6	2.77	1.48	42.03	46.24	350.6	-	-	-
54.4	2.78	1.75	42.55	46.79	353.1	-	-	-
70.9	2.73	2.25	42.55	46.62	338.9	-	-	-
71.3	2.73	2.29	42.82	47.02	349.8	-	-	-
72.6	2.75	2.43	43.38	47.50	343.1	106.0	-	-
75.4	2.77	2.69	43.55	47.72	347.3	113.3	-	-
86.9	2.73	4.13	43.70	47.85	345.6	-	-	-
96.5	2.75	4.30	42.32	46.45	344.0	-	13.6	3.9
100.6	2.75	4.25	42.58	46.80	351.4	135.3	-	-
103.6	2.75	4.10	41.83	46.08	353.9	-	-	-
109.9	2.73	4.12	40.80	45.00	349.8	-	-	-
122.7	2.73	3.10	40.23	44.45	351.4	-	13.2	3.2
123.8	2.74	2.90	40.61	44.31	349.8	141.4	-	-
131.0	2.76	3.04	41.85	46.08	352.3	-	-	-

Experiment 7 Tubular Fouling Reactor 4

Time	F_r	ΔP	T_i	T_{ii}	Thermal Power	Thickness
0	2.74	0.58	36.55	40.73	348.1	0
0.1	2.78	0.58	36.40	40.58	348.1	-
3.9	2.73	0.58	36.36	40.59	352.3	-
11.8	2.75	0.59	36.80	41.29	373.9	-
22.2	2.75	0.58	38.40	42.62	351.4	-
25.5	2.76	0.58	41.40	45.62	351.4	10.8
28.2	2.75	0.59	42.61	46.95	361.4	-
30.0	2.78	0.65	43.81	47.98	347.3	-
35.0	2.73	1.06	45.40	49.52	343.1	-
35.4	2.74	1.09	45.78	49.97	348.9	-
37.0	2.78	1.38	45.53	49.73	353.9	104.1
47.6	2.74	2.76	46.04	50.05	340.0	-
48.0	2.76	2.81	46.03	50.21	348.1	-
51.2	2.74	3.15	45.80	50.00	349.7	190.4
84.4	2.77	1.15	40.95	45.20	353.9	-
100.7	2.74	1.00	40.84	45.18	361.4	-
101.8	2.76	1.01	40.22	44.41	348.9	260.5, 234.4, 230.6

Experiment 8 Tubular Fouling Reactor 4

Time	F_r	ΔP	T_i	T_{ii}	Thermal Power	Thickness	Ca^{++} (mg/l)	Mg^{++} (mg/l)
0	2.76	0.58	35.60	39.80	349.8	0	30.5	6.3
11.2	2.73	0.57	35.63	39.80	347.3	-	-	-
25.0	2.75	0.56	37.17	41.48	358.9	-	-	-
25.5	2.73	0.56	37.18	41.42	353.1	-	-	-
32.2	2.77	0.56	36.99	41.19	349.8	-	-	-
36.5	2.75	0.58	39.40	43.80	366.4	-	-	-
47.3	2.89	0.77	41.03	45.25	351.4	-	-	-
47.5	2.64	0.72	41.34	45.54	349.8	13.4	-	-
51.3	2.77	0.77	38.00	42.20	349.8	-	-	-
57.8	2.76	1.42	41.20	45.58	364.8	-	-	-
58.0	2.17	0.57	42.53	46.74	350.6	-	-	-
58.3	2.92	1.39	40.57	44.83	354.8	-	-	-
58.5	2.74	1.57	41.03	45.21	348.1	-	-	-
60.4	2.74	2.07	41.79	45.99	349.8	-	-	-
70.4	2.87	1.50	38.50	42.58	339.8	-	-	-
70.7	2.75	1.36	38.83	43.04	350.6	99.9	-	-
76.0	2.76	1.60	41.41	45.60	348.9	-	-	-
80.3	2.49	2.57	46.17	50.21	336.5	-	-	-
80.6	2.89	3.03	45.85	50.03	348.1	-	-	-
80.7	2.76	2.91	45.92	50.07	345.6	-	-	-
81.2	2.76	3.06	45.84	50.18	361.4	256.7, 208	-	-
85.1	2.73	3.08	41.10	45.38	356.4	-	-	-
99.5	2.51	3.85	44.13	48.05	326.5	-	-	-
100.2	2.29	3.21	45.87	49.85	331.5	-	-	-
100.5	1.29	1.07	51.8	55.8	333.1	-	-	-
100.8	2.73	4.55	42.70	46.90	349.8	108.1, 99	-	-
106.7	2.77	4.05	42.63	46.98	362.3	-	-	-
107.5	2.78	4.06	42.80	47.00	349.8	-	-	-
118.9	2.66	4.20	40.32	44.45	343.9	-	-	-
121.0	2.77	4.30	41.08	45.38	358.1	-	-	-
124.7	2.75	4.38	43.43	47.65	351.4	-	-	-
128.0	2.76	4.25	44.42	48.78	338.2	-	-	-
128.3	2.75	4.24	44.05	48.35	358.1	164.5	-	-
167.6	2.66	4.20	39.25	43.42	347.3	-	-	-
167.9	2.92	4.34	39.14	43.35	350.6	-	-	-
168.7	2.73	4.21	39.02	43.19	347.3	-	-	-

Experiment 9 Tubular Fouling Reactor 4

Time	F_r	ΔP	T_i	T_{ii}	Thermal Power	Thickness	Ca^{++} (mg/l)	Mg^{++} (mg/l)
0	2.76	0.58	39.07	43.32	353.9	0	121.8	38.1
0.2	2.78	0.57	38.95	43.03	339.8	-	-	-
7.7	2.75	0.59	39.24	43.51	355.6	-	-	-
11.1	2.74	0.57	39.22	43.51	357.3	-	112.2	44.9
11.7	2.76	0.57	39.12	43.30	348.1	-	-	-
22.8	2.75	0.58	39.18	43.27	340.6	-	-	-
23.7	2.73	0.58	39.66	43.90	353.1	-	114.6	43.4
27.8	2.76	0.58	40.62	44.86	353.1	-	-	-
29.6	2.77	0.59	41.46	45.81	362.3	-	-	-
34.3	2.74	0.58	39.99	44.20	350.6	-	-	-
51.4	2.73	0.58	41.00	45.26	354.8	-	-	-
57.6	2.73	0.58	43.39	47.63	353.1	36.6	102.6	39.0
59.5	2.75	0.59	42.90	47.20	358.1	-	-	-
81.9	2.56	1.71	45.35	49.41	338.1	-	-	-
82.2	2.75	1.94	45.19	49.38	348.9	84.0, 139	101.8	51.2
83.6	2.78	2.08	44.40	48.59	348.9	-	-	-
93.4	2.73	3.10	45.97	50.01	336.5	-	-	-
94.1	2.62	3.12	46.46	50.62	346.4	-	-	-
94.6	2.21	2.43	47.98	52.1	343.1	-	-	-
95.0	1.83	1.61	50.1	54.2	341.5	-	-	-
95.2	1.43	1.03	53.7	57.9	349.8	-	-	-
96.0	2.76	3.62	45.83	50.17	361.4	-	-	-
97.4	2.75	3.30	44.78	48.92	344.8	-	-	-
98.1	2.77	3.30	45.01	49.21	349.8	128	-	-
105.9	2.74	2.95	45.80	50.04	353.1	-	93.8	42.9
107.3	2.75	3.11	45.81	50.03	351.4	122, 114	-	-
119.6	2.76	3.54	45.20	49.22	334.8	-	-	-
120.3	2.74	3.56	45.78	49.98	349.8	-	-	-
124.8	2.75	3.73	46.20	50.40	349.8	-	-	-
130.1	2.75	4.18	46.22	50.48	354.8	-	73.8	28.3
143.8	2.77	3.78	43.45	47.65	349.8	-	-	-
147.1	2.84	3.85	44.00	48.22	351.4	-	-	-
147.4	2.16	2.52	45.40	49.50	341.5	-	-	-
147.7	1.57	1.46	48.80	53.0	349.8	-	-	-
148.2	3.30	5.04	43.38	47.62	353.1	-	-	-
148.6	2.72	3.60	44.17	48.35	348.1	90.5	-	-
156.7	2.78	3.72	46.40	50.60	349.8	-	-	-

Experiment 10 Tubular Fouling Reactor 4

Time	F_r	ΔP	T_i	T_{ii}	Thermal Power	Thickness
0	2.76	0.58	40.42	44.72	358.1	0
45.5	2.73	0.59	40.22	44.40	348.1	0
70.5	2.73	0.59	40.38	44.63	353.9	0
94.1	2.74	0.60	40.34	44.64	358.1	0
143.0	2.76	0.59	40.70	45.10	366.4	0
165.8	2.78	0.58	40.83	45.19	363.1	0
191.3	2.78	0.58	40.63	44.80	347.3	0
312.2	2.75	0.61	40.70	44.84	344.8	0

ANNULAR FOULING REACTOR

S_i = Inlet Nutrient Concentration

T_b = Bulk Fluid Temperature

Re = Reynolds Number = $2bv_m/\nu$

where b = width of annulus

ν = kinematic viscosity

v_m = Mean Fluid Velocity

τ_o = Initial Wall Shear Stress = $T_q/2\pi R_o^2 H$

where R_o = radius of AFR outer cylinder

H = height of AFR inner cylinder

Ta = Taylor Number = $\Omega R_m^{1/2} b^{3/2} / \nu Fg$

where R_m = mean annulus radius

$$Fg = \text{geometric factor} = \frac{\pi^2}{41.2} \left(\frac{1-b}{2R_m}\right)^{-1} P^{-1/2}$$

$$P = 0.0571 \left(1 - 0.652 \frac{b/R_m}{1-b/2R_m}\right) + 0.00056 \left(1 - 0.652 \frac{b/R_m}{1-b/2R_m}\right)^{-1}$$

Ω = Rotational Velocity

Time = Experimental Run Time

T_q = Torque on Inner Cylinder

f_a = Friction Factor = $\dfrac{T_q}{\Omega^2 \pi f R_i^3 (R_o + R_i) H}$

where f = density of water

R_i = radius of AFR inner cylinder

Th = Biofilm Thickness

S = Limiting Nutrient Concentration (glucose)

X = Biomass Concentration in Bulk Fluid

AFR 1

S_i (mg/l): 5 T_b (°C): 30 Re: 366

v_m (cm/sec): 82.5 τ_o (N/m^2): 1.62 Ta: 203

Ω: 150

TIME (h)	T_q (N-cm)	f_a	Th (μm)	S (mg/l)	X (mg/l)	S_i (mg/l)
0	0.5789	0.1074	-	-	-	2.6
6	-	-	-	2.00	-	-
12	0.7695	0.1427	-	-	-	-
14	0.9813	0.1820	-	-	-	-
16	1.0872	0.2016	36.1	-	-	-
18	1.1719	0.2173	-	1.55	1.0	-
23	1.5108	0.2802	47.8	-	-	-
36	1.7155	0.3182	-	1.20	5.0	-
37	-	-	71.4	-	-	-
42	-	-	-	-	4.0	-
47	2.0756	0.3850	88.9	-	-	-
48	-	-	-	0.55	3.5	-
61	2.0403	0.3784	-	-	4.0	-
62	-	-	103.3	-	-	-
71	2.0050	0.3719	-	0.40	4.0	-
72	-	-	103.8	-	-	-
74	-	-	-	-	-	-

AFR 2

S_i (mg/l): 20 T_b (°C): 30 Re: 366

v_m (cm/sec): 82.5 τ_o (N/m^2): 1.62 Ta: 203

Ω: 150

TIME (h)	T_q (N-cm)	f_a	Th (μm)	S (mg/l)	X (mg/l)	S_i (mg/l)
0.0	0.8683	0.1004	-	-	-	11.0
4.6	-	-	-	10.2	-	-
8.6	-	-	-	9.1	0.7	-
12.6	-	-	-	7.5	1.8	-
16.9	0.8754	0.1012	-	-	-	-
17.0	-	-	-	5.4	5.8	-
17.7	-	-	-	-	-	-
18.1	0.9036	0.1045	13.4	-	-	-
24.3	1.8920	0.2187	-	-	-	-
24.5	-	-	-	2.6	6.5	-
24.7	1.9979	0.2310	-	-	-	-
25.0	-	-	83.2	-	-	-
28.5	-	-	-	2.4	4.3	-
32.5	-	-	-	2.4	4.3	-
32.5	-	-	-	2.3	4.4	-
36.5	-	-	-	1.6	5.4	-
39.8	3.0428	0.3517	-	-	-	-
41.4	3.0569	0.3534	-	-	-	-
42.0	-	-	93.3	1.1	5.7	-
46.6	2.5627	0.2962	-	-	-	-
47.0	-	-	67.6	-	-	-
53.0	-	-	-	0.5	4.8	-
57.0	-	-	-	-	5.4	-
61.0	-	-	71.8	-	-	7.7
61.6	3.0216	0.3493	-	-	-	-
62.0	-	-	-	0.4	6.4	-
62.1	-	-	-	-	-	-

AFR 3

S_i (mg/l): 20 T_b (^oC): 30 Re: 366

v_m (cm/sec): 82.5 τ_o (N/m^2): 1.62 Ta: 203

Ω : 150

TIME (h)	T_q (N-cm)	f_a	Th (μm)	S (mg/l)	X (mg/l)	S_i (mg/l)
0	0.5718	0.1065	-	-	-	9.2
4	-	-	-	3.00	-	-
8	-	-	-	4.75	4	-
11	0.5859	0.1091	-	-	-	-
15	1.3202	0.2458	-	4.70	5	-
16	1.4967	0.2787	35.9	-	-	-
17	1.6167	0.3011	-	-	-	-
24	2.0968	0.3905	67.7	-	-	-
25	-	-	-	2.25	5	-
28	-	-	-	2.15	7	-
32	-	-	-	1.80	-	-
36	-	-	-	2.30	5	-
37	1.6732	0.3116	108.9	-	-	-
38	1.6167	0.3011	-	-	-	-
41	1.7085	0.3182	136.3	-	-	-
45	-	-	-	1.50	7	-
48	1.6026	0.2984	-	-	-	-
53	-	-	-	2.50	6	-
60	1.3908	0.2590	112.9	-	-	-

AFR 4

S_i (mg/l): 5 T_b (^oC): 30 Re: 366

v_m (cm/sec): 82.5 τ_o (N/m^2): 1.62 Ta: 203

Ω: 150

TIME (h)	T_q (N-cm)	f_a	Th (μm)	S (mg/l)	X (mg/l)	S_i (mg/l)
0.0	0.8542	0.0991	-	-	-	2.6
4.0	-	-	-	0.1	-	-
8.0	-	-	-	0.4	0.5	-
12.0	-	-	-	2.0	1.6	-
14.2	0.8542	0.0991	-	-	-	-
18.0	0.9036	0.1049	-	0.1	2.5	-
18.5	-	-	17.5	-	-	-
18.7	-	-	-	-	-	-
21.6	0.9178	0.1065	-	-	-	-
22.0	-	-	-	0.3	1.5	-
26.0	-	-	-	-	-	-
26.5	1.4755	0.1713	-	-	-	-
26.9	1.5390	0.1786	40.0	-	-	-
27.0	-	-	-	0.5	1.5	-
27.9	1.5955	0.1852	-	-	-	-
29.3	-	-	-	0.7	2.0	-
33.3	-	-	-	0.3	2.0	-
37.3	-	-	-	0.1	1.7	2.8
38.2	2.3227	0.2696	95.5	-	-	-
39.6	2.3933	0.2778	-	-	-	-
43.2	2.3015	0.2671	-	0.1	1.7	-
62.0	2.1462	0.2491	93.6	0.1	1.6	-
62.1	-	-	-	-	-	-
67.8	-	-	-	-	2.5	-
68.5	2.2874	0.2655	89.2	-	-	-

ρ_f, biofilm density = 13.8 mg/cm^3

S_i (mg/l): 12.5 T_b (^oC): 30 Re: 366

v_m (cm/sec): 82.5 τ_o (N/m^2): 1.62 Ta: 203

Ω: 150

TIME (h)	T_q (N-cm)	f_a	Th (μm)	S (mg/l)	X (mg/l)	S_i (mg/l)
0.0	0.7201	0.1042	-	-	-	6.6
4.5	-	-	-	5.5	-	-
8.5	0.7977	0.1154	-	4.8	1.1	-
11.0	0.7977	0.1154	-	-	-	-
12.0	0.8683	0.1256	-	2.5	2.0	-
12.6	0.9389	0.1359	36.3	-	-	-
13.0	1.0166	0.1471	-	-	-	-
13.9	1.3696	0.1982	-	-	-	-
14.7	1.7932	0.2595	-	-	-	-
15.6	2.1603	0.3126	-	-	-	-
16.0	-	-	-	0.3	2.4	-
16.1	2.2945	0.3320	75.0	-	-	-
21.5	3.0852	0.4464	96.3	0.3	3.2	-
26.4	-	-	-	0.2	3.0	-
30.4	-	-	-	0.2	3.0	-
34.4	-	-	-	-	3.1	-
37.6	3.2758	0.4740	113.3	0.2	-	-
37.7	-	-	-	-	2.9	-
42.2	3.2758	0.4740	-	0.3	3.0	-
45.8	3.2829	0.4750	111.6	0.6	2.8	-
45.9	-	-	-	-	-	-
52.2	-	-	-	0.4	3.8	-
58.2	-	-	-	0.1	-	-
59.7	3.2405	0.4689	106.2	-	-	-

ρ_f, biofilm density = 25.5 mg/cm^3

AFR 6

S_i (mg/l): 12.5 T_b (^oC): 30 Re: 366

v_m (cm/sec): 82.5 τ_o (N/m^2): 1.62 Ta: 203

Ω: 150

TIME (h)	T_q (N-cm)	f_a	Th (μm)	S (mg/l)	X (mg/l)	S_i (mg/l)
0.0	0.7201	0.1042	-	-	-	6.8
4.5	-	-	-	0.9	0.3	-
8.5	-	-	-	0.8	0.6	-
12.5	0.8048	0.1164	-	4.2	1.5	-
13.0	0.8472	0.1226	-	-	-	-
14.2	0.9884	0.1430	25.2	-	-	-
15.0	1.2002	0.1736	-	-	-	-
15.6	1.4473	0.2094	-	-	-	-
16.0	-	-	-	0.7	1.5	-
16.1	1.6873	0.2441	-	-	-	-
16.4	1.7861	0.2584	-	-	-	-
18.6	2.4004	0.3473	49.4	-	-	-
22.3	2.8240	0.4086	84.4	0.3	-	-
22.4	-	-	-	-	2.4	-
26.2	-	-	93.2	2.1	-	-
30.2	-	-	-	-	1.8	-
34.2	-	-	-	0.3	2.4	-
35.8	-	-	-	-	-	-
37.0	-	-	-	-	-	-
37.1	-	-	-	-	-	-
39.4	-	-	-	-	3.3	-
41.4	3.0358	0.4392	91.3	-	-	-
45.8	-	-	-	-	3.5	-
59.6	2.9652	0.4290	105.1	-	5.0	-

ρ_f, biofilm density = 41.6 mg/cm^3

S_i (mg/l): 20 T_b (^oC): 30 Re: 366

v_m (cm/sec): 82.5 τ_o (N/m^2): 1.62 Ta: 203

Ω: 150

TIME (h)	T_q (N-cm)	f_a	Th (μm)	S (mg/l)	X (mg/l)	S_i (mg/l)
0.0	0.8542	0.0991	-	-	-	9.2
4.5	-	-	-	4.0	-	-
8.5	-	-	-	5.6	1.5	-
13.0	1.3061	0.1516	-	-	-	-
13.7	1.7297	0.2008	-	-	-	-
14.1	1.8920	0.2196	-	-	-	-
14.4	1.9979	0.2319	-	3.4	-	-
14.8	2.1462	0.2491	-	-	-	-
15.2	-	-	44.4	-	-	-
17.5	2.6828	0.3114	-	1.2	3.4	-
23.4	2.9652	0.3441	91.9	-	-	-
24.5	-	-	-	0.7	3.9	-
28.5	-	-	-	0.6	4.7	-
32.5	-	-	-	0.6	5.6	-
34.5	-	-	-	-	-	-
39.4	2.3298	0.2704	76.4	0.7	5.1	-
48.9	2.2945	0.2663	-	0.5	6.7	-
54.9	-	-	-	-	5.6	-
59.8	2.2945	0.2663	87.5	0.8	6.8	-

ρ_f, biofilm density = 18.4 mg/cm^3

AFR 8

S_i (mg/l): 5 T_b (^oC): 30 Re: 366

v_m (cm/sec): 82.5 τ_o (N/m^2): 1.62 Ta: 203

Ω: 150

TIME (h)	T_q (N-cm)	f_a	Th (μm)	S (mg/l)	X (mg/l)	S_i (mg/l)
0.0	0.5718	0.1065	-	-	-	3.1
8.4	-	-	-	1.0	0.5	-
12.4	-	-	-	1.0	1.2	-
13.5	0.6071	0.1131	-	-	-	-
14.4	0.6142	0.1144	-	-	-	-
16.4	0.6283	0.1170	-	0.8	1.3	-
17.8	0.6848	0.1275	-	-	-	-
19.5	0.7130	0.1328	-	-	-	-
23.8	0.8613	0.1604	32.9	0.9	1.5	-
28.0	-	-	-	-	1.8	-
32.0	-	-	-	-	1.3	-
34.1	1.8850	0.3510	57.8	-	-	-
37.2	1.9909	0.3707	-	-	-	-
38.6	2.0615	0.3839	-	-	-	-
41.8	2.2067	0.4102	82.8	-	-	-
42.1	-	-	-	0.7	1.5	-
61.3	2.1674	0.4036	95.9	-	-	-
63.2	-	-	-	1.0	2.4	-
69.2	-	-	-	0.7	2.6	-
73.1	2.1674	0.4036	-	-	-	-
75.2	-	-	-	1.0	2.5	-
86.0	2.1321	0.3970	102.6	-	-	-
86.1	-	-	-	-	-	-

ρ_f, biofilm density = 28.3 mg/cm^3

S_i (mg/l): 5 T_b (^oC): 30 Re: 366
v_m (cm/sec): 82.5 τ_o (N/m^2): 1.62 Ta: 203
Ω: 150

TIME (h)	T_q (N-cm)	f_a	Th (μm)	S (mg/l)	X (mg/l)	S_i (mg/l)
0.0	0.8683	0.1004	-	-	-	0.4
4.5	-	-	-	0.2	-	-
8.5	-	-	-	0.2	0.7	-
12.5	-	-	-	0.5	-	-
16.4	0.9107	0.1053	-	-	-	-
16.7	-	-	-	0.1	-	-
21.5	1.0166	0.1175	-	0.1	-	-
22.3	1.0872	0.1257	26.0	-	-	-
24.4	1.1578	0.1338	-	0.1	1.3	-
28.4	-	-	-	0.0	0.6	-
32.4	-	-	-	0.0	2.1	-
34.8	1.6873	0.1951	-	-	-	-
37.4	1.7932	0.2073	50.2	0.0	2.3	-
42.3	2.0403	0.2359	-	-	-	-
43.8	2.1321	0.2465	-	0.1	2.4	-
48.3	2.1815	0.2522	45.9	-	-	-
52.5	-	-	-	0.0	1.6	-
58.5	-	-	-	0.2	1.4	-
60.2	2.1462	0.2481	67.5	-	-	-
64.6	-	-	-	0.1	1.4	-
66.0	2.1321	0.2465	62.8	-	-	-

ρ_f, biofilm density = 39.4 mg/cm^3

AFR 10

S_i (mg/l): 20 T_b (^oC): 30 Re: 366

v_m (cm/sec): 82.5 τ_o (N/m^2): 1.62 Ta: 203

Ω: 150

TIME (h)	T_q (N-cm)	f_a	Th (μm)	S (mg/l)	X (mg/l)	S_i (mg/l)
0.0	0.5789	0.1074	-	-	-	11.0
4.1	-	-	-	1.4	1.2	-
8.1	-	-	-	1.1	2.5	-
12.1	-	-	-	4.0	3.5	-
13.0	0.5930	0.1100	-	-	-	-
16.0	0.6142	0.1139	-	-	-	-
17.3	0.6283	0.1165	-	4.7	2.5	-
18.2	0.6424	0.1192	-	-	-	-
20.1	0.6918	0.1283	-	-	-	-
22.8	1.2849	0.2383	-	2.9	3.7	-
25.0	1.8003	0.3339	35.9	-	-	-
26.2	-	-	-	1.1	4.0	-
30.2	-	-	-	1.0	5.7	-
36.2	-	-	-	0.8	5.9	-
39.3	2.5486	0.4727	-	-	-	-
42.6	2.5416	0.4714	85.7	1.1	6.3	-
48.3	2.6263	0.4871	92.4	0.8	5.7	-

ρ_f, biofilm density = 48.5 mg/cm^3

AFR 11

S_i (mg/l): 12.5 T_b (^oC): 30 Re: 366

v_m (cm/sec): 82.5 τ_o (N/m^2): 1.62 Ta: 203

Ω: 150

TIME (h)	T_q (N-cm)	f_a	Th (μm)	S (mg/l)	X (mg/l)	S_i (mg/l)
0.0	0.7201	0.1042	-	-	-	7.3
4.3	-	-	-	0.5	2.4	-
8.3	-	-	-	0.5	2.0	-
9.5	0.7201	0.1042	-	-	-	-
12.5	0.9319	0.1348	-	-	-	-
13.0	1.1084	0.1604	31.7	0.6	-	-
13.8	1.4261	0.2063	-	-	-	-
14.0	-	-	-	0.5	2.3	-
14.1	1.5320	0.2217	-	-	-	-
14.4	-	-	-	0.6	-	-
14.8	1.6802	0.2431	-	-	-	-
17.8	2.1674	0.3136	62.9	-	-	-
19.0	-	-	-	0.5	3.0	-
23.0	-	-	-	0.7	3.2	-
29.0	-	-	-	0.7	5.9	-
31.3	2.3792	0.3442	-	-	-	-
37.7	2.3298	0.3371	79.2	0.6	6.5	7.1
43.4	2.3086	0.3340	-	0.7	5.3	-
49.4	-	-	-	0.7	3.3	-
58.7	2.3792	0.3442	73.9	0.7	4.7	-

ρ_f, biofilm density = 10.7 mg/cm^3

AFR 12

S_i (mg/l): 12.5 T_b (^oC): 30 Re: 366

v_m (cm/sec): 82.5 τ_o (N/m^2): 1.62 Ta: 203

Ω: 150

TIME (h)	T_q (N-cm)	f_a	Th (μm)	S (mg/l)	X (mg/l)	S_i (mg/l)
0.0	0.7201	0.0142	-	-	-	6.6
4.2	-	-	-	1.7	-	-
9.6	0.7907	0.1144	-	1.1	3.1	-
11.3	1.6379	0.2370	-	1.2	2.0	-
11.8	1.8144	0.2625	-	-	-	-
11.9	1.8850	0.2727	34.0	-	-	-
13.0	2.1674	0.3136	-	-	-	-
14.4	2.3792	0.3442	-	-	-	-
15.0	-	-	-	0.7	4.4	-
20.9	2.5204	0.3647	56.6	0.5	3.0	-
27.1	-	-	-	0.7	2.0	-
33.1	-	-	-	0.7	3.0	-
35.0	1.7791	0.2574	34.6	-	-	-

AFR 13

S_i (mg/l): 12.5 T_b (^oC): 30 Re: 366

v_m (cm/sec): 82.5 τ_o (N/m^2): 1.62 Ta: 203

Ω: 150

TIME (h)	T_q (N-cm)	f_a	Th (μm)	S (mg/l)	X (mg/l)	S_i (mg/l)
0.0	0.7201	0.1042	-	-	-	7.4
4.3	-	-	-	0.5	1.9	-
8.3	-	-	-	0.5	2.9	-
11.9	1.0943	0.1583	23.5	-	-	-
12.4	1.1719	0.1696	-	-	-	-
12.9	1.4049	0.2033	-	-	-	-
13.5	1.6873	0.2441	-	-	-	-
14.4	1.9697	0.2850	-	1.2	3.3	-
15.0	2.1462	0.3105	-	-	-	-
15.2	-		-	2.1	-	-
17.3	2.3933	0.3463	-	-	-	-
17.9	-	-	-	1.3	5.0	-
18.1	2.4639	0.3565	49.1	-	-	-
23.8	2.3933	0.3463	59.7	1.1	3.2	-
34.7	1.6873	0.2441	-	0.1	3.3	-
36.4	1.6167	0.2339	46.5	-	-	-
41.5	1.3696	0.1982	42.6	0.7	2.8	-
48.4	1.2284	0.1777	-	-	-	-
52.4	-	-	-	0.6	1.0	-
60.4	1.0166	0.1471	33.4	0.4	1.4	6.6

ρ_f, biofilm density = 34.4 mg/cm^3

AFR 14

S_i (mg/l): 5 T_b (^oC): 30 Re: 366

v_m (cm/sec): 82.5 τ_o (N/m^2): 1.62 Ta: 203

Ω: 150

TIME (h)	T_q (N-cm)	f_a	Th (μm)	S (mg/l)	X (mg/l)	S_i (mg/l)
0.0	0.8683	0.1004	-	-	-	2.7
10.2	1.0166	0.1175	-	-	-	-
11.5	1.3343	0.1542	30.2	0.7	1.5	-
13.3	1.9062	0.2203	-	0.6	1.8	-
14.4	2.1815	0.2522	-	-	-	-
17.1	2.4568	0.2840	-	0.6	1.9	-
22.8	2.7675	0.3199	53.9	0.8	2.7	-
40.7	2.7816	0.3215	58.5	0.6	2.9	-
66.1	2.4286	0.2807	52.6	1.1	2.4	-

ρ_f, biofilm density = 45.5 mg/cm^3

AFR 15

S_i (mg/l): 25 T_b (°C): 30 Re: 366

v_m (cm/sec): 82.5 τ_o (N/m^2): 1.62 Ta: 203

Ω: 150

TIME (h)	T_q (N-cm)	f_a	Th (μm)	S (mg/l)	X (mg/l)	S_i (mg/l)
0	0.7201	0.1042	-	-	-	14.2
11.9	0.8190	0.1185	-	9.8	1.7	-
12.8	0.9107	0.1318	-	-	-	-
13.6	1.0096	0.1461	-	-	-	-
14.2	1.1508	0.1665	-	8.7	1.7	-
14.6	1.2002	0.1737	-	-	-	-
15.2	1.3485	0.1951	-	-	-	-
15.7	1.5250	0.2206	-	-	-	-
16.2	1.8000	0.2604	-	-	-	-
16.7	1.9062	0.2758	34.6	-	-	-
24.9	2.0615	0.2983	58.9	2.5	1.4	-
31.5	1.8991	0.2733	-	1.7	4.0	-
37.4	1.5391	0.2227	53.4	1.1	3.2	-
51.7	1.1690	0.1706	43.0	1.1	4.3	15.3
60.5	1.5038	0.2176	55.1	1.3	3.8	-
77.9	1.3908	0.2012	44.7	0.8	3.7	-

AFR HEAT TRANSFER EXPERIMENT

S_i (mg/l): 12.5 T_b (^oC): 46.9 Re: 366

v_m (cm/sec): 93.5 τ_o (N/m^2): 20.3 Ta: 258

Ω: 170

Influent Dilution Water Temp: 30^oC

TIME (h)	T_q (N-cm)	f_a	Th (μm)	S (mg/l)	X (mg/l)	Effluent Temp. (^oC)	Surface Temp. (^oC).
0	0.72	0.10	-	-	-	36.8	47.0
7.0	0.74	0.11	-	-	-	36.8	46.9
10.9	1.51	0.22	-	-	-	36.9	46.9
11.2	1.66	0.24	-	-	-	37.0	46.9
12.0	1.87	0.27	-	-	-	36.9	46.9
12.6	2.07	0.30	36.9	-	-	36.9	46.9
22.7	2.87	0.41	55.5	-	-	36.9	46.9
28.5	3.02	0.44	-	-	-	37.1	46.9
31.4	3.02	0.44	-	-	-	37.2	46.9
34.2	2.97	0.43	-	-	-	37.0	46.9
36.5	3.02	0.44	57.6	-	-	36.9	46.9
46.8	2.97	0.43	-	-	-	36.6	46.9
48.1	2.87	0.41	54.7	-	-	36.5	46.9
51.0	2.67	0.39	-	-	-	36.5	46.9
53.4	2.73	0.40	-	-	-	36.6	46.9
55.8	2.87	0.41	-	-	-	36.6	47.0
59.8	2.77	0.40	48.0	-	-	36.5	47.0

ρ_f, biofilm density = 14.4 mg/cm^3

TAFRI EXPERIMENT*

S_i (mg/l): 12.5 τ_o (N/cm^2): 2.00 T_b (°C): 30

TIME (h)	TUBULAR FOULING REACTOR Δp	f_a	Th (μm)	ANNULAR FOULING REACTOR T_q (N-cm)	f_a	Th (μm)	COMBINED REACTOR SYSTEM S_i (mg/l)	S (mg/l)	X (mg/l)
-10.5	1.10	0.0090							
0				0.52	0.0847				
8.2	1.75	0.0137					6.2		1.0
12.4	1.85	0.0133						1.2	
16.2	1.80	0.0126	79					1.3	4
17.5				0.55	0.0897				
19.5				0.59	0.0962				
20.8	1.90	0.0134						0.5	7
23.4				0.61	0.0995				
26.3	2.40	0.0172						1.6	6
27.8				0.66	0.1076				
28.4	2.40	0.0172	75				5.0		
28.7	2.25	0.0145						3.6	3
30.7				0.71	0.1156	31.3			
35.5	2.50	0.0184							
41.7				1.22	0.1991				
43.0				1.24	0.2023	62.0			
45.2				1.24	0.2023				
48.0				1.24	0.2023				
52.7	2.10	0.0164							
53.3	1.70	0.0112							
53.8	1.80	0.0122							
67.5				1.06	0.1730	63.1			

*This experiment was conducted with the feed solution entering the fermenter in the TFR1 system. The AFR received effluent from the TFR1 fermenter and was an integral part of the TFR1 recycle line. Hydraulic residence time in the AFR was approximately 1 minute.